Technische Universität München

WACKER-Lehrstuhl für Makromolekulare Chemie

Development and Application of Novel Cobalt and Rare Earth Metal Single-Site Catalysts for the Polymerization of Polar Monomers

Peter Thomas Altenbuchner

Vollständiger Abdruck der von der Fakultät für Chemie der Technischen Universität München zur Erlangung des akademischen Grades eines

Doktors der Naturwissenschaften

genehmigten Dissertation.

Vorsitzender:	Univ.-Prof. Dr. Tom Nilges
Prüfer der Dissertation:	1. Univ.-Prof Dr. Dr. h.c. Bernhard Rieger
	2. Univ.-Prof. Dr. Lukas Hintermann
	3. Univ. Prof. Dr. Gerhard Erker, Westfälische Wilhelms-Universität Münster, (schriftliche Beurteilung)
	Univ.-Prof. Dr. Klaus Köhler, (mündliche Prüfung)

Die Dissertation wurde am 30.06.2015 bei der Technischen Universität München eingereicht und durch die Fakultät für Chemie am 31.08.2015 angenommen.

Danksagung

Mein besonderer Dank gilt Prof. Dr. Dr. h.c. Bernhard Rieger für die Aufnahme in den Arbeitskreis und die interessante Themenstellung. Ihre richtungsweisenden Ratschläge bei anregenden Diskussionen und die mir gewährten wissenschaftlichen Freiheiten, auch im Rahmen von Industriekooperation, sind das Fundament dieser Arbeit. Die Möglichkeit Forschung ohne die Einschränkung auf Themengebiete zu betreiben hat mich fasziniert und meine Zeit an Ihrem Lehrstuhl wie im Flug verstreichen lassen.

Dr. Carsten Troll und Dr. Sergei Vagin gebührt mein Dank für die Organisation des Lehrstuhls und der Unterstützung bei jeglichen Problemen. Bei Annette Bauer und Sabine Saul-Hubrich möchte ich mich für Ihre Hilfe bei organisatorischen Problemen bedanken.

Der BASF SE möchte ich für die finanzielle Unterstützung danken. Im Besonderen gilt mein Dank Dr. Anna Brym, Dr. Uwe Seemann, Dr. Maximilian Lehenmeier, Dr. Robert Reichardt, Dr. Robert Loos und Dr. Peter Deglmann.

Allen Doktoranden und Mitarbeitern am Wacker-Lehrstuhl möchte ich für die angenehme Atmosphäre und gute Zusammenarbeit danken. Meinen Laborkollegen Patrick Werz, Benedikt Soller und Ignaz Höhlein gilt desweiteren mein Dank für die fachlichen Diskussionen und die tolle Stimmung im Labor. Stefan Kissling, Alexander Kronast, Richard Reithmeier, Nicole Zollbrecht sei zudem für die schöne Zeit auf Konferenzen, im Kaffezimmer und im Labor gedankt.

Allen Studenten, die Praktika, Bachelorarbeiten und/oder Masterarbeiten bei mir gemacht haben danke ich dafür, dass sie mich durch Ihren Eifer und Fleiß tatkräftig unterstützt haben: Thomas Bachmann, Marina Reiter, Friederike Adams, Dominik Reiter, Anna Neumann, Luisa Lempenauer, Hanusch Grab, Qian Sun und Leon Serc.

Dr. Eberhardt Herdtweck und Dr. Alexander Pöthig gilt mein Dank für die Röntgenkristallstrukturanalyse. Mein Dank geht auch an das Team für Elementaranalyse des Anorganisch-chemischen Instituts der TUM, insbesondere an Ulrike Ammari für ihre stete Hilfe.

Zu großem Dank verpflichtet bin ich meinen Eltern, meinen Geschwistern und Großeltern für Ihre Unterstützung während des gesamten Studiums und der Promotion. Patricia Schöppner gilt mein Dank für aufmunternden Worte, Geduld und Unterstützung.

Table of Contents

Table of Abbreviations

BDSA	bisdimethylsilylamide
BL	β-butyrolactone
CCS	carbon capture and Storage
DAVP	dialkyl vinylphosphonate
DEVP	diethyl vinylphosphonate
DIVP	diisopropyl vinylphosphonate
DMAA	*N,N*-dimethyl acrylamide
EGDM	ethylene glycol dimethacrylate
GTP	group transfer polymerization
HPPO	hydrogen peroxide to propylene oxide
I*	initiator efficiency
IPOx	isopropenyloxazoline
LA	lactide
LCST	lower critical solution temperature
MALS	multi angle light scattering
MBTU	mega British thermal units
MTP	methanol to propene
NAFTA	North American Free Trade Agreement
PCHC	poly(cyclohexene carbonate)
PDI	polydispersity index
PHB	poly(3-hydroxybutyrate)
PPC	poly(propylene carbonate)
PO	propylene oxide
R&D	Research and Development
RDS	rate determining step
SI-GTP	surface initiated - GTP
TBAB	tetrabutylammonium bromide
TBD	1,5,7-triazabicyclo[4,4,0] dec-5-ene
^{t}Bu	*tert*-butyl
thf	tetrahydrofurane (ligand)
THF	tetrahydrofurane (solvent)
TOF	turn over frequency
UCST	upper critical solution temperature

1. Introduction

The global chemical industry has seen stunning growth since the mid-1980s at a rate of 7 per cent annually and with respect to value creation was the fourth best performing sector from 2007 to 2011 of all industries.[1] The majority of the overall growth was generated in Asia, which currently accounts for almost half of the global chemical sales. Projections for the next 20 years predict a diverging trend for Asia and Europe and if current global trends continue, Asia will grow by 3 per cent over the next 20 years while Europe is expected to lag behind with only 1 per cent growth.[1a]

The industry faces tremendous changes and challenges which reshape value chains, the competitive environment and upheaval the global playing field. Five to eight companies in the global top 10 players are forecasted to come from Asia and the Middle East in 2030.[1a] European and American companies are expected to be superseded by predominantly state-controlled giants such as *ChemChina*, *Sinopec*, and *PetroChina* (table 1).[1a,2] What are the driving forces behind this projected trend and what can be done from a European perspective to confront them?

Table 1. Top chemicals players (Sales EUR billion[a], market share in %)[1a]

1985				2010			2030[b]
1	Bayer	14	2.8%	BASF	48	2.0%	Europe 2-3[c]
2	BASF	13	2.8%	Dow Chemical	41	1.7%	
3	Hoechst	13	2.6%	Exxon Mobil	40	1.7%	
4	ICI	10	2.1%	SABIC	35	1.5%	NAFTA 1-2[c]
5	Dow Chemical	8	1.7%	Sinopec	33	1.4%	
6	DuPont	8	1.7%	Royal Dutch Shell	30	1.3%	Middle East 2-3[c] Asia 3-5[c]
7	Ciba-Geigy	7	1.5%	DuPont	24	1.0%	
8	Montedison	7	1.4%	LyondellBasell	24	1.0%	
9	Rhône-Poulenc	6	1.2%	Ineos Group	21	0.9%	
10	Monsanto	5	1.0%	Mitsubishi Chemical	21	0.9%	

a assumed exchange rate is $1.39/EUR
b Assumes the following growth rates 2010 – 30: Asia 5%, Europe 1%, NAFTA 1.2%, Rest of world 3%
c Number of players by region

The recent global economic downturn (2007 – 2009) highlighted the diverging structural background to the economic models. Especially emerging markets were hit harder than their competitors in industrialized countries which reflects in the poor performance over the last 5 years. The reason for this is the focus of emerging markets chemical industry, mostly state owned enterprises, on local or regional markets while at the same time their business model is focused on vulnerable base chemicals and polymers. Predictions about the ascent of Asia's chemical industry are founded on the increasing maturity of chemical companies in emerging markets and their effort to move into downstream chemicals and enhanced value products in coming years.[2] Furthermore, Asian and Middle Eastern producers derive added benefit from state subsidies (e.g. 0.75 $/MBTU (Mega British thermal units) of natural gas for Saudi Basic Industry Corporation (*SABIC*)[3]).

Also North American companies put increased pressure on their European competitors as the shale gas boom has reversed their energy supply situation and cut the shale gas price from $12/MBTU in 2008 to $3/MBTU in 2012.[4] The opportunity of inexpensive energy supply and raw material for a foreseeable future has the potential to shift the balance toward US based growth in the industry.

European chemical companies are well positioned in their home markets but hold weak positions in overseas markets.[1a,3] They have various tools at hand how to improve their performance in an increasingly competitive global market. Possibilities are for example the increased utilization of technology, opening up new markets by entering a new region or by introducing their products to new applications and even business model changes. Three main trends which can currently be observed within the industry are firstly the restructuring of the portfolio to shed businesses with low profits, secondly increased number of mergers creating multispecialty companies, such as *Rhodia-Solvay* and *Clariant-Süd-Chemie*, and thirdly increased tendency towards global merger and acquisition activities.[1b,2,5]

Additionally, research and development (R&D) spending is in steady decline across integrated, specialty and commodity chemical companies.[6] A study by *Boston Consulting Group* showed that increased R&D spending does not correlate with commercial success in terms of total shareholder return.[2]

Rather the R&D strategy of chemical companies has to be reevaluated and transformed from a blockbuster approach towards customer oriented solutions and innovations research bolstered by state funded research at university level.[7] Furthermore, research and development is increasingly relocating to Asia to allow customer proximity and availability of talent.

Industrial R&D programs can not fulfill the sustained capital influx for fundamental research over prolonged periods of time without generating revenue. However, this basic research creates the foundation for future marketable ideas and products. Therefore, state financed research at universities plays a pivotal role in pushing the boundaries in chemical mechanistic understanding, cutting edge synthetic techniques and available high performance materials.[8] A close integration between universities and industry has the potential to be one of the deciding factors in the global competitive race of coming decades. The main advantage of Europe as hub for chemical companies is the mature scientific infrastructure comprised of extraordinary universities, and other scientific institutes (e.g. *Frauenhofer Institute*, *Max-Planck Institute*).

In summary, the global chemical industry is at the verge of fundamental changes and developments. On the path towards ever more globalized markets, trends in production, energy supply and innovation have to be closely monitored to keep a competitive edge. Especially European chemical companies face demanding and exciting future challenges within a globally connected market with an increasing number of strong competitors. Close cooperation between industry and publicly financed institutions can bolster the competitive edge over North America and Asia in coming decades.

2. Utilization of Carbon Dioxide for the Generation of Polycarbonates

Carbon dioxide has inspired many scientists to pursue the dream of its utilization as raw material in synthetic chemistry. Contrary to popular opinion, chemical processes can not impact the carbon dioxide levels in the atmosphere (400 pm) due to small volume and its limited long term storage capacity within the synthesized materials.[9] For this purpose, carbon capture and storage techniques (CCS) are the more promising approach.[10] However, chemical processes utilizing carbon dioxide can shift production pathways away from fossil resource based chemistry and thereby have positive influence on the overall sustainability.

One of the most prominent possible applications of carbon dioxide is the replacement of phosgene in the synthesis of polycarbonates and polyurethanes.[11] A substitution of the phosgene process would lead to the evasion of highly toxic phosgene and concomitant hydrochloride and other byproducts during production process.[12]

The high oxidation state of carbon in carbon dioxide is the biggest hurdle in accessing the potential reactant as it requires large quantities of energy to convert it to the desired products. Elegant access to polycarbonates and polyurethanes from carbon dioxide is possible *via* high-energy small-membered ring molecules, *e.g.* epoxides. Most common representatives of relevant epoxides for the polycarbonate synthesis are cyclohexene oxide and propylene oxide. Poly(propylene carbonate) (PPC) in particular has interesting properties such as biodegradability and biocompatability.[13]

Aside from carbon dioxide and an epoxide, a catalyst is necessary for the selective and efficient conversion to polycarbonates. Heterogeneous catalysis dominates the industrial production and also receives great interest from research facilities.[10c,14] However, mechanistic studies and the targeted approach towards new polymer architectures is performed with homogeneous single-site catalyst systems of the general structure L_nMR, where M is the active metal center combined with an organic ligand framework and R as initiating group.

Properties such as molecular weight, polydispersity, endgroups, stereochemistry, and comonomer incorporation can be addressed and controlled by tuning the ligand, metal center, and initiating group. The carbon dioxide utilization for the production of polycarbonates has grown to a mature field of research since its early discoveries by Prof. Inoue.[15] The reader shall be referred to recently published elaborate review articles covering the complete historic developments.[14b,16] In this work, the focus is on cobalt based catalyst systems and their activity, selectivity, and stability.[17]

2.1 Mechanism of Catalytic CO_2/Epoxide Copolymerization

The copolymerization of epoxides and carbon dioxide is strongly dependent on the reaction conditions and employed catalyst system. A binary copolymerization mechanism for which either a second catalyst molecule or a cocatalyst is necessary to activate the epoxide and stabilize the growing polymer chain has been identified to be prevailing mechanism in the majority of catalytic systems.[18] Aside from polycarbonate formation (A) two other processes can take place, polyether (B) and cyclic carbonate (C) formation (Figure 1).[17,19] Polyether formation is the result of consecutive epoxide insertion into the growing polymer chain. Cyclic carbonate is generated by intramolecular elimination of cyclic carbonate, so called backbiting, which can proceed *via* two mechanisms, one involving the metal center and the coordinated polymer chain while the other occurs with the detached polymer chain. The cyclic elimination from a detached polymer chain was found to have a lower activation barrier and is hence favoured at elevated temperatures and the presence of excess nucleophilic cocatalyst.

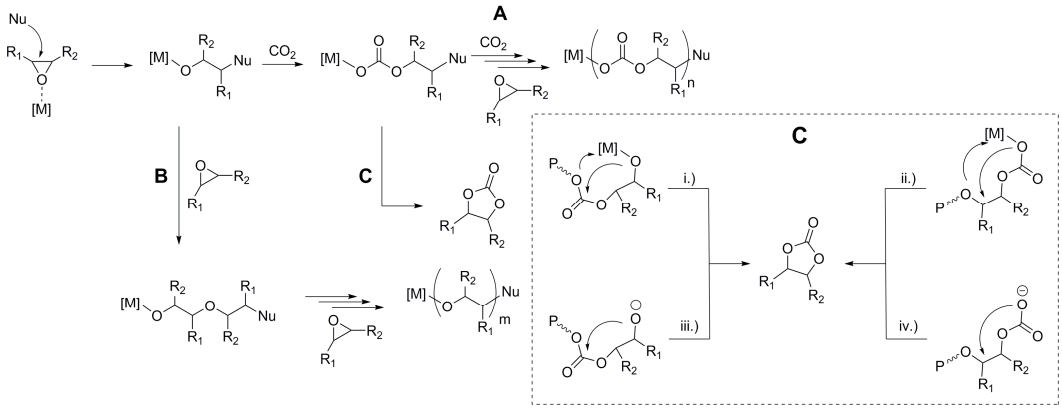

Figure 1. Copolymerization of carbon dioxide and epoxides to polycarbonates and possible side reactions.

Five-membered cyclic carbonates are thermodynamically more stable than the corresponding polycarbonate and the selective poylcarbonate formation is further complicated by the small difference in activation energy for cyclic carbonate and copolymer formation.[20] Therefore, cyclic carbonate is predominately formed at elevated temperatures and high conversions. The stereochemistry of polycarbonate is heavily affected by the regioselectivity of the epoxide ring opening step. Ring opening at the methylene carbon-oxygen bond proceeds under retention of the stereochemistry while ring opening at the methine carbon proceeds under inversion of the configuration. Hence, in an alternating copolymer head-to-tail, head-to-head, and tail-to-tail carbonate linkages can be present depending on the ring opening step.

2.2 Cobalt Catalysts for the Copolymerization Carbon Dioxide and Epoxides

Reports of cobalt catalysts for the coupling of CO_2 and epoxides were scarce in literature and limited to $Co(OAc)_2$ with acetic acid as cocatalyst (TOF = 0.06 h^{-1}) until 2002 when HE reported the formation of ethylene carbonate with a binary catalyst system comprised of (salen)Co(II) and Bu_4NBr (salen = *N,N'-bis*(3,5-di-*tert*-burtylsalicylidene)-1,2-cyclohexanediamine).[21] Subsequent reports of cobalt(II) catalysts showed the successful synthesis of various cyclic carbonates from their respective epoxides and CO_2.[22] Based on the work of JACOBSEN on ring-opening of epoxides with (salen)Co(III) carboxylates COATES developed [(salen)CoOAc] catalysts for the highly selective polycarbonate formation (>99%) from propylene oxide and carbon dioxide (25 °C, 56 bar, TOF = 81 h^{-1}).[23] In comparison to chromium salen catalysts the [(salen)CoOAc] afforded polycarbonate without the necessary additon of a cocatalyst.

This publication sparked the race towards ever more active Co(III) catalyst systems. The introduction of bifunctional cobalt catalysts which have a cocatalyst covalently bound to the ligand framework, allowed for another leap forward with respect to polymerization activity. Various elegantly designed structures were introduced by different groups (Figure 2).[24] The pinnacle of catalytic activity was so far reached with a binary system based on (salen)Co(III)X in combination with a quaternary ammonium salt.[25] Systematic alterations to the initially developed system by LEE resulted in the development of a catalyst system which exhibits turn over frequencies up to 26 000 h^{-1} for the copolymerization of propylene oxide

and carbon dioxide while retaining almost perfect polycarbonate selectivity at elevated temperatures and low catalyst loadings (80 °C, [PO]/[cat] = 25000/1).

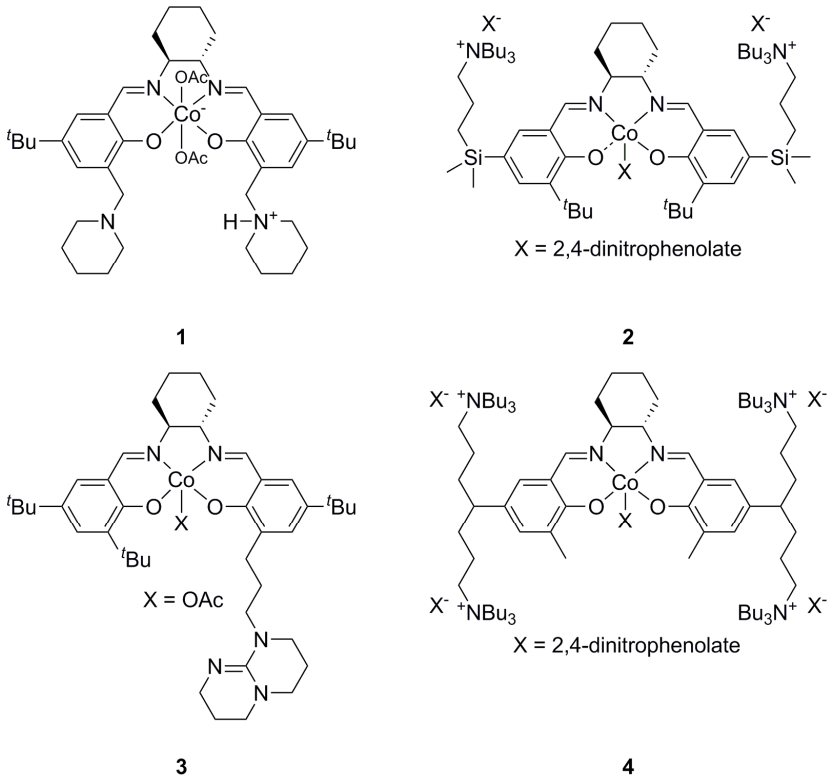

1 **2** **3** **4**

Figure 2. Bifunctional Co(III) catalysts (1-4) for the copolymerization of epoxides and carbon dioxide.

Apart from activity also the reaction conditions, especially the carbon dioxide pressure, are highly relevant factors for a possible industrial application. The copolymerization at ambient pressure reduces the necessary energy input and thereby reduces costs. Currently, few catalysts exist which can copolymerize at ambient pressure.[18a,24c,26] In 2010, WILLIAMS successfully synthesized bimetallic Co(II) (TOF = 172 h^{-1}) (**5**) and mixed metallic Co(II)/Co(III) (TOF = 159 h^{-1}) (**6**) catalysts which are capable catalysts for the CHO/CO_2 copolymerization and an order of magnitude more active than their zinc counterparts (Figure 3, table 2).[18e,26h]

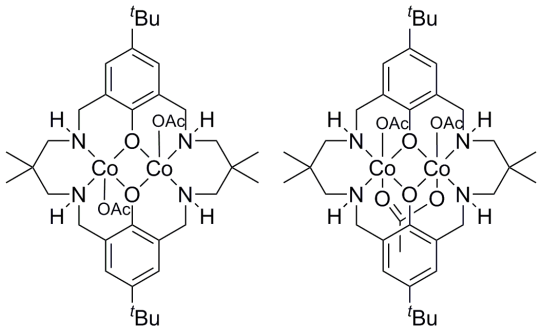

Figure 3. Dinuclear Robson-type Co(II) (5) and Co(II)/Co(III) (6) catalysts.

Table 2. Copolymerizations of CHO and carbon dioxide with catalyst 5 and 6 at 80 °C and 1 atm CO_2.[26h]

catalyst	time [h]	TOF[a] [h^{-1}]	Selectivity[b] [%]	M_n[c] [g/mol]	PDI
5	2	172	>99	5100	1.26
6	3	159	>99	6300/2800	1.04/1.14

[a] TOF = TON per hour. [b] determined by comparison of the integrals of signals arizing from the methylene protons in the ^{1}H NMR spectra due to copolymer carbonate linkages (δ = 4.65 ppm), copolymer ether (δ = 3.45 ppm), and the signals due to cyclic carbonate byproduct (δ = 4.0 ppm). [c] Determined by SEC, in THF, using narrow polystyrene standards as calibrants. All the copolymers contained >99% carbonate linkages, as observed by ^{1}H NMR.

2.3 Deactivation of Cobalt(III) Catalysts During the Copolymerization

Deactivation of cobalt(III) catalysts during the copolymerization have often been reported in literature. However only few detailed investigations exist about the proceedings during such deactivation processes. Early on it was postulated that the presence of cocatalysts helps to prevent the reduction but no additonal experiments were performed.[16c,27]

LU used in depth mass spectrometry (ESI-MS) and infrared spectroscopy studies with a bifunctional (salen)Co(III) catalyst with an anchored organic base 1,5,7-triazabicyclo[4,4,0] dec-5-ene (TBD) and found that the covalently linked TBD arm plays a distinct role in maintaining thermal stability and activity (Figure 4).[24c] It is postulated that the propagating carboxylate species originating from the nucleophilic anion and the nucleophilic cocatalyst successively stabilize the metal center from the reduction to Co(II) also at low CO_2 pressure and elevated temperatures by reversible intramolecular Co-O bond formation and dissociation (Figure 4).

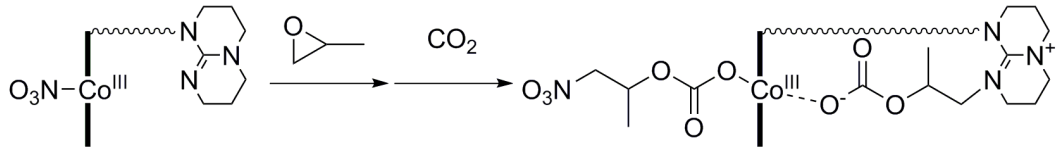

3

Figure 4. Proposed stabilization of Co(III) by successive, intramolecular Co-O bond formation and dissociation.[24c]

Subsequent stability studies of catalyst 3 during the hydrolytic kinetic resolution of racemic epoxides unveiled a redox reaction between Co(III) and the hydrolyzed product to Co(II) and α-hydroxy ketones.[28] The authors propose the reduction of Co(III) *via* a highly reactive Co(IV) intermediate which in turn is responsible for the epoxide oxidation to α-hydroxy ketones. Other catalyst systems, namely non-bifunctional salen and porphyrin catalysts also show more or less pronounced tendency towards reduction and therewith complete loss of activity under copolymerization conditions. The deactivation of catalysts is strongly related to the formation of alcoxy cobalt species.[29]

RIEGER investigated the behavior of (porphyrin)Co(III)X and (salen)Co(III)X systems under copolymerization conditions of propylene oxide and carbon dioxide. UV-Vis, NMR and X-ray crystalstructure analytics corroborate the stabilizing function of the coordinated carboxylate chain end. An autoreduction mechanism on basis of the experimental data is postulated which proceeds *via* a (salen)Co(III)-alkoxide intermediate (Figure 5).[30] Additionally, it was found that the hydrolysis of the Co(III)-alkoxide species by water may accelerate formation of Co(II).[28]

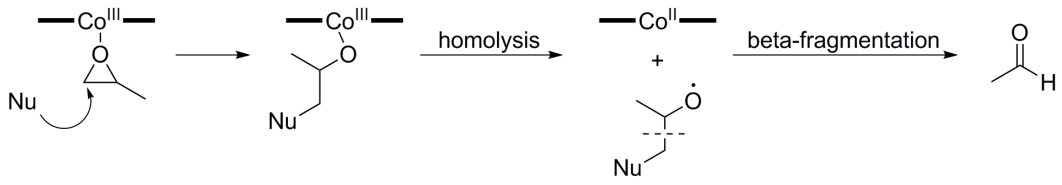

Figure 5. Postulated deactivation mechanism for Co(III)-porphyrin/salen systems in the presence of propylene oxide.[30]

Prevention of the deactivation of cobalt catalysts is possible through the reduction of the lifetime of the autoreducible cobalt-alkoxide species by introducing a covalently bound cocatalyst or increasing the carbon dioxide pressure and thereby fast CO_2 insertion.

2.4 Aim of this Work: Cobalt(II) Catalysts for the Copolymerization of Carbon Dioxide and Epoxides

Interestingly, all catalysts which have been studied for their deactivation behavior are completely inactive for the copolymerization of epoxides and carbon dioxide in their reduced form. Porphyrin, salen and derivatives thereof become completely inactive as Co(II) complexes (*vide supra*). In recent years, researchers have started to investigate Co(II) complexes for their copolymerization ability and so far only one catalyst system was found which allows the successful copolymerization of epoxide (CHO) and CO_2. The cobalt(II) catalyst is even able to match the activity of the mixed valence (Co(II)/Co(III)) counterpart.

Recently, amine-*bis*(phenolato)catalysts were introduced for the coupling of CO_2 and epoxides. Promising results were obtained with chromium and cobalt(II/III) systems and structural variations have been synthesized and characterized.[31] Although only chromium based amine-*bis*(phenolato)systems showed the ability to produce polycarbonates.

Amine-*bis*(phenolato)complexes are still at the early stages of their implementation as catalysts the copolymerization of epoxides and carbon dioxide. The ligand motif is easily accessible *via* Mannich-reaction and offers numerous possibilities to tune its steric and electronic properties.

Bifunctional cobalt(III) catalysts are currently the most active category within the plethora of copolymerization catalysts, however their deactivation to inactive compounds under polymerization conditions leaves room for improvement. Especially since the potential of cobalt(II) based catalyst systems has been neglected until recently.

The creation of highly active, amine-*bis*(phenolato)-cobalt(II) based catalysts is desirable to assess their potential polymerization abilities and to circumvent catalyst deactivation through reduction.

2.5 Manuscript: Amine-bis(phenolato)cobalt(II) Catalysts for the Formation of Organic Carbonates from Carbon Dioxide and Epoxides

Status	Published online: 27th February 2015
Journal	European Journal of Inorganic Chemistry
Publisher	Wiley-VCH Verlag GmbH & Co. KGaA
Article type	Full paper
DOI	10.1002/ejic.201403087

Authors	Marina Reiter*; Peter T. Altenbuchner*; Stefan Kissling; Eberhardt Herdtweck; Bernhard Rieger

*Contributed equally

Content

New monometallic amine-*bis*(phenolato)cobalt(II) [(ONNO)^{R}Co(II)] (R = CMe_2Ph; Cl; Br) complexes have been synthesized and fully characterized. These novel Co(II) complexes show good activities for the formation of cyclic propylene carbonate in combination with tetrabutylammonium bromide (TBAB) as cocatalyst. Reaction conditions such as carbon dioxide pressure, cocatalyst loadings and temperature were varied to determine the ideal reaction conditions. These catalysts were also tested in copolymerization reactions of cyclohexene oxide/CO_2 and propylene oxide/CO_2. [(ONNO)^{Cl}Co(II)]*(MeOH) was found to copolymerize cyclohexene oxide (CHO) and CO_2 which makes the catalyst the first reported amine-*bis*(phenolato)cobalt(II) complex to be active in the copolymerization of CO_2 and CHO. In-depth stability studies were conducted (Evans' Method) to ensure Co(II) as the active species for the copolymerization. Endgroup analysis *via* NMR, ESI-MS and MALDI-TOF showed 4-dimethylaminopyridine (DMAP) and methoxy terminated chains.

JOHN WILEY AND SONS LICENSE TERMS AND CONDITIONS

Apr 14, 2015

This Agreement between Peter Altenbuchner ("You") and John Wiley and Sons ("John Wiley and Sons") consists of your order details and the terms and conditions provided by John Wiley and Sons and Copyright Clearance Center.

License Number	3607661255122
License date	Apr 14, 2015
Licensed Content Publisher	John Wiley and Sons
Licensed Content Publication	European Journal of Inorganic Chemistry
Licensed Content Title	Amine-bis(phenolato)cobalt(II) Catalysts for the Formation of Organic Carbonates from Carbon Dioxide and Epoxides
Licensed Content Author	Marina Reiter,Peter T. Altenbuchner,Stefan Kissling,Eberhardt Herdtweck,Bernhard Rieger
Licensed Content Date	Feb 27, 2015
Pages	9
Type of use	Dissertation/Thesis
Requestor type	Author of this Wiley article
Format	Print and electronic
Portion	Full article
Will you be translating?	No
Title of your thesis / dissertation	Development and Application of Novel Cobalt and Rare Earth Metal Single-Site Catalysts for the Polymerization of Polar Monomers
Expected completion date	Jul 2015
Expected size (number of pages)	250
Requestor Location	Peter Altenbuchner Kolomanstr 23 None None Ismaning, Germany 85737 Attn: Peter Altenbuchner
Billing Type	Invoice
Billing Address	Peter Altenbuchner Kolomanstr 23 None None Ismaning, Germany 85737 Attn: Peter Altenbuchner
Total	**0.00 EUR**

EurJIC European Journal of Inorganic Chemistry
ChemPubSoc Europe
FULL PAPER

DOI:10.1002/ejic.201403087

Amine-bis(phenolato)cobalt(II) Catalysts for the Formation of Organic Carbonates from Carbon Dioxide and Epoxides

Marina Reiter,[a][‡] Peter T. Altenbuchner,[a][‡] Stefan Kissling,[a] Eberhardt Herdtweck,[b] and Bernhard Rieger*[a]

Keywords: Carbon dioxide fixation / Copolymerization / Cyclic carbonates / Epoxides / Cobalt

New monometallic amine-bis(phenolato)cobalt(II) [(ONNO)^{R}-Co^{II}] (R = CMe_2Ph; Cl; Br) complexes have been synthesized and fully characterized including X-ray crystallographic analysis. These Co^{II} complexes show good activity for the formation of cyclic propylene carbonate in combination with tetrabutylammonium bromide (TBAB) as a co-catalyst. The reaction parameters such as carbon dioxide pressure, co-catalyst loadings and temperature were varied to determine the ideal reaction conditions. These catalysts were also employed in copolymerization reactions of cyclohexene oxide/CO_2 and propylene oxide/CO_2. [(ONNO)^{Cl}Co^{II}]$^{\bullet}$(MeOH) was found to effectively copolymerize cyclohexene oxide (CHO) and CO_2. This is the first reported amine-bis(phenolato) cobalt(II) complex to be active in the copolymerization of CO_2 and CHO. In-depth stability studies were conducted (Evan's method) to validate Co^{II} as the active species required for copolymerization. End-group analysis via NMR, ESI-MS and MALDI-TOF revealed the presence of 4-(dimethylamino)pyridine (DMAP) and methoxy terminated chains.

Introduction

Carbon dioxide is non-toxic, abundant, renewable, and a low cost C_1-building block. By virtue of these attributes, CO_2 is an increasingly attractive material for economic and academic use.[1–4] The industrial application of CO_2 is currently limited to the production of urea, methanol, cyclic carbonate, and salicylic acid.[2,3,5–10] Since Inoue et al. discovered the coupling of thermodynamically stable CO_2 with epoxides in 1969, a plethora of homogeneous catalysts have been developed.[5,10–13] Cyclic carbonates are in high industrial demand,[14,15] given their use as precursors to polycarbonates,[14,16] electrolytes in lithium ion batteries,[17–19] additives to gasolines,[20] thickeners of cosmetics,[18] and as so called "green solvents".[21–23] Moreover, polycarbonates derived from CO_2 have promising physical properties like durability, biodegradability, high transparency, heat resistance, and gas permeability which make them possible candidates for applications in the automotive, medical and electronics industries.[10,24–26] Catalysts for polycarbonate or cyclic carbonate synthesis often rely on porphyrin, β-diiminate- and salen-ligands in combination with various metals like zinc, iron, magnesium, aluminum, chromium, and cobalt.[15,27–38] The adequate choice of catalyst is essential to achieving reaction selectivity. Owing to the desire for high selectivities and activities, in recent years, catalyst design has shifted towards bifunctional and bimetallic catalysts.[1,5,10,12] Bifunctional complexes combine the active metal site, coordinated by an organic ligand framework, with a covalently bound co-catalyst whereas for bimetallic catalysts the co-catalyst is replaced by a second metal center. The highest activities reported in the literature paired with exceptional selectivities for the copolymerization of propylene oxide/cyclohexene oxide and CO_2 have been achieved using ionic salen-cobalt(III) catalysts[32] and dinuclear zinc catalysts.[34]

Published reports of Co^{II} catalysts for the coupling of CO_2 and epoxides are rare and limited to $Co(OAc)_2$ with acetic acid as co-catalyst for a substantial period of time (TOF = 0.06 h^{-1}).[39] In recent years Lu et al. were able to utilize immobilized Co^{II} catalysts for the coupling of ethylene oxide and carbon dioxide under harsh conditions for 24 h without loss of activity.[40] In 2010, Williams et al. successfully synthesized bimetallic Co^{II} (TOF = 172 h^{-1}) and mixed metallic Co^{II}/Co^{III} (TOF = 159 h^{-1}) catalysts which were active for the copolymerization of CHO/CO_2 at ambient pressure.[41,42] Recently, amine-bis(phenolato) catalysts were introduced for the coupling of CO_2 and epoxides. Promising results were obtained with chromium and

[a] WACKER-Lehrstuhl für Makromolekulare Chemie, Technische Universität München, Lichtenbergstraße 4, 85747 Garching, Germany
E-mail: rieger@tum.de
http://www.makro.ch.tum.de
[b] Anorganisch-Chemisches Institut, Lehrstuhl für Anorganische Chemie, Technische Universität München, Lichtenbergstraße 4, 85747 Garching, Germany
[‡] The authors contributed equally.
Supporting information for this article is available on the WWW under http://dx.doi.org/10.1002/ejic.201403087.

$Co^{II/III}$ systems although only the chromium-based amine-bis(phenolato) systems generated polycarbonates.[43–45] The amine-bis(phenolate) ligand structure is versatile and offers numerous possibilities for electronic and steric alteration.[46–53] Contradicting reports exist in the literature regarding the role and respective activity of Co^{II} and Co^{III} catalysts for the copolymerization of epoxides and carbon dioxide.[54–57] In some cases, complete loss of activity upon reduction to Co^{II} is reported whereas in other cases, activities remain in the same order of magnitude for the Co^{II} and Co^{III} species.[42–44,55,56] The increased Lewis acidity of Co^{III} is generally advantageous for copolymerization; it facilitates epoxide activation and ring opening and concomitantly suppresses the undesired dissociation of the growing polymer chain from the metal and subsequent back-biting. The tendency of Co^{III} to be reduced to Co^{II} is detrimental, especially during the copolymerization, since it changes the electronics and therefore the carefully designed characteristics of the catalyst. Accordingly, a loss or decisive drop in activity is observed.

We were interested in designing a Co^{II} catalyst system for the copolymerization of carbon dioxide and epoxides based on the work of Kozak et al. that circumvents in situ degradation of the active species. We were curious to see if amine-bis(phenolato)cobalt(II) catalysts, in particular, can be modified and subsequently used for copolymerization of CO_2 and epoxides.

Results and Discussion

Substituted amine-bis(phenolate) ($LigH^1$–$LigH^4$) compounds were prepared by modified literature procedures employing Mannich condensation of the corresponding amine, phenol and formaldehyde in a one pot reaction with water or methanol as solvent (Scheme 1).[58,59]

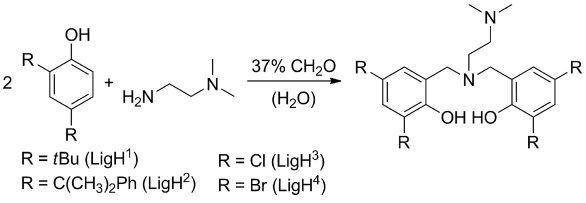

Scheme 1. Synthesis of amine-bis(phenolate) ligands $LigH^1$–$LigH^4$.

Co^{II} complexes were prepared by reacting 2.2 equiv. of potassium hydroxide with the respective ligand in a methanol/toluene solution (1:1) followed by addition of cobalt acetate. After refluxing for 18 h under an inert atmosphere purple solids were formed and catalysts **2**–**4** were isolated following recrystallization. Catalyst **1** was synthesized according to a previously published procedure (Figure 1).[47]

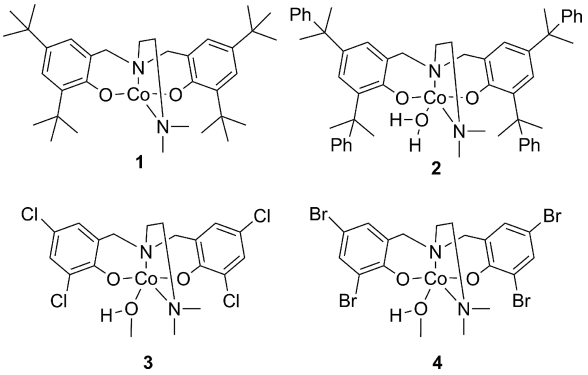

Figure 1. Structure of amine-bis(phenolato)cobalt(II) complexes **1**–**4**.

Crystallography

Recrystallization from hexane (catalyst **2**) or methanol (catalysts **3**, **4**) yields purple crystals, suitable for single-crystal X-ray diffraction studies. The molecular structures and selected bond lengths of catalysts **2**·H_2O, **3**·MeOH and **4**·MeOH are shown in Figures 2, 3 and 4 and are given in Table 1. (For more detailed information see Supporting Information.) An equatorial plane is formed by the Co^{II} ion, two phenolate oxygens O(2) and O(3) and a dimethylamino donor N(1) in all presented crystal structures. The

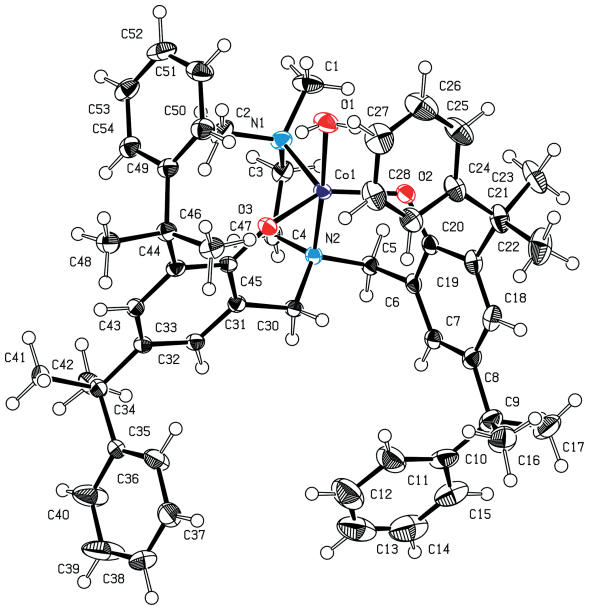

Figure 2. ORTEP view of the molecular structure of catalyst **2** with 50% thermal ellipsoid probability. Selected bond lengths [Å] and angles [°]: Co1–O1 2.1538(11), Co1–O2 1.9607(10), Co1–O3 1.9563(9), Co1–N1 2.1199(12), Co1–N2 2.1262(11), O1–Co1–O2 89.26(5), O1–Co1–O3 86.33(4), O2–Co1–O3 130.66(4), O1–Co1–N1 92.78(5), O1–Co1–N2 175.61(5), O2–Co1–N1 118.23(4), O3–Co1–N1 111.06(4), O2–Co1–N2 94.10(4), O3–Co1–N2 93.61(4), N1–Co1–N2 83.13(4).

nitrogen donor N(2) of the ligand backbone and the oxygen of the water molecule O(1) (or methanol molecule, respectively) are located in apical positions. Therefore, these complexes exhibit a distorted trigonal bipyramidal coordination sphere. Regarding the Co(1)–O(2) or Co(1)–O(3) distances, there is an observable difference between complex **2** and complexes **3** and **4**. Shorter Co(1)–O(2) bonds of 1.9345 Å (complex **3**) and 1.9364 Å (complex **4**) are observed for the bromo- or chloro-substituted complexes compared to a Co(1)–O(2) distance of 1.9607 Å of complex **2** with a cumyl substituent in the ligand backbone (Table 1).

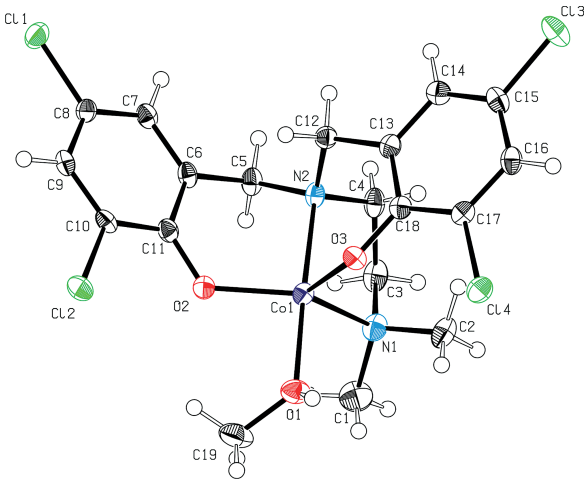

Figure 3. ORTEP view of the molecular structure of catalyst **3** with 50% thermal ellipsoid probability. Solvent molecule (MeOH) is refined for clarity. Selected bond lengths [Å] and angles [°]: Co1–O1 2.0946(11), Co1–O2 1.9345(10), Co1–O3 1.9446(10), Co1–N1 2.1129(13), Co1–N2 2.1965(12), O1–Co1–O2 90.34(4), O1–Co1–O3 91.44(4), O2–Co1–O3 121.77(4), O1–Co1–N1 93.80(5), O1–Co1–N2 175.92(5), O2–Co1–N1 129.82(5), O3–Co1–N1 108.11(4), O3–Co1–N2 90.80(4), O2–Co1–N2 91.37(4), N1–Co1–N2 82.26(5).

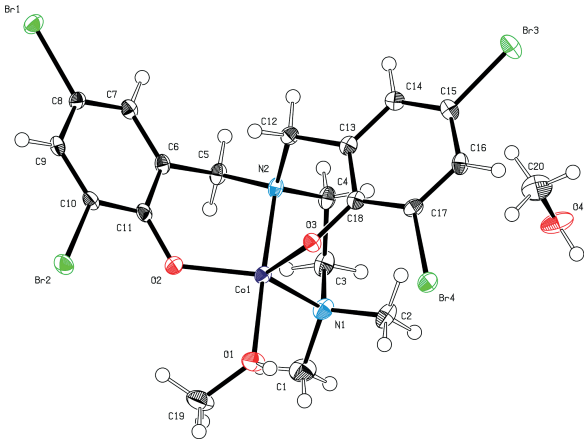

Figure 4. ORTEP view of the molecular structure of catalyst **4** with 50% thermal ellipsoid probability. Selected bond lengths [Å] and angles [°]: Co1–O1 2.0980(15), Co1–O2 1.9364(14), Co1–O3 1.9485(14), Co1–N1 2.1134(17), Co1–N2 2.2002(16), O1–Co1–O2 90.26(6), O1–Co1–O3 91.96(6), O2–Co1–O3 121.40(6), O1–Co1–N1 93.87(6), O1–Co1–N2 175.67(6), O2–Co1–N1 129.31(6), O3–Co1–N1 108.93(6), O3–Co1–N2 90.71(6), O2–Co1–N2 91.25(6), N1–Co1–N2 82.04(6).

Table 1. Selected bond lengths [Å] for **2**, **3** and 4.

Entry	Complex	Co1–O1	Co1–O2	Co1–O3
1	**2**·H_2O	2.1538(11)	1.9607(10)	1.9563(9)
2	**3**·MeOH	2.0947(11)	1.9345(10)	1.9449(10)
3	**4**·MeOH	2.0980(15)	1.9364(14)	1.9485(14)

Coupling Reactions of CO_2 and Epoxides

Catalysts **1**–**4** were employed in coupling reactions of carbon dioxide and propylene oxide under various reaction conditions (Table 2). Catalyst **1** was developed in the group of Kozak et al. and preliminary tests of the coupling of CO_2 and propylene oxide were conducted.[44] Due to the purification via crystallization, complex **2** was only used as **2**·H_2O, and complexes **3** and **4** were employed as **3**·MeOH/**3**·Acetone and **4**·MeOH species. Since tetrabutylammonium halides are claimed to be catalysts for the formation of cyclic carbonates from CO_2 and epoxides, an experiment was conducted using only TBAB.[24] Neither TBAB, nor catalyst **1**, by themselves, enabled formation of cyclic carbonates, polyethers or polycarbonates at 60 °C and 30 bar. Catalyst **1** and TBAB were found to be active in coupling of PO and CO_2 and were used to screen for optimal pressure, temperature and co-catalyst. The CO_2 pressure was varied from 10 to 40 bar at 60 °C ([Cat]:[CoCat] = 1:1). The results of these trials revealed an independence of the reaction velocity from CO_2 pressure within the tested pressure range (Table 2). This suggest that the rate-determining step during the reaction is not the insertion of CO_2, but rather, the coordination and ring opening of the epoxide, as is consistent with literature.[34,55,60] Reaction temperatures evaluated ranged from room temperature up to 80 °C (30 bar, [Cat]:[CoCat] = 1:1). With elevated temperatures the production of cyclic propylene carbonate (cPC) increased in

Table 2. Optimization of reaction temperature, pressure and co-catalyst to catalyst ratio for formation of cyclic propylene carbonate.[a]

Entry	Catalyst	*T* [°C]	p(CO_2) [bar]	TBAB/cat	TON[b]	Yield [%][c]
1	**1**	60	10	1	485	20
2	**1**	60	20	1	520	25
3	**1**	60	30	1	500	20
4	**1**	60	40	1	510	20
5	**1**	25	30	1	130	5
6	**1**	40	30	1	340	15
7	**1**	80	30	1	620	30
8	**1**	60	30	0.5	415	20
9	**1**	60	30	2	630	30
10	**3**·MeOH	60	30	1	1400	60
11	**3**·MeOH	80	30	1	2060	85
12	**4**·MeOH	80	30	1	2050	85

[a] Reaction conditions: cat/PO = 1:2150, cobalt catalyst (0.03 mmol), TBAB (0.03 mmol), 18 h, 5 mL of PO (neat). [b] Mol of propylene carbonate produced per mol cobalt complex. [c] Yields determined on basis of mass.

an approximately linear fashion as was expected and has previously been observed for salen systems.[37,61] Additionally, the co-catalyst ratio was varied from 0.5 to 2 equiv. at 60 °C and 30 bar (Table 2, Entries 3, 8, 9). Again, an approximately linear dependence between turn over number (TON) and co-catalyst ratio was observed. The highest TON of 2060 for the formation of cPC was obtained with catalyst **3**·MeOH and TBAB at 80 °C and 30 bar (Table 2, Entry 11). The high activity of complex **3** relative to the other catalysts can be explained by the electron-withdrawing property of the chloro substituents. The Lewis acidity of the cobalt center is increased and, therefore, the propylene oxide is coordinated more strongly to the metal center. Similar activities could be observed utilizing complex **4**. Kleij et al. observed the same trend for chloro substituents on amino-*tris*(phenolato)aluminum complexes with respect to cyclic carbonate formation.[30]

In an in situ ATR IR, which can be applied for continuous monitoring experiments using IR spectroscopy and an attenuated total reflectance probe, the decrease of the stretching carbonyl vibration of carbon dioxide at 2350 cm^{-1} and the increase of the carbonyl vibration of cyclic carbonate at 1797 cm^{-1} was monitored during the reaction of CO_2 and propylene oxide for all four catalysts **1**–**4**. The initial linear slope of each curve obtained with catalyst **1**–**4** at 60 °C, 30 bar and using a 1:1 co-catalyst to catalyst ratio was measured (Figure 5). Notably, catalyst **3** exhibited the highest activity ($v_{obs'}$ = 0.83 h^{-1}), whereas catalyst **2** displayed the lowest activity ($v_{obs'}$ = 0.15 h^{-1}).

This increase can be attributed to the positive influence of electron-withdrawing groups in *ortho*- and *para*-positions of the ligands. The comparison of chloro- and bromo-substituted complexes **3** and **4** reveals no significant difference in activity as was expected (R = Cl, $v_{obs'}$ = 0.83 h^{-1}; R = Br, $v_{obs'}$ = 0.81 h^{-1}). This is likely attributable to the similarity of the chloride and bromide moieties.

The main focus of this work was to develop enhanced synthesis of polycarbonates with amine-bis(phenolato)cobalt(II) catalysts. Therefore, reaction variables such as temperature, pressure and nature of the co-catalyst were evaluated. Some experiments were performed with DMAP as the co-catalyst instead of TBAB (Table 3, Entries 6, 7). The use of DMAP and catalyst **1** or **3**·MeOH failed to afford poly(propylene carbonate) (PPC), polyether or the cyclic product. However, reactions at 50 bar CO_2, 80 °C, cat/PO = 1:500 with TBAB as co-catalyst afforded cPC in 90–95% yield (Table 3, Entries 8, 9), but no polycarbonate. Under these conditions neither catalyst **1** nor catalyst **3**·MeOH with TBAB or DMAP as co-catalyst were able to produce PPC.

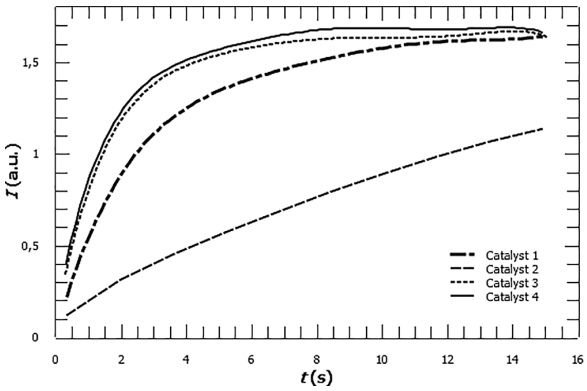

Figure 5. Intensity progress of the carbonyl vibration band of cyclic propylene carbonate at 1797 cm^{-1} against time in the ATR-IR. Reaction conditions: p(CO_2) = 30 bar, 60 °C, cat/PO = 1:2150, cobalt catalyst (0.03 mmol), TBAB (0.03 mmol), 5 mL of PO (neat). Determination of the initial slopes for catalyst **1**–**4**: $v_{obs'}$: 0.50 h^{-1} (catalyst **1**), 0.15 h^{-1} (catalyst **2**·H_2O), 0.83 h^{-1} (catalyst **3**·MeOH), 0.81 h^{-1} (catalyst **4**·MeOH).

The inability of catalysts **1**–**4**·MeOH to polymerize propylene oxide and carbon dioxide led us to cyclohexene oxide as a viable alternative for use in further investigating the capabilities of the Co^{II}-catalyst system. The reason behind the switch of monomer, from propylene oxide to cyclohexene oxide, is the reluctance of CHO and carbon dioxide to form cyclic carbonates. The depolymerization (back-biting) is several orders of magnitude slower for poly(cyclohexene

Table 3. CO_2 coupling reactions with cyclohexene oxide and propylene oxide.[a].

Entry	Catalyst	Co-catalyst	[cat]/[cocat]/[epoxide]	Epoxide	Product	Polycarbonate/cyclic carbonate/ether linkages [%]	TON[b]	Yield [%][c]	M_n [g/mol][d]	PDI[d]
1	**3**·MeOH	DMAP	1:1:500	CHO	PCHC	99:1:0	120	25	4000	1.48
2	**3**·MeOH	DMAP	1:3:500	CHO	PCHC	96:4:0	95	20	1600[e]	1.49[e]
3	**1**	DMAP	1:1:500	CHO	–	–	0	0	–	–
4	**3**·MeOH	DMAP	1:1:100	CHO	PCHC	99:1:0	20	20	n.d.	n.d.
5	**3**·Acetone	DMAP	1:1:500	CHO	PCHC	97:3:0	60	13	6700	1.35
6	**3**·MeOH	DMAP	1:1:500	PO	–	–	0	0	–	–
7	**1**	DMAP	1:1:500	PO	–	–	0	0	–	–
8	**3**·MeOH	TBAB	1:1:500	PO	cPC	0:100:0	480	95	–	–
9	**1**	TBAB	1:1:500	PO	cPC	0:100:0	450	90	–	–
10	**3**·MeOH	TBAB	1:1:500	CHO	–	–	0	0	–	–
11	**1**	TBAB	1:1:500	CHO	–	–	0	0	–	–

[a] Reaction conditions: cat/epoxide = 1:500, cat/DMAP = 1, 18 h, 80 °C, 50 bar, 4 mL of epoxide (neat). [b] mol of PCHC per mol cobalt complex or mol of cyclic propylene carbonate produced per mol cobalt complex. [c] Yield determined by weight of the precipitated polymer or by weight of the produced cyclic propylene carbonate. [d] Determined by GPC, calibrated with polystyrene standard in $CHCl_3$. [e] Unprecipitated polymer was used for GPC analysis.

carbonate) (PCHC) than for PPC. Therefore, the deleterious pathway to cyclic product can be suppressed by switching from CHO to PO.[37,62,63]

We tested our catalyst systems **1** and **3**·MeOH for the copolymerization reaction of cyclohexene oxide and carbon dioxide.[56] First the adequate co-catalyst had to be found and copolymerization experiments with catalysts **1** and **3**·MeOH, in combination with TBAB were conducted. These experiments did not yield PCHC (Table 3, Entries 10, 11). However, using DMAP as co-catalyst with compound **3**·MeOH enabled copolymerization of carbon dioxide and cyclohexene oxide at 80 °C and a pressure of 50 bar whereas reference system **1** failed to generate any PCHC (Table 3, Entry 3). In this case, the Lewis acidity at the cobalt center might be too low for CHO/CO_2 copolymerization. Catalyst **3** is the first example of an amine-bis(phenolato)cobalt(II) catalyst able to produce polycarbonate through copolymerization of CO_2 and CHO. It exhibits very high selectivity for carbonate linkages (99%), a TON of 120 and provides a reaction yield of 24% (Table 3, Entry 1). GPC measurements show a monomodal M_n distribution with a narrow PDI of 1.48 (Supporting Information Figure S12). The isolated poly(cyclohexene oxide) was subjected to ^{13}C NMR analysis which revealed that the isolated polymer is atactic (Figure 6); it consists of mainly isotactic and a significant percentage of syndiotactic PCHC (Table 3, Entry 1). ESI-MS-based end-group analyses of oligomeric cyclohexene carbonate, obtained using catalyst **3**·MeOH and DMAP as the co-catalyst, (Table 3, Entry 4) revealed signals corresponding to [17 (OH) + 142 *n* (repeating unit) + 82 (C_6H_{10}) + 122 ($C_7H_{10}N_2$)] (Supporting Information Figure S6).

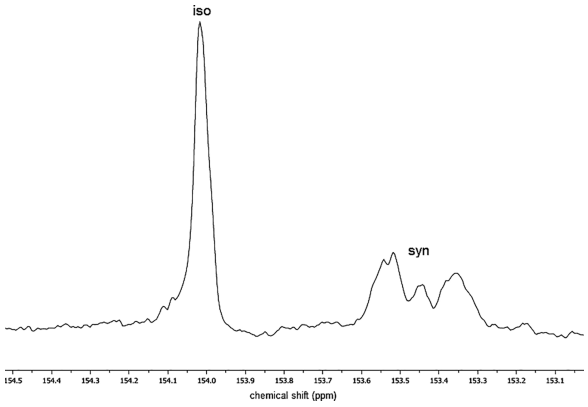

Figure 6. Carbonyl region of the ^{13}C spectrum of atactic poly(cyclohexene carbonate) prepared at 80 °C, 50 bar and DMAP as co-catalyst (Table 3, Entry 1).

MALDI-TOF analysis of the PCHC sample confirmed the ESI-MS results and gave a series consisting of [17 (OH) + 142 *n* (repeating unit) + 82 (C_6H_{10}) + 122 ($C_7H_{10}N_2$)], indicating that DMAP is the only initiating group and that no chain transfer reaction is occurring (Figure 7). ESI-MS and MALDI-TOF are very sensitive methods for detection of positive charged molecules and as the DMAP end-capped polymer chains are positively charged, the intensity of other polymer chains without a charge is probably very low compared to the charged polymer. Therefore, ^1H NMR spectroscopy and HSQC NMR spectroscopy were performed. These analyses revealed the presence of methoxy end-groups for the produced PCHC (Figure 8, Supporting Information FigureS7). The ^1H NMR spectra of isolated PCHC showed no signals corresponding to DMAP-initiated polymer chains. Therefore, we conducted an experiment with catalyst **3**·MeOH and a three-fold excess of DMAP to indirectly show the effect of DMAP on polymerization. The molecular mass of PCHC dropped significantly relative to samples prepared with only one equiv. DMAP (Table 3, Entries 1, 2), indirectly showing that DMAP can act as the initiator for copolymerization.

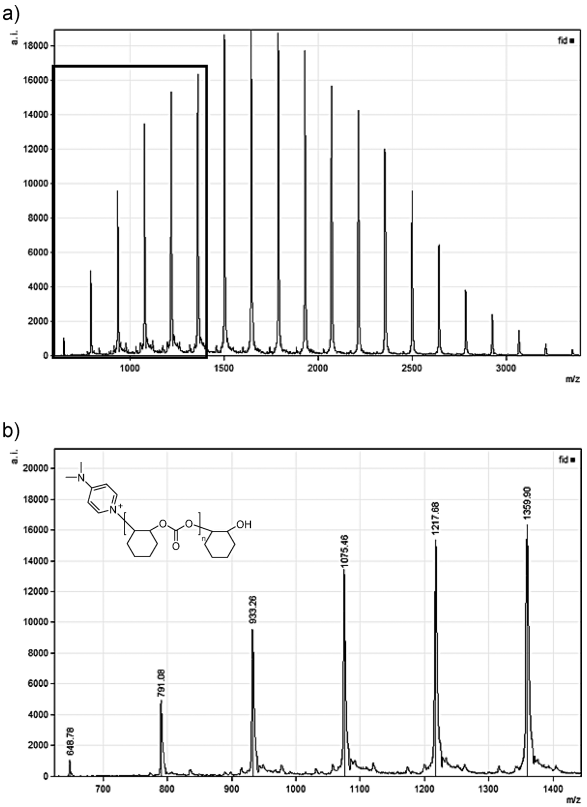

Figure 7. Top = a) MALDI-TOF MS of PCHC produced according to Table 3, Entry 1. Bottom = b) Labeled section of MALDI spectrum a (600–1400 g/mol) with modeled polymer chain containing a DMAP initiating group.

As already mentioned, complex **3**·MeOH was always isolated through crystallization meaning that two molecules of methanol were concomitantly present for every molecule of catalyst. Alcohols are known to function as chain transfer agents during catalytic copolymerizations and can influence activity, selectivity and polymer characteristics such as molecular weight and PDI.[25–28,64] Therefore, catalyst **3**·MeOH was isolated as **3**·Acetone from a saturated acetone solution and used for copolymerization.

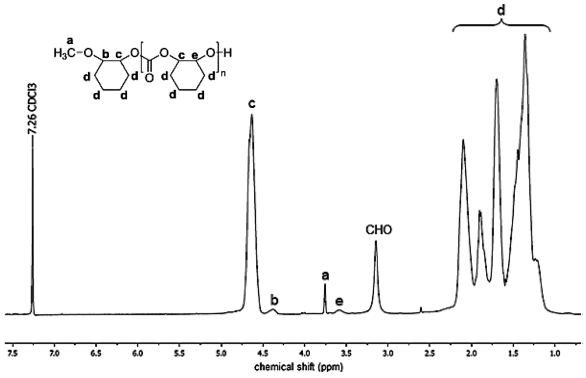

Figure 8. ^{1}H NMR of the polycarbonate catalyzed by **3**·MeOH (500 MHz, $CDCl_3$, 298 K).

The role and capabilities of methanol as a chain transfer agent in the copolymerization with **3**·MeOH should be evaluated. Catalyst **3**·Acetone proved to be active for the copolymerization of CHO/CO_2 (Table 3, Entry 5) and, as expected, produced PCHC with increased molecular weight.[25,64] Comparison of the polymer ^{1}H NMR spectra between catalyst **3**·MeOH-and **3**·Acetone-derived material showed that no methoxy end-groups are present in the case of poly(cyclohexene carbonate) produced with **3**·Acetone (Supporting Information Figure S9). MALDI-TOF analysis showed signals corresponding to a DMAP end-group [17 (OH) + 142 *n* (repeating unit) + 82 (C_6H_{10}) + 122 ($C_7H_{10}N_2$)] (Supporting Information Figure S8). Thus, the direct comparison of **3**·MeOH and **3**·Acetone in the copolymerization of CHO and carbon dioxide is in good agreement with previously described effects of chain transfer agents in copolymerization reactions.[25–27,64] Increased activity for the copolymerization with **3**·MeOH is observed compared to **3**·Acetone. Altogether the polymerization results of both catalysts are similar and show the minor influence of methanol on the copolymerization in case of **3**·MeOH.

Identifying the Active Species for Copolymerization of Carbon Dioxide and Cyclohexene Oxide

The stability of our amine-bis(phenolato)cobalt(II) catalyst system **3**·MeOH against in situ oxidation during copolymerizations was evaluated using NMR spectroscopy, ESI-MS and susceptibility measurements (Evan's method).[65,66] Following copolymerization of CHO and CO_2 with catalyst **3**·MeOH, the catalyst could be separated from the oligomer via filtration, as the solubility of the oligomer in methanol is better than that of the catalyst (Table 3, Entry 4). ^{1}H NMR spectra taken before and after reaction were paramagnetic in nature and the constant purple color of the reaction mixture indicated that the catalyst did not change its oxidation state during the polymerization; even small quantities of Co^{III} are strongly coloring (Supporting Information Figure S15). The Evan's method is an NMR technique for determining paramagnetic susceptibility of a substance in solution.[65,66] Experiments employing the Evan's NMR method to study the magnetic susceptibility of catalyst **3**·MeOH during reaction were performed to observe the catalyst oxidation behavior (detailed information are given in the Supporting Information). The oxidation of catalysts **1** and **3**·MeOH with 3 equiv. $AgNO_3$ in $CDCl_3$ at 40 °C was monitored by periodic measurements of the magnetic moment. Catalyst **1** displayed a faster rate of oxidation than did compound **3**·MeOH. The magnetic susceptibility of **1** dropped from 3.7 μ_B to 3.4 μ_B within 5 h whereas catalyst **3**·MeOH displayed a smaller decrease (4.3 μ_B to 4.2 μ_B) over the same period of time. After 24 h at 40 °C the magnetic moment of **3**·MeOH dropped significantly and reached a value of 3.5 μ_B; this was accompanied by a color change to dark brown. In contrast, complete oxidation could be observed with catalyst **1** at 40 °C after the same period of time. Hence, catalyst **3**·MeOH exhibits remarkable stability failing to undergo oxidization to Co^{III} even under forcing conditions compared to catalyst **1** (Supporting Information Table S6, S7). Further stability measurements were conducted by systematically varying conditions of the cobalt(II) catalyst **3**·MeOH; conditions such as temperature, pressure and composition of the solution were varied. Catalyst **3**·MeOH in both $CDCl_3$ and [D_2]tetrachloroethane was found to possess a solution magnetic moment of 4.3 μ_B. In the presence of one equiv. DMAP, this value was unchanged. Experiments at elevated temperatures were conducted in tetrachloroethane to allow the monitoring of the magnetic susceptibility up to those of established copolymerization conditions. Catalyst **3**·MeOH, in combination with one equiv. DMAP and an excess of CHO under argon atmosphere, showed no immediate change in its magnetic moment. Prolonged heating of the sample to 80 °C and measurements at regular intervals revealed that μ_B stayed constant at 4.3 even after 15 h. To exclude CO_2 as a possible oxidizing agent, a Young tube was charged with catalyst **3**·MeOH, co-catalyst (DMAP), cyclohexene oxide under an argon atmosphere, subsequently pressurized with 1 bar of CO_2 and heated to 80 °C. The solution magnetic moment stayed constant at 4.3 μ_B over a period of 21 h. The same experiment was conducted under an air atmosphere; under these aerobic conditions a slight change of 0.1 μ_B after 21 h was noted. Since copolymerizations are conducted at 50 bar CO_2 pressure, the stability of complex **3**·MeOH was further evaluated at 50 bar CO_2 pressure in the presence of one equiv. DMAP and an excess of CHO in tetrachloroethane. All components were charged in a suitable glass vessel, put into a standard autoclave and pressured with 50 bar CO_2. After 15 h at 80 °C the autoclave was cooled to –78 °C to avoid loss of volume, solvent or CHO, and the CO_2 was slowly released. The magnetic susceptibility of the catalyst was measured and found to have undergone no change in solution magnetic moment (4.3 μ_B). Moreoever, this post-reaction sample retained its original purple color. These experiments indicate the profound stability of catalyst **3**·MeOH against oxidation under all tested conditions and especially under copolymerization reaction conditions.

Conclusions

We investigated the formation of cyclic propylene carbonate from carbon dioxide and propylene oxide, as well as the copolymerization of carbon dioxide and cyclohexene oxide with new monometallic amine-bis(phenolato)cobalt(II) (**2**–**4**) complexes. Catalysts **2**–**4** were used with their coordinated solvent molecules in the copolymerization experiments. Nevertheless, all catalysts enabled the coupling reaction of PO and carbon dioxide to afford cPC. The dichloro-substituted catalyst **3**·MeOH achieved turnover numbers up to 2060 for the formation of cPC. Reaction parameters for the coupling of propylene oxide and CO_2, such as temperature, pressure range and catalyst to co-catalyst ratio were varied to optimize the reaction conditions (80 °C, 30 bar CO_2, [Cat]:[TBAB] = 1:1). Complexes **1** and **3**·MeOH, in combination with TBAB, did not yield any polycarbonate in copolymerization experiments with PO/CO_2 and CHO/CO_2. However, DMAP and catalyst **3**·MeOH readily copolymerized CHO and CO_2 to generate atactic, low molecular weight polycarbonates with narrow polydispersities (80 °C, 50 bar CO_2, [Cat]:[TBAB] = 1:1, PDI = 1.48). End-group analyses using ESI-MS, MALDI-TOF and NMR measurements of the produced poly(cyclohexene) carbonate unveiled DMAP and methoxy terminated polymer chains. This finding indicates that DMAP initiates the copolymerization and that, due to the presence of an excess amount of methanol, chain-transfer reactions occur. Catalyst **3**·MeOH and **3**·Acetone were used in copolymerization reactions to investigate the effect of methanol as a chain transfer agent. Increased activity and reduced molecular weight products were obtained with catalyst **3**·MeOH which can be attributed to the presence of methanol in the copolymerization. Catalyst **3** is the first example of an amine-bis(phenolato)cobalt(II) catalyst active in copolymerization reactions of CHO/CO_2. Therefore, particular attention was given to the oxidation state of cobalt in this catalyst. The nature of the active species during copolymerization was scrutinized using Evan's NMR method under various conditions; no observable oxidation of catalyst **3**·MeOH was noted under polymerization conditions. Hence, all experiments conducted with catalyst [(ONNO)^{Cl}Co^{II}]*(MeOH) indicate that the catalyst retains the Co^{II} state under polymerization conditions and that this represents the active species. Therefore, we conclude that the copolymerization of CHO and CO_2 is, in fact, catalyzed by the newly developed catalyst [(ONNO)^{Cl}Co^{II}]*(MeOH).

Experimental Section

Methods and Materials: Unless otherwise stated, all manipulations were performed under an argon atmosphere using standard Schlenk techniques or an MBraun glovebox. Chemicals were purchased from Sigma–Aldrich or Acros Organics and used without further treatment if not otherwise stated. All glassware was heat-dried under vacuum prior to use. Toluene, CH_2Cl_2, Et_2O, pentane and THF were dried applying an MBraun SPS-800 and used as received. Monomers were dried with calcium hydride and distilled prior to polymerization. NMR spectra were recorded with a Bruker AVIII-300, AVIII-500 spectrometer. ^{1}H NMR spectroscopic chemical shifts δ are reported in ppm relative to tetramethylsilane and calibrated to the residual proton signal of the deuterated solvent. Deuterated solvents were obtained from Sigma Aldrich and used as received. ESI-MS analytical measurements were performed in acetonitrile solutions with a Varian 500 MS spectrometer. Magnetic measurements in solution were performed using Evan's method with a Bruker AVIII-300 spectrometer with a coaxial insert (Wilmad).[65,66] $CDCl_3$ and $C_2D_2Cl_4$ were used as solvent and TMS as reference. In-situ IR measurements were carried out under an argon atmosphere using an ATR-IR Mettler Toledo system. IR spectra were performed with a Bruker Vertex 70 spectrometer with a Bruker Platinum ATR setup and the integrated MCT detector. MALDI-TOF mass spectrometry was carried out using a Bruker Ultraflex III, with a dithranol matrix and sodium trifluoroacetate as cationizing agent. Polymer, Matrix and sodium trifluoroacetate were dissolved at a concentration of 5 mg mL^{-1} in THF and premixed at a ratio of 1:1:1. Gel permeation chromatography (GPC) analysis was performed with a Varian PL-GPC 50 Plus at 30 °C equipped with a PLgel Olexis Column Set (300 × 7.5 mm). $CDCl_3$ (HPLC grade) was used as solvent together with tetrabutylammonium tetrafluoroborate at a flow rate of 1 mL/min and a polystryrene standard. Elemental analysis was performed at the microanalytic laboratory of the Department of Inorganic Chemistry at the Technical University of Munich.

Coupling Reaction of CO_2 and PO: All standard coupling reactions were performed in 100 mL steel autoclaves equipped with glass inlay, magnetic stirring, and oil bath heating. The autoclaves were heated to 130 °C and dried in an oven under vacuum prior to use to remove trace water. The catalyst and co-catalyst were transferred into the autoclave in the desired ratio, followed by addition of PO (5 mL). No additional solvent was used. The reactor was closed, pressurized with CO_2 and heated to the desired temperature for 18 h. After cooling down the reaction vessel to 0 °C, CO_2 was slowly released. The remaining PO was removed under vacuum and afterwards yield was determined by mass weight.

Copolymerization Procedure: All standard copolymerization experiments were performed in 100 mL steel autoclaves equipped with glass inlay, magnetic stirring, and oil bath heating. The autoclaves were heated to 130 °C and dried in an oven under vacuum prior to use to remove trace water. The catalyst and co-catalyst were transferred into the autoclave in the desired ratio, followed by addition of CHO (4.0 mL) and no additional solvent. The reactor was closed, pressurized with CO_2 and heated to 80 °C for 18 h. After cooling down the reaction vessel to 0 °C, CO_2 was slowly released. After a small sample of the crude material was removed for characterization, the product was dissolved in CH_2Cl_2, and the polymer was precipitated from methanol. The product was then dried in vacuo to constant weight.

Ligand Synthesis: A solution of the disubstituted phenol (2.00 equiv.), *N*,*N* dimethylethylenamine (1.00 equiv.) and 37% aqueous formaldehyde (2.00 equiv.) in dist. water (LigH^2) or methanol (LigH^4) was stirred and refluxed for 18 h. The mixture was cooled to room temperature and the supernatant liquid decanted. The remaining oil was recrystallized from ethanol, affording colorless crystals.

H_2[ONNO]^{CMe2Ph} (LigH^2): Yield 40%. $C_{54}H_{64}N_2O_2$ (773.11): calcd. C 83.89, H 8.34, N 3.62; found C 84.13, H 8.49, N 3.83. ^{1}H NMR (300 MHz, $CDCl_3$, 298 K): δ = 9.49 (br. s, 2 H, OH), 7.24–7.04 (m, 22 H, H_{Ar}), 6.69 (d, ^3J = 3 Hz, 2 H, H_{Ar}), 3.36 [s, 4 H, N(CH_2)$_2$], 2.27 (t, ^3J = 6 Hz, 2 H, NCH_2), 2.08 (t, ^3J = 6 Hz, 2 H,

NCH_2), 1.65 (s, 12 H, $ArCH_3$), 1.62–1.61 [m, 18 H, $ArCH_3$, $N(CH_3)_2$] ppm. ^{13}C NMR (75 MHz, $CDCl_3$, 298 K): δ = 153.42, 152.16, 151.89, 139.93, 136.13, 128.30, 127.82, 127.54, 127.21, 126.44, 125.78, 125.43, 125.05, 122.88, 56.86, 56.25, 49.13, 44.48, 42.81, 42.40, 31.28, 29.52 ppm. MS (ESI) *m/z* (%, ion): 773.7 g/mol [$[M - H]^+$].

H_2[ONNO]^{Br} (LigH^4): Yield 55%. $C_{18}H_{20}Br_4N_2O_2$ (615.98): calcd. C 35.10, H 3.27, N 4.55; found C 35.45, H 3.25, N 4.52. ^1H NMR (300 MHz, CD_2Cl_2, 298 K): δ = 7.56 (d, ^3J = 3.0 Hz, 2 H, H_{Ar}), 7.12 (d, ^3J = 3.0 Hz, 2 H, H_{Ar}), 3.63 [s, 4 H, $N(CH_2)_2$], 2.64 [s, 4 H, $N(CH_2CH_2)$], 2.36 [s, 6 H, $N(CH_3)_2$] ppm. ^{13}C NMR (75 MHz, CD_2Cl_2, 298 K): δ = 153.98, 135.37, 132.39, 125.55, 112.22, 110.75, 56.24, 56.16, 49.58, 45.06 ppm. MS (ESI) *m/z* (%, ion): 617.0 g/mol ($[M - H]^+$).

Complex Synthesis: 1.00 equiv of the ligand, 1.00 equiv cobalt-acetate-tetrahydrate and 2.20 equiv potassium hydroxide were refluxed in a mixture of dry toluene and methanol (1:1) under argon atmosphere for 18 h. After cooling to room temperature a violet solid precipitates. The solvent was removed under vacuum and the residue was solved in CH_2Cl_2. After filtration the solvent was again removed under vacuum. Once prepared these complexes are air stable. Purification was carried out through crystallization in different solvents.

Complex 2·H_2O: Violet crystals were obtained from a saturated hexane solution at room temperature, yield 25%. $C_{54}H_{64}CoN_2O_3$ (848.04): calcd. C 76.48, H 7.61, N 3.30; found C 76.68, H 7.76, N 3.36. ESI-MS: 829.9 g/mol [$M - H_2O + H]^+$. μ_{eff} ($CDCl_3$, 298 K) = 4.0 μ_B. IR (neat): $\tilde{\nu}$ = 700 (s), 765 (m), 784 (m), 804 (m), 885 (m), 936 (w), 1035 (m), 1110 (m), 1148 (w), 1203 (w), 1306 (m), 1417 (w), 1441 (m), 1461 (m), 1493 (w), 1599 (w), 2867 (w), 2963 (w), 3051 (w), 3495 (w), 3561 (w) cm^{-1}.

Complex 3·MeOH: Violet crystals were obtained from a saturated methanol solution at room temperature, yield 57%. $C_{20}H_{26}Cl_4CoN_2O_4$ (559.18): calcd. C 42.96, H 4.69, N 5.01; found C 42.66, H 4.69, N 4.94. ESI-MS: 495.3 g/mol [M – MeOH + $H]^+$. μ_{eff} ($CDCl_3$, 298 K) = 4.3 μ_B. IR (neat): $\tilde{\nu}$ = 741 (s), 864 (s), 942 (w), 1022 (m), 1034 (m), 1103 (w), 1173 (m), 1308 (m), 1369 (s), 1428 (s), 1454 (s), 1583 (w), 2846 (w), 2927 (s), 3074 (br) cm^{-1}.

Complex 4·MeOH: Violet crystals were obtained from a saturated methanol solution at room temperature, yield 47%. $C_{20}H_{26}Br_4CoN_2O_4$ (736.99): calcd. C 32.37, H 3.15, N 3.97; found C 32.69, H 3.59, N 3.78. ESI-MS: 673.1 g/mol [M – MeOH + $H]^+$. μ_{eff} ($CDCl_3$, 298 K) = 4.1 μ_B. IR (neat): $\tilde{\nu}$ = 636 (m), 699 (s), 761 (w), 778 (w), 866 (s), 940 (m), 1019 (s), 1031 (s), 1104 (w), 1154 (m), 1272 (m), 1306 (w), 1366 (m), 1432 (s), 1450 (s), 1575 (w), 2843 (w), 2926 (w), 3237 (br) cm^{-1}.

X-ray Structural Determination: The instrumental setup is given in the Supporting Information. CCDC-1018316, -1018317 and -1018318 contain the supplementary crystallographic data for this paper. These data can be obtained free of charge from The Cambridge Crystallographic Data Centre via www.ccdc.cam.ac.uk/data_request/cif.

Supporting Information (see footnote on the first page of this article): Details of the X-ray structure determination, NMR spectra of all complexes, kinetic investigations, GPC and NMR analysis of polymers, ESI-MS studies and tables of magnetic susceptibility measurements (Evan's method) are given in Supporting Information.

Acknowledgments

The authors thank Richard Reithmeier for support with the preparation of this paper, Dr. Malte Winnacker for measuring MALDI-TOF experiments and Dr. Alexander Pöthig for additional crystallographic measurements and editorial corrections.

[1] M. Cokoja, C. Bruckmeier, B. Rieger, W. A. Herrmann, F. E. Kuehn, *Angew. Chem. Int. Ed.* **2011**, *50*, 8510–8537; *Angew. Chem.* **2011**, *123*, 8662.
[2] M. Aresta, *Carbon Dioxide as Chemical Feedstock*, Wiley-VCH, Weinheim, Germany, **2010**.
[3] H. Arakawa, M. Aresta, J. N. Armor, M. A. Barteau, E. J. Beckman, A. T. Bell, J. E. Bercaw, C. Creutz, E. Dinjus, D. A. Dixon, K. Domen, D. L. DuBois, J. Eckert, E. Fujita, D. H. Gibson, W. A. Goddard, D. W. Goodman, J. Keller, G. J. Kubas, H. H. Kung, J. E. Lyons, L. E. Manzer, T. J. Marks, K. Morokuma, K. M. Nicholas, R. Periana, L. Que, J. Rostrup-Nielson, W. M. H. Sachtler, L. D. Schmidt, A. Sen, G. A. Somorjai, P. C. Stair, B. R. Stults, W. Tumas, *Chem. Rev.* **2001**, *101*, 953–996.
[4] M. Aresta, A. Dibenedetto, I. Tommasi, *Energy Fuels* **2001**, *15*, 269–273.
[5] D. J. Darensbourg, S. J. Wilson, *Green Chem.* **2012**, *14*, 2665–2671.
[6] S. Klaus, M. W. Lehenmeier, C. E. Anderson, B. Rieger, *Coord. Chem. Rev.* **2011**, *255*, 1460–1479.
[7] F. Shi, Y. Deng, T. SiMa, J. Peng, Y. Gu, B. Qiao, *Angew. Chem. Int. Ed.* **2003**, *42*, 3257–3260; *Angew. Chem.* **2003**, *115*, 3379.
[8] C.-C. Tai, M. J. Huck, E. P. McKoon, T. Woo, P. G. Jessop, *J. Org. Chem.* **2002**, *67*, 9070–9072.
[9] A. Sclafani, L. Palmisano, G. Farneti, *Chem. Commun.* **1997**, 529–530.
[10] M. R. Kember, A. Buchard, C. K. Williams, *Chem. Commun.* **2011**, *47*, 141–163.
[11] S. Inoue, H. Koinuma, T. Tsuruta, *J. Polym. Sci., Part B: Polym. Lett.* **1969**, *7*, 287–292.
[12] X.-B. Lu, D. J. Darensbourg, *Chem. Soc. Rev.* **2012**, *41*, 1462–1484.
[13] G. W. Coates, D. R. Moore, *Angew. Chem. Int. Ed.* **2004**, *43*, 6618–6639; *Angew. Chem.* **2004**, *116*, 6784.
[14] S. Fukuoka, M. Kawamura, K. Komiya, M. Tojo, H. Hachiya, K. Hasegawa, M. Aminaka, H. Okamoto, I. Fukawa, S. Konno, *Green Chem.* **2003**, *5*, 497–507.
[15] M. North, R. Pasquale, C. Young, *Green Chem.* **2010**, *12*, 1514–1539.
[16] G. Rokicki, *Prog. Polym. Sci.* **2000**, *25*, 259–342.
[17] J. H. Clements, *Ind. Eng. Chem. Res.* **2003**, *42*, 663–674.
[18] A.-A. G. Shaikh, S. Sivaram, *Chem. Rev.* **1996**, *96*, 951–976.
[19] T. Sakakura, K. Kohno, *Chem. Commun.* **2009**, 1312–1330.
[20] R. Zevenhoven, S. Eloneva, S. Teir, *Catal. Today* **2006**, *115*, 73–79.
[21] J. Bayardon, J. Holz, B. Schäffner, V. Andrushko, S. Verevkin, A. Preetz, A. Börner, *Angew. Chem. Int. Ed.* **2007**, *46*, 5971–5974; *Angew. Chem.* **2007**, *119*, 6075.
[22] M. North, M. Omedes-Pujol, *Tetrahedron Lett.* **2009**, *50*, 4452–4454.
[23] J. H. Clements, *Ind. Eng. Chem. Res.* **2003**, *42*, 663–674.
[24] G. A. Luinstra, E. Borchardt, *Polym. Rev.* **2008**, *48*, 192–219.
[25] A. Cyriac, S. H. Lee, J. K. Varghese, E. S. Park, J. H. Park, B. Y. Lee, *Macromolecules* **2010**, *43*, 7398–7401.
[26] A. Cyriac, S. H. Lee, J. K. Varghese, J. H. Park, J. Y. Jeon, S. J. Kim, B. Y. Lee, *Green Chem.* **2011**, *13*, 3469–3475.
[27] M. R. Kember, C. K. Williams, *J. Am. Chem. Soc.* **2012**, *134*, 15676–15679.
[28] K. Nakano, T. Kamada, K. Nozaki, *Angew. Chem. Int. Ed.* **2006**, *45*, 7274–7277; *Angew. Chem.* **2006**, *118*, 7432.

[29] C. Chatterjee, M. H. Chisholm, *Inorg. Chem.* **2011**, *50*, 4481–4492.
[30] C. J. Whiteoak, N. Kielland, V. Laserna, F. Castro-Gomez, E. Martin, E. C. Escudero-Adan, C. Bo, A. W. Kleij, *Chem. Eur. J.* **2014**, *20*, 2264–2275.
[31] C. J. Whiteoak, B. Gjoka, E. Martin, M. M. Belmonte, E. C. Escudero-Adan, C. Zonta, G. Licini, A. W. Kleij, *Inorg. Chem.* **2012**, *51*, 10639–10649.
[32] J. K. Min, J. E. Seong, S. J. Na, B. Y. Lee, *Angew. Chem. Int. Ed.* **2008**, *47*, 7306–7309; *Angew. Chem.* **2008**, *120*, 7416.
[33] M. North, R. Pasquale, *Angew. Chem. Int. Ed.* **2009**, *48*, 2945–2948.
[34] M. W. Lehenmeier, S. Kissling, P. T. Altenbuchner, C. Bruckmeier, P. Deglmann, A.-K. Brym, B. Rieger, *Angew. Chem. Int. Ed.* **2013**, *52*, 9821–9826; *Angew. Chem.* **2013**, *125*, 10004.
[35] C. T. Cohen, T. Chu, G. W. Coates, *J. Am. Chem. Soc.* **2005**, *127*, 10869–10878.
[36] S. Klaus, S. I. Vagin, M. W. Lehenmeier, P. Deglmann, A. K. Brym, B. Rieger, *Macromolecules* **2011**, *44*, 9508–9516.
[37] D. J. Darensbourg, J. C. Yarbrough, C. Ortiz, C. C. Fang, *J. Am. Chem. Soc.* **2003**, *125*, 7586–7591.
[38] S. D. Allen, D. R. Moore, E. B. Lobkovsky, G. W. Coates, *J. Am. Chem. Soc.* **2002**, *124*, 14284–14285.
[39] K. Soga, K. Hyakkoku, S. Ikeda, *Makromol. Chem.* **1978**, *179*, 2837–2843.
[40] X.-B. Lu, J.-H. Xiu, R. He, K. Jin, L.-M. Luo, X.-J. Feng, *Appl. Catal. A* **2004**, *275*, 73–78.
[41] M. R. Kember, F. Jutz, A. Buchard, A. J. P. White, C. K. Williams, *Chem. Sci.* **2012**, *3*, 1245–1255.
[42] M. R. Kember, A. J. P. White, C. K. Williams, *Macromolecules* **2010**, *43*, 2291–2298.
[43] L. N. Saunders, M. E. Pratt, S. E. Hann, L. N. Dawe, A. Decken, F. M. Kerton, C. M. Kozak, *Polyhedron* **2012**, *46*, 53–65.
[44] L. N. Saunders, N. Ikpo, C. F. Petten, U. K. Das, L. N. Dawe, C. M. Kozak, F. M. Kerton, *Catal. Commun.* **2012**, *18*, 165–167.
[45] R. K. Dean, K. Devaine-Pressing, L. N. Daweb, C. M. Kozak, *Dalton Trans.* **2013**, *42*, 9233–9244.
[46] R. K. Dean, S. L. Granville, L. N. Dawe, A. Decken, K. M. Hattenhauer, C. M. Kozak, *Dalton Trans.* **2010**, *39*, 548–559.
[47] U. K. Das, J. Bobak, C. Fowler, S. E. Hann, C. F. Petten, L. N. Dawe, A. Decken, F. M. Kerton, C. M. Kozak, *Dalton Trans.* **2010**, *39*, 5462–5477.
[48] R. R. Chowdhury, A. K. Crane, C. Fowler, P. Kwong, C. M. Kozak, *Chem. Commun.* **2008**, 94–96.
[49] K. Hasan, C. Fowler, P. Kwong, A. K. Crane, J. L. Collins, C. M. Kozak, *Dalton Trans.* **2008**, 2991–2998.
[50] K. Hasan, L. N. Dawe, C. M. Kozak, *Eur. J. Inorg. Chem.* **2011**, 4610–4621.
[51] S. Groysman, I. Goldberg, M. Kol, E. Genizi, Z. Goldschmidt, *Organometallics* **2003**, *22*, 3013–3015.
[52] E. Y. Tshuva, I. Goldberg, M. Kol, Z. Goldschmidt, *Organometallics* **2001**, *20*, 3017–3028.
[53] P. T. Altenbuchner, B. S. Soller, S. Kissling, T. Bachmann, A. Kronast, S. I. Vagin, B. Rieger, *Macromolecules* **2014**, *47*, 7742–7749.
[54] R. L. Paddock, Y. Hiyama, J. M. McKay, S. T. Nguyen, *Tetrahedron Lett.* **2004**, *45*, 2023–2026.
[55] D. J. Darensbourg, *Chem. Rev.* **2007**, *107*, 2388–2410.
[56] W.-M. Ren, Z.-W. Liu, Y.-Q. Wen, R. Zhang, X.-B. Lu, *J. Am. Chem. Soc.* **2009**, *131*, 11509–11518.
[57] Y. M. Shen, W. L. Duan, M. Shi, *J. Org. Chem.* **2003**, *68*, 1559–1562.
[58] A. M. Reckling, D. Martin, L. N. Dawe, A. Decken, C. M. Kozak, *J. Organomet. Chem.* **2011**, *696*, 797–794.
[59] E. Y. Tshuva, I. Goldberg, M. Kol, *Organometallics* **2001**, *20*, 3017–3028.
[60] E. N. Jacobsen, *Acc. Chem. Res.* **2000**, *33*, 421–431.
[61] D. J. Darensbourg, *Inorg. Chem.* **2010**, *49*, 10765–10780.
[62] M. W. Lehenmeier, C. Bruckmeier, S. Klaus, J. E. Dengler, P. Deglmann, A.-K. Ott, B. Rieger, *Chem. Eur. J.* **2011**, *17*, 8858–8869.
[63] Y. Xiao, Z. Wang, K. Ding, *Macromolecules* **2006**, *39*, 128–137.
[64] W. J. van Meerendonk, R. Duchateau, C. E. Koning, G.-J. M. Gruter, *Macromolecules* **2005**, *38*, 7306–7313.
[65] D. F. Evans, *J. Chem. Soc.* **1959**, 2003–2005.
[66] E. M. Schubert, *J. Chem. Educ.* **1992**, *69*, 62.

Received: November 13, 2014
Published Online: February 27, 2015

3 Synthesis of Poly(3-hydroxybutyrate) by Stereoselective Ring-Opening Polymerization of β-Butyrolactone

Poly(3-hydroxybutyrate) (PHB) is a polyester produced by bacteria as carbon and energy storage material. Natural PHB is strictly (*R*)-isotactic and has a melting point close to its decomposition temperature of 180 °C. PHB possesses young modulus, tensile strength, UV stability, and oxygen permeability comparable to isotatic polypropylene and is additionally biodegradable.[32] Therefore it has potential applications as commodity polymer e.g. as packaging material.[33] However, naturally derived PHB has major drawbacks such as low strain elongation due to its brittle nature and the aforementioned high melting point which hampers the processability.

Aside from the unfavorably high melting temperature of PHB also the currently employed synthetic pathways to obtain PHB require improvement. Biochemical fermentation has major drawbacks as it competes with food production, is expensive and lacks necessary levers to alter the polymer tacticity.[34] Homogeneous catalysis in turn offers an excellent alternative to biochemical processes as it can produce varying levels of tactic PHB through the ring-opening polymerization of β-butyrolactone (Figure 6, step 5).[35]

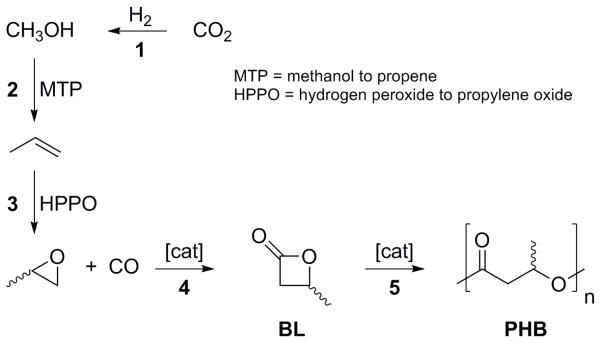

Figure 6. Synthesis of Poly(3-hydroxybutyrate) starting from carbon dioxide and hydrogen.

Biodegradable PHB synthesized by means of catalytic chemical processes offers access to a fully biobased commodity polymer (Figure 6). The separate steps can be gradually shifted from fossil based towards renewable feedstock, as renewable resources become more competitive and more available.

3.1 Catalytic Ring-Opening Polymerization of β-Butyrolactone

The production of PHB with controlled molecular weights and dispersities can proceed *via* ROP of enantiomerically pure BL or *via* the stereoselective polymerization of a racemic mixture. Enantiopure β-butyrolactone can be prepared through direct carbonylation of the corresponding enantiopure propylene oxide.[36] However, this elegant pathway is still in its infancy (Figure 6, step 4). In contrast, racemic BL is cheaper and a widely available feedstock. Stereoselective ROP provides a convenient route to a broad range of varying tacticities through the choice of a suitable initiator. The polymerization of BL can take place *via* anionic, cationic, enzymatic, organo-catalyzed, and coordination-insertion processes.[35c,37]

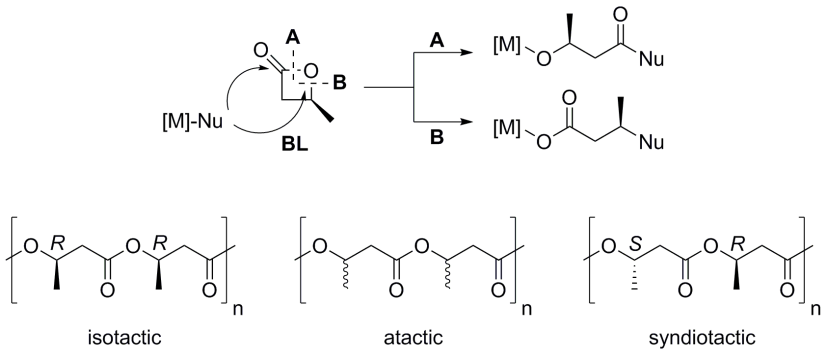

Figure 7. ROP of β-butyrolactone *via* acyl-oxygen (A), and alkyl-oxygen (B) cleavage under retention (A) and inversion (B) of the stereoconfiguration and the possible resulting PHB tacticities.

Coordination-insertion polymerization of BL may proceed *via* retention and/or inversion of the stereoconfiguration depending on the mode of ring-opening. Acyl-oxygen (A) cleavage by the attacking nucleophile leads to retention while alkyl-oxygen cleavage (B) inverses the stereoconfiguration (Figure 7). Both pathways can occur during the polymerization which limits the degree of stereocontrol. Depending on the employed initiator and polymerization conditions different side-reactions may be present during the ROP of BL. Transesterifications, chain-transfer, and multiple hydrogen transfer reactions lead to undesired chain-end functionalities (crotonate, carboxylic acid) and the loss of polymerization control.[35c] The most promising approach is through coordination-insertion polymerization *via* highly tunable homogeneous single-site catalysts. The tacticity of PHB can be determined by assessing the methyl and carbonyl region in the ^{13}C NMR spectra.[38] The resonances can be assigned at

the triad level and the degree of tacticity is given as probability of racemic linkages (P_r) or meso linkages ($P_m = 1\text{-}P_r$) between β-butyrolactone units (Figure 8).

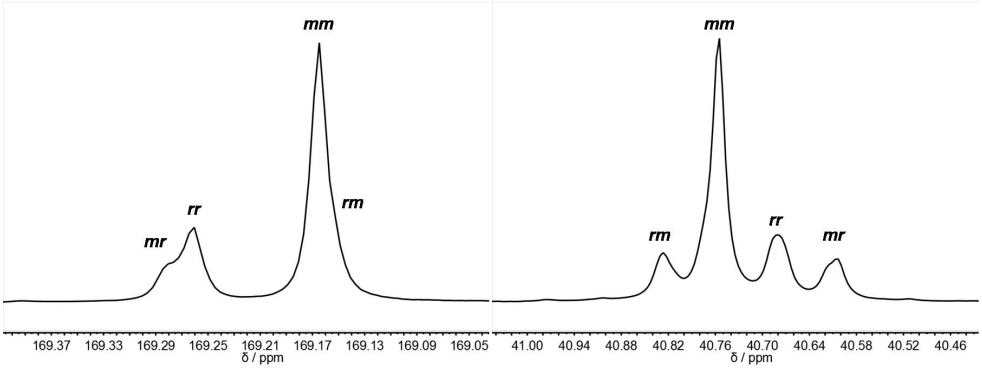

Figure 8. ^{13}C NMR of isoenriched-PHB: Carbonyl region (left) and methylene region (right).

3.2 Single-Site Catalysts for the Stereoselective ROP of BL

Homogeneous single-site catalysts for the ROP of BL have been synthesized with various metal centers and ancillary ligand systems.[35b,35c] On the path towards the development of an easily tunable, highly active and stereoselective catalyst system major progress has been made and a selection of the most important catalysts shall be presented in short.

COATES employed β-diiminate zinc alkoxide complex **7** for the controlled polymerization of BL with good rates and under mild reaction conditions.[39] Although these catalysts are able to produce tactic PLA from meso- and *rac*-lactides by a chain-end control mechanism, they only generate atactic PHB through selective acyl-cleavage.[40]

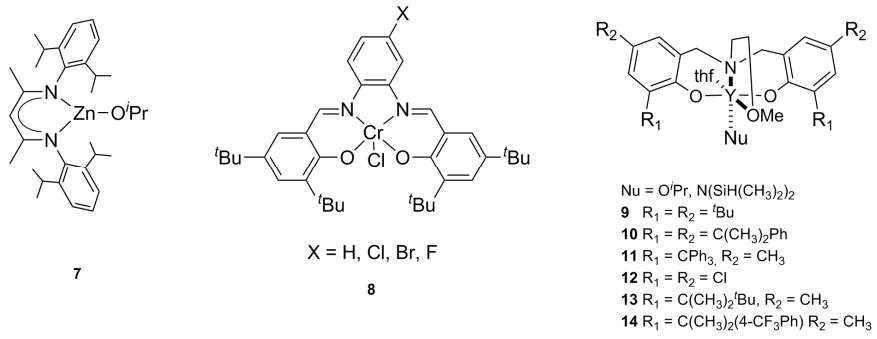

Figure 9. Selected catalysts for the ROP of *rac*-BL.

RIEGER reported on achiral chromium(III)-salophen complexes **8** as efficient initiators of the ROP of BL.[41] These catalysts exhibit fairly high activities and are able to produce isoenriched, high molecular weight PHB (P_m ~ 0.66, M_W = 780 kg/mol). Rather broad polydispersities (PDI = 5.2 – 9.6) are obtained probably due to the reluctant initiation of the chloride.

The highest stereoselectivities are so far obtained with group 3 and rare earth metal complexes (**9**-**14**).[42] The polymerization proceeds under very mild conditions, with excellent activities and productivities. The remarkable stability allows for the addition of over stoichiometric amounts of chain-transfer agent, transforming the living-type polymerization into an immortal ROP.[43] Dependencies of the tacticity on the solvent were observed. Catalyst **10** produced PHB with lower syndiotacticities in thf (P_r = 0.83) compared to toluene (P_r = 0.94) while for *rac*-LA the reverse trend is observed.[44] Highly syndiotactic PHB (P_r = 0.94) exhibits elevated melting transition temperatures of up to 183 °C which is slightly above the melting temperature of (*R*)-*i*-PHB (T_m ~ 180 °C).[38d]

Mechanistic studies of the ROP of BL with catalysts **9**-**10** revealed that the polymerization proceeds *via* acyl-oxygen cleavage and on the basis of NMR studies the authors proposed a monometallic coordination-insertion mechanism.[38d] Furthermore, *Bernoullian* analysis indicates that the syndioselectivity originates from a chain-end-control mechanism.

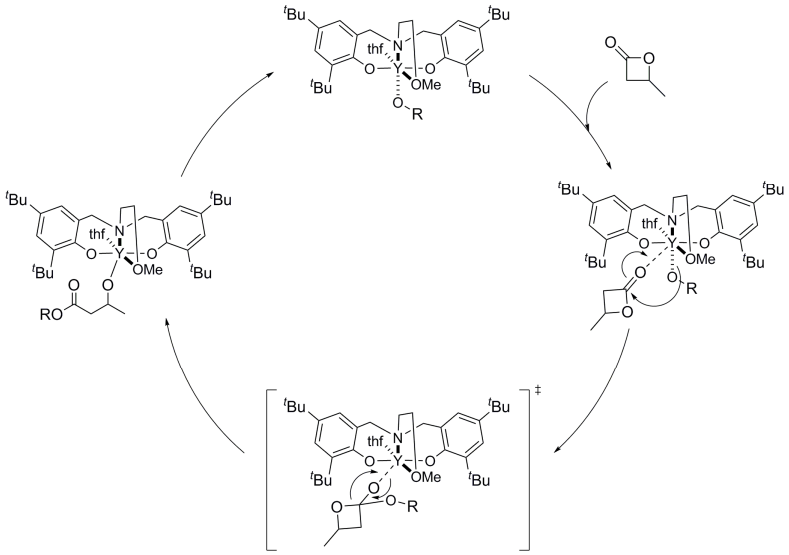

Figure 10. Proposed mechanism for the ROP of BL.[38d]

Steric and electronic alterations to the 2-methoxyethylaminobis-(phenolate)-yttrium system gave preliminary insight into correlations between increased steric crowding and activity as well as tacticity of the resulting PHB.[42b] In case of catalyst **12** the reduced steric demand in *ortho* position led to the formation of a dimer structure with drastically reduced activity and loss of stereoselectivity (P_r = 0.42; TOF < 12 h^{-1}), while catalyst **11** with its bulky trityl group gave the highest syndiotacticities (P_r = 0.94; TOF = 9400h^{-1}) and **10** exhibited the highest activities with a TOF of 22080 h^{-1} (P_r = 0.89). Recently published results for the ROP of β-malolactones reported the highest syndiotacticities with catalyst **12**.[45] Hence, no clear trend between steric crowding, electronic alteration, and tacticity could be found so far.

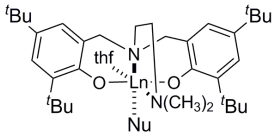

Ln = Y(**15**), Yb(**16**), Er(**17**), Sm(**18**),
Nu = alcoxide

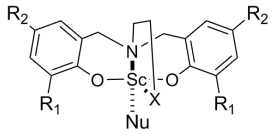

19 $R_1 = R_2 = C(CH_3)_2Ph$, X = OCH_3
20 $R_1 = C(CH_3)_2Ph$, $R_2 = CH_3$, X = OCH_3
21 $R_1 = C(CH_3)_2(p\text{-ClPh})$, $R_2 = CH_3$, X = OCH_3
22 $R_1 = C(CH_3)_2Ph$, $R_2 = CH_3$, X = $N(CH_3)_2$

Figure 11. Bis(phenolate)-lanthanide complexes.

WANG and coworkers reported about ROP of BL with bis(phenolate) catalyst structures (**15**-**18**) with varying metal ionic radii and found that the metal radius does not have an influence on the tacticity (P_r ~ 0.83) but on the activity.[42c] Higher activities were observed for smaller radii in the order of Yb > Er > Y >> Sm. Interestingly, the authors describe an inverse correlation between metal radii and activity for the polymerization of *rac*-LA. In case of Scandium bis(phenolate) systems (**19**–**22**) the small ionic radius does not allow the coordination of thf to the metal. A complete loss of activity is reported for the ROP of BL even at elevated temperatures and prolonged reaction time (60 °C, 24 h, [cat]:[BL]:[^{i}PrOH]=1:100:1).[42d] In contrast, identical Yttrium based systems are able to polymerize BL and show syndiotacticities in the range of 0.81 to 0.88.

3.3 Aim of this work: Understanding the Stereoselective ROP of β-Butyrolactone with 2-Methoxyethylaminobis-(phenolate)-metal Catalysts

The synthesis of isoenriched, and isotactic PHB from *rac*-BL has so far not been achieved although the material would have the potential to be used as commodity polymer in various applications. Highly active and stereoselective Yttrium and other rare earth metal bis(phenolate) complexes have been thoroughly investigated and a chain-end control monometallic coordination-insertion mechanism has been proposed on grounds of NMR studies and *Bernoullian* analysis.

However, in depth mechanistic understanding of the relationship between metal ionic radii, activity and tacticity are currently missing for 2-methoxyethylaminobis(phenolate)-metal catalysts. Hence, kinetic investigations and temperature dependent measurements in correlation with DFT-calculations could pinpoint possible structural motifs to tune the stereoselectivity towards isotactic PHB.

3.4 Manuscript: Mechanistic Investigations of the Stereoselective Rare Earth Metal-Mediated Ring-Opening Polymerization of β-Butyrolactone

Status	Published online: 11th August 2015
Journal	Chemistry – A European Journal
Publisher	Wiley-VCH Verlag GmbH & Co. KGaA
Article type	Full paper
DOI	DOI: 10.1002/chem.201501156
Authors	Peter T. Altenbuchner; Alexander Kronast; Stefan Kissling; Sergei I. Vagin; Eberhardt Herdtweck; Alexander Pöthig; Peter Deglmann; Robert Loos; Bernhard Rieger

Content

Nature produces poly(3-hydroxybutyrate) (PHB) only in its strictly isotactic (*R*) form, while homogeneous catalysis, when starting from racemic β-butyrolactone (BL) as monomer, can in fact produce a wide variety of tacticities through stereoselective ring-opening polymerization. The variation of the metal center and the surrounding ligand structure enable activity as well as tacticity tuning. However, to date no homogeneous catalyst exists which is easy to modify, highly active and able to attain PHB with high isotacticities from *rac*-β-BL. Therefore, in this work reaction kinetics of various 2-methoxyethylamino-*bis*(phenolate)-lanthanide (Ln = Sm, Tb, Y, Lu) catalysts are examined in detail. The order in monomer and catalyst are determined to elucidate the reaction mechanism, results are correlated with DFT calculations of the catalytic cycle. Furthermore, the enthalpies and entropies of the rate determining steps are determined through temperature dependent *in situ* IR measurements. Experimental and computational results converge in one specific mechanism for the ring opening poylmerization of BL and even allow to rationalize the preference for syndiotactic PHB.

Title:	Mechanistic Investigations of the Stereoselective Rare Earth Metal-Mediated Ring-Opening Polymerization of β-Butyrolactone
Author:	Peter T. Altenbuchner,Alexander Kronast,Stefan Kissling,Sergei I. Vagin,Eberhardt Herdtweck,Alexander Pöthig,Peter Deglmann,Robert Loos,Bernhard Rieger
Publication:	Chemistry - A European Journal
Publisher:	John Wiley and Sons
Date:	Aug 11, 2015

Order Completed

Thank you for your order.

This Agreement between Peter Altenbuchner ("You") and John Wiley and Sons ("John Wiley and Sons") consists of your license details and the terms and conditions provided by John Wiley and Sons and Copyright Clearance Center.

Your confirmation email will contain your order number for future reference.

Get the printable license.

License Number	3717760389699
License date	Sep 28, 2015
Licensed Content Publisher	John Wiley and Sons
Licensed Content Publication	Chemistry - A European Journal
Licensed Content Title	Mechanistic Investigations of the Stereoselective Rare Earth Metal-Mediated Ring-Opening Polymerization of β-Butyrolactone
Licensed Content Author	Peter T. Altenbuchner,Alexander Kronast,Stefan Kissling,Sergei I. Vagin,Eberhardt Herdtweck,Alexander Pöthig,Peter Deglmann,Robert Loos,Bernhard Rieger
Licensed Content Date	Aug 11, 2015
Licensed Content Pages	9
Type of use	Dissertation/Thesis
Requestor type	Author of this Wiley article
Format	Print and electronic
Portion	Full article
Will you be translating?	No
Title of your thesis / dissertation	Development and Application of Novel Cobalt and Rare Earth Metal Single-Site Catalysts for the Polymerization of Polar Monomers
Expected completion date	Jul 2015
Expected size (number of pages)	250
Requestor Location	Peter Altenbuchner Kolomanstr 23 Ismaning, Germany 85737 Attn: Peter Altenbuchner
Billing Type	Invoice
Billing address	Peter Altenbuchner Kolomanstr 23 Ismaning, Germany 85737

	Attn: Peter Altenbuchner
Total	0.00 EUR

ORDER MORE CLOSE WINDOW

ChemPubSoc Europe

DOI: 10.1002/chem.201501156

CHEMISTRY
A European Journal
Full Paper

Reaction Mechanisms |*Hot Paper*|

Mechanistic Investigations of the Stereoselective Rare Earth Metal-Mediated Ring-Opening Polymerization of β-Butyrolactone

Peter T. Altenbuchner,[a] Alexander Kronast,[a] Stefan Kissling,[a] Sergei I. Vagin,[a] Eberhardt Herdtweck,[b] Alexander Pöthig,[b] Peter Deglmann,[c] Robert Loos,[c] and Bernhard Rieger*[a]

Abstract: Poly(3-hydroxybutyrate) (PHB) is produced by numerous bacteria as carbon and energy reserve storage material. Whereas nature only produces PHB in its strictly isotactic (*R*) form, homogeneous catalysis, when starting from racemic (*rac*) β-butyrolactone (BL) as monomer, can in fact produce a wide variety of tacticities. The variation of the metal center and the surrounding ligand structure enable activity as well as tacticity tuning. However, no homogeneous catalyst exists to date that is easy to modify, highly active, and able to produce PHB with high isotacticities from *rac*-β-BL. Therefore, in this work, the reaction kinetics of various 2-methoxyethylamino-bis(phenolate) lanthanide (Ln = Sm, Tb, Y, Lu) catalysts are examined in detail. The order in monomer and catalyst are determined to elucidate the reaction mechanism and the results are correlated with DFT calculations of the catalytic cycle. Furthermore, the enthalpies and entropies of the rate-determining steps are determined through temperature-dependent in situ IR measurements. Experimental and computational results converge in one specific mechanism for the ring-opening polymerization of BL and even allow us to rationalize the preference for *syndiotactic* PHB.

Introduction

Poly(3-hydroxybutyrate) (PHB) is produced by numerous bacteria, for example, *Bacillus megaterium*, as carbon and energy reserve storage material.[1] Whereas nature only synthesizes PHB in its strictly isotactic (*R*) form, homogeneous catalysis is so far unable to produce isotactic PHB when starting from racemic β-butyrolactone (BL) as monomer, whereas it is able to give access to a wide variety of other tacticities.[2] The stereochemistry of the polymer chain plays a decisive role for the physical, mechanical and, most importantly, degradation properties.[3] Biodegradable, tailor-made, high precision polymers obtained through selective catalysis have the potential to answer the continuously increasing demands of industry and consumers.[4] A broad range of catalysts for the ring-opening polymerization (ROP) of lactones are known in the literature.[5] These systems range from β-diiminate zinc[6] catalysts, which mainly produce atactic PHB, to rare earth metal 2-methoxyethylamino-bis(phenolate) complexes, which are able to produce highly *syndiotactic* PHB with narrow molecular weight distributions at ambient temperature from *rac*-BL.[5a] Apart from a monometallic propagation mechanism,[6a] coordinative-anionic polymerizations may also follow a bimetallic mechanism in which one metal center activates the monomer and the other stabilizes the growing chain end. Bimetallic mechanisms are known for the copolymerization of carbon dioxide and epoxides[7] and for group-transfer polymerizations of group IV metal complexes.[8] Predictions for the mechanism at work during the ROP of lactones and its rate-determining step (RDS) are difficult and were found to strongly depend on the metal center, the ligand structure, and the monomer.[6a,9] Elaborate studies by the group of Carpentier show the influence of different electronic and steric alterations on the polymerization behavior of 2-methoxyethylamino-bis(phenolate)-yttrium systems on the tacticity and activity for the ROP of BL.[5h,i] In particular the *ortho* position within the ligand appears to have pronounced influence on the resulting tacticities also in the case of structurally related β-malolactones.[10] NMR studies with 2-methoxyethylamino-bis(phenolate)-yttrium complexes of the ring-opening polymerization of BL were able to show that the ROP proceeds through a coordination–insertion pathway under retention of the configuration at the methine carbon.[11]

However, there is so far no study that further investigates the mechanistic proceedings and the implications for the generated microstructure of 2-methoxyethylamino-bis(phenolate) complexes. An encompassing understanding of the mechanism of the highly active 2-methoxyethylamino-bis(phenolate) lanthanide catalysts might allow us to formulate predictions

[a] *P. T. Altenbuchner, A. Kronast, S. Kissling, Dr. S. I. Vagin, Prof. Dr. B. Rieger*
Technische Universität München
WACKER-Lehrstuhl für Makromolekulare Chemie
Lichtenbergstrasse 4, 85748 Garching (Germany)
E-mail: rieger@tum.de

[b] *Prof. E. Herdtweck, Dr. A. Pöthig*
Technische Universität München
Lehrstuhl für Anorganische Chemie Lichtenbergstrasse 4
85748 Garching (Germany)

[c] *Dr. P. Deglmann, Dr. R. Loos*
BASF SE, GM 67056 Ludwigshafen (Germany)

Supporting information for this article is available on the WWW under http://dx.doi.org/10.1002/chem.201501156.

concerning the stereoregularity of the ROP of BL and promote further catalyst design. Therefore, detailed experimental and theoretical investigations of the kinetic behavior of 2-methoxyethylamino-bis(phenolate) lanthanide catalysts [(ONOO)-*t*BuLn(bdsa)(thf)] (Ln = Sm, Tb, Y and Lu; bdsa = bis-dimethylsilylamide) are presented in this manuscript to elucidate the propagation mechanism and tacticity control. The presented results enable the target-oriented synthesis of new catalyst structures for the production of isotactic PHB (Scheme 1).

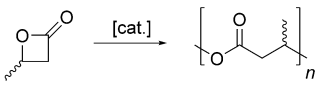

Scheme 1. Catalyzed ring-opening polymerization of *rac*-β-butyrolactone to poly(3-hydroxybutyrate).

Results and Discussion

Catalysts **1**–**4** are accessible through a straightforward synthesis from readily available compounds in good yields (Scheme 2).[12] The ligand $H_2(ONOO)^{tBu}$ is treated with one equivalent of the respective lanthanide precursor $[Ln(bdsa)_3(thf)_2]$ (bdsa = bis-dimethylsilylamide) in a mixture of pentane and toluene at ambient temperature to generate the catalysts. Recrystallization from a pentane/toluene solution afforded the catalysts with the general structure $[(ONOO)^{tBu}Ln(bdsa)(thf)]$ (Ln = Sm, Tb, Y and Lu). Instead of alkoxide initiators, bis-dimethylsilylamide was used as anionic ligand to enter into the catalytic ring-opening polymerization in our study. Nevertheless, the polymerization of β-butyrolactone proceeded in a more or less controlled fashion, resulting in PHBs with slightly broadened polydispersity indexes (PDIs; $M_w/M_n \leq 1.8$). Catalyst **3** has already been studied in previous reports for the ROP of BL and no side products such as *trans*-crotonate and carboxy groups were observed.[5i,11] Notably, this observation is also valid in the cases of catalysts **1**, **2**, and **4** and no initiation period is observed.

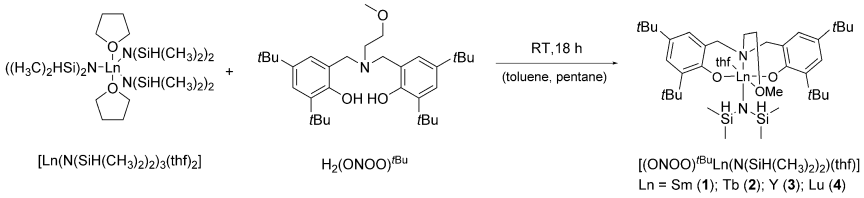

Scheme 2. General catalyst synthesis of the employed catalyst systems [(ONOO)*t*BuLn(N{SiH(CH$_3$)$_2$}$_2$)(thf)] (**1**–**4**; Ln = Sm, Tb, Y, Lu) in the kinetic studies.

The initiation mechanism was elucidated by end-group analysis of oligomeric PHB generated by treating $[(ONOO)^{tBu}Y(bdsa)(thf)]$ with 10 equivalents of *rac*-BL and monitoring the reaction by using NMR spectroscopy. The subsequent ESI-MS analysis of the sample found exclusively signals with $m^oz = nxM_{Mon} + M_{Na^+}$, where Na^+ is charge carrier. The absence of bdsa groups on the oligomers indicates that in the ESI-MS an olefinic end group is generated through elimination of bis-dimethylsilylamine (Supporting Information, Figure S9). Time-resolved ^{1}H NMR spectra however show the decreasing signal of coordinated N(SiH(CH$_3$)$_2$)$_2$, which can be monitored in relation to the increasing $C_{(Polymer)}N(SiH(CH_3)_2)_2$ signal at the oligomer chain end (Supporting Information, Figure S10).

Crystallographic data

The molecular structures of complexes **1** and **2** are depicted in Figure 1. In **1** and **2** the catalyst adopts a mononuclear structure in the solid state with a hexacoordinated metal center in an octahedral surrounding. The solid-state structures of yttrium- and lanthanum-based systems have been previously described in literature and shall be included in the discussion.[12,13] The lanthanide-O(methoxy) bond length in compound **1** (Sm(1)–O(3), 2.508(2) Å) is slightly longer than those in catalysts **2** (Tb(1)–O(3), 2.443(2 Å) and **3** (Y(1)–O(3), 2.414(2) Å)[12] and slightly shorter than that in the lanthanum complex (2.647(3) Å).[13] All other bond lengths also show this trend as result of the major influence of the effective ionic radii of the metal centers.[14] It assumed that for a chain-end control mechanism observed for the yttrium species, the bond angles of the trans-located oxygen atoms of the phenolates (O(1)-Ln(1)-O(2)) play a crucial role: La 127.39(12);[13] Sm 150.59(6); Tb 153.30(6); Y 153.97(8).[12] Together with the methyl ether and tertiary amine donor they define the reactive pocket for the ring-opening polymerization. There is less systematics in the angles between the methyl ether and the THF ligands (O(3)-Ln-(O(4)): La 167.3(1);[13] Sm 152.88(6); Tb 155.93(8)/150.9(2) [disordered, see the Supporting Information]; Y 157.09(8)[12]) and the angle of the *trans*-located N(amine) and N(amide) [N(2)-Ln-N(1): La 144.0(1);[13] Sm 163.27(7); Tb 162.31(7); Y 165.80(9)[12]].

Kinetic investigations

Kinetic investigations were conducted in steel autoclaves and the carbonyl vibration of the monomer as well as the polymer was monitored using an in situ attenuated total reflectance (ATR)-IR. The precipitation of PHB from the reaction mixture of lactone, catalyst, and polymer has to be suppressed until high conversions to allow successful measurements. Additionally, the viscosity has to be kept low. Thus, instead of toluene or tetrahydrofurane, dichloromethane was used as the solvent because of its superior solvation characteristics for *syndiotactic* PHB. As known from the literature, the solvent can have a pronounced effect on the stereoselectivity of the produced PHB, therefore polymerizations were also conducted in toluene. Generally, two mechanisms can

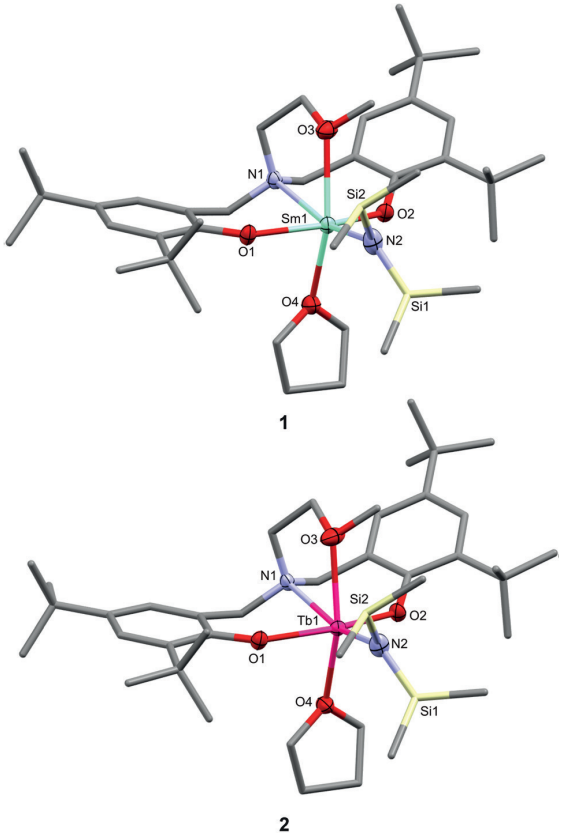

Figure 1. Molecular structures of complexes **1** and **2**.[29]

occur during the ROP of *rac*-BL: either a chain-end control or an enantiomorphic site control mechanism. Stereocontrol is defined as probability of racemic (P_r) or *meso* ($P_m = 1-P_r$) placements of monomer units in the polymer chain.[11] Catalyst [(ONOO)*t*BuY(bdsa)(thf)] in dichloromethane ($P_r = 0.82$) produced PHBs with identical *syndiotactities* as reported for toluene ($P_r = 0.81$).[5a] The catalyst systems investigated herein showed an increasing catalytic activity with decreasing ionic radius (Sm < Tb < Y < Lu; Table 1).

Within the investigated temperature range (273–308 K), a slight decrease of the syndiotacticity was observed at elevated temperatures. Interestingly, apart from the activity also the tacticity of the resulting polymer samples varied significantly. Contrary to previous studies,[15] the complexes produced increasingly *syndiotactic* PHB with decreasing radius of the metal center ($M_{(Pr(298\ K)}$: Sm (0.56); Tb (0.77); Y (0.82); Lu (0.88)). It has been previously reported for the polymerization of racemic-lactide (*rac*-LA) with bis(phenolate)-rare earth metal catalysts that increasing heteroselectivity is observed with decreasing metal ionic radius.[5h,16] The trend of increasing syndiotacticity with decreasing radius has not been described in literature for the ROP of BL. Generally, the ROP of BL exhibits diverging trends with regard to activity and tacticity as compared with lactide polymerization, which can be attributed to the size of monomer, and overall structure of LA. A more constrained geometry around the metal center induces a more pronounced selectivity towards *syndiotactic* polyester because of the smaller ionic radius. The general rate law for catalyzed polymerizations reads:

$$r = k \times [\text{Cat.}]^m \times [\text{M}]^n \quad (1)$$

Thus, for the determination of the reaction orders, first, the initial monomer concentration is kept constant to determine the order in catalyst (m). For different catalyst concentrations of otherwise identical reaction conditions, the maximum rate is consistently reached at similar conversions (< 5 %). Therefore, the residual monomer concentration is assumed to be constant. The plot of ln(r) against ln([Cat.]) yields a reaction order of $m = 1$ (Figure 2).

Consequently, rare earth-mediated ROP of β-butyrolactone follows a monometallic propagation mechanism. Furthermore the order in monomer was determined according to Equation (2):

$$r = k \times [\text{M}]^n \quad (2)$$

The reaction rate was measured for different monomer concentrations at otherwise identical conditions. Plotting ln(r) against ln([M]) gave the order in monomer $n = 1$ (Figure 3). These results show that the rare earth-mediated ROP of β-butyrolactone follows a monometallic coordination–insertion mechanism with coordination of the BL and subsequent ring opening.

Through these results, no explanation for the influence of the metal radii on the catalytic activity can be given. Hence, temperature-dependent kinetic analysis was undertaken to determine the activation enthalpies $\Delta H^{\neq}$ and entropies $\Delta S^{\neq}$ according to the Eyring Equation (3):

Table 1. ROP with catalysts of the general structure [(ONOO)*t*BuLn(N{SiH(CH$_3$)$_2$}$_2$)(thf)] (**1**–**4**).[a]

Entry	[Ln]	t [min]	Conv.[b] [%]	$M_{n,calcd}$[c] ($\times 10^3$) [g mol^{-1}]	$M_{n,exptl}$ ($\times 10^3$)[c] [g mol^{-1}]	M_w/M_n[d]	P_r[e]	TOF [h^{-1}]
1	Sm[f]	165	50	8.6	13.3	1.7	0.56	1800
2	Tb	20	40	20.7	69.7	1.8	0.77	2200
3	Y	60	89	46.0	79.6	1.8	0.82	4900
4	Lu	20	73	37.7	91.0	1.6	0.88	6900

[a] Reactions performed with M = 14.9 mmol, cat. = 20.3 μmol at 25 °C in 5 mL dichloromethane. [b] Conversions determined by ^{1}H NMR spectroscopy. [c] $M_{n,calcd}$ from $M_{n,calcd} = M \times (([M]/[Cat.]) \times \text{conversion})$ and $M_{n,exptl}$ determined by GPC in $CHCl_3$ versus polystyrene standards. [d] M_w/M_n values determined by GPC. [e] P_r is the probability of racemic linkages between monomer units and is determined by ^{13}C NMR spectroscopy. [f] Reactions performed with [M] = 14.9 mmol, [Cat.] = 60.7 μmol at 25 °C in 5 mL dichloromethane.

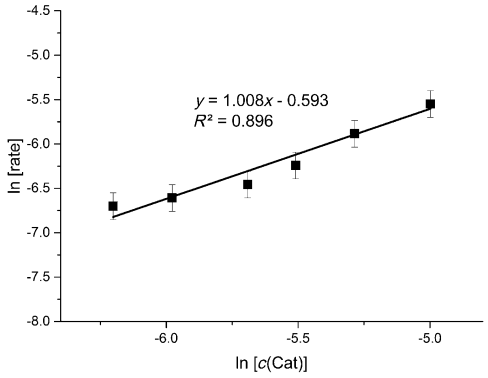

Figure 2. Order in catalyst for [(ONOO)*t*BuY(N{SiH(CH$_3$)$_2$}$_2$)(thf)] (12–41 μmol of catalyst, 14.9 mmol BL, 5 mL CH_2Cl_2 20 °C).

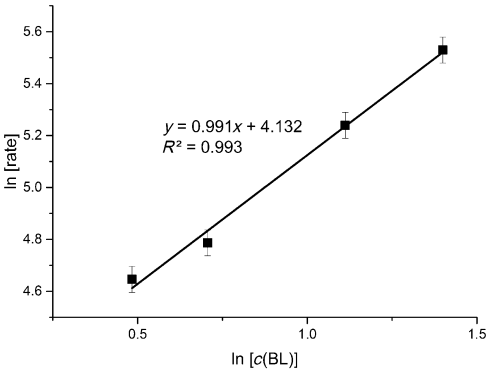

Figure 3. Order in monomer for [(ONOO)*t*BuY(N{SiH(CH$_3$)$_2$}$_2$)(thf)] (10–24 mmol of BL, 20 μmol of catalyst, 5 mL CH_2Cl_2, 20 °C).

$$\ln\frac{k}{t} = -\frac{\Delta H^{\ddagger}}{RT}\frac{1}{T} + \ln\frac{k_B}{h} + \frac{\Delta S^{\ddagger}}{R} \quad (3)$$

in which k is the rate constant, T is the temperature, R is the ideal gas constant, k_B is the Boltzmann constant, and h is the Planck constant. Plotting ln(k/T) against 1/T gives the activation enthalpy and entropy of the rate-determining step. The measurements were conducted with catalysts **1**–**4** (in order of decreasing metal ionic radius)[14] and BL as monomer.

For the ROP of BL, $\Delta H^{\ddagger}$ and $\Delta S^{\ddagger}$ are strongly affected by the ionic radius of the metal center. Thus, entropic effects such as the coordination of BL with the respective bond strength and the metallacycle ring strain as a function of the Lewis acidity contribute strongly to the activity of the respective catalyst. For the studied catalysts no linear correlation was found for $\Delta H^{\ddagger}$ and $\Delta S^{\ddagger}$ and their respective metal radius. Rather, a maximum enthalpy was determined for [(ONOO)*t*BuTb(bdsa)(thf)] together with a maximum in entropic contribution (Table 2).

The lowest enthalpy and entropy was found for [(ONOO)*t*BuLu(bdsa)(thf)] with 28 kJ mol^{-1} and −161 J K mol^{-1}, respectively. The application of the Gibbs–Helmholtz equation on the obtained enthalpies and entropies demonstrates nicely the temperature-dependent variation of $\Delta G^{\ddagger}$ (Figure 4) and highlights that at low temperatures $\Delta G^{\ddagger}$ of the Sm catalyst drops below the Tb catalyst because of the reduced importance of the entropic contribution at these conditions. This decrease will result in increased activity of **1** as compared to **2** at lower temperatures than those studied here.

Table 2. Activation enthalphy $\Delta H^{\ddagger}$ and entropy $\Delta S^{\ddagger}$ and the dependence on the ionic radius.

[Ln^{3+}], [(ONOO)*t*BuLn(N{SiH(CH$_3$)$_2$}$_2$)(thf)]	Sm	Tb	Y	Lu
ionic radius [Å]	1.219	1.180	1.159	1.117
$\Delta H^{\ddagger}$ (±5) [kJ mol^{-1}]	42	64	43	28
$-\Delta S^{\ddagger}$ (±10) [J K mol^{-1}]	122	41	107	161
$\Delta G^{\ddagger}$ [kJ mol^{-1}], 273 K	75.3	75.2	72.2	71.9

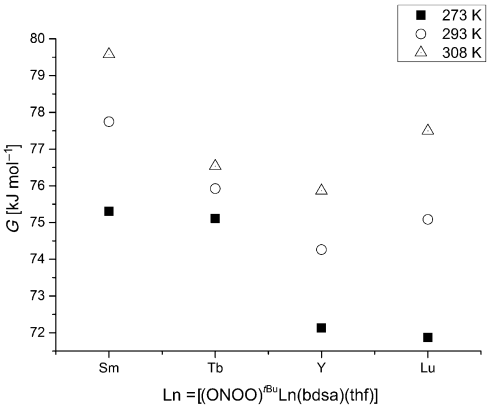

Figure 4. Gibbs free energy plotted for selected temperatures (273, 293, 308 K) for catalysts **1**–**4** (Sm, Tb, Y, Lu).

Theoretical study

Quantum chemical studies were performed to rationalize the observed rate laws, gain insight into the nature of the rate-limiting step, and to identify with this knowledge potential directions of future catalyst development.

Catalytic cycle

The postulated catalytic cycle involves (after initiation and dissociation of the rather weakly coordinated and dilute ligand THF) alkoxide species that propagate through carbonyl addition–elimination reactions, which is supported by the retention of stereochemistry observed for this type of catalysts.[5a,i,11] Computed thermodynamic functions (Gibbs free energies G and enthalpies H) of intermediates and transition states for different reactive pathways are given in Scheme 3 for yttrium as metal center. A general feature of the [Y(ONOO)*t*Bu]$^{+}$ unit is its preference for an overall coordination number of six or seven, which means that apart from the anionic polymer chain end one or two neutral donors can bind to Y. Under the conditions of catalysis, these can be either the monomer or further ester functionalities from the growing polymer chain.

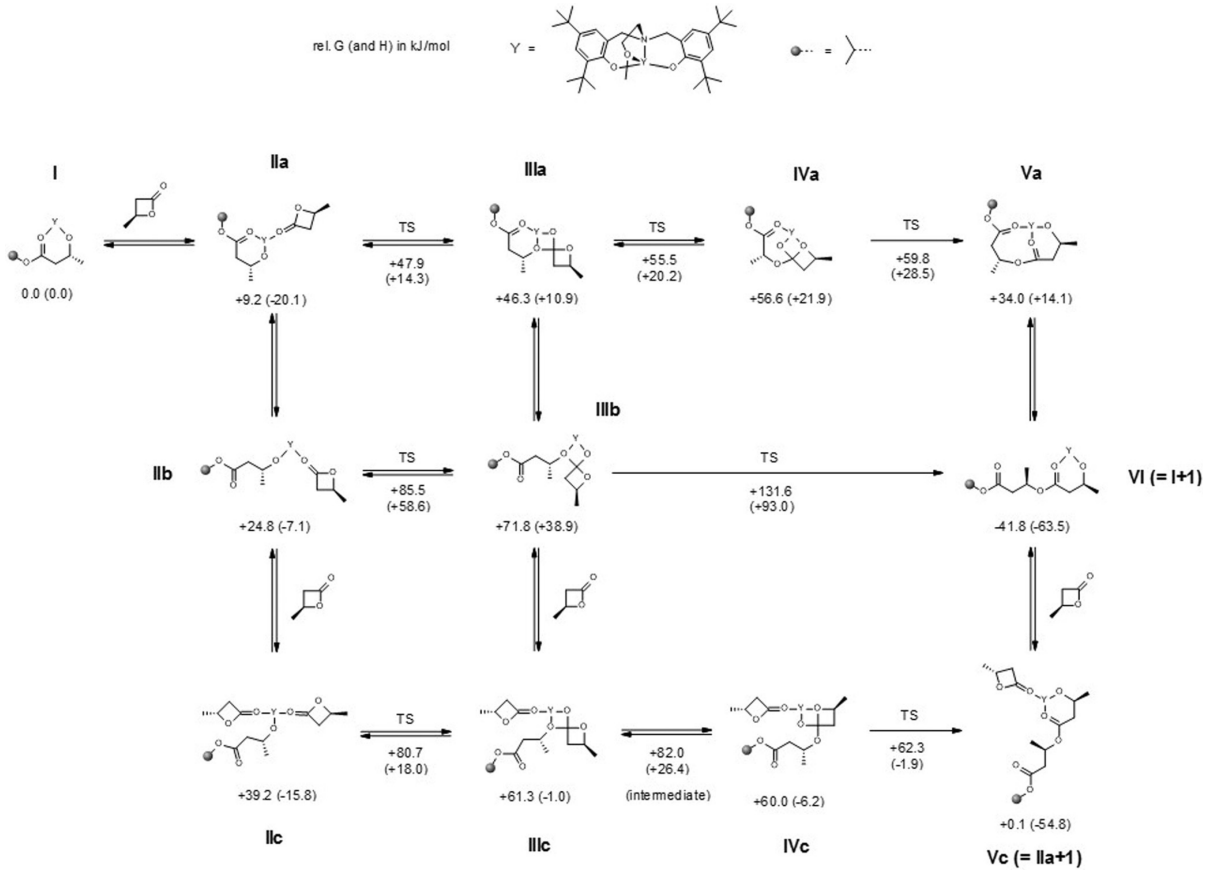

Scheme 3. Computed thermodynamic functions, that is, Gibbs free energies, *G*, and enthalpies, *H* (in brackets) for intermediates and transition states of catalytic β-butyrolactone ring opening leading to an *r*-dyad (*syndiotactic* product).

The two phenolate donors of (ONOO)*t*Bu are always more or less on opposite sides of the Y-center and are connected by the amine donor to which also the ether donor is attached. In the case of a coordination number of six, a roughly octahedral environment is found around Y in which the two further donors are necessarily *cis* with respect to each other. In the structures with sevenfold coordination, the three non-(ONOO)-*t*Bu donor sites are also arranged more or less in a row, which can be significantly distorted by the chelates resulting from multiple coordination of the polymeric chain end ligand. Generally, there seems to be a certain preference for a coordination of the anionic chain end donor opposite to N of (ONOO)*t*Bu; at least, this is the case in practically for all lowest energy isomers of the species considered in the following. However, structures with the anionic donor *cis* with respect to the amine are typically only a few kJ mol^{-1} higher in energy; a fast equilibration through the addition and dissociation of ligands between all species that are rather low in energy can be postulated due to the very similar *G* of six- and sevenfold coordination.

The catalyst resting state, that is, the species with minimal *G*, is computed to be a complex of the latter type in which the penultimate ester carbonyl O-atom coordinates to yttrium, thus the chelating polymeric ligand and the metal center form a six-membered ring (I). The addition of one monomer to this complex results in a slight decrease of *H* but in an increase of *G* for entropic reasons (**IIa**).

A further addition of monomer is only possible after a previous dissociation of the polymeric ester donor to yield a κ^1-alkoxide ligand (**IIb** and **IIc**). From these three species, propagation through addition–elimination chemistry has been considered for the case that chain end and monomer exhibit different stereochemistry at their chiral C-centers, that is, for a *syndio*-attack. The most favorable carbonyl addition step, which is in fact part of the preferred catalytic pathway, starts from the κ^2-bound polymer chain; it exhibits a relative *G* of $+49.7$ kJ mol^{-1} for TS(**IIa**→**IIIa**) and leads to a spiro-bicyclic intermediate (**IIIa**).

With a relative *G* not much lower than that of the transition state itself, it is not expected that such intermediates can be observed experimentally. A subsequent ring-opening ester elimination now requires a change in the polymeric ligand coordination mode if generation of a free alkoxide is to be avoided. This switching between neutral O-donor atoms can either occur through dissociation or as a simultaneous exchange; the

latter pathway is computed to be preferred. Ring opening of the resulting intermediate (**IVa**) yields a κ^3-coordinated polymer (**Va**), which then stabilizes itself by dissociation of the penultimate ester donor to yield the propagated resting state (**VI**). Around intermediate **IVa**, the potential energy surface is quite flat, which is reflected in the fact that the computed relative *G* of **IVa** is even minimally higher than that of the transition state generating it from **IIIa**: This unphysical result is a consequence of the fact that, as usual when performing quantum chemical studies of larger systems, the structure optimization has been performed at another level of theory than the final energy calculation (furthermore, also the zero-point vibrational energy cannot be computed for every single optimization step so that its influence is not included as well when localizing stationary points on the potential energy surface). TS(**IIIa**→**IVa**) is quite product-like and TS(**IVa**→**Va**), which represents the highest point of the catalytic cycle and thus the rate limiting step, is quite reactant-like, that is, both are very similar to **IVa** itself with respect to structure and energy. It is actually also found that all three species exhibit the very same most stable conformation: The anionic *ortho*-esterate O-donor of the polymer chain end being also here always *trans* with respect to the amine donor of the (ONOO)*t*Bu ligand and the spectator polymer chain ester O-donor always *trans* with respect to the etheric ligand O-donor. This at least suggests that TS(**IIIa**→**IVa**), **IVa**, or TS(**IVa**→**Va**) can equally serve to rationalize polymerization selectivity between *syndio*- and *iso*-attack. With its 28.5 kJ mol^{-1}, the relative *H* of **IV** as highest point on the potential energy surface is somewhat lower than the experimental activation enthalpy of 43 kJ mol^{-1}, whereas the calculated activation entropy amounts to -107 J K mol^{-1}, which is even the very same value as in the experiment (Table 2).

There are alternative catalytic pathways involving carbonyl attack of the β-butyrolactone monomer by a κ1-coordinated polymer chain, TS(**IIb**→**IIIb**) and TS(**IIc**→**IIIc**); in the latter case, a further lactone is coordinated as a spectator ligand to the metal center. However, both these transition states are significantly higher in *G* than even the highest point TS(**IVa**→**Va**) of the catalytic pathway discussed before. Although **IIIb** and **IIIc** as well as subsequent chemistry starting from them can in principle also take place through penultimate ester dissociation from **IIIa** (and if necessary β-butyrolactone coordination), such pathways can be ruled out due to the high *G* of **IIIb** and **IIIc** and the even higher *G* of TS(IIIb→Vb) [here, exchange of coordinating O-donor and C–O dissociation occur simultaneously] or the dissociative intermediate (i.e., with a κ1-coordinated polymer chain end) between **IIIc** and **IVc**.

Rationalization of stereoselectivity

Because of the aforementioned clear preference for propagation involving a κ^2-coordinated polymer chain end and just the monomer that is being attacked, Scheme 4 compares *syndio*- with *iso*-propagation only for this pathway.

As already found for the *syndio*-case, the alkoxide addition to the lactone monomer, TS(**IIa**→**IIIa**), is not the point of highest *G* within the *iso*-pathway as well. In contrast to *syndio*-propagation, it turned out that the ring-opening C–O bond dissociation step immediately connects **IIIa**(*iso*) and **Va**(*iso*), that is, exchange of neutral O-donor ligand and C–O dissocia-

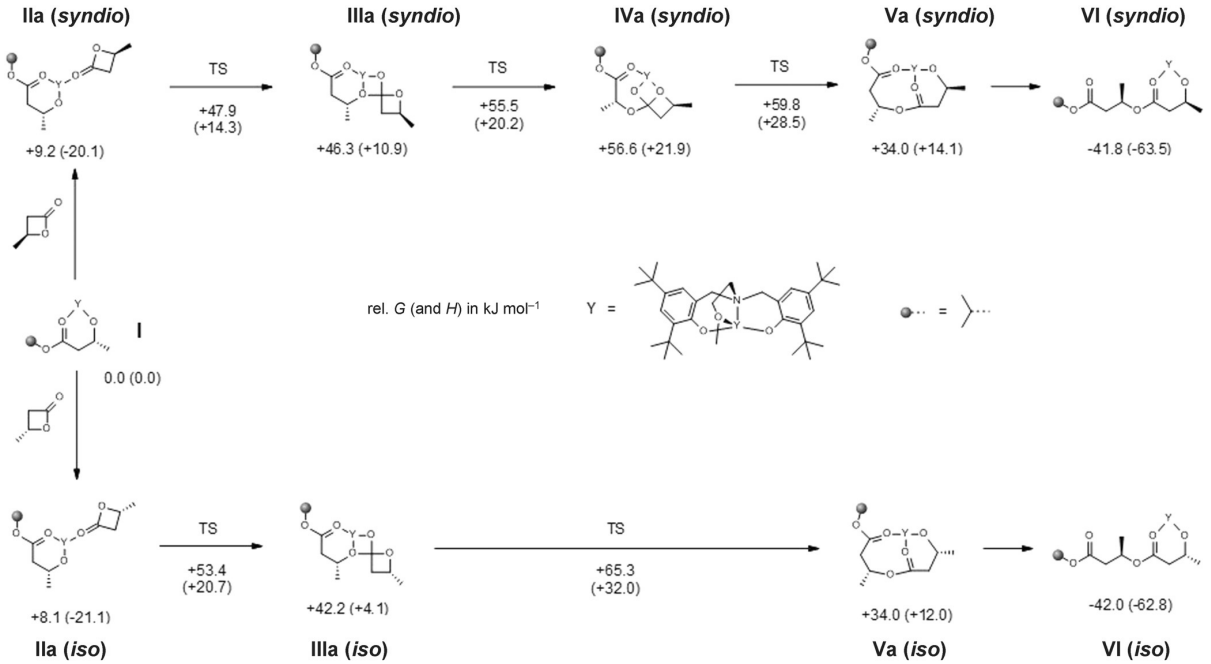

Scheme 4. Computed thermodynamic functions, that is, Gibbs free energies, *G*, and enthalpies, *H* (in brackets) for intermediates and transition states of the clearly preferred catalytic β-butyrolactone ring-opening pathway leading to either an *r*- or *m*-dyad (*syndiotactic* or *isotactic* product, respectively).

tion take place simultaneously (as was the case for TS(**IIIb**→**Vb**) upon *syndio*-propagation). The *iso*-propagation is 5.5 kJ mol^{-1} higher in *G* than that of *syndio*-propagation, which fits to the experimental preference for the latter tacticity (a P_r of around 0.9 would be concluded from this difference which is in line with the experimental P_r of 0.81). The reason that there is for the [(ONOO)*t*BuLn]-type catalysts (in contrast to, e.g., the Zn catalysts of Coates et al.),[6a] a certain extent of stereocontrol appears to be a consequence of the tridentate nature of the propagating reactive centers, as will be discussed in the following. This chain-end control can be rationalized from the transition-state structures of TS(**IVa**→**Va**)(*syndio*) and TS(**IIIa**→**Va**)(iso), given in Figure 5. As mentioned before, in TS(**IVa**→**Va**)(*syndio*), the attacked lactone moiety is located *cis* with respect to the (ONOO)*t*Bu ligand ether O-donor; it forms itself a monoanionic κ^2-ligand within which the anionic O is swapped upon C–O dissociation. Whereas the former lactone carbonyl O atom is positioned most closely to the ether, the neutral lactone O atom of **Va**(*syndio*) is located quite close to the phenolate O-donor and thus also close to its bulky *ortho*-substituent (one of the *tert*-butyl groups).

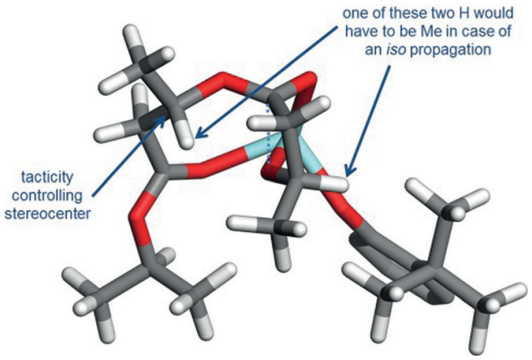

Figure 5. Detail within structure of the lowest energy conformer of the rate limiting transition state of β-butyrolactone ring opening leading to the *syndiotactic* product and rationalization why this conformation disfavors an *isotactic* lactone incorporation.

However, in the case of the *syndio*-propagation, a potential steric repulsion is minimized as the lactone methyl group points away from the *tert*-butyl group. This would not be the case for an *iso*-propagation in which either this methyl group would directly interfere with the bulky *ortho*-substituent or alternatively the penultimate ester donor would have to adopt a very unfavorable conformation as shown in Figure 5. If there would be no coordination of the penultimate ester group, the secondary C-atom stereocenter belonging to the attacking polymer chain end could adopt numerous conformations in TS(**IVa**→**Va**) [*syndio*] (methyl group and dangling polymer chain end are similar in size) so that stereocontrol would be most probably lost. As a consequence of the strong preference of κ^3-coordinated C–O dissociation transition states, the most favorable *iso*-propagation in fact proceeds through a transition state in which the tridentate reactive center has been rotated

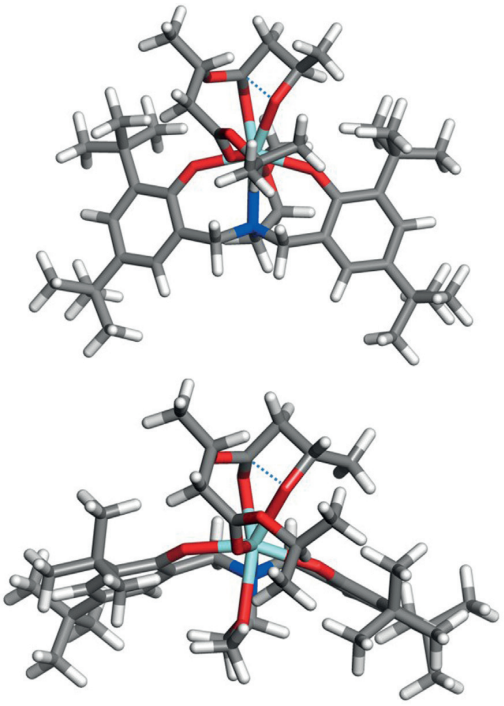

Figure 6. Structures of lowest energy conformers of the rate-limiting transition states of β-butyrolactone ring opening leading to either *syndiotactic* (top) or *isotactic* (bottom) product.

by around 180° with respect to the (ONOO)*t*Bu ligand, which reduces steric repulsion with the *tert*-butyl group (Figure 6).

Conclusion

2-Methoxyethylamino-bis(phenolate) lanthanide bisdimethylsilylamide catalysts [(ONOO)*t*BuLn(bdsa)(thf)] (Ln = Sm, Tb, Y, and Lu) have been synthesized for mechanistic investigations of the ring-opening polymerization of β-butyrolactone. Kinetic measurements supported by extensive DFT calculations revealed a monometallic coordination–insertion mechanism with coordination of the lactone and subsequent ring opening for the ROP of BL. Eyring-plot analysis for catalysts **1**–**4** explains the varying influence of temperature onto the respective activities of the catalysts. A distinct influence of the metal ionic radii on activity and stereoselectivity was observed, in which smaller radii led to increased activity as well as to higher syndiotacticity: the latter effect is most probably a result of increasing steric congestion at the catalyst center. The rationalization of the preference for *syndio*- over *iso*-propagation through DFT calculations pinpoints for the first time ligand features that are responsible for the preferred *syndiotactic* PHB production with [(ONOO)*t*BuLn(bdsa)(thf)] catalyst systems. For the investigated 2-methoxyethylamino-bis(phenolate) lanthanide system, stereocontrol is the consequence of the tridentate nature of the propagating reactive centers rooted in the strong preference of κ^3-coordinated C–O dissociation transi-

tion states. In the case of *syndio*-propagation, potential steric repulsion between the ligands *tert*-butyl group and the lactone methyl moiety is minimized and therefore energetically preferred compared to *iso*-propagation. On the basis of these results, future catalyst design with the aim to end up with *iso*-enriched poly(3-hydroxybutyrate) would most probably have to avoid κ^3-coordinated transition states (i.e., metal centers with too many free coordination sites) but at the same time be rigid enough to promote one stereospecific mode of attack through chain-end control or enantiomorphic site control.

Experimental Section

Computational methods

All calculations were performed with the program package TURBOMOLE[17] employing, where applicable, the efficient RI-J approximation.[18] Structure optimizations took place at the Becke–Perdew-86[19] (BP86) level of theory and with a def-SV(P)[20] basis set and assuming an electric conductor (dielectric constant $\varepsilon=\infty$) according to the solvation model COSMO.[21]

Thermodynamic functions were evaluated for a temperature of 20 °C. Methylene chloride was chosen as a model solvent. A solvation treatment of reaction thermodynamics was performed using the COSMO-RS method,[22] which means an explicit consideration of electrostatic effects on intermolecular interactions and can be highly beneficial for a more quantitative picture of kinetics and thermodynamics in the condensed phase.[23] This requires further calculations at the BP86 level with a def-TZVP[24] basis set, assuming both a gas and an electric conductor environment.

As DFT method for single-point energy calculations, the B3-LYP[19c,25] functional including Grimme's dispersion corrections[26] was chosen in combination with a def2-TZVP[27] basis set.

Thermodynamic functions were evaluated according to standard statistic thermodynamic expressions. However, because of the size of the species involved, this was done by only considering the lowest energy conformer of each species involved. Furthermore, because systems with 80–100 atoms typically exhibit very low energy vibrations for which a computation of the vibrational partition function within the harmonic approximation would lead to artefacts, the entropic contributions from vibrational partition functions were computed instead for small models; see the Supporting Information in which additional conformational corrections are given as well.

Instrumentation and materials

All reactions were carried under argon atmosphere using standard Schlenk or glovebox techniques. All glassware was heat dried under vacuum prior to use. Unless otherwise stated, all chemicals were purchased from Sigma–Aldrich, Acros Organics, or ABCR and used as received. Toluene, THF and pentane were dried using an MBraun SPS-800 solvent purification system. Hexane and isopropanol were dried over 3 Å molecular sieves. The precursor complexes $[Ln(bdsa)_3(thf)_2]$, ligand $H_2(ONOO)tBu$ as well as catalyst **1** and **3** were prepared according to literature procedures.[12,28] The monomer, β-butyrolactone, was dried over calcium hydride and distilled prior to use. NMR spectra were recorded on a Bruker AVIII-300 spectrometer. ^{1}H- and ^{13}C NMR spectroscopic chemical shifts δ are reported in ppm relative to the residual proton signal. δ (^{1}H) is calibrated to the residual proton signal, δ (^{13}C) to the carbon signal of the solvent. Deuterated solvents were obtained from Sigma-Aldrich and dried over 3 Å molecular sieves. Elemental analyses were measured at the Laboratory for Microanalysis at the Institute of Inorganic Chemistry at the Technische Universität München. ESI-MS analytical measurements were performed with methanol and isopropanol solutions on a Varian 500-MS spectrometer. GPC was carried out on a Polymer Laboratories GPC50 Plus chromatograph. As eluent, chloroform with 1.5 g L^{-1} tetrabutylammonium tetrafluoroborate was used. Polystyrene standards were used for calibration. In situ ATR-IR measurements were carried out using a Mettler–Toledo React-IR system under argon atmosphere.

Activity measurements and kinetic analysis

For activity measurements, the stated amount of catalyst (12–61 μmol) is dissolved in dichloromethane (5 mL), the reaction mixture is transferred into the in situ ATR-IR autoclave and the temperature is set. Then, the stated amount of monomer (10–24 mmol) is added. During the course of the experiment the temperature is kept isotherm (±2 K). After the stated reaction time, the reaction is quenched by addition of deuterated hydrous chloroform (0.5 mL) and an aliquot is taken to determine the conversion. The polymer is precipitated in excess methanol, filtered off and dried under vacuum.

Catalyst synthesis

General procedure for the synthesis of [(ONOO)*t*BuLn(bdsa)(thf)] (1–4): One equivalent of proligand $H_2(ONOO)tBu$ in toluene is added to a stirred solution of $[Ln(bdsa)_3(thf)_2]$ in pentane. The resulting solution is stirred, overnight, at room temperature. The solvent is removed in vacuo, and the resulting solid is washed with pentane. Crystallization from pentane, toluene afforded the respective complexes.

[(ONOO)*t*BuSm(bdsa)(thf)] (1): Yield: 2.7 g white powder (3.1 mmol, 70%); elemental analysis calcd (%) for $C_{41}H_{73}SmN_2O_4Si_2$: C 56.96, H 8.51, N 3.24; found: C 56.59, H 8.62, N 3.30

[(ONOO)*t*BuTb(bdsa)(thf)] (2): Yield: 2.0 g white powder (2.3 mmol, 67%); elemental analysis calcd (%) for $C_{41}H_{73}TbN_2O_4Si_2$: C 56.40, H 8.43, N 3.21; found: C 57.04, H 8.51, N 3.22

[(ONOO)*t*BuY(bdsa)(thf)] (3): Yield: 2.2 g white powder (2.7 mmol, 63%) ^{1}H NMR (298 K, 300 MHz, C_6D_6): $\delta=7.61$ (d, $^4J=2.5$ Hz, 2H), 7.10 (d, $^4J=2.3$ Hz, 2H), 5.23–5.00 (m, 2H), 3.83 (m, 6H), 3.00 (d, $^2J=12.6$ Hz, 2H), 2.84 (s, 3H), 2.70 (t, $^3J=5.5$ Hz, 2H), 2.30 (t, $^3J=5.5$ Hz, 2H), 1.79 (s, 18H), 1.47 (s, 18H), 1.16 (s, 4H), 0.50 ppm (d, $^4J=3.0$ Hz, 12H); ^{13}C NMR (298 K,75 MHz, C_6D_6): $\delta=161.63$, 136.77, 125.64, 124.35, 73.33, 71.53, 64.72, 60.69, 49.61, 35.71, 34.29, 32.31, 30.54, 25.15, 4.48 ppm; elemental analysis calcd (%) for $C_{41}H_{73}YN_2O_4Si_2$: C 61.32, H 9.16, N 3.49; found: C 61.42, H 9.17, N 3.47

[(ONOO)*t*BuLu(bdsa)(thf)] (4): Yield: 2.4 g white powder (2.7 mmol, 66%); ^{1}H NMR (298 K, 300 MHz, C_6D_6): $\delta=7.63$ (d, $^4J=2.6$ Hz, 2H), 7.08 (d, $^4J=2.6$ Hz, 2H), 5.11–5.02 (m, 2H), 3.97–3.75 (m, 6H), 2.95 (d, $^2J=12.7$ Hz, 2H), 2.83 (s, 3H), 2.74 (t, $^3J=5.5$ Hz, 2H), 2.28 (t, $^3J=5.6$ Hz, 2H), 1.80 (s, 18H), 1.47 (s, 18H), 0.51 ppm (d, $^4J=3.1$ Hz, 12H); ^{13}C NMR (298 K, 75 MHz, C_6D_6): $\delta=162.12$, 137.31, 136.72, 125.48, 124.47, 124.09, 73.74, 71.99, 64.95, 60.90, 35.71, 34.28, 32.32, 30.62, 25.16, 4.67 ppm; elemental analysis calcd (%) for $C_{41}H_{73}LuN_2O_4Si_2$: C 55.38, H 8.28, N 3.15; found: C 55.56, H 7.95, N 3.11

Acknowledgements

The authors thank the BASF SE for financial support.

Keywords: density functional calculations · kinetics · polymers · rare earths · ring-opening polymerization

[1] a) A. Rodríguez-Contreras, M. Koller, M. Miranda-de Sousa Dias, M. Calafell-Monfort, G. Brauneggk M. S. Marques-Calvo, *J. Appl. Microbiol.* **2013**, *114*, 1378 – 1387; b) A. Steinbüchel, *Macromol. Biosci.* **2001**, *1*, 1 – 24.

[2] a) M. J. L. Tschan, E. Brule, P. Haquette, C. M. Thomas, *Polym. Chem.* **2012**, *3*, 836 – 851; b) C. M. Thomas, *Chem. Soc. Rev.* **2010**, *39*, 165 – 173; c) J.-F. Carpentier, *Macromol. Rapid Commun.* **2010**, *31*, 1696 – 1705.

[3] a) B. M. Bachmann, D. Seebach, *Macromolecules* **1999**, *32*, 1777 – 1784; b) H. Abe, I. Matsubara, Y. Doi, Y. Hori, A. Yamaguchi, *Macromolecules* **1994**, *27*, 6018 – 6025; c) Y. Tabata, H. Abe, *Macromolecules* **2014**, *47*, 7354 – 7361; d) B. Wu, R. W. Lenz, T. M. Scherer, *Macromol. Chem. Phys.* **1998**, *199*, 2079 – 2085; e) H. Abe, Y. Doi, *Macromolecules* **1996**, *29*, 8683 – 8688; f) W. Amass, A. Amass, B. Tighe, *Polym. Int.* **1998**, *47*, 89 – 144; g) D. Kai, X. J. Loh, *ACS Sustainable Chem. Eng.* **2013**, *1*, 106 – 119.

[4] a) T. Iwata, *Angew. Chem. Int. Ed.* **2015**, *54*, 3210 – 3215; *Angew. Chem.* **2015**, *127*, 3254 – 3260; b) S. Mecking, *Angew. Chem. Int. Ed.* **2004**, *43*, 1078 – 1085; *Angew. Chem.* **2004**, *116*, 1096 – 1104.

[5] a) A. Amgoune, C. M. Thomas, S. Ilinca, T. Roisnel, J.-F. Carpentier, *Angew. Chem. Int. Ed.* **2006**, *45*, 2782 – 2784; *Angew. Chem.* **2006**, *118*, 2848 – 2850; b) N. Ajellal, G. Durieux, L. Delevoye, G. Tricot, C. Dujardin, C. M. Thomas, R. M. Gauvin, *Chem. Commun.* **2010**, *46*, 1032 – 1034; c) R. Reichardt, S. Vagin, R. Reithmeier, A. K. Ott, B. Rieger, *Macromolecules* **2010**, *43*, 9311 – 9317; d) J. W. Kramer, D. S. Treitler, E. W. Dunn, P. M. Castro, T. Roisnel, C. M. Thomas, G. W. Coates, *J. Am. Chem. Soc.* **2009**, *131*, 16042 – 16044; e) C. Bakewell, T.-P.-A. Cao, N. Long, X. F. Le Goff, A. Auffrant, C. K. Williams, *J. Am. Chem. Soc.* **2012**, *134*, 20577 – 20580; f) S. I. Vagin, R. Reichardt, S. Klaus, B. Rieger, *J. Am. Chem. Soc.* **2010**, *132*, 14367 – 14369; g) E. Grunova, E. Kirillov, T. Roisnel, J.-F. Carpentier, *Dalton Trans.* **2010**, *39*, 6739 – 6752; h) A. Amgoune, C. M. Thomas, T. Roisnel, J.-F. Carpentier, *Chem. Eur. J.* **2006**, *12*, 169 – 179; i) M. Bouyahyi, N. Ajellal, E. Kirillov, C. M. Thomas, J.-F. Carpentier, *Chem. Eur. J.* **2011**, *17*, 1872 – 1883; j) J. Fang, M. J. L. Tschan, T. Roisnel, X. Trivelli, R. M. Gauvin, C. M. Thomas, L. Maron, *Polym. Chem.* **2013**, *4*, 360 – 367; k) Y. Chapurina, J. Klitzke, O. d. L. Casagrande, Jr., M. Awada, V. Dorcet, E. Kirillov, J.-F. Carpentier, *Dalton Trans.* **2014**, *43*, 14322 – 14333; l) M. A. Sinenkov, G. K. Fukin, A. V. Cherkasov, N. Ajellal, T. Roisnel, F. M. Kerton, J.-F. Carpentier, A. A. Trifonov, *New J. Chem.* **2011**, *35*, 204 – 212; m) A. Sauer, A. Kapelski, C. Fliedel, S. Dagorne, M. Kol, J. Okuda, *Dalton Trans.* **2013**, *42*, 9007 – 9023; n) A. Stopper, J. Okuda, M. Kol, *Macromolecules* **2012**, *45*, 698 – 704; o) J. S. Klitzke, T. Roisnel, E. Kirillov, O. d. L. Casagrande, Jr., J.-F. Carpentier, *Organometallics* **2014**, *33*, 309 – 321; p) J. S. Klitzke, T. Roisnel, E. Kirillov, O. d. L. Casagrande, J.-F. Carpentier, *Organometallics* **2014**, *33*, 5693 – 5707.

[6] a) L. R. Rieth, D. R. Moore, E. B. Lobkovsky, G. W. Coates, *J. Am. Chem. Soc.* **2002**, *124*, 15239 – 15248; b) C. G. Jaffredo, J.-F. Carpentier, S. M. Guillaume, *Macromolecules* **2013**, *46*, 6765 – 6776.

[7] a) M. W. Lehenmeier, S. Kissling, P. T. Altenbuchner, C. Bruckmeier, P. Deglmann, A.-K. Brym, B. Rieger, *Angew. Chem. Int. Ed.* **2013**, *52*, 9821 – 9826; *Angew. Chem.* **2013**, *125*, 10004 – 10009; b) D. R. Moore, M. Cheng, E. B. Lobkovsky, G. W. Coates, *J. Am. Chem. Soc.* **2003**, *125*, 11911 – 11924; c) P. Altenbuchner, S. Kissling, B. Rieger, in *Carbon Dioxide as C-1 Block for the Synthesis of Polycarbonates* (Eds.: B. M. Bhanage, M. Araï), Springer, Berlin, **2014**, pp. 163 – 200.

[8] a) Y. Li, D. G. Ward, S. S. Reddy, S. Collins, *Macromolecules* **1997**, *30*, 1875 – 1883; b) R. Sustmann, W. Sicking, F. Bandermann, M. Ferenz, *Macromolecules* **1999**, *32*, 4204 – 4213; c) S. Salzinger, B. Rieger, *Macromol. Rapid Commun.* **2012**, *33*, 1327 – 1345.

[9] a) L. Wang, M. Bochmann, R. D. Cannon, J.-F. Carpentier, T. Roisnel, Y. Sarazin, *Eur. J. Inorg. Chem.* **2013**, 5896 – 5905; b) K. Ding, M. O. Miranda, B. Moscato-Goodpaster, N. Ajellal, L. E. Breyfogle, E. D. Hermes, C. P. Schaller, S. E. Roe, C. J. Cramer, M. A. Hillmyer, W. B. Tolman, *Macromolecules* **2012**, *45*, 5387 – 5396; c) M. P. F. Pepels, M. Bouyahyi, A. Heise, R. Duchateau, *Macromolecules* **2013**, *46*, 4324 – 4334; d) L. M. Alcazar-Roman, B. J. O'Keefe, M. A. Hillmyer, W. B. Tolman, *Dalton Trans.* **2003**, 3082 – 3087; e) H.-Y. Chen, B.-H. Huang, C.-C. Lin, *Macromolecules* **2005**, *38*, 5400 – 5405; f) J.-C. Wu, B.-H. Huang, M.-L. Hsueh, S.-L. Lai, C.-C. Lin, *Polymer* **2005**, *46*, 9784 – 9792; g) Z. Zhong, P. J. Dijkstra, J. Feijen, *J. Am. Chem. Soc.* **2003**, *125*, 11291 – 11298; h) S. M. Guillaume, L. Annunziata, I. d. Rosal, C. Iftner, L. Maron, P. W. Roesky, M. Schmid, *Polym. Chem.* **2013**, *4*, 3077 – 3087.

[10] C. G. Jaffredo, Y. Chapurina, S. M. Guillaume, J.-F. Carpentier, *Angew. Chem. Int. Ed.* **2014**, *53*, 2687 – 2691; *Angew. Chem.* **2014**, *126*, 2725 – 2729.

[11] N. Ajellal, M. Bouyahyi, A. Amgoune, C. M. Thomas, A. Bondon, I. Pillin, Y. Grohens, J.-F. Carpentier, *Macromolecules* **2009**, *42*, 987 – 993.

[12] C.-X. Cai, L. Toupet, C. W. Lehmann, J.-F. Carpentier, *J. Organomet. Chem.* **2003**, *683*, 131 – 136.

[13] C.-X. Cai, A. Amgoune, C. W. Lehmann, J.-F. Carpentier, *Chem. Commun.* **2004**, 330 – 331.

[14] A. Fr. Hollemann, E. Wiberg, in *Lehrbuch der Anorganischen Chemie (Textbook of Inorganic Chemistry,* Engl. Transl.), de Gruyter, Berlin, **2007**.

[15] K. Nie, L. Fang, Y. Yao, Y. Zhang, Q. Shen, Y. Wang, *Inorg. Chem.* **2012**, *51*, 11133 – 11143.

[16] a) C. Bakewell, A. J. P. White, N. J. Long, C. K. Williams, *Angew. Chem. Int. Ed.* **2014**, *53*, 9226 – 9230; *Angew. Chem.* **2014**, *126*, 9380 – 9384; b) A. Amgoune, C. M. Thomas, J.-F. Carpentier, *Pure Appl. Chem.* **2007**, *79*, 2013 – 2030.

[17] R. Ahlrichs, M. Bär, H. Horn, C. Kölmel, *Chem. Phys. Lett.* **1989**, *162*, 165 – 169.

[18] K. Eichkorn, O. Treutler, H. Ohm, M. Haser, R. Ahlrichs, *Chem. Phys. Lett.* **1995**, *242*, 652 – 660.

[19] a) A. D. Becke, *Phys. Rev. A* **1988**, *38*, 3098 – 3100; b) J. Perdew, *Phys. Rev. B* **1986**, *33*, 8822 – 8824; c) S. H. Vosko, L. Wilk, M. Nusair, *Can. J. Phys.* **1980**, *58*, 1200 – 1211.

[20] A. Schäfer, H. Horn, R. Ahlrichs, *J. Chem. Phys.* **1992**, *97*, 2571 – 2577.

[21] A. Klamt, G. Schüürmann, *J. Chem. Soc. Perkin Trans. 2* **1993**, 799 – 805.

[22] A. Klamt, F. Eckert, *Fluid Phase Equilib.* **2000**, *172*, 43 – 72.

[23] P. Deglmann, I. Müller, F. Becker, A. Schäfer, K.-D. Hungenberg, D. Weiß, *Macromol. React. Eng.* **2009**, *3*, 469 – 515.

[24] A. Schäfer, C. Huber, R. Ahlrichs, *J. Chem. Phys.* **1994**, *100*, 5829 – 5835.

[25] a) P. J. Stephens, F. J. Deylin, C. F. Chabalowski, M. J. Frisch, *J. Chem. Phys.* **1994**, *98*, 11623 – 11627; b) C. Lee, W. Yang, R. G. Parr, *Phys. Rev. B* **1988**, *37*, 785 – 789; c) A. D. Becke, *J. Chem. Phys.* **1993**, *98*, 5648 – 5652.

[26] S. Grimme, J. Antony, S. Ehrlich, H. Krieg, *J. Chem. Phys.* **2010**, *132*, 154104.

[27] F. Weigend, R. Ahlrichs, *Phys. Chem. Chem. Phys.* **2005**, *7*, 3297 – 3305.

[28] a) E. Y. Tshuva, S. Groysman, I. Goldberg, M. Kol, Z. Goldschmidt, *Organometallics* **2002**, *21*, 662 – 670; b) J. Eppinger, PhD Thesis, Technische Universität München, Garching bei München, **1999**; c) H. E. Dyer, S. Huijser, N. Susperregui, F. Bonnet, A. D. Schwarz, R. Duchateau, L. Maron, P. Mountford, *Organometallics* **2010**, *29*, 3602 – 3621.

[29] CCDC 1040217 (**1**) and 1040218 (**2**) contain the supplementary crystallographic data for this paper. These data are provided free of charge by The Cambridge Crystallographic Data Centre.

Received: March 24, 2015
Revised: June 2, 2015
Published online on August 11, 2015

4 Rare Earth Metal-Mediated Group Transfer Polymerization

The year 1992 marks the beginning of controlled polymerization of acrylic monomers with discrete metallocene complexes. Two independent groups simultaneously published the successful polymerization of methyl methacrylate (MMA) with narrow molecular weight distributions (PDI = 1.02 – 1.05) and high conversions to PMAA.[46] YASUDA employed neutral single-site lanthanocenes while COLLINS and coworkers utilized a two component group 4 metallocene system. Due to the mechanistic similarities to silyl ketene actetal-initiated group transfer polymerization (GTP), it is referred to as transition metal-mediated GTP.[47]

Since then, great progress has been made especially in the field of discrete lanthanide catalysts. Advances in catalyst development for the coordinative anionic polymerization of polar monomers resulted in enhanced activities and stereocontrol. Building on these developments new monomer feedstock could be unlocked, in particular the controlled polymerization of vinylphosphonates. This group of heteroatom functionalized, polar vinyl monomers posed a challenge to radical and anionic polymerization procedures and literature reports where either unsuccessful or resulted in the production of low molecular weight material concomitantly with various side products.[48]

4.1 REM-GTP of Phosphorous containing Monomers

In 2010 RIEGER reported on the first successful, controlled polymerization of diethyl vinylphoshonate (DEVP) with late lanthanide metallocenes (Cp_2YbMe, Cp_2YbCl).[49] Copolymerization studies of DEVP with the structurally and electronically related MMA pointed towards a group transfer polymerization type mechanism. However, contrary to the observed trend of polymerization activity with MMA, polymerization studies of lanthanide metallocene systems with DEVP showed increased activity with decreasing metal ionic radius.[50] The proof of mechanism for the rare earth metal-mediated (REM) polymerization of DEVP was left unanswered.

The initiation of REM-GTP can proceed *via* three different mechanisms. The strongly basic, alkyl initiators are inefficient and slow at initiating the polymerization of DEVP by deprotonation of the acidic α–CH (A).

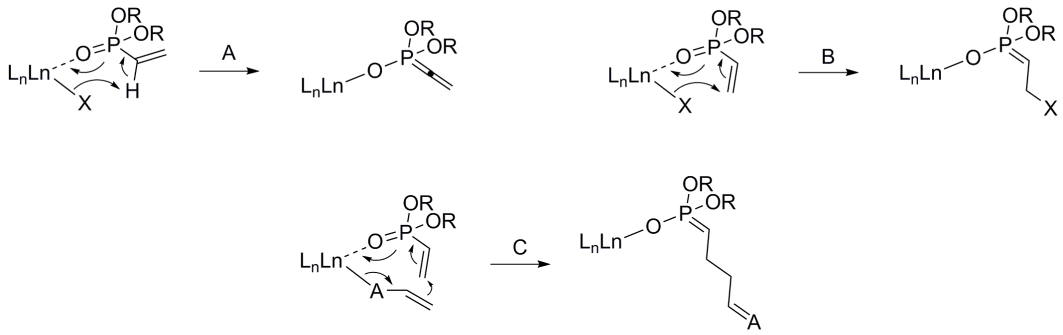

Figure 12. Possible initiation pathways (A,B and C) of REM-GTP depicted for DEVP.

Other pathways initiate *via* nucleophilic transfer of X (*e.g.* Cp or SR) to a coordinated monomer (B) or *via* monomer induced ligand-exchange processes (C). Alkoxides are employed as initiators for the ring-opening polymerization of lactones. Theoretical calculations for the initiation of MMA with isopropyl indicated an unlikely endothermic formation of a MMA isopropyloxide adduct.[51]

In 2013 an in depth study of lanthanide metallocene systems for the REM-GTP of dialkyl vinylphosphonates (DAVP) was published.[52] Determination of the monomer and catalyst order showed that also the polymerization of DAVP monomers proceeds *via* a *Yasuda*-type monometallic propagation mechanism (Figure 13).

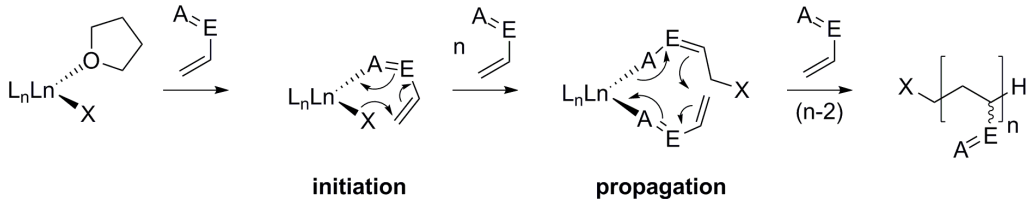

Figure 13. Yasuda-type monometallic propagation mechanism of a general *Michael*-type monomer structure *via* an initiation through nucleophilic transfer of X onto a coordinated monomer (B) (*vide supra*).

The rate determining step (RDS) was found to be a S_N2-type associative displacement of the polymer phophonate ester by an incoming monomer (Figure 14). As with the earlier described lanthanide metallocene catalysts a strong dependency of the initiator efficiency was observed in the mechanistic studies. Hence, normalization of activity by the active amount of catalyst (TOF/I*) was necessary to achieve comparability in between systems.[52] Temperature

dependent activity measurements were conducted to rationalize the observed effect of metal ionic radii (Tb, Y, Tm, Lu) and monomer size (DEVP, diisoproyl vinylphophonate (DIVP)) on the polymerization activity. Activation enthalpies $\Delta H^{\ddagger}$ and entropies $\Delta S^{\ddagger}$ were determined according to the Eyring equation. The determined enthalpic values for both monomers were not affected by the metal radius however the enthalpies showed a linear dependency. Differences in activation barriers $\Delta G^{\ddagger}$ are therefore a result of changes in the entropic term $-T\Delta S^{\ddagger}$ and were found to increase linearly with decreasing metal ionic radius. Also the polymerization activity is mainly determined by the steric demand of the growing polymer chain rather than the type of incoming monomer.

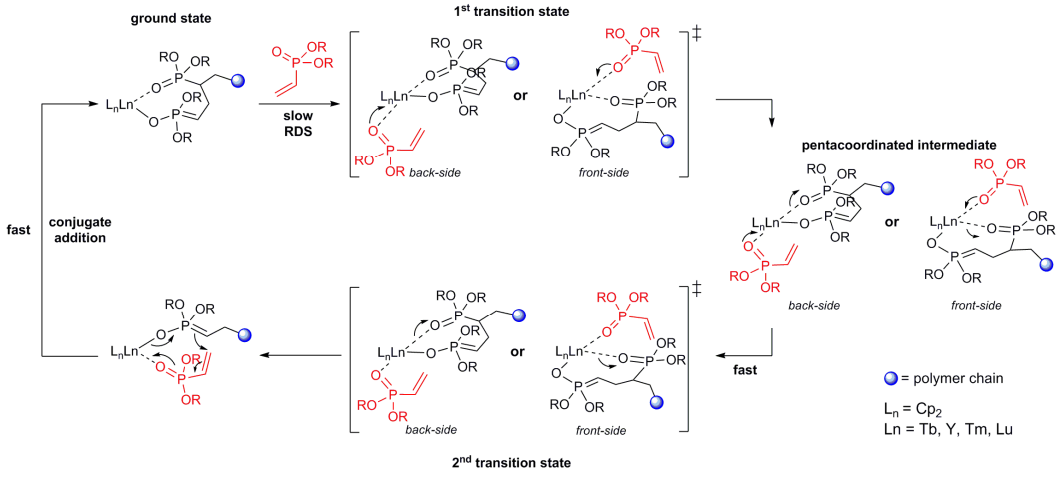

Figure 14. REM-GTP of DAVP with lanthanocene catalysts (Tb, Y, Tm, Lu): The rate-determining step (RDS) is an S_N2-type associative displacement of the polymer phosphonate ester by a vinylphosphonate monomer, presumably *via* a pentacoordinated intermediate.

Hence, the development of highly efficient initiators was a pressing necessity. Rare earth metals can form stable compounds from σ-bond metathesis and are known in literature for C-H bond activation of methane[53], internal alkynes[54], heteroaromatic substrates[55] and hydrocarbons[56,57]. Therefore, C-H bond activation through alkylyttrium mediated σ-bond metathesis depicts a promising strategy to introduce capable initiators into the catalyst structures. MASHIMA employed Yttrium catalysts in oligomerization studies and utilized the C-H bond activation of hetereoaromatics and alkynes for the introduction of functional endgroups.[58] The initiation of 2-vinylpyridine (2VP) proceeded in all cases *via* a nucleophilic transfer of the initiator (B,C, Figure 12).

Building on those oligomerization studies our group evaluated the potency of 2,4,6-trimethylpyridine as initiator for REM-GTP with $Cp_2Y(CH_2TMS)(thf)$.[59]

Polymerization experiments found the fast and complete initiation of DEVP polymerization without an initiation period which was attributed to an initiation *via* an enamide transition state similar to the propagating species.

4.2 Properties and Applications of Polyvinylphosphonates

The solubility of polyvinylphosphonates varies depending on the substitution at the ester side chain. In aqueous solutions PDEVP exhibit a lower critical solution temperature (LCST) close to the physiological range (T_{LCST} = 40 – 46 °C). LCST is the point below which and accordingly the upper critical solution temperature (UCST) is the temperature above which a polymer solution is a one phase system. Apart from the molecular weight of PDEVP also the concentration determines the characteristics of the LCST. Through random copolymerization of DEVP, dimethyl vinyphophonate (DMVP) and di-*n*-propyl vinylphosphonate (DPVP) the thermoresponsive behavior can be tuned and adjusted in the range of 5 to 92 °C by changing the feed composition.[60] Also the surface initiated GTP (SI-GTP) was investigated which allows the modification of silicon surfaces, microspheres and silicon nanocrystals with defined polymer brushes which is particularly interesting for biomedical applications (Figure 15).[61]

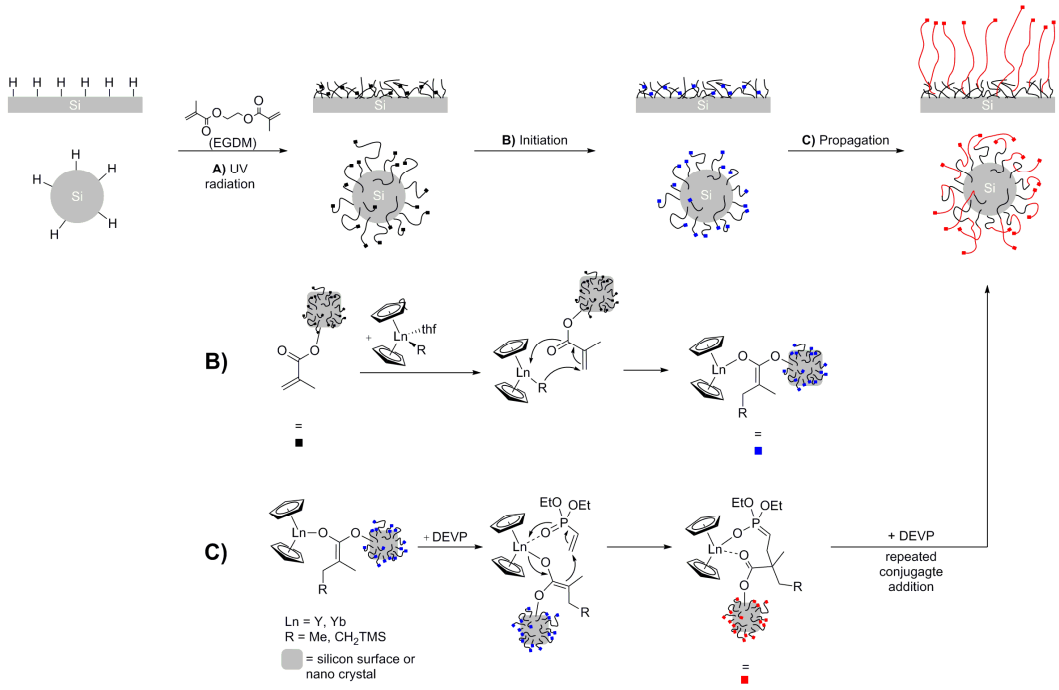

Figure 15. SI-GTP on hydrogen terminated silicon wafer or silicon nanocrystals. Synthesis of methyl methacrylate binding sites (black), initiation *via* nucleophilic attack of the alkyl ligand (blue), and propagation *via* eight-membered ring transition state (red).

4.3 Application of REM-GTP to Nitrogen-coordinating Monomers

Broadening the scope of catalysis with regard to available monomers has the potential to unlock so far unattainable material properties. The living and highly controlled group transfer polymerization with its ability to introduce an outstanding level of precision in combination with the possibility to add functional endgroups is the perfect tool to achieve functionality and precision in new polymeric homo- and copolymers.

Early experiments with simple lanthanocene systems such as Cp_2YbMe showed their ability to polymerize IPOx, DEVP, MMA and 2VP with great control and decent activities.[62] The highest activities were observed for polymerizations of DEVP.

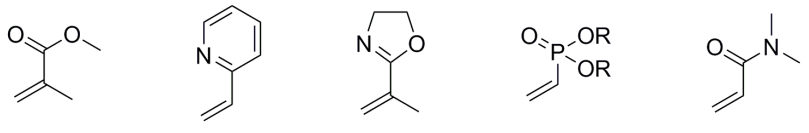

Figure 16. *Michael*-type monomers accessible through REM-GTP.

However the activities of rare earth metallocenes, e.g. Cp_2YbMe for IPOx (TOF = 380 h^{-1}) and especially 2VP (TOF = 44 h^{-1}) are unsatisfactory and leave the need for highly active catalysts unanswered.[62] For MMA a wide variety of nonmetallocene catalyst systems have been evaluated and those or similar systems might also be viable options for the polymerization of IPOx, 2VP, and other monomers.[47b]

Aminebis(phenolate)-yttrium systems known for their activity in ROP of lactones (*vide supra*), were also employed in attempts to polymerize MMA.[63] Aminebis(phenolate)-yttrium(CH_2TMS) (**23**) did not show any activity while aminebis(phenolate)-yttrium bisdimethylsilylamide (BDSA) (**24**) produced very low yields of slightly isoenriched PMMA. Recently, elegantly crafted ene-diamido yttrium catalysts (**25**) were tested for their ability to oligomerize 2VP and introduce functional endgroups *via* CH-bond activation.[58]

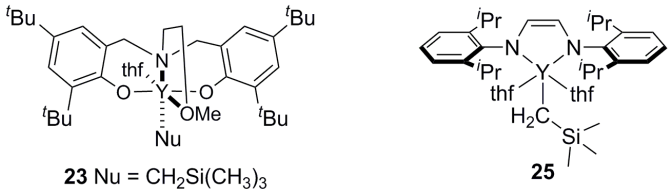

23 Nu = $CH_2Si(CH_3)_3$
24 Nu = $N(SiHMe_2)_2$

25

Figure 17. Selected nonmetallocene catalysts.

Homo- and copolymers of P2VP exhibit promising material properties for applications in nanotechnology.[64] Shape changing nanoparticles have emerged just recently and allow the utilization of pH-sensitive behavior of P2VP within a block copolymer.[65] Also the application for electronic devices is tested with block copolymer structures of P2VP.[66] The direct access to well defined, high molecular weight P2VP at ambient conditions through REM-GTP is highly desirable as anionic and radical polymerization procedures are hampered by side reactions, lack of control and fragile reaction conditions.[67]

4.4 Aim of this Work: 2-Methoxyethylaminobis(phenolate)-yttrium Catalysts for the Polymerization of *Michael*-type Monomers

The polymerization of *Michael*-type monomers, in particular 2VP, with non-metallocene rare earth metal catalysts has only been achieved in few cases and only with low activities. The development of a new catalyst system for the polymerization of *Michael*-type monomers, e.g. 2VP, is hence desirable.

On the basis of easily tunable and accessible 2-methoxyethylaminbis-(phenolate) ligands rare earth metal catalysts can be developed and tested for their activity in REM-GTP of various monomers. Mechanistic investigations are necessary to ensure the validity of the REM-GTP mechanism, especially the desired living character of the polymerization.

4.5 Manuscript: Versatile 2-Methoxyethylaminobis(phenolate)-yttrium Catalysts: Catalytic Precision Polymerization of Polar Monomers via Rare Earth Metal-Mediated Group Transfer Polymerization

Status	Published online: 10th November 2014
Journal	Macromolecules
Publisher	American Chemical Society
Article type	Full paper
DOI	10.1021/ma501754u
Authors	Peter T. Altenbuchner; Benedikt S. Soller; Stefan Kissling; Thomas Bachmann; Alexander Kronast; Sergei I. Vagin; Bernhard Rieger

Content

Rare earth metal-mediated group-transfer polymerization (REM-GTP) with non-metallocene catalyst systems is evaluated for various *Michael*-type monomers and β-butyrolactone. 2-Methoxyethylamino-bis(phenolate)-yttrium trimethylsilyl-methyl complexes with varying steric demand were synthesized and showed moderate to high activities in the REM-GTP of 2-vinylpyridine, 2-isopropenyl-2-oxazoline, diethyl vinylphosphonate, diisopropyl vinylphosphonate and *N,N*-dimethylacrylamide as well as in the ring-opening polymerization of β-butyrolactone. Mechanistic studies found the reaction order in catalyst and monomer to be one for the REM-GTP of 2-vinylpyridine. Hence, the catalyst systems follow a living monometallic group-transfer polymerization mechanism. Temperature dependent reaction kinetics were conducted and allowed conclusions about the influence of the bulky substituents around the metal center. Block copolymerizations with precise molecular-weight control and very narrow molecular weight distributions are possible.

Title: Versatile 2-Methoxyethylaminobis(phenolate)yttrium Catalysts: Catalytic Precision Polymerization of Polar Monomers via Rare Earth Metal-Mediated Group Transfer Polymerization

Author: Peter T. Altenbuchner, Benedikt S. Soller, Stefan Kissling, et al

Publication: Macromolecules

Publisher: American Chemical Society

Date: Nov 1, 2014

PERMISSION/LICENSE IS GRANTED FOR YOUR ORDER AT NO CHARGE

This type of permission/license, instead of the standard Terms & Conditions, is sent to you because no fee is being charged for your order. Please note the following:

- Permission is granted for your request in both print and electronic formats, and translations.
- If figures and/or tables were requested, they may be adapted or used in part.
- Please print this page for your records and send a copy of it to your publisher/graduate school.
- Appropriate credit for the requested material should be given as follows: "Reprinted (adapted) with permission from (COMPLETE REFERENCE CITATION). Copyright (YEAR) American Chemical Society." Insert appropriate information in place of the capitalized words.
- One-time permission is granted only for the use specified in your request. No additional uses are granted (such as derivative works or other editions). For any other uses, please submit a new request.

Macromolecules

Article

pubs.acs.org/Macromolecules

Versatile 2-Methoxyethylaminobis(phenolate)yttrium Catalysts: Catalytic Precision Polymerization of Polar Monomers via Rare Earth Metal-Mediated Group Transfer Polymerization

Peter T. Altenbuchner, Benedikt S. Soller, Stefan Kissling, Thomas Bachmann, Alexander Kronast, Sergei I. Vagin, and Bernhard Rieger*

WACKER-Lehrstuhl für Makromolekulare Chemie, Technische Universität München, Lichtenbergstraße 4, 85748 Garching bei München, Germany

Supporting Information

ABSTRACT: The present study is one of the first examples for rare earth metal-mediated group transfer polymerization (REM-GTP) with non-metallocene catalyst systems. 2-Methoxyethylaminobis(phenolate)yttrium trimethylsilylmethyl complexes were synthesized and showed moderate to high activities in the rare earth metal-mediated group transfer polymerizations of 2-vinylpyridine, 2-isopropenyl-2-oxazoline, diethyl vinylphosphonate, diisopropyl vinylphosphonate, and *N*,*N*-dimethylacrylamide as well as in the ring-opening polymerization of β-butyrolactone. Reaction orders in catalyst and monomer were determined for the REM-GTP of 2-vinylpyridine. The mechanistic studies revealed that the catalyst systems follow a living monometallic group transfer polymerization mechanism allowing a precise molecular-weight control of the homopolymers and the block copolymers with very narrow molecular weight distributions. Temperature-dependent reaction kinetics were conducted and allowed conclusions about the influence of the bulky substituents around the metal center on the polymerization activity. Additional polymerization experiments concerning the combination of REM-GTP and ROP to obtain block copolymers were performed.

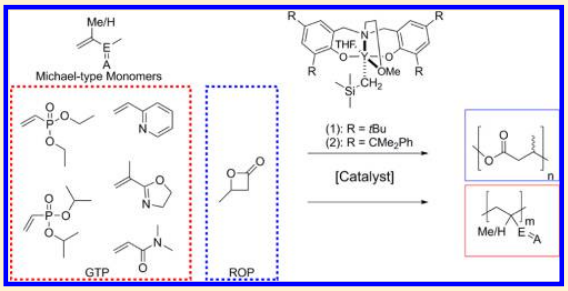

INTRODUCTION

The metal-mediated group transfer polymerization (GTP) was first employed in 1992 by two independent groups. Yasuda et al. used samarocene $[Cp^*_2SmH]_2$ catalysts for the polymerization of methyl methacrylate (MMA) whereas Collins and Ward employed a two-component group 4 metallocene system.[1] Since then, great effort has been put into the development of new and more efficient catalysts as well as into the expansion of the accessible monomers through GTP. Apart from MMA, dialkyl vinyl phosphonates (DAVP), 2-isopropenyl-2-oxazoline (IPOx), *N*,*N*-dimethylacrylamide (DMAA), and 2-vinylpyridine (2VP) were successfully homo- and copolymerized.[2] So far, only a few examples for non-metallocene rare earth metal catalysts for the polymerization of Michael-type monomers can be found in the literature, and the predominant catalyst systems are still of the general structure $[Cp^R_2LnX]$.[2d,3] The general ability of non-metallocene yttrium complexes as initiators for the GTP of MMA was previously studied via DFT calculations.[4] The results indicated that alcoholate initiators are not able to polymerize MMA due to an endothermic limitation of the initiation but DFT signified toward amido initiators as valid options for the GTP of MMA.[4] In a recent effort the mechanistic proceedings during the REM-GTP were elucidated and shown to have a monometallic propagation mechanism via an eight-membered-ring intermediate.[5] Contrary to the monometallic propagation of lanthanide catalysts, a monometallic as well as a bimetallic pathway is thought possible for group 4 metal catalysts.[2d,6] In the bimetallic mechanism one catalyst molecule bears the growing chain end, while the other activates the monomer. P2VP is an underrepresented polymer in the literature, and only scarce examples for controlled polymerization are available although interesting material properties for membranes and drug delivering carriers are reported for P2VP copolymers.[7] The polymerization of 2VP to poly(2-vinylpyridine) can be achieved via anionic polymerization or REM-GTP.[2a,3a,8] Compared to the simple anionic polymerization, REM-GTP has several advantages, e.g., strictly linear polymer growth, very narrow molecular weight distributions ($D < 1.1$), and increased operation temperature of the polymerization. The living character makes REM-GTP particularly suitable for block copolymerizations.[2a,7e] The currently available metallocene catalyst systems lack the activities necessary to further explore the potential applications of homo- and copolymer structures of

Received: August 26, 2014
Revised: October 15, 2014
Published: November 10, 2014

Scheme 1. Synthesis of 2-Methoxyethylaminobis(phenolate)yttrium Trimethylsilylmethyl Complexes [(L)M($CH_2Si(CH_3)_3$)(thf)]

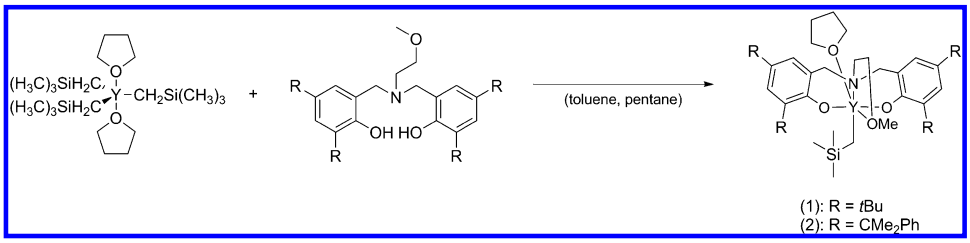

P2VP. The metallocene system Cp_2YbMe yielded turnover frequencies (TOF) of 44 h^{-1} for the REM-GTP of 2VP and molecular weights up to 14 kg/mol.[2a] Other literature reports of the REM-GTP of 2VP did not focus on the polymerization itself rather produced oligomeric P2VP and investigated the possibilities for the end-group functionalization through C−H bond activation.[3a]

However, to this date no highly active catalyst for the controlled polymerization of 2VP has been described in the literature. Mechanistic studies on initiation, propagation, and rate-determining step (RDS) of the 2VP polymerization have so far not been conducted.

Therefore, in this work the authors report the synthesis of highly versatile and highly active 2-methoxyethylaminobisphenolate yttrium catalysts for the homopolymerization and block copolymerization of Michael-type monomers such as 2VP, DEVP, DIVP, IPOx, and DMAA. The newly developed system was furthermore employed in mechanistic studies. The steric influence around the reactive metal center was evaluated using kinetic *in situ* ATR-IR measurements. The determination of the reaction order in catalyst and monomer combined with temperature-dependent reaction kinetics (Eyring plot) further elucidates the processes during the polymerization. The results presented in this article add valuable insight into the general picture of the REM-GTP mechanism and introduce a highly active catalyst system for the precise polymerization of functional monomers for the synthesis of high performance, high precision materials.

DISCUSSION

The REM-GTP of 2VP was investigated with 2-methoxyethylaminobis(phenolate)yttrium trimethylsilylmethyl complexes [$(ONOO)^{R}M(CH_2Si(CH_3)_3)$(thf)] which differ in the nature of the *o*-phenolate substituents (R) (Scheme 1). The catalysts are accessible through a straightforward synthesis from readily available compounds in good yields. The respective ligand is reacted with 1 equiv of $[Y(CH_2Si(CH_3)_3)_3(thf)_2]$ in a mixture of pentane and toluene at ambient temperature to generate the catalyst.

The homopolymerizations of 2VP, DEVP, DIVP, IPOx, and DMAA with catalysts **1** and **2** proceed rapidly under mild conditions. The respective ligands were chosen to address the question of steric influence on the REM-GTP. According to the small steric demand of Cp ligands, only atactic P2VP has so far been produced with those systems. Mashima et al. however obtained isotactic oligomeric P2VP with yttrium ene−diamido complexes.[3a] As we synthesized 2-methoxyethylaminobis(phenolate)yttrium trimethylsilylmethyl complexes with increased steric demand around the yttrium center, we expected to restrict the accessibility and thereby influence the activities of the catalysts and possibly also the tacticities of the resulting polymers. First, the initiation mechanism was elucidated by end-group analysis of oligomeric P2VP generated by reacting $(ONOO)^{tBu}Y(CH_2Si(CH_3)_3)$(thf) with 10 equiv of 2VP and monitoring the reaction via NMR. Time-resolved ^1H NMR spectra show a shift of the respective $CH_2Si(CH_3)_3$ methyl groups (Figure S18). The subsequent ESI-MS analysis found signals corresponding to $n \times M_{Mon} + M_I$ with either H^+ or Na^+ as charge carrier ($M_I = CH_2Si(CH_3)_3$).

The initiating $CH_2Si(CH_3)_3$ groups were clearly visible in the ESI-MS; therefore, a transfer of the coordinated ligand during the initiation through a six-membered intermediate is evident (Figure 1). Our studies showed no activity of 2-methoxyethylaminobis(phenolate)yttrium bisdimethylsilylamide complexes for the REM-GTP of Michael-type monomers. The alkyl initiators of catalysts **1** and **2** however initiate the polymerization of β-butyrolactone (BL), DEVP, DIVP, 2VP, IPOx, and DMAA at room temperature. Catalyst **1** showed the highest activities for the polymerization of DMAA with quantitative conversion of 200 equiv of monomer in 15 min at 0 °C. The activity of catalyst **1** decreased in the order of DMAA > IPOx > 2VP > DEVP > DIVP (Tables 1 and 2). The polymerization of DMAA at room temperature proceeded in an uncontrolled fashion producing PDMAA with broad PDI within less than 1 min. At 0 °C it was possible to control the polymerization and achieve quantitative yields of atactic PDMAA within 15 min with slightly broadened PDI (1.69) due to the high activity.

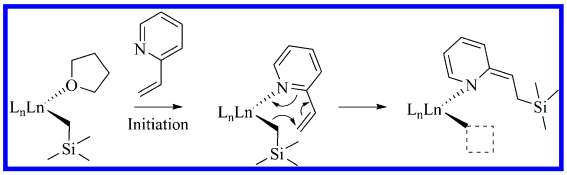

Figure 1. Six-membered initiation mechanism for 2VP and $L_nLn(CH_2Si(CH_3)_3)$.

The polymerization of 2VP proceeds in a living fashion, as discernible by the narrow polydispersities ($1.01 \leq x \leq 1.07$) and the good match between experimentally determined and the theoretically expected M_n values (Figure 3). To further examine the character of the polymerization with our 2-methoxyethylaminobis(phenolate)yttrium trimethylsilylmethyl complexes aliquots were taken at regular time intervals during the polymerization. These aliquots were analyzed by gel permeation chromatography multiangle light scattering (GPC-MALS) to obtain the absolute molecular mass (M_n) against the monomer (2VP) conversion as can be seen in Figure 3. The plots reveal a linear relationship between M_n and

Table 1. REM-GTP and ROP Polymerization Results of Catalyst 1[a]

entry	[M]/[Cat]	[M]	solvent	time [h]	conv [%]	$M_{n,calc}$ ($\times 10^4$)[b] [g/mol]	$M_{n,exp}$ ($\times 10^4$) [g/mol]	M_w/M_n	I^*[c]	P_r[d]	TOF [h^{-1}]
1	200	2VP	toluene	2	99	2.2	2.2	1.01	0.99		1100
2	200	DEVP	toluene	3.3	99	3.3	9.0	1.10	0.36		480
3	200	DIVP	toluene	5	25	1.0	3.4	1.09	0.28		42
4	200	IPOx	toluene	0.17	99	2.2	2.4	1.12	0.93		1500
5	600	2VP	toluene	4	99	6.6	11.0	1.02	0.60		420
6[e]	200	DMAA	CH_2Cl_2	0.25	99	2.0	6.2	1.69	0.32		
7[f]	600	BL	CH_2Cl_2	1	89	4.6	8.6[g]	1.50[g]	0.54	0.81	6000

[a]Reactions performed with [M] = 27 mmol at 25 °C in 20 mL of solvent, conversions determined by gravimetry, and $M_{n,expd}$ determined by GPC-MALS. [b]$M_{n,calc}$ from $M_{n,calc} = M \times (([M]/[Cat]) \times \text{conversion})$. [c]$I^* = M_{n,calc}/M_{exp}$. [d]$P_r$ is the probability of racemic linkages between monomer units and is determined by ^{13}C NMR spectroscopy. [e]Reaction conducted at −78 °C. [f]Reaction performed with [*rac*-BL] = 8.57 mmol at 25 °C in 5 mL of CH_2Cl_2 and conversion determined by ^1H NMR spectroscopy. [g]$M_{n,exp}$ and M_w/M_n values determined by GPC in $CHCl_3$ vs polystyrene standards.

Table 2. REM-GTP and ROP Polymerization Results of Catalyst 2[a]

entry	[M]/[Cat]	[M]	solvent	time [h]	conv [%]	$M_{n,calc}$ ($\times 10^3$)[b] [g/mol]	$M_{n,exp}$ ($\times 10^3$) [g/mol]	M_w/M_n	I^*[c]	P_r[d]	TOF [h^{-1}]
1	200	2VP	toluene	1.5	99	2.1	2.9	1.03	0.72		430
2	600	2VP	toluene	3	82	5.2	11.2	1.04	0.46		230
3[e]	600	BL	CH_2Cl_2	1	99	5.2	14.2[f]	1.60[f]	0.36	0.88	15800

[a]Reactions performed with [M] = 27 mmol at 25 °C in 20 mL of solvent, conversions determined by gravimetry, and $M_{n,expd}$ determined by GPC-MALS. [b]$M_{n,calc}$ from $M_{n,calc} = M \times (([M]/[Cat]) \times \text{conversion})$. [c]$I^* = M_{n,calc}/M_{exp}$. [d]$P_r$ is the probability of racemic linkages between monomer units and is determined by ^{13}C NMR spectroscopy. [e]Reaction performed with [*rac*-BL] = 8.57 mmol at 25 °C in 5 mL of CH_2Cl_2 and conversion determined by ^1H NMR spectroscopy. [f]$M_{n,expd}$ and M_w/M_n values determined by GPC in $CHCl_3$ vs polystyrene standards.

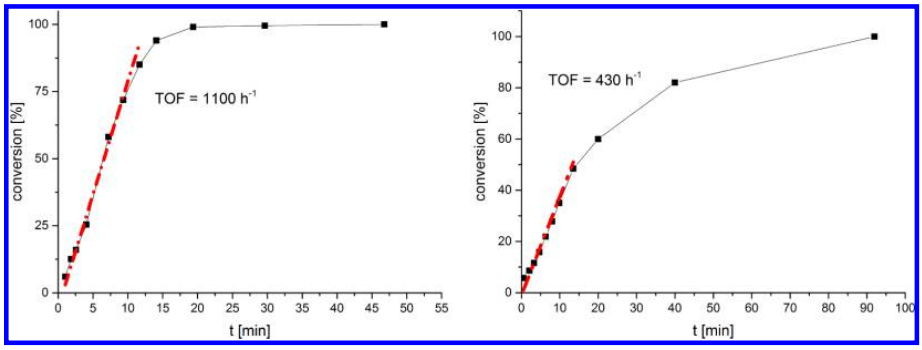

Figure 2. (left) Determination of catalytic activity of $(ONOO)^{tBu}Y(CH_2Si(CH_3)_3)(thf)$ (catalyst 135 μmol, 2VP 27 mmol, toluene 20 mL, T = 25 °C). (right) Determination of catalytic activity of $(ONOO)^{CMe2Ph}Y(CH_2Si(CH_3)_3)(thf)$ (catalyst 135 μmol, 2VP 27 mmol, toluene 20 mL, T = 25 °C).

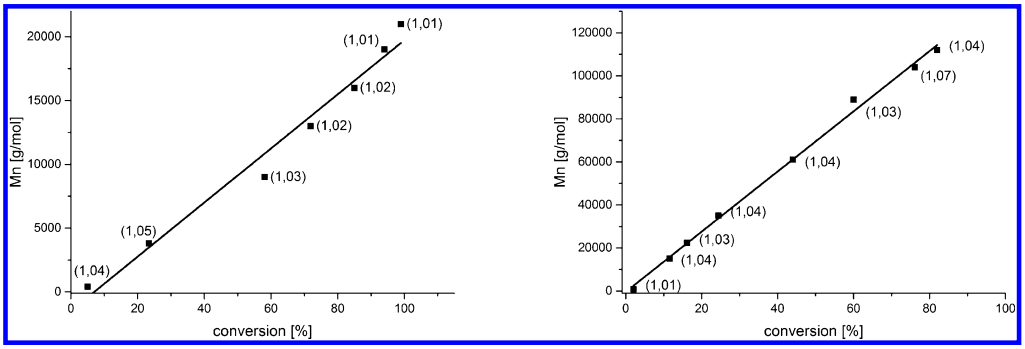

Figure 3. Linear growth of the absolute molecular weight (M_n) determined by GPC-MALS as a function of monomer conversion (determined gravimetically), with respective PDI values shown in parentheses: (left) catalyst **1**, 135 μmol, 2VP 27 mmol, toluene 20 mL, 25 °C; (right) catalyst **2**, 43 μmol, 2VP 27 mmol, toluene 20 mL.

conversion while retaining a very narrow PDI throughout the polymerization (PDI < 1.05).

Catalyst **1** yields atactic polymer in the case of P2VP, PDEVP, PDIVP, and PDMAA at ambient conditions. Catalyst

dx.doi.org/10.1021/ma501754u | *Macromolecules* 2014, 47, 7742−7749

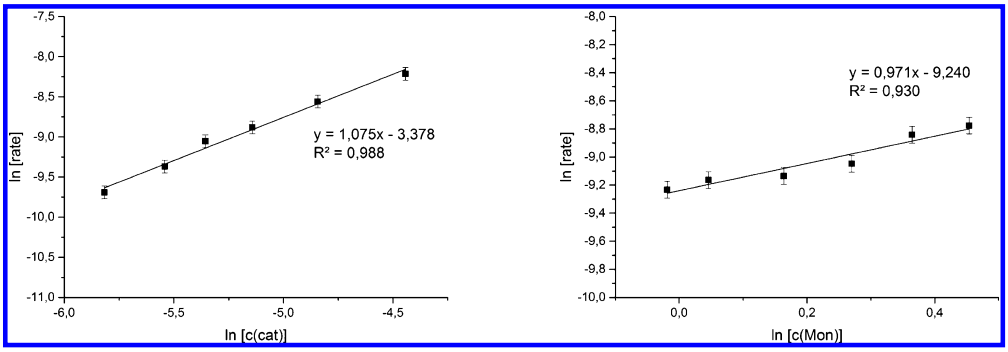

Figure 4. (left) Determination of catalyst order (ONOO)^{tBu}Y(CH$_2$Si(CH$_3$)$_3$)(thf) (catalyst 22−85 μmol, 2VP 8.6 mmol, toluene 5.5 mL). (right) Determination of monomer order (ONOO)^{tBu}Y(CH$_2$Si(CH$_3$)$_3$)(thf) (catalyst 42 μmol, 2VP 7−11.5 mmol, toluene 5.5 mL).

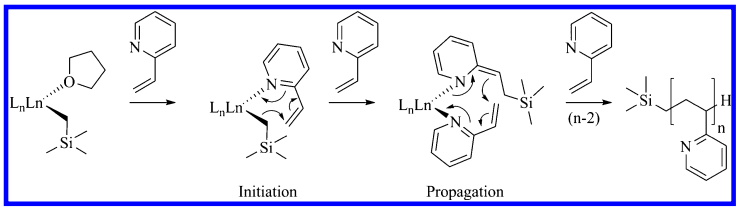

Figure 5. Schematic illustration concerning the initiation and propagation of REM-GTP of 2VP.

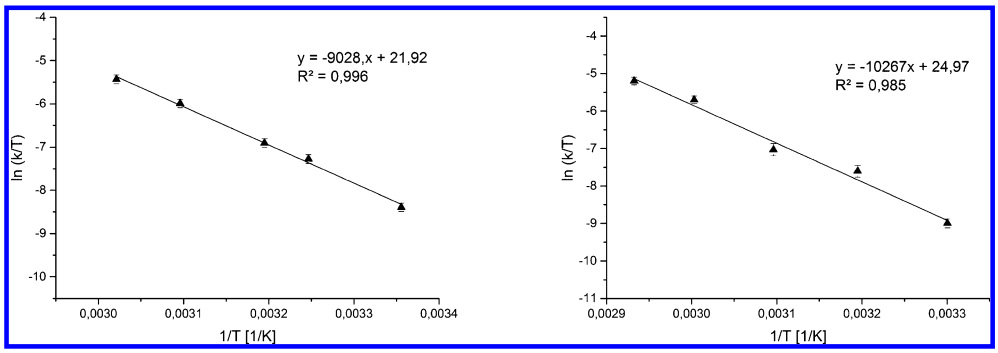

Figure 6. (left) Eyring plot for (ONOO)^{tBu}Y(CH$_2$Si(CH$_3$)$_3$)(thf) the polymerization of 2VP (catalyst 42 μmol, 2VP 8.6 mmol, toluene 5.5 mL, temperature 298−331 K). (right) Eyring plot for (ONOO)^{CMe2Ph}Y(CH$_2$Si(CH$_3$)$_3$)(thf) the polymerization of 2VP (catalyst 42 μmol, 2VP 8.6 mmol, toluene 5.5 mL, temperature 303−333 K).

2 was not active for the polymerization of DEVP, DIVP, and also produced atactic P2VP. Temperature variations between −20 and 60 °C did not change the tacticities of the resulting polymer. The generally occurring color change of the polymerization solution of 2VP probably due to the coordination to the catalyst was not observed at −78 °C. Also, prolonged stirring at this temperature did not produce polymer. We attribute this to the inability of 2VP to coordinate to the catalyst, replacing the coordinated THF molecule. Consequently, no initiation and polymerization could be observed until the temperature was elevated to −20 °C. The effect of the steric influence of catalysts **1** and **2** on the activity in the 2VP GTP was investigated through gravimetric kinetic measurements. For 2-methoxyethylaminobis(phenolate)yttrium trimethylsilylmethyl complexes the activity for GTP decreases with increased steric demand. The activity for the 2VP GTP dropped from 1100 h^{-1} with catalyst **1** to 430 h^{-1} with catalyst **2**. Catalyst **2** showed no activity for the polymerization of DEVP and DIVP.

To ensure that the activity differences are not only differences in initiator efficiency (I*), aliquots were taken from the reaction and I* was determined through GPC analysis. For catalyst **1** the I* was found to be 99%, whereas for catalyst **2** I* was only 72% at 25 °C. The measured I* made the direct comparison of both catalysts possible and showed that the activity difference is due to the steric destabilization of the intermediate eight-membered transition state during the polymerization which increases the activation barrier for the S$_N$2-type associative dissplacement of the polymer by a 2VP monomer. Previous studies showed that the S$_N$2-type associative dissplacement is the rate-determining step (RDS) for the metallocene REM-GTP of phosphorus-containing vinyl polymers.[5a]

Kinetics. Generally, a monometallic as well as a bimetallic mechanism is thought possible for the GTP depending on the

Table 3. Activation Enthalpy $\Delta H^{\ddagger}$ and Entropy $\Delta S^{\ddagger}$ and the Dependence on the Steric Demand of the Ligand Structure

	$(ONOO)^{tBu}Y(CH_2Si(CH_3)_3)(thf)$	$(ONOO)^{CH2Ph}Y(CH_2Si(CH_3)_3)(thf)$
$\Delta H^{\ddagger}$ (±2) (kJ/mol)	75.1	85.4
$-\Delta S^{\ddagger}$ (±3) (J/(K mol))	15.3	10.1

employed catalyst system. Therefore, kinetic *in situ* ATR-IR measurements were conducted for the REM-GTP of 2VP with catalysts **1** and **2**. The formal rate law for catalyzed polymerizations reads

$$r = k \times [\mathrm{Cat}]^m \times [\mathrm{Mon}]^n \quad (1)$$

Thus, for the determination of the reaction orders, first, the initial monomer concentration is kept constant to determine the order in catalyst (m). For different catalyst concentrations of otherwise identical reaction conditions, the plot of $\ln(r)$ against $\ln([\mathrm{Cat}])$ yields a reaction order of $m = 1$ (Figure 4, left). Furthermore, the order in monomer was determined according to eq 2.

$$r = k \times [\mathrm{Mon}]^n \quad (2)$$

For different monomer concentrations at otherwise identical conditions the reaction rate was measured. Plotting $\ln(r)$ against $\ln([\mathrm{Mon}])$ gave the order in monomer $n = 1$ (Figure 4, right). These results show that the REM-GTP of 2VP with 2-methoxyethylaminobis(phenolate)yttrium catalysts follows a monometallic Yasuda-type polymerization mechanism (Figure 5) as was also found for metallocene systems with phosphorus-containing monomers.[5a]

Through these results no exact explanation for the steric influence of the ligand on the catalytic activity can be given. Hence, temperature-dependent kinetic measurements were undertaken to determine the activation enthalpies $\Delta H^{\ddagger}$ and entropies $\Delta S^{\ddagger}$ according to the Eyring equation

$$\ln\frac{k}{T} = -\frac{\Delta H^{\ddagger}}{RT}\frac{1}{T} + \ln\frac{k_B}{h} + \frac{\Delta S^{\ddagger}}{R} \quad (3)$$

with the rate constant k, the temperature T, the ideal gas constant R, the Boltzmann constant k_B, and the Planck constant h. Plotting $\ln(k/T)$ against $1/T$ gives the activation enthalpy and entropy of the rate-determining step. The measurements were performed with catalyst $(ONOO)^{tBu}Y(CH_2Si(CH_3)_3)$-(thf) and $(ONOO)^{CMe2Ph}Y(CH_2Si(CH_3)_3)(thf)$ under identical conditions in an ATR-IR autoclave.

Eyring plot studies for the polymerization of polar monomers are rare in the literature.[9] The activities in previous studies were found to be mainly determined by entropic effects. REM-GTP Eyring plot measurements with different lanthanides (Y, Tb, Tm, and Lu) were performed with DEVP and DIVP.[5a] A decreased entropic contribution was observed with a decreased metal radius (i.e., faster propagation rates), and an increased entropic influence was found for sterically more demanding monomers (i.e., slower propagation rates). The 2-methoxyethylaminobis(phenolate)yttrium trimethylsilylmethyl complexes used for the Eyring plot measurements with 2VP show a different trend compared the lanthanocene catalysts. An increased steric demand in *ortho*-position of these complexes leads to an increase in both the $\Delta H^{\ddagger}$ and the $-T\Delta S^{\ddagger}$. Bulkier ligands around the metal center destabilize the propagation ground state by restraining the eight-membered transition state. The increased steric crowding furthermore interferes with the associative displacement of the polymer by a 2VP monomer.

These destabilizing effects are of enthalpic and of entropic nature. The enthalpic $\Delta H^{\ddagger}$ contribution to the RDS is increased from 75.1 kJ/mol for catalyst **1** to 85.4 kJ/mol for catalyst **2**. The entropic $-\Delta S^{\ddagger}$ contribution has a minor influence but nevertheless is also raised from 15.3 J/(K mol) for catalyst **1** to 10.1 J/ (K mol) for the more sterically crowded catalyst **2**.

ROP of β-Butyrolactone. The activities of both 2-methoxyethylaminobis(phenolate)yttrium catalysts were tested for the ring-opening polymerization (ROP) of BL. In general, initiators for the polymerization of lactones are alcoholates and amides, whereas alkyl initiators are not commonly used for the ROP with lanthanide catalysts. As expected, narrow polydispersities for PHB were achieved (<1.6), and the measured molecular weights are in good agreement with the theoretically calculated values (Tables 1 and 2). Both polymerization types, the REM-GTP[5a,10] as well as the ROP,[11] have a monometallic initiation and propagation mechanism with first-order kinetics in catalyst and monomer. In the literature similar 2-methoxyethylaminobis(phenolate)yttrium catalysts were previously used for the ring-opening polymerization (ROP) of β-butyrolactone.[12] Catalysts **1** and **2** show good activities (TOF = 6000 and 15 800 h^{-1}) toward the ROP and produced syndiotactic PHB (P_r = 0.81−0.88). The order in activity for catalysts **1** and **2** for the ROP is reversed compared to the GTP. The bulky catalyst **2** is more active for ROP whereas the less crowded complex **1** shows higher activities for GTP. For a good ROP and GTP catalyst a balance has to be found for the steric crowding introduced through the ligand. Bulkier ligands increase the activity for the ROP as dimer formation is suppressed, and the carbonyl-alkoxy chelate during the ROP is not hindered. Catalyst **2** exhibits an activity almost 3 times higher than catalyst **1** for the ring-opening polymerization of BL. GTP, however, proceeds faster with catalyst **1** as the eight-membered transition state for the propagation of polar monomers is sterically more demanding and destabilized by catalyst **2**. Catalyst **1** (1100 h^{-1}) is more than twice as fast as catalyst **2** (430 h^{-1}) for the polymerization of 2VP.

Block Copolymerization. In the literature numerous examples can be found for the copolymerization of lactones[13] and the copolymerization of Michael-type monomers.[2a,d] Only a few examples can be found for the combination of GTP and ROP, and they are limited to the copoylmerization of (meth)acrylate and ε-caprolactone and δ-valerolactone.[14] The use of anionic initiators has been reported for trials to produce polyester and polyhydrocarbon copolymers, but only homopolymer formation with very broad molecular weight distributions could be observed.[15] Also modified PHB has been investigated to afford macromolecular initiators which produce polymeric material with narrow dispersities.[16] There, PHB modifications prior to the polymerization are necessary which enable the radical copolymerization of PHB and acrylates. As our compounds **1** and **2** were suitable catalysts for the GTP and ROP we were interested if these different polymerization methods can be combined and utilized to produce block copolymers.

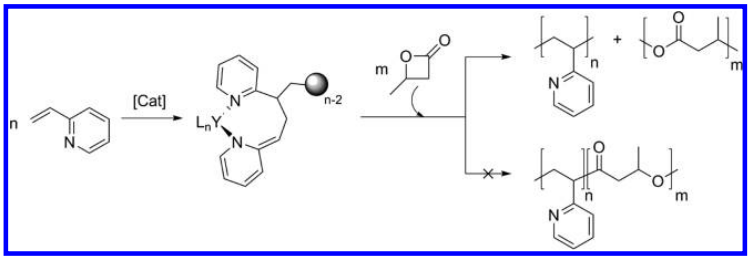

Figure 7. Experimental steps toward the attempted block copolymerization of 2VP and BL (catalyst **1** 34 μmol, [Cat]:[2VP]:[BL] = 1:100:100, 25 °C, 5 mL of CH_2Cl_2).

Table 4. Copolymerization Experiments with Catalyst 1

		$M_{n,expd}$[a] ($\times 10^4$) [g/mol]	$M_{n,calcd}$ ($\times 10^4$) [g/mol]	PDI[b]	comonomer ratio A/B[c]	yield[d] [%]	I^*[e]
1	$P2VP_{100}$-*b*-$PDEVP_{100}$	3.0	2.7	1.05	1:1.1	96	0.90
2	$P2VP_{100}$-*b*-$PIPOx_{100}$	2.6 (1.3)	2.2	1.03 (1.01)	1:1.2	97	0.85
3	$P2VP_{100}$-*b*-$PDMAA_{100}$[f]	3.3 (1.6)	2.0	1.24 (1.04)	1:1.6	97	0.63

[a]Reactions performed with [M] = 4.3, [Cat] = 43 μmol at 25 °C in 5 mL of CH_2Cl_2; numbers in parentheses give the respective data for the aliquot sample taken in the case of bimodal distributions. [b]Determined by GPC-MALS. [c]Determined by ^{1}H NMR. [d]Determined by weighing of the components. [e]$I^* = M_{n,calc}/M_{n,exp}$; numbers in parentheses give the I^* of the macroinitiator for polymerization of block B (in the case of bimodal distributions). [f]Reaction performed at 0 °C.

In comparison to other Michael-type monomers, 2VP coordinates the weakest to the metal center (DEVP > MMA > IPOx > 2VP).[2a] For REM-GTP the addition sequence of the monomers is crucial for monomers with different coordination strength. In our study we picked up on the concept and tried to use the low coordination strength of P2VP to the metal center to obtain block copolymer structures by sequential addition (Figure 7). Low-temperature polymerization experiments showed that at −78 °C 2VP is not polymerized. For a successful block copolymerization, BL needs to be able to replace the coordinated eight-membered intermediate of the REM-GTP while the P2VP chain end needs to have enough nucleophilicity to ring-open the coordinated lactone. Therefore, we chose 2VP as monomer to obtain P2VP and use the pending polymer chain on the yttrium catalyst as macroinitiator for the subsequent ROP of BL. The very high initiator efficiencies of catalyst **1** should suppress homopolymer formation of PHB and facilitate the subsequent isolation of the block copolymer. The polymerization of block A (P2VP) is conducted in dichloromethane to ensure complete conversion without precipitation of P2VP. An aliquot is taken for later GPC-MALS analysis, and subsequently, BL is added and stirred for an additional 2 h after which an aliquot NMR is once again taken to ensure full conversion of BL. The separation of the block-AB-copolymer is attempted by precipitation with hexane and washing cycles with methanol and thf, but only homopolymers were isolated (Figure 7).

Possible reasons for the inability to produce block copolymers might stem from the inadequate nucelophilicity of macroinitiator at the catalyst or chain scission of P2VP-*b*-PHB. Furthermore, the formation of PHB homopolymer could be explained by traces of unreacted catalyst molecules. The general activity of the pending P2VP chain toward block copolymerization was successfully tested with Michael-type monomers (*vide infra*, Table 4) and yielded block copolymers to ensure the livingness of the P2VP chain. Ensuing, the reaction conditions were systematically varied. Excess of BL was added as well as catalyst concentration, monomer loading of monomer A, solvent, and temperature screened. Aside from 2VP, other Michael-type monomers such as DEVP and IPOx were employed in copolymerization experiments with BL and did not show any block copolymer formation either. Under all tested conditions homopolymer could be isolated, but no block copolymer formation was observed.

The initiation of the ROP of BL was still puzzling as the initiator efficiency of catalyst **1** under the reaction conditions was 99%. Of course, trace quantities of catalyst which catalyze the ROP of BL might be a possible explanation for the generation of PHB homopolymer. Therefore, GPC measurements of the isolated PHB homopolymers were performed. They showed average M_n (PDI ∼ 1.5) and I^* of around 20−30%. The PHB homopolymer signals do not exhibit any initiating group. From NMR measurements crotonic end groups can be excluded as they show characteristic shifts and are visible already at very low concentrations (see Figures S6 and S7). Therefore, the hypothesis of trace amounts of catalyst initiating the BL polymerization can be discarded. The experimental results point toward a deprotonation of BL and a subsequent anionic ROP or chain scission. Further mechanistic studies have to be performed to reveal the mechanism in detail.

The general ability of our catalyst system was tested in block copolymerization experiments with Michael-type monomers. REM-GTP block copolymerization was conducted with 2VP as block A and DEVP, IPOx, and DMAA as block B. As with the previous copolymerization attempts with BL also here samples were taken after 2 h for later GPC-MALS analysis. Monomodal distribution was found for P2VP-*b*-PDEVP (Table 4, entry 1). In the GPC of the other copolymers (P2VP-*b*-PIPOx; P2VP-*b*-PDMAA) remaining P2VP block was observed which could be unambiguously assigned through the comparison with GPCs of the aliquot samples. The remaining P2VP is probably the result of quenching processes though trace amounts of water in the monomer B. The separation of the P2VP-*b*-PDMAA block copolymers was achieved through washing cycles with toluene and water.

The PDIs of the obtained block copolymers were narrow (PDI = 1.03−1.24), and the calculated M_n fit well to the

experimentally determined values. More defined polymer structures were obtained during block copolymerization of 2VP and DMAA due to the employed P2VP macroinitiator. The PDI of PDMAA was 1.69, whereas for the $P2VP_{100}$-*b*-$PDMAA_{100}$ block copolymer a PDI of 1.24 could be achieved. The significant decrease of the polydispersity can be attributed to a different initiation mechanism of the macroinitiator P2VP compared to alkyl initiators. Similar results were achieved for the polymerization of DMAA with zirconocenes using enolates as initiating ligands.[2b,10] For α-acid monomers like DMAA, initiation can proceed via either deprotonation of the α-CH or nucleophilic transfer, both being six-electron processes. The P2VP macroinitiator is supposed to coordinate to the metal via an enamide and can initiate via an eight-membered ring, matching the propagation step during the polymerization and therefore initiate uniformly.

CONCLUSION

2-Methoxyethylaminobis(phenolate)yttrium trimethylsilylmethyl complexes $[(ONOO)^{R}Y(CH_2Si(CH_3)_3)(thf)]$ were synthesized and showed moderate to high activities in the rare earth metal-mediated group transfer polymerization of 2-vinylpyridine, diethyl vinylphosphonate, diisopropyl vinylphosphonate, *N*,*N*-dimethylacrylamide, and 2-isopropenyl-2-oxazoline as well as in the ring-opening polymerization of β-butyrolactone. The present study is one of the first examples for REM-GTP with non-metallocene catalyst systems covering a large variety of polar monomers. Catalyst **1** exhibits the highest TOF for the REM-GTP of 2-vinylpyridine reported in the literature. The reaction orders in catalyst and monomer were determined, and temperature-dependent reaction kinetics (Eyring plot) were conducted for the polymerization of 2-vinylpyridine. The mechanistic studies through kinetic *in situ* ATR-IR measurements of the 2VP polymerization revealed that 2-methoxyethylaminobis(phenolate) catalyst systems follow a living monometallic group transfer polymerization mechanism allowing a precise molecular weight control of the homopolymers and the block copolymers with very narrow molecular weight distributions. Generally the steric demand of the *ortho*-position in the ligand structure had a pronounced influence on the catalytic activity. For the REM-GTP less sterically demanding catalysts exhibited higher activities contrary to the activities in the ROP where higher steric crowding gave increased activities. This can be attributed to the difference in steric demand of the different propagation mechanisms. The combination of REM-GTP and ROP to form block copolymers was investigated. Efforts to utilize the versatility of the catalyst system to produce block copolymer structures for a mechanistic crossover of GTP and ROP proved unsuccessful probably due to inadequate nucleophilicity of the Michael-type monomers used as macroinitiator. However, REM-GTP block copolymerization of 2VP with DEVP, IPOx, and DMAA with high activities were possible with 2-methoxyethylaminobis(phenolate)yttrium trimethylsilylmethyl complexes.

EXPERIMENTAL SECTION

General. All reactions were carried under an argon atmosphere using standard Schlenk or glovebox techniques. All glassware was heat-dried under vacuum prior to use. Unless otherwise stated, all chemicals were purchased from Sigma-Aldrich, Acros Organics, or ABCR and used as received. Toluene, thf, and pentane were dried using an MBraun SPS-800 solvent purification system. Hexane was dried over 3 Å molecular sieves. The precursor complex $Ln(CH_2Si(CH_3)_3)_3(thf)_2$ is prepared according to literature procedure.[17,18] The monomers, 2-vinylpyridine, diethyl vinylphosphonate, diisopropyl vinylphosphonate, 2-isopropenyl-2-oxazoline, *N*,*N*-dimethylacrylamide, and β-butyrolactone were dried over calcium hydride and distilled prior to use.

NMR spectra were recorded on a Bruker AVIII-300 spectrometer. ^1H and ^{13}C NMR spectroscopic chemical shifts δ are reported in ppm relative to the residual proton signal. δ (^1H) is calibrated to the residual proton signal and δ (^{13}C) to the carbon signal of the solvent. Deuterated solvents were obtained from Sigma-Aldrich and dried over 3 Å molecular sieves. Elemental analysis were measured at the Laboratory for Microanalysis at the Institute of Inorganic Chemistry at the Technische Universität München. ESI-MS analytical measurements were performed with methanol and isopropanol solutions on a Varian 500-MS spectrometer. GPC was carried out on a Varian LC-920 equipped with two PL Polargel columns. As eluent a mixture of THF and 6 g L^{-1} tetrabutylammonium bromide (TBAB) was used. Absolute molecular weights have been determined online by multiangle light scattering (MALS) analysis using a Wyatt Dawn Heleos II in combination with a Wyatt Optilab rEX as concentration source. GPC for poly(hydroxybutyrate) was carried out on a Polymer Laboratories GPC50 Plus chromatograph. As eluent, chloroform with 1.5 g L^{-1} tetrabutylammonium tetrafluoroborate was used. Polystyrene standards were used for calibration. *In situ* IR measurements were carried out using a Mettler−Toledo system under an argon atmosphere.

Kinetics by the Aliquots Method. After dissolving 0.14 mmol of $(ONOO)^{tBu}Y(CH_2Si(CH_3)_3)(thf)$ in 20 mL of toluene at room temperature, the corresponding amount of monomer (27 mmol) was added in one injection. Aliquots were taken from the reaction solution at regular time intervals and quenched by addition of MeOH. For each aliquot, the conversion is determined by gravimetry, and the molecular weight of the polymer is measured by GPC-MALS analysis.

Catalyst Synthesis. *General Procedure for the Synthesis of (L)Y(CH$_2$Si(CH$_3$)$_3$)(thf).* One equivalent of proligand $H_2(ONOO)^{X}$ in toluene is added to a stirred solution of $Ln(CH_2Si(CH_3)_3)_3(thf)_2$ in pentane. The resulting solution is stirred overnight at room temperature. The solvent is removed *in vacuo*, and the resulting solid is washed with pentane.

*$(ONOO)^{tBu}Y(CH_2Si(CH_3)_3)(thf)$ (**1**).* ^1H NMR (298 K, 300 MHz, C_6D_6): δ = 7.61 (m, 2H), 7.09 (m, 2H), 3.97−3.86 (m, 4H), 3.79 (m, 2H), 2.90 (m, 2H), 2.78 (s, 3H), 2.43 (m, 2H), 2.26−2.15 (m, 2H), 2.11 (s, 3H), 1.81 (s, 18H), 1.46 (s, 18H), 1.23−1.09 (m, 4H), 0.51 (s, 4H), −0.38 (m, 2H). ^{13}C NMR (298 K, 75 MHz, C_6D_6): δ = 161.67, 161.64, 136.73, 129.33, 125.65, 124.47, 124.16, 74.08, 71.88, 64.89, 61.36, 49.31, 35.65, 34.29, 32.31, 30.36, 25.58, 25.07, 4.91. EA: calculated: C 64.97, H 9.31, N 1.85; found: C 65.02, H 9.44, N 1.85.

*$(ONOO)^{CMe2Ph}Y(CH_2Si(CH_3)_3)(thf)$ (**2**).* ^1H NMR (298 K, 300 MHz, C_6D_6): δ = 7.63 (m, 2H), 7.51−7.37 (m, 8H), 7.28−7.14 (m, 8H), 7.17−7.04 (m, 2H), 7.00−6.88 (m, 2H), 6.78 (m, 2H), 3.30 (d, ^2J = 12.4 Hz, 2H), 2.96 (m, 4H), 2.72 (s, 3H), 2.48 (m, 2H), 2.38 (m, 2H), 2.07 (s, 6H), 1.95 (m, 2H), 1.78 (s, 24H), 1.05 (s, 2H), 0.47 (s, 9H), −0.82 (m, 2H). ^{13}C NMR (298 K, 75 MHz, C_6D_6): δ = 161.16, 153.15, 152.45, 136.11, 136.02, 128.29, 127.92, 127.31, 126.55, 125.85, 125.79, 124.52, 124.45, 73.76, 70.89, 63.99, 60.97, 48.93, 42.74, 32.44, 31.79, 31.66, 28.51, 25.07, 5.22. EA: calculated: C 72.81, H 7.81, N 1.39; found: C 73.10, H 7.77, N 1.57.

ASSOCIATED CONTENT

Supporting Information

Oligomer analysis and GPC data, conversion vs reaction time diagrams for DEVP, DIVP, and PIPOx, LCST behavior of P2VP, additional ^1H NMR spectra of the catalysts, DSC and TGA data. This material is available free of charge via the Internet at http://pubs.acs.org.

AUTHOR INFORMATION

Corresponding Author

*E-mail rieger@tum.de; Tel +49-89-289-13570; Fax +49-89-289-13562 (B.R.).

Notes

The authors declare no competing financial interest.

ACKNOWLEDGMENTS

The authors thank BASF SE for financial support.

ABBREVIATIONS

BL, β-butyrolactone; REM-GTP, rare earth metal-mediated group transfer polymerization; MMA , methyl methacrylate; DAVP, dialkyl vinyl phosphonates; IPOx, 2-isopropenyl-2-oxazoline; DMAA, *N*,*N*-dimethylacrylamide; 2VP, 2-vinylpyridine; RDS, rate-determining step.

REFERENCES

(1) (a) Yasuda, H.; Yamamoto, H.; Yokota, K.; Miyake, S.; Nakamura, A. *J. Am. Chem. Soc.* **1992**, *114*, 4908. (b) Collins, S.; Ward, D. G. *J. Am. Chem. Soc.* **1992**, *114*, 5460.

(2) (a) Zhang, N.; Salzinger, S.; Soller, B. S.; Rieger, B. *J. Am. Chem. Soc.* **2013**, *135*, 8810. (b) Mariott, W. R.; Chen, E. Y. X. *Macromolecules* **2005**, *38*, 6822. (c) Chen, E. Y. X. *Dalton Trans.* **2009**, 8784. (d) Chen, E. Y. X. *Chem. Rev.* **2009**, *109*, 5157. (e) Salzinger, S.; Rieger, B. *Macromol. Rapid Commun.* **2012**, *33*, 1327. (f) Rabe, G. W.; Komber, H.; Haussler, L.; Kreger, K.; Lattermann, G. *Macromolecules* **2010**, *43*, 1178. (g) Salzinger, S.; Seemann, U. B.; Plikhta, A.; Rieger, B. *Macromolecules* **2011**, *44*, 5920. (h) He, J.; Zhang, Y.; Chen, E. Y. X. *Synlett* **2014**, *25*, 1534.

(3) (a) Kaneko, H.; Nagae, H.; Tsurugi, H.; Mashima, K. *J. Am. Chem. Soc.* **2011**, *133*, 19626. (b) Hu, Y.; Wang, X.; Chen, Y.; Caporaso, L.; Cavallo, L.; Chen, E. Y. X. *Organometallics* **2013**, *32*, 1459.

(4) Fang, J.; Tschan, M. J. L.; Brule, E.; Robert, C.; Thomas, C. M.; Maron, L. *Dalton Trans.* **2013**, *42*, 9226.

(5) (a) Salzinger, S.; Soller, B. S.; Plikhta, A.; Seemann, U. B.; Herdtweck, E.; Rieger, B. *J. Am. Chem. Soc.* **2013**, *135*, 13030. (b) Zhang, Y.; Ning, Y.; Caporaso, L.; Cavallo, L.; Chen, E. Y. X. *J. Am. Chem. Soc.* **2010**, *132*, 2695.

(6) (a) Collins, S.; Ward, D. G.; Suddaby, K. H. *Macromolecules* **1994**, *27*, 7222. (b) Li, Y.; Ward, D. G.; Reddy, S. S.; Collins, S. *Macromolecules* **1997**, *30*, 1875.

(7) (a) Hayward, R. C.; Chmelka, B. F.; Kramer, E. J. *Adv. Mater.* **2005**, *17*, 2591. (b) Sun, W.; Wang, Z.; Yao, X.; Guo, L.; Chen, X.; Wang, Y. *J. Membr. Sci.* **2014**, *466*, 229. (c) Popescu, M.-T.; Korogiannaki, M.; Marikou, K.; Tsitsilianis, C. *Polymer* **2014**, *55*, 2943. (d) Klinger, D.; Wang, C. X.; Connal, L. A.; Audus, D. J.; Jang, S. G.; Kraemer, S.; Killops, K. L.; Fredrickson, G. H.; Kramer, E. J.; Hawker, C. J. *Angew. Chem., Int. Ed.* **2014**, *53*, 7018. (e) Soller, B. S.; Zhang, N.; Rieger, B. *Macromol. Chem. Phys.* **2014**, *215*, 1946−1962.

(8) (a) Tsitsilianis, C.; Voulgaris, D. *Macromol. Chem. Phys.* **1997**, *198*, 997. (b) Hückstädt, H.; Göpfert, A.; Abetz, V. *Macromol. Chem. Phys.* **2000**, *201*, 296. (c) Gohy, J.-F.; Antoun, S.; Jerome, R. *Macromolecules* **2001**, *34*, 7435. (d) Natalello, A.; Tonhauser, C.; Berger-Nicoletti, E.; Frey, H. *Macromolecules* **2011**, *44*, 9887. (e) Atanase, L. I.; Riess, G. *J. Colloid Interface Sci.* **2013**, *395*, 190. (f) Tanaka, S.; Goseki, R.; Ishizone, T.; Hirao, A. *Macromolecules* **2014**, *47*, 2333.

(9) Frauenrath, H.; Keul, H.; Hoecker, H. *Macromolecules* **2001**, *34*, 14.

(10) Miyake, G.; Caporaso, L.; Cavallo, L.; Chen, E. Y. X. *Macromolecules* **2009**, *42*, 1462.

(11) (a) Ding, K.; Miranda, M. O.; Moscato-Goodpaster, B.; Ajellal, N.; Breyfogle, L. E.; Hermes, E. D.; Schaller, C. P.; Roe, S. E.; Cramer, C. J.; Hillmyer, M. A.; Tolman, W. B. *Macromolecules* **2012**, *45*, 5387. (b) Pepels, M. P. F.; Bouyahyi, M.; Heise, A.; Duchateau, R. *Macromolecules* **2013**, *46*, 4324. (c) Wang, L.; Bochmann, M.; Cannon, R. D.; Carpentier, J.-F.; Roisnel, T.; Sarazin, Y. *Eur. J. Inorg. Chem.* **2013**, *2013*, 5896.

(12) Amgoune, A.; Thomas, C. M.; Ilinca, S.; Roisnel, T.; Carpentier, J.-F. *Angew. Chem., Int. Ed.* **2006**, *45*, 2782.

(13) (a) Jaffredo, C. G.; Carpentier, J.-F.; Guillaume, S. M. *Macromolecules* **2013**, *46*, 6765. (b) Bouyahyi, M.; Duchateau, R. *Macromolecules* **2014**, *47*, 517−524. (c) Jaffredo, C. G.; Chapurina, Y.; Guillaume, S. M.; Carpentier, J.-F. *Angew. Chem., Int. Ed.* **2014**, in press. (d) Hong, M.; Chen, E. Y. X. *Macromolecules* **2014**, *47*, 3614. (e) Du, G.; Wei, Y.; Zhang, W.; Dong, Y.; Lin, Z.; He, H.; Zhang, S.; Li, X. *Dalton Trans.* **2013**, *42*, 1278.

(14) (a) Kostakis, K.; Mourmouris, S.; Karanikolopoulos, G.; Pitsikalis, M.; Hadjichristidis, N. *J. Polym. Sci., Part A: Polym. Chem.* **2007**, *45*, 3524. (b) Ihara, E.; Morimoto, M.; Yasuda, H. *Macromolecules* **1995**, *28*, 7886. (c) Yasuda, H.; Ihara, E. *Macromol. Chem. Phys.* **1995**, *196*, 2417.

(15) Solaro, R.; Cantoni, G.; Chiellini, E. *Eur. Polym. J.* **1997**, *33*, 205.

(16) (a) Arslan, H.; Menteş, A.; Hazer, B. *J. Appl. Polym. Sci.* **2004**, *94*, 1789. (b) Arslan, H.; Hazer, B.; Kowalczuk, M. *J. Appl. Polym. Sci.* **2002**, *85*, 965. (c) Arslan, H.; Yeşilyurt, N.; Hazer, B. *J. Appl. Polym. Sci.* **2007**, *106*, 1742. (d) Nguyen, S.; Marchessault, R. H. *Macromolecules* **2004**, *38*, 290. (e) Zhang, X.; Yang, H.; Liu, Q.; Zheng, Y.; Xie, H.; Wang, Z.; Cheng, R. *J. Polym. Sci., Part A: Polym. Chem.* **2005**, *43*, 4857.

(17) Hultzsch, K. C.; Voth, P.; Beckerle, K.; Spaniol, T. P.; Okuda, J. *Organometallics* **2000**, *19*, 228.

(18) (a) Tshuva, E. Y.; Groysman, S.; Goldberg, I.; Kol, M.; Goldschmidt, Z. *Organometallics* **2002**, *21*, 662−670. (b) Amgoune, A.; Thomas, C. M.; Roisnel, T.; Carpentier, J.-F. *Chem.−Eur. J.* **2005**, *12*, 169−179.

4.6 Manuscript: Stereospecific Catalytic Precision Polymerization of 2-Vinylpyridine via Rare Earth Metal-Mediated Group Transfer Polymerization with 2-Methoxyethylamino-bis(phenolate)-Yttrium Complexes

Status	Published online: 13th August 2015
Journal	Polymer Chemistry
Publisher	RSC Publishing
Article type	Communication
DOI	DOI: 10.1039/c5py01146a
Authors	Peter T. Altenbuchner; Friederike Adams; Alexander Kronast; Eberhardt Herdtweck; Alexander Pöthig; Bernhard Rieger

Content

2-Methoxyethylamino-bis(phenolate)-yttrium complexes were employed in the catalytic precision polymerization of 2-vinylpyridine (2VP). The newly developed C_1-symmetric catalyst systems are able to isospecifically polymerize prochiral 2-vinylpyridine with moderate to high activities. The degree of tacticity of P2VP was found to depend on the steric bulk of the *ortho*-position on the phenolate rings. Tacticities ranging from atactic to isotactic can be achieved (P_m = 0.54-0.74). All tested catalyst systems follow a living type group transfer polymerization mechanism allowing precise molecular weight control with very narrow molecular weight distributions. Mechanistic studies through ^{13}C NMR microstructure analysis of the resulting isotactic P2VP show an enantiomorphic site control mechanism.

Polymer Chemistry

COMMUNICATION

View Article Online
View Journal | View Issue

Cite this: *Polym. Chem.*, 2015, **6**, 6796

Received 22nd July 2015,
Accepted 11th August 2015

DOI: 10.1039/c5py01146a

www.rsc.org/polymers

Stereospecific catalytic precision polymerization of 2-vinylpyridine *via* rare earth metal-mediated group transfer polymerization with 2-methoxyethylamino-bis(phenolate)-yttrium complexes†

P. T. Altenbuchner,[a] F. Adams,[a] A. Kronast,[a] E. Herdtweck,[b] A. Pöthig[b] and B. Rieger*[a]

2-Methoxyethylamino-bis(phenolate)-yttrium complexes were employed in the catalytic precision polymerization of 2-vinylpyridine (2VP). The C_1-symmetric catalyst systems are able to isospecifically polymerize prochiral 2-vinylpyridine with moderate to high activities. Tacticities ranging from atactic to isotactic can be achieved (P_m = 0.54–0.74). Mechanistic studies through ^{13}C NMR microstructure analysis of the resulting isotactic P2VP show an enantiomorphic site control mechanism.

Poly-(2-vinylpyridine) (P2VP) and in particular its copolymers and terpolymers have various applications in electrochemistry, optics, medicine, nano- and membrane technology due to their versatile properties regarding self-assembly and micelle formation.[1–23] Until the 1960s only radical poylmerization of 2-vinylpyridine (2VP) to atactic P2VP was possible.[24,25] The group of Natta introduced the anionic polymerization of 2VP with metallorganic compounds in the early 60s.[26,27] They were able to obtain isotactic P2VP with magnesium amides. Subsequent mechanistic studies of Soum and Fontanille with organomagnesium compounds revealed that the stereocontrol derives from a Markov-chain end control through a favoured *gauche* coordination of two monomers to the metal cation.[28–31] Apart from the mentioned examples only few groups investigated the stereospecific polymerization of 2VP.[32–36] In addition Frustrated Lewis pair,[37,38] anionic[39–44] and radical[45–48] polymerizations have been applied to synthesize functional but atactic P2VP based materials. Rare earth metal-mediated group transfer polymerization (REM-GTP) in contrast is a relatively recent polymerization method for 2VP.[21,36,49] GTP has several advantages *e.g.* strictly linear polymer growth, very narrow molecular weight distributions ($Đ$ < 1.1) and increased operation temperature of the polymerization. Recently, our group reported on the utilization of a new class of 2-methoxyethylamino-bis(phenolate)-yttrium catalysts for the homo- and copolymerization of 2VP with diethyl vinyl phosphonate (DEVP), 2-isopropenyl-2-oxazoline (IPOx), and *N*,*N*′-dimethylacrylamide (DMAA).[49] Mechanistic studies revealed a living monometallic group-transfer polymerization mechanism and kinetic studies showed the exceptional activity for the polymerization of 2VP.[49] A correlation between the steric demand of the *ortho* position in the ligand structure and the activity was observed. Less steric crowding led to higher activities, but the initially tested 2-methoxyethylamino-bis(phenolate) systems did not show any tacticity control for 2VP. However, exerting tacticity control during the polymerization is of upmost interest to adequately explore potential applications of tactic, P2VP based materials. Therefore, we focused our efforts on the structural variation of 2-methoxyethylamino-bis(phenolate)-yttrium catalysts for the stereospecific polymerization. REM-GTP of 2VP was investigated with C_1-symmetric 2-methoxyethylamino-bis(phenolate)-yttrium complexes $(ONOO)^RY(CH_2Si(CH_3)_3)(thf)$ which differ in the nature of the *ortho*- and *para*-phenolate substituents (R) (Scheme 1).

Symmetrically substituted 2-methoxyethylamino-bis(phenolate) ligands can be synthesized through modified Mannich condensation of the respective phenol with the corresponding amine.[50] The asymmetric ligands however pose a more challenging synthetic goal as their synthesis was not possible through stepwise amination and reduction sequences as previously described for symmetric, sterically more demanding 2-methoxyethylamino-bis(phenolate) ligands.[51] The synthesis was hampered by the formation of large quantities of symmetric ligand and only traces of the desired compound were obtained. Therefore, an alternative approach was develo-

[a]*WACKER-Lehrstuhl für Makromolekulare Chemie, Technische Universität München, Lichtenbergstraße 4, 85748 Garching bei München, Germany. E-mail: rieger@tum.de; http://www.makro.ch.tum.de; Fax: +49-89-289-13562; Tel: +49-89-289-13570*
[b]*Chair of Inorganic Chemistry/Molecular Catalysis, Catalysis Research Center, Technische Universität München, Ernst-Otto-Fischer-Straße 1, 85748 Garching bei München, Germany*

†Electronic supplementary information (ESI) available: Detailed procedures, GPC-MALS data, NMR spectra and crystallographic data. CCDC 1040219. For ESI and crystallographic data in CIF or other electronic format see DOI: 10.1039/c5py01146a

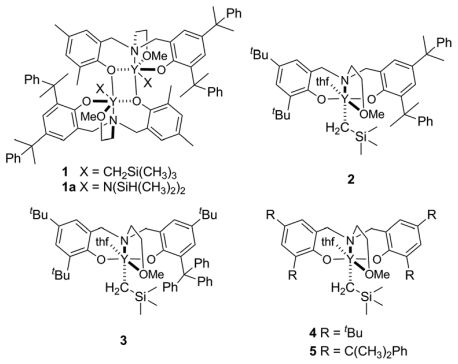

Scheme 1 2-Methoxyethylamino-bis(phenolate)-yttrium complexes (**1–5**) for the rare earth metal-mediated group-transfer polymerization of 2-vinylpyridine.

ped in which the respective aldehyde is transformed to a bromomethylphenol which subsequently can be reacted with a secondary amine to afford the desired structure in yields of 40–70% (Scheme 2). The ligands $H_2(ONOO)^R$ (L1–L3) are then reacted with one equivalent of lanthanide precursor ($Y(CH_2Si(CH_3)_3)_3(thf)_2$) in a mixture of pentane and toluene at 0 °C to generate the catalysts.

Recrystallization affords the desired complexes with the general structure $(ONOO)^RY(CH_2Si(CH_3)_3)(thf)$ (**1–3**) in good yields. The characterization was achieved by NMR spectroscopy, elemental analysis and, in case of compound **1a**, X-ray diffraction analysis. Crystals were grown through slow diffusion of pentane into a saturated THF solution at room temperature. The solid state structure supports the assumption of a dimeric structure deducted from ^{1}H NMR measurements (Fig. S3†) as was previously described for similar symmetrically substituted complexes.[51] Complexes **1–5** served as catalysts for the polymerization of 2VP in toluene at room temperature to give P2VP with very narrow molecular weight distributions (M_w/M_n = < 1.18, Table 1).

The initiation was observed *via* ^{1}H NMR and ESI-MS analysis and proceeds *via* a six-membered insertion of 2VP into the $Y–CH_2Si(CH_3)_3$ bond as was described in previous work.[36,49] REM-GTP of 2VP proceeds rapidly and the primary limitation is an inefficient initiation. Hence, the initiator efficiency (I^*) changes throughout the polymerization and to ensure comparability of the catalytic activity, I_t^* needs to be considered as the average initiator efficiency at the maximum rate of monomer conversion. Normalization of activity can be achieved by TOF/I_t^*.

The I_t^* of catalyst **1** is drastically reduced compared to the other tested compounds **2–5**. Due to its dimeric structure monomer coordination and initiation (I_t^* = 12%) are hampered. Normalized activity of catalyst **1** (410 h^{-1}) however is comparable to the activities obtained with catalyst **2** and **3** (entries 2 and 3, Table 1). Quantitative conversion is achieved after 5.5 hours and only slight broadening of the PDI to 1.18 is observed. Asymmetric catalysts **2** and **3** exhibit improved I_t^* up to 0.71–0.76 compared to compound **1** and no initiaton period for the polymerization of 2VP. These efficiencies compare well to the symmetrically substituted catalyst **5** (0.72).

Previous studies showed that complex **4** is the most active (1100 h^{-1}) catalyst for the polymerization of 2VP reported in literature and that increased steric demand (catalyst **5**, 600 h^{-1}) of the ligand led to decreased catalytic activities in the GTP of 2VP.[49] Hence, the slight decrease in activity through the introduction of increasing steric bulk (**1–3**) was to be expected. The activities of catalyst **2** and **3** remained moderate at 440 h^{-1} and 360 h^{-1} and decreased with increasing steric bulk (Fig. 1). Variations of the polymerization conditions with catalyst **3**, such as decreased temperatures (−30 °C) led to lower conversion and polymerization activity due to lower initiator efficiency (I^* = 26%) (ESI†). At −78 °C no initiation was observed. Elevated polymerization temperature of 50 °C

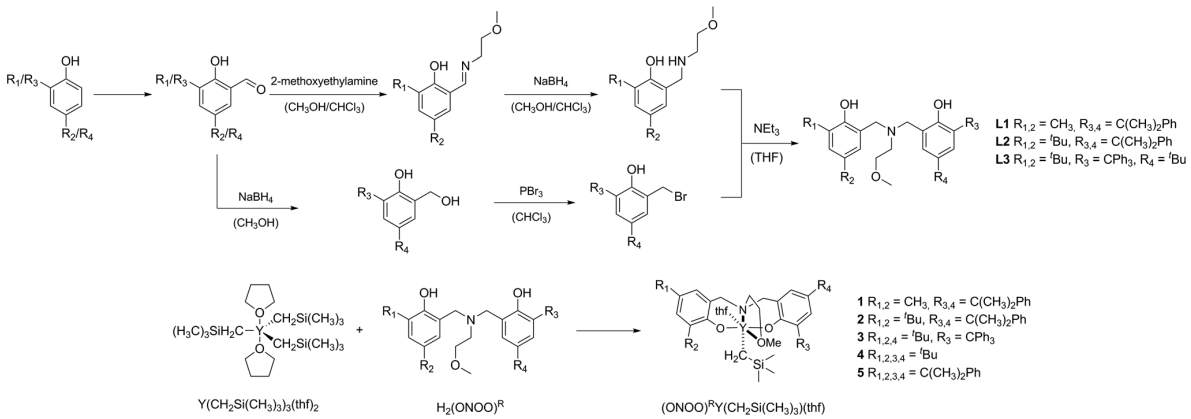

Scheme 2 Synthesis of 2-methoxyethylamino-bis(phenolate) ligands (**L1–L3**) and 2-methoxyethylamino-bis(phenolate)-yttrium trimethylsilylmethyl complexes $(ONOO)^RY(CH_2Si(CH_3)_3)(thf)$ (**1–5**).

Table 1 REM-GTP results of catalyst **1–5** of 2VP[a]

Entry	[Cat]	Time [h]	Conversion [%]	$M_{n,calc}$ (-10^4)[b] [g mol^{-1}]	$M_{n,exp}$ ($\times10^4$) [g mol^{-1}]	M_w/M_n	I_t^* [c]	P_m [d]	TOF* [e] [h^{-1}]
1	**1**	6.1	>99	2.0	13.7	1.18	0.12	0.63	410
2	**2**	2.0	>99	2.2	3.9	1.00	0.71	0.57	440
3	**3**	2.8	>99	2.0	3.3	1.06	0.76	0.74	360
4[49]	**4**	2.0	>99	2.2	2.2	1.01	0.99	0.55	1100
5[49]	**5**	1.5	>99	2.1	2.9	1.03	0.72	0.54	600

[a] Reactions performed with [2VP] = 27 mmol, [2VP]/[Cat] = 200/1, at 25 °C in 20 mL solvent, conversions determined by gravimetry and $M_{n,exp}$ determined by GPC-MALS. [b] $M_{n,calc} = M \times (([2VP]/[Cat]) \times \text{conversion})$. [c] $I_t^* = M_{n,calc}/M_{n,exp}$; I_t^* at the maximum rate. [d] P_m is the probability of *meso* linkages between monomer units and is determined by ^{13}C NMR spectroscopy. [e] TOF* = TOF/I_t^*.

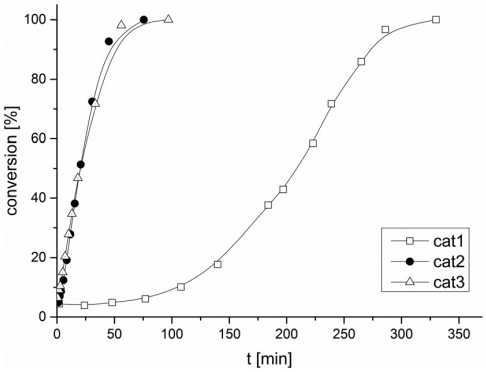

Fig. 1 Catalytic activity of catalyst **1** (hollow square), **2** (black circle) and **3** (hollow triangle) (catalyst 135 μmol, 2VP 27 mmol, toluene 20 mL, T = 25 °C).

respectively led to full conversion within 45 minutes and to an initiator efficiency (I^*) of 57% with catalyst **3**. The polymerization of 2VP was additionally conducted in coordinating solvent THF and dichloromethane. The presence of THF slowed down the polymerization significantly and only 10% conversion were achieved after 2 hours compared to full conversion in toluene and CH_2Cl_2 after the same period of time.

More importantly, the structural modifications of the 2-methoxyethylamino-bis(phenolate) ligand lead to significant alterations of the polymer microstructure of P2VP. Catalysts **1–3** are able to generate P2VP with tacticities ranging from atactic to isotactic (P_m = 0.55–0.74). Interestingly, catalyst **2** exhibits no influence on the P2VP microstructure while catalyst **1** induces a certain degree of isotacticity which translates to increased mmmm- and mmmr-pentades in the ^{13}C NMR of the aromatic quaternary carbon (P_m = 0.63; ESI†). Catalyst **3** with its bulky C_1-symmetric ligand induces the highest degree of tacticity (P_m = 0.74, Fig. 3). Solvent and temperature variations did not affect P2VP tacticity (P_m = 0.73 (THF), 0.75 (CH_2Cl_2); Table S3†).

It is the first 2-methoxyethylamino-bis(phenolate) based catalyst which is able to stereospecifically polymerize 2VP (Fig. 4). Fig. 3 depicts the direct comparison of the aromatic quaternary ^{13}C NMR resonances of P2VP generated with catalyst **3** and **4** in toluene.

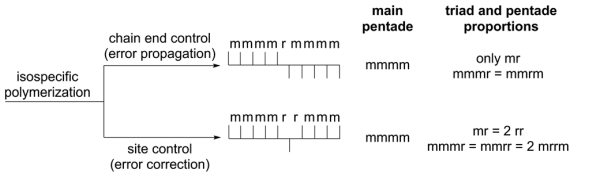

Fig. 2 Chain end control *vs.* enantiomorphic site control and the respective stereoerrors.

The pronounced increase in mmmm and mmmr pentades within the iso-region of the ^{13}C NMR highlights the substantial difference in the P2VP microstructure generated by catalyst **3**. As catalyst **3** marks a significant advancement from catalyst **4** and **5**, the origin of stereocontrol in the REM-GTP of 2VP was investigated in more detail. Defects in the pentade splitting pattern of the tactic polymer can be used for the evaluation of the polymerization mechanism. Generally, chain end control (Bernoulli, Markov) or enantiomorphic site control regime can be responsible for the tacticity control of homogeneous catalysts.[30,52,53] In case the pentade structure is adequately resolved a comparison of the respective intensities allows the deduction of the polymerization mechanism according to the principle depicted in Fig. 2. Closer examination of the pentade separation of the aromatic quaternary carbon of P2VP showed substantial overlap of the [mmmr], [mmrr], and [rmmr] signals which made the determination of integrals and the subsequent comparison of pentade proportions unfeasible (Fig. 3 and ESI†). However, on triad level an assignment and integration is possible and through the bernoullian- (1) and enantiomorphic site control triad test (2) a clear conclusion can be drawn about the prevailing mechanism of stereospecific 2VP polymerization:

$$B = \frac{4 \times [\text{mm}] \times [\text{rr}]}{[\text{mr}]^2} \quad (1)$$

$$E = \frac{2 \times [\text{rr}]}{[\text{mr}]} \quad (2)$$

The Bernoulli model triad test B, where $B = (4[\text{mm}][\text{rr}])/[\text{mr}]^2$), was considered as possibility and the calculated values are shown in Table 2. However, the obtained values are far

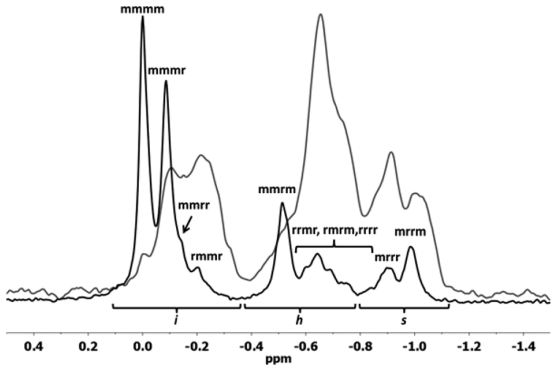

Fig. 3 Aromatic quaternary ^{13}C NMR resonances (i, h, s proportions of isotactic, heterotactic and syndiotactic) of poly(2-vinylpyridine) (30 mg P2VP in 0.6 mL CD_3OD) produced with (black) catalyst **3** and (grey) catalyst **4** ([Cat] : [2VP] = 1 : 200, [M] = 27 mmol, 20 mL toluene, 25 °C), chemical shifts are further explained in ESI.†

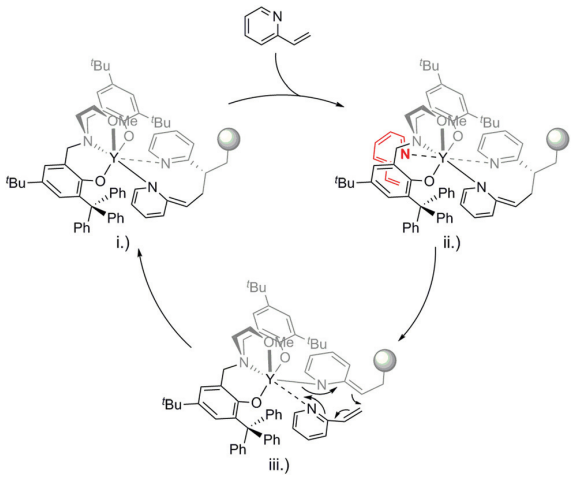

Fig. 4 Stereospecific rare earth metal-mediated GTP of 2-vinylpyridine with catalyst **3**: (i) ground state (ii) heptacoordinated intermediate (iii) 8-membered propagation.

from the theoretical value of $B = 1$ for chain end control mechanism (Table 2). Rather, the enantiomorphic site control triad test E, where $E = (2[rr])/[mr])$, gave values ranging from $E = 1.03$ to 1.07, which is very close to the theoretical value of 1 for a perfect enantiomorphic site control (Table 2). Also the theoretically calculated triad distributions compare very well with the experimentally determined (^{13}C) values. Hence, the tacticity control of the developed C_1-symmetric 2-methoxyethylaminobis-(phenolate) catalysts derives from an enantiomorphic site control mechanism (Fig. 4).

Conclusions

In conclusion, we have developed an efficient synthetic approach for the synthesis of (C_1) asymmetric 2-methoxyethylaminobis-(phenolate)-yttrium catalysts and their subsequent application in the rare earth metal-mediated GTP of 2-vinylpyridine. The polymerization exhibits a strictly living nature and very narrow molecular weight distributions were obtained (PDI < 1.18). Influence of increased, asymmetric steric bulk in *ortho* position of the catalyst on the polymerization behaviour was evaluated. Varying degrees of tactic P2VP are produced with the generated catalyst structures **1–3** (P_m = 0.54–0.75). Catalyst **3** is the first 2-methoxyethylamino-bis(phenolate) based catalyst able to produce isotactic P2VP through stereospecific polymerization of prochiral 2VP with moderate activity (360 h^{-1}). Detailed microstructural analysis of P2VP allowed mechanistic examination of the tacticity control. Bernoulli- and enantiomorphic site control triad tests were conducted and showed that the observed isoselectivity of the catalyst systems derives from an enantiomorphic site control mechanism.

Table 2 Experimental and calculated triad distributions for the aromatic quaternary carbon of P2VP[a]

	Triad distributions									
	Experimental values				Theoretical values[c]					
Catalyst	i	h	s	P_m [b]	i	h	s	B[d]	E[e]	σ[f]
1	0.44	0.37	0.19	0.63	0.45	0.37	0.18	2.44	1.03	0.755
2	0.35	0.43	0.22	0.57	0.36	0.43	0.21	1.67	1.02	0.687
3	0.61	0.26	0.13	0.74	0.61	0.26	0.13	4.69	1.00	0.846
4	0.34	0.43	0.23	0.55	0.32	0.45	0.23	1.69	1.07	0.658
5	0.31	0.45	0.24	0.54	0.34	0.44	0.22	1.47	1.07	0.673

[a] 75 mg P2VP in 0.6 mL CD_3OD; NMR AV500C, AV900C; ^{13}C NMR resonances of poly(2-vinylpyridine) produced with catalyst **1–5**, at 25 °C, ([Cat] : [2VP] = 1 : 200, [M] = 27 mmol, 20 mL toluene). [b] P_m is the probability of meso linkages between monomer units and is determined by ^{13}C NMR spectroscopy. [c] Theoretical triad distributions calculated for enantiomorphic site control model. [d] Bernoulli model triad test B, where $B = (4[mm][rr])/[mr]^2)$. [e] Enantiomorphic site control triad test E, where $E = (2[rr])/[mr])$. [f] Probability of prochiral monomer addition *via re* or *si* side of the catalyst, where $P_m = m = \sigma^2 + (1 - \sigma)^2$; $P_r = 1 - P_m$; mm = P_m^2; mr = P_mP_r; rr = P_r^2.

Acknowledgements

The authors thank BASF SE for the financial support. We thank Patrick Werz, Ignaz Höhlein, Sergei Vagin and Benedikt Soller for the valuable discussions.

Notes and references

1 H. Hückstädt, A. Göpfert and V. Abetz, *Macromol. Chem. Phys.*, 2000, **201**, 296–307.
2 M. S. Rahman, S. Samal and J.-S. Lee, *Macromolecules*, 2006, **39**, 5009–5014.
3 M. S. Rahman, S. Samal and J.-S. Lee, *Macromolecules*, 2007, **40**, 9279–9283.
4 M. A. Dyakonova, N. Stavrouli, M. T. Popescu, K. Kyriakos, I. Grillo, M. Philipp, S. Jaksch, C. Tsitsilianis and C. M. Papadakis, *Macromolecules*, 2014, **47**, 7561–7572.
5 M.-T. Popescu, M. Korogiannaki, K. Marikou and C. Tsitsilianis, *Polymer*, 2014, **55**, 2943–2951.
6 T. Higashihara, S. Ito, S. Fukuta, T. Koganezawa, M. Ueda, T. Ishizone and A. Hirao, *Macromolecules*, 2015, **48**, 245–255.
7 L. M. Bronstein, S. N. Sidorov, P. M. Valetsky, J. Hartmann, H. Cölfen and M. Antonietti, *Langmuir*, 1999, **15**, 6256–6262.
8 S. Mössmer, J. P. Spatz, M. Möller, T. Aberle, J. Schmidt and W. Burchard, *Macromolecules*, 2000, **33**, 4791–4798.
9 R. C. Hayward, B. F. Chmelka and E. J. Kramer, *Adv. Mater.*, 2005, **17**, 2591–2595.
10 M. Brautigam, P. Weyell, T. Rudolph, J. Dellith, S. Krieck, H. Schmalz, F. H. Schacher and B. Dietzek, *J. Mater. Chem. A*, 2014, **2**, 6158–6166.
11 Y. Fan, S. Tang, E. L. Thomas and B. D. Olsen, *ACS Nano*, 2014, **8**, 11467–11473.
12 D. Klinger, C. X. Wang, L. A. Connal, D. J. Audus, S. G. Jang, S. Kraemer, K. L. Killops, G. H. Fredrickson, E. J. Kramer and C. J. Hawker, *Angew. Chem., Int. Ed.*, 2014, **53**, 7018–7022.
13 S. G. Jang, E. J. Kramer and C. J. Hawker, *J. Am. Chem. Soc.*, 2011, **133**, 16986–16996.
14 S. G. Jang, D. J. Audus, D. Klinger, D. V. Krogstad, B. J. Kim, A. Cameron, S.-W. Kim, K. T. Delaney, S.-M. Hur, K. L. Killops, G. H. Fredrickson, E. J. Kramer and C. J. Hawker, *J. Am. Chem. Soc.*, 2013, **135**, 6649–6657.
15 M. R. Talingting, P. Munk, S. E. Webber and Z. Tuzar, *Macromolecules*, 1999, **32**, 1593–1601.
16 A. Bauer, S. Hauschild, M. Stolzenburg, S. Förster and C. Mayer, *Chem. Phys. Lett.*, 2006, **419**, 430–433.
17 R. P. Quirk and S. Corona-Galvan, *Macromolecules*, 2001, **34**, 1192–1197.
18 N. Hameed, J. Liu and Q. Guo, *Macromolecules*, 2008, **41**, 7596–7605.
19 M. Changez, N.-G. Kang, D. W. Kim and J.-S. Lee, *Nanoscale*, 2013, **5**, 11554–11560.
20 N.-G. Kang, B. Cho, B.-G. Kang, S. Song, T. Lee and J.-S. Lee, *Adv. Mater.*, 2012, **24**, 385–390.
21 N. Zhang, S. Salzinger, B. S. Soller and B. Rieger, *J. Am. Chem. Soc.*, 2013, **135**, 8810–8813.
22 N.-G. Kang, B.-G. Kang, H.-D. Koh, M. Changez and J.-S. Lee, *React. Funct. Polym.*, 2009, **69**, 470–479.
23 M. Changez, H.-D. Koh, N.-G. Kang, J.-G. Kim, Y.-J. Kim, S. Samal and J.-S. Lee, *Adv. Mater.*, 2012, **24**, 3253–3257.
24 S. L. Aggarwal and F. A. Long, *J. Polym Sci.*, 1953, **11**, 127–138.
25 G. E. Ham, *US Pat.*, 2643990 A 19530630, 1953.
26 G. Natta, G. Mazzanti, P. Longi, G. Dall'Asta and F. Bernardini, *J. Polym Sci.*, 1961, **51**, 487–504.
27 G. Natta, G. Mazzanti, G. Dall'asta and P. Longi, *Die Makromolekulare Chemie*, 1960, **37**, 160–162.
28 A. Soum and M. Fontanille, *Die Makromolekulare Chemie*, 1980, **181**, 799–808.
29 A. Soum and M. Fontanille, *Die Makromolekulare Chemie*, 1981, **182**, 1743–1750.
30 A. Soum and M. Fontanille, *Die Makromolekulare Chemie*, 1982, **183**, 1145–1159.
31 M. Brigodiot, H. Cheradame, M. Fontanille and J. P. Vairon, *Polymer*, 1976, **17**, 254–256.
32 K. Matsuzaki, T. Kanai, T. Matsubara and S. Matsumoto, *J. Polym. Sci., Polym. Lett. Ed.*, 1976, **14**, 1475–1484.
33 A. Dworak, W. J. Freeman and H. J. Harwood, *Polym. J.*, 1985, **17**, 351–361.
34 G. Helary, M. Fontanille, I. M. Khan and T. E. Hogen-Esch, *Die Makromolekulare Chemie*, 1989, **190**, 341–348.
35 D. K. Dimov and T. E. Hogen-Esch, *Macromolecules*, 1995, **28**, 7394–7400.
36 H. Kaneko, H. Nagae, H. Tsurugi and K. Mashima, *J. Am. Chem. Soc.*, 2011, **133**, 19626–19629.
37 J. He, Y. Zhang, L. Falivene, L. Caporaso, L. Cavallo and E. Y. X. Chen, *Macromolecules*, 2014, **47**, 7765–7774.
38 J. He, Y. Zhang and E. Y. X. Chen, *Synlett*, 2014, 1534–1538.
39 C. Tsitsilianis and D. Voulgaris, *Macromol. Chem. Phys.*, 1997, **198**, 997–1007.
40 J.-F. Gohy, S. Antoun and R. Jerome, *Macromolecules*, 2001, **34**, 7435–7440.
41 A. Natalello, C. Tonhauser, E. Berger-Nicoletti and H. Frey, *Macromolecules*, 2011, **44**, 9887–9890.
42 L. I. Atanase and G. Riess, *J. Colloid Interface Sci.*, 2013, **395**, 190–197.
43 S. Tanaka, R. Goseki, T. Ishizone and A. Hirao, *Macromolecules*, 2014, **47**, 2333–2339.
44 W. L. Jenkins, C. F. Tien and T. E. Hogen-Esch, *J. Polym. Sci., Polym. Lett. Ed.*, 1978, **16**, 501–506.
45 I. Chalari, S. Pispas and N. Hadjichristidis, *J. Polym. Sci., Part A: Polym. Chem.*, 2001, **39**, 2889–2895.
46 J. Luo, M. Li, M. Xin and W. Sun, *Macromol. Chem. Phys.*, 2015, **216**, 1646–1652.
47 A. J. Convertine, B. S. Sumerlin, D. B. Thomas, A. B. Lowe and C. L. McCormick, *Macromolecules*, 2003, **36**, 4679–4681.

48 S. Kumar, M. Changez, C. N. Murthy, S. Yamago and J.-S. Lee, *Macromol. Rapid Commun.*, 2011, **32**, 1576–1582.
49 P. T. Altenbuchner, B. S. Soller, S. Kissling, T. Bachmann, A. Kronast, S. I. Vagin and B. Rieger, *Macromolecules*, 2014, **47**, 7742–7749.
50 E. Y. Tshuva, S. Groysman, I. Goldberg, M. Kol and Z. Goldschmidt, *Organometallics*, 2002, **21**, 662–670.
51 M. Bouyahyi, N. Ajellal, E. Kirillov, C. M. Thomas and J.-F. Carpentier, *Chem. – Eur. J.*, 2011, **17**, 1872–1883.
52 N. Ajellal, M. Bouyahyi, A. Amgoune, C. M. Thomas, A. Bondon, I. Pillin, Y. Grohens and J.-F. Carpentier, *Macromolecules*, 2009, **42**, 987–993.
53 A. D. Bolig and E. Y. X. Chen, *J. Am. Chem. Soc.*, 2004, **126**, 4897–4906.

5 Summary and Outlook

In the first project of the PhD-thesis, novel amine-*bis*(phenolato)-cobalt^{II} catalysts were synthesized and evaluated for their activity in the coupling reaction of propylene oxide and carbon dioxide in combination with tetrabutylammonium bromide as cocatalyst (Scheme 1). The developed systems exhibit good activities for the formation of cyclic propylene carbonate. All catalysts were tested for their activity in the copolymerization of cyclohexene oxide and carbon dioxide as well as propylene oxide and CO_2. Catalyst [(ONNO)^{Cl}Co(II)]*(MeOH) is the first cobalt based amine-*bis*(phenolato)-based catalyst system able to polymerize CHO/CO_2. In depth stability investigations of the developed catalyst were conducted under polymerization conditions and no decomposition or *in situ* oxidation could be observed to the respective Co^{III} species which underlines the excellent stability.

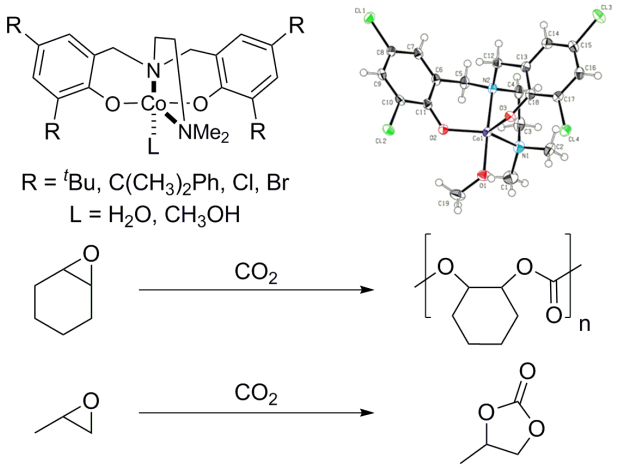

Scheme 1. Coupling and copolymerization of epoxides and carbon dioxide utilizing amine-*bis*(phenolato)-cobalt^{II} catalyst.

The second project was focused on elucidating the mechanism of the stereoselective ring-opening polymerization of racemic β-butyrolactone with rare earth metal 2-methoxyethyl-aminobis(phenolate) catalysts (Scheme 2). The influence of the metal ionic radius on polymerization activity and tacticity was investigated and a correlation between decreasing polymerization activity and stereoselectivity with increasing metal ionic radius was found. Temperature dependent activity measurements correlated with DFT calculations enabled to uncover the step-by-step mechanism of the ring-opening polymerization and rationalized the observed stereoselectivities with the employed catalysts.

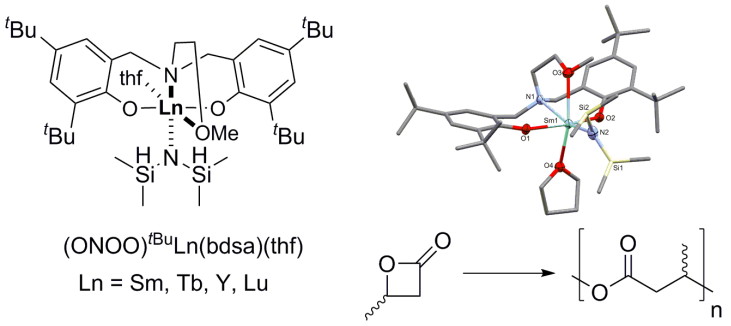

Scheme 2. Stereoselective ring-opening polymerization of *rac*-β-butyrolactone with 2-methoxyethyl-aminobis(phenolate) catalysts (Sm, Tb, Y, Lu).

The last project investigated the development of homogeneous single-site nonmetallocene catalysts for the rare earth metal-mediated group transfer polymerization of *Michael*-type monomers such as dialkyl vinylphosphonates, 2-vinylpyridine, isopropenyloxazoline and *N,N*-dimethylacrylamide (Scheme 3). 2-Methoxyethylaminobis(phenolate)-yttrium catalysts with varying steric demand were synthesized and tested for the REM-GTP. They showed moderate to high activities in the polymerization experiments (DMAA>2VP~IPOX>DEVP>DIVP) and steric crowding proofed to be disadvantageous to enhancing the activity. Mechanistic investigations revealed that 2-methoxyethylamino-bis(phenolate)-yttrium catalysts follow a living monometallic group transfer mechanism allowing for precise molecular weight control and the production of blockcopolymers.

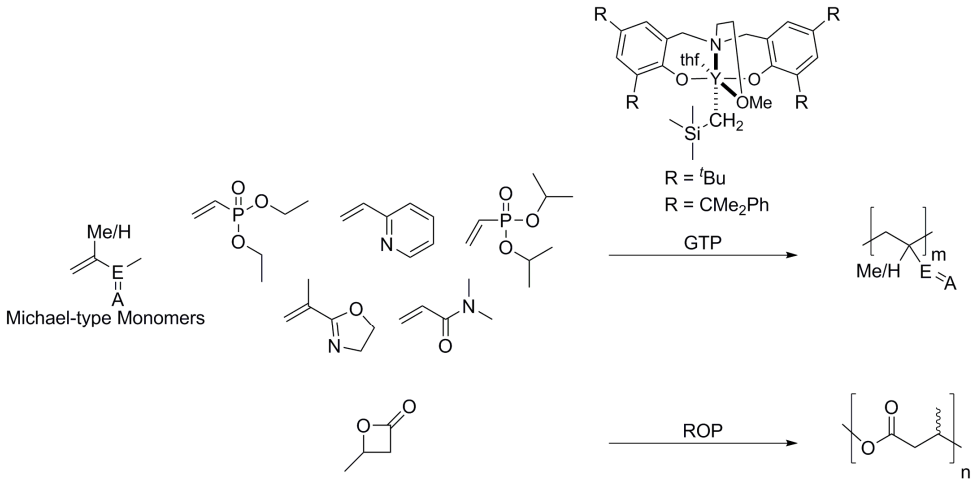

Scheme 3. Rare earth metal-mediated group transfer polymerization of *Michael*-type monomers with 2-methoxyethylaminobis(phenolate)-yttrium catalysts.

Temperature dependent reaction kinetics were performed to rationalize the observed differences between sterically less and more demanding catalysts.

Attempts to produce blockcopolymer structures from an *in situ* combination of REM-GTP and ROP did only result in the formation of homopolymers.

Based on the versatile 2-methoxyethylamino-bis(phenolate) framework catalyst structures capable of exerting significant control over the polymer microstructure of poly(2-vinylpyridine) were developed (Scheme 4). These catalysts retain the advantageous characteristics of REM-GTP such as the living fashion of the polymerization and very narrow molecular weight distributions while a completely new level of complexity is unlocked through microstructure control. In addition, the origin of the tacticity control was elucidated through mechanistic studies utilizing high resolution ^{13}C NMR spectroscopy. Experimental and calculated triad distribution tests evidence that the induced stereocontrol stems from an enantiomorphic site control.

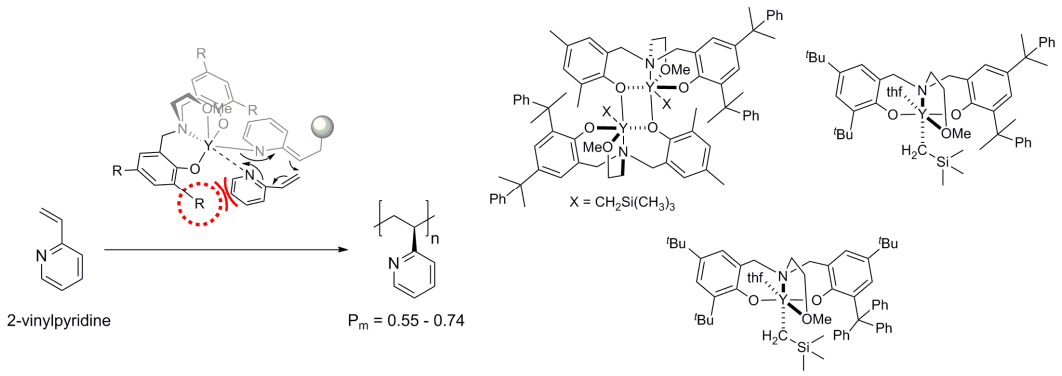

Scheme 4 Stereospecific Catalytic Precision Polymerization of 2-Vinylpyridine via Rare Earth Metal-Mediated Group Transfer Polymerization with 2-Methoxyethylamino-bis(phenolate)-Yttrium Complexes.

In conclusion, the investigations presented in this PhD-thesis pave the way towards new catalyst systems based on bisphenolate ligand structures in three major areas of research: carbon dioxide utilization, synthesis of biodegradable polyesters and the catalytic precision polymerization of polar monomers.

The synthesis of highly stable and highly active Co(II) systems for the copolymerization of epoxides and carbon dioxide can be based on the developed system. Incorporation of structural features from already established Co(III) catalysts might enable activity increases and in combination with the enhanced stability of Co(II) under polymerization conditions could result in a palpable reduction of catalyst costs.

Mechanistic investigations and kinetic studies paired with DFT calculations pinpoint possible pathways towards isospecific polymerization of *rac*-BL. This so far unachievable goal could be reached by rare earth metal bisphenolate systems and the conclusions drawn from the mechanistic investigations. A targeted approach can be made towards a defined single-site catalyst capable of producing isoenriched polyhydroxybutyrate.

The introduction of highly active 2-methoxyethyl-aminobis(phenolate)-yttrium catalysts to the rare earth metal-mediated group transfer polymerization enables access to the vast potential of nitrogen containing monomers e.g. 2-vinylpyridine. P2VP and in particular its copolymers and terpolymers have various applications in electrochemistry, optics, medicine, nano- and membrane technology due to their properties regarding self-assembly and micelle formation. Tactic P2VP generated by REM-GTP is therefore of upmost interest to adequately explore the applications of P2VP based materials. Homopolymer and more importantly copolymer structures with vinylphosphonates can have a major impact in applications such as self assembly, electronics and biomedical applications (e.g. drug delivery) due to their versatile properties (amphiphilic, pH-switchable, tunable LCST).

6 Publications Beyond the Scope of this Thesis

6.1 Carbon Dioxide as C-1 Block for the Synthesis of Polycarbonates

Status	Published online: 13th January 2014
Book	Transformation and Utilization of Carbon Dioxide
Publisher	Springer
Article type	Review Article
DOI	10.1007/978-3-642-44988-8_7
Authors	Peter T. Altenbuchner; Stefan Kissling; Bernhard Rieger

Abstract

The chapter summarizes the recent developments in catalyst synthesis, polymer analytics and material properties of polycarbonates produced from carbon dioxide and epoxides. The physical behaviour of the two most important and well researched polycarbonates: poly(propylene carbonate) (PPC) and poly(cyclohexene carbonate) (PCHC) do not meet the desired characteristics of structure polymers, yet. Terpolymerization, blending, end-capping and increasing the molecular weight are just a few examples which are more closely covered in this chapter and could be methods for adjusting PPC and PCHC properties. NMR analytics are one of the mayor analytical tools for the characterization of the polymer microstructure and are also included in this chapter. Today, the focus for homogeneous catalysts is shifting towards sustainable and cheap metals e.g. magnesium and zinc. Studies with heterogeneous and homogeneous structures indicate a strong dependence of the activity on the distance between the metal sites. Bimetallic systems try to exploit this correlation. Kinetic studies supported by DFT calculations have been performed, which support the hypothesis and show up new ways towards even higher activities in the copolymerization of carbon dioxide and epoxides.

6.2 Mechanistic Aspects of a Highly Active Dinuclear Zinc Catalyst for the Copolymerization of Epoxides and CO_2

Status	Published online: 20th April 2015
Journal	Chemistry – A European Journal
Publisher	Wiley-VCH Verlag GmbH & Co. KGaA
Article type	Full Paper
DOI	10.1002/chem.201406055
Authors	Stefan Kissling; Peter T. Altenbuchner; Maximilian W. Lehenmeier; Eberhardt Herdtweck; Peter Deglmann; Uwe B. Seemann; Bernhard Rieger

Abstract

The dinuclear zinc complex reported by us is to date the most active zinc catalyst for the co-polymerization of cyclohexene oxide (CHO) and carbon dioxide. However, co-polymerization experiments with propylene oxide (PO) and CO_2 revealed surprisingly low conversions. Within this work, we focused on clarification of this behavior through experimental results and quantum chemical studies. The combination of both results indicated the formation of an energetically highly stable intermediate in the presence of propylene oxide and carbon dioxide. A similar species in the case of cyclohexene oxide/CO_2 co-polymerization was not stable enough to deactivate the catalyst due to steric repulsion.

6.3 Dinuclear Zinc Catalysts with Unprecedented Activities for the Copolymerization of Cyclohexene Oxide and CO_2

Status	Published online: 10th February 2015
Journal	Chemical Communications
Publisher	RSC Publishing
Article type	Communication
DOI	10.1039/C5CC00784D
Authors	Stefan Kissling; Maximilian W. Lehenmeier; Peter T. Altenbuchner; Alexander Kronast; Marina Reiter; Peter Deglmann; Uwe B. Seemann; Bernhard Rieger

RIEGER *Cem Commun* 2015 DOI 10.1039/C5CC00784D. Abstract reproduced with permission of the Royal Society of Chemistry.

Abstract

A variety of new dinuclear zinc catalysts was developed and tested for the copolymerization of cyclohexene oxide and carbon dioxide. Electron-withdrawing groups thereby led to unprecedented activities with turnover frequencies up to 155 000 h^{-1}. These are by far the highest polymerization rates ever reported for the copolymerization of cyclohexene oxide and CO_2.

6.4 Zinc-Catalyzed Transformation of Carbon Dioxide

Status	Published online: 6th February 2015
Book	Zinc Catalysis: Applications in Organic Synthesis
Publisher	Wiley-VCH Verlag GmbH & Co. KGaA
Article type	Review Article
DOI	10.1002/9783527675944.ch8
Authors	Stefan Kissling; Peter T. Altenbuchner; Teemu Niemi; Timo Repo; Bernhard Rieger

Abstract

This chapter gives an overview of the already existing systems and recent trends in the catalysis of copolymerization of epoxides and carbon dioxide using zinc-based catalysts. The zinc-catalyzed copolymerization of epoxides and carbon dioxide to polycarbonates is supposed to proceed *via* a bimetallic mechanism. Functionalized epoxides have been directly applied in the copolymerization with carbon dioxide. Catalysts used by the chemical industry to produce cyclic carbonates from carbon dioxide include organotin and organoantimony compounds. The two main synthetic strategies for this transformation are cycloaddition of CO_2 and epoxides, and cyclization of diols and carbon dioxide. The chapter covers recent developments in zinc-catalyzed synthesis of cyclic carbonate utilizing carbon dioxide as a chemical feedstock. It explores the scope of the synthetic methodologies as well as the effect of reaction condition. In addition, the reaction mechanisms for these zinc catalysts are surveyed.

6.5 Flexibly Tethered Dinuclear Zinc Complexes: A Solution to the Entropy Problem in CO_2/Epoxide Copolymerization Catalysis?

Status	Published online: 19th July 2013
Journal	Angewandte Chemie International Edition
Publisher	Wiley-VCH Verlag GmbH & Co. KGaA
Article type	Communication
DOI	10.1002/anie.201302157
Authors	Maximilian W. Lehenmeier; Stefan Kissling; Peter T. Altenbuchner; Christian Bruckmeier; Peter Deglmann; Anna-Katharina Brym; Bernhard Rieger

Abstract

The authors report the first dinuclear zinc catalyst which shows a shift in the rate-determining step from ring opening of the epoxide to carbon dioxide insertion for the copolymerization of cyclohexene oxide and carbon dioxide. The reason for this behavior is the similarity of the activation barriers of the ring opening and insertion reactions, which is achieved by linking the two active centers with a flexible tether. These attributes lead to very high activities for the copolymerization reaction. To achieve even higher activities, according to our study, an additional decrease of the activation energy of the ring-opening step is necessary. The match between experimental and theoretical results delivers a tool for further catalyst development. Currently, modifications of these catalysts is under investigation.

7 Appendix

7.1 Supporting Information: Amine-bis(phenolato)cobalt(II) Catalysts for the Formation of Organic Carbonates from Carbon Dioxide and Epoxides

Status	Published online: 27th February 2015
Journal	European Journal of Inorganic Chemistry
Publisher	Wiley-VCH Verlag GmbH & Co. KGaA
Article type	Full paper
DOI	10.1002/ejic.201403087
Authors	Marina Reiter;* Peter T. Altenbuchner;* Stefan Kissling; Eberhardt Herdtweck; Bernhard Rieger

*Contributed equally

Eur. J. Inorg. Chem. **2015** · ISSN 1099–0682

SUPPORTING INFORMATION

DOI: 10.1002/ejic.201403087
Title: Amine-bis(phenolato)cobalt(II) Catalysts for the Formation of Organic Carbonates from Carbon Dioxide and Epoxides
Author(s): Marina Reiter, Peter T. Altenbuchner, Stefan Kissling, Eberhardt Herdtweck, Bernhard Rieger*

TABLE OF CONTENT

1. Single Crystal X-Ray Determination

General: Data were collected on an X-ray single crystal diffractometer equipped with a CCD detector (Bruker APEX II, κ-CCD), a fine-focus sealed tube with MoK_α radiation (λ = 0.71073 Å), and a graphite monochromator by using the APEX 2 software package. [1] The measurements were performed on a single crystal coated with perfluorinated ether. The crystal was fixed on the top of a cactus prickle and transferred to the diffractometer. The crystal was frozen under a stream of cold nitrogen. A matrix scan was used to determine the initial lattice parameters. Reflections were merged and corrected for Lorenz and polarization effects, scan speed, and background using SAINT. [2] Absorption corrections, including odd and even ordered spherical harmonics were performed using SADABS. [2] Space group assignments were based upon systematic absences, E statistics, and successful refinement of the structures. Structures were solved by direct methods with the aid of successive difference Fourier maps, [1] and were refined against all data using SHELXL-97[3] in conjunction with SHELXLE. [4] If not mentioned otherwise, non-hydrogen atoms were refined with anisotropic displacement parameters. Hydrogen atoms were placed in ideal positions using the SHELXL riding model. Full-matrix least-squares refinements were carried out by minimizing Σw(Fo2-Fc2)2 with SHELXL-97 [3] weighting scheme. Neutral atom scattering factors for all atoms and anomalous dispersion corrections for the non-hydrogen atoms were taken from International Tables for Crystallography. [6] Images of the crystal structures were generated by PLATON. [5]

[1] APEX suite of crystallographic software. “APEX 2” Version 2008.4. Bruker AXS Inc., Madison, Wisconsin, USA (2008).

[2] SAINT, Version 7.56a and SADABS Version 2008/1. Bruker AXS Inc., Madison, Wisconsin, USA (2008).

[3] Sheldrick, G. M. "SHELXL-97", University of Göttingen, Göttingen, Germany, (1998).

[4] Huebschle, C. B.; Sheldrick, G. M.; Dittrich, B. (2011). “SHELXLE” J. Appl. Cryst., 44, (2011) 1281 - 1284.

[5] Spek, A. L. "PLATON", A Multipurpose Crystallographic Tool, Utrecht University, Utrecht, The Netherlands, (2010).

[6] International Tables for Crystallography, Vol. C, Tables 6.1.1.4 (pp. 500-502), 4.2.6.8 (pp. 219-222), and 4.2.4.2 (pp. 193-199), Wilson, A. J. C., Ed., Kluwer Academic Publishers, Dordrecht, The Netherlands, 1992.

Special: Compound 2 (CCDC 1018316)

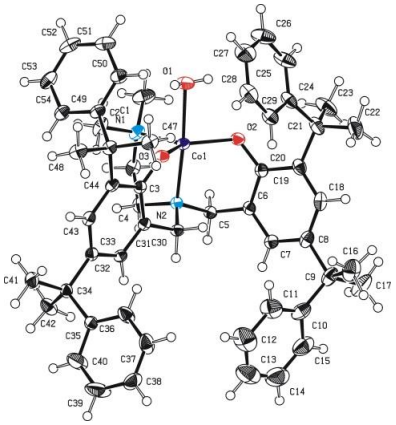

Crystal data

$C_{54}H_{64}CoN_2O_3$	
M_r = 848.00	D_x = 1.216 Mg m^{-3}
Monoclinic, $P2_1/n$	Melting point: ? K
Hall symbol: -P 2yn	Mo $K\alpha$ radiation, λ = 0.71073 Å
a = 17.6630 (5) Å	Cell parameters from 9533 reflections
b = 10.8393 (3) Å	θ = 2.1–25.4°
c = 24.3282 (6) Å	μ = 0.42 mm^{-1}
β = 96.0267 (11)°	T = 123 K
V = 4632.0 (2) Å^3	Fragment, purple
Z = 4	0.36 × 0.36 × 0.25 mm
F(000) = 1812	

Data collection

Bruker APEX-II CCD diffractometer	8501 independent reflections
Radiation source: fine-focus sealed tube	7704 reflections with $I > 2\sigma(I)$
graphite	R_{int} = 0.022
Detector resolution: 16 pixels mm^{-1}	θ_{max} = 25.4°, θ_{min} = 2.1°
phi– and ω–rotation scans	h = −21 21
Absorption correction: multi-scan *SADABS*, Bruker, 2008b	k = −13 13
T_{min} = 0.704, T_{max} = 0.745	l = −29 29

101028 measured reflections	

Refinement

Refinement on F^2	Secondary atom site location: difference Fourier map
Least-squares matrix: full	Hydrogen site location: inferred from neighbouring sites
$R[F^2 > 2\sigma(F^2)]$ = 0.028	H atoms treated by a mixture of independent and constrained refinement
$wR(F^2)$ = 0.074	Weighting scheme based on measured s.u.'s $w = 1/[\sigma^2(F_o^2) + (0.0343P)^2 + 2.3881P]$ where $P = (F_o^2 + 2F_c^2)/3$
S = 1.02	$(\Delta/\sigma)_{max}$ = 0.001
8501 reflections	$\Delta\rho_{max}$ = 0.29 e Å^{-3}
559 parameters	$\Delta\rho_{min}$ = −0.27 e Å^{-3}
0 restraints	Extinction correction: none
0 constraints	
Primary atom site location: structure-invariant direct methods	

Compound 3 (CCDC 1018317)

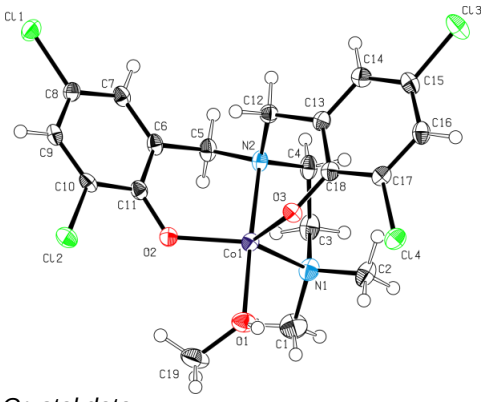

Crystal data

$C_{19}H_{22}Cl_4CoN_2O_3{\cdot}CH_4O$	V = 2416.32 (13) Å^3
M_r = 559.16	Z = 4
Monoclinic, $P2_1/c$	Mo $K\alpha$ radiation
a = 12.7311 (4) Å	μ = 1.18 mm^{-1}
b = 12.3138 (4) Å	T = 123 K
c = 16.0769 (5) Å	0.50 × 0.30 × 0.30 mm
β = 106.519 (2)°	

Data collection

Bruker APEX-II CCD diffractometer	4482 independent reflections
Absorption correction: multi-scan *SADABS*, Bruker, 2008b	4293 reflections with i > 2σ(i)
T_{min} = 0.655, T_{max} = 0.745	R_{int} = 0.021
85815 measured reflections	θ_{max} = 25.5°

Refinement

$R[F^2 > 2\sigma(F^2)]$ = 0.020	0 restraints
$wR(F^2)$ = 0.052	H atoms treated by a mixture of independent and constrained refinement
S = 1.08	$\Delta\rho_{max}$ = 0.26 e Å^{-3}
4482 reflections	$\Delta\rho_{min}$ = −0.29 e Å^{-3}
292 parameters	

Compound 4 (CCDC 1018318)

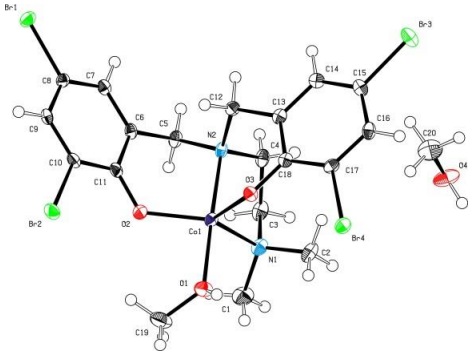

Crystal data

$C_{19}H_{22}Br_4CoN_2O_3{\cdot}CH_4O$	?
M_r = 736.96	D_x = 1.947 Mg m^{-3}
Monoclinic, $P2_1/c$	Melting point: ? K
Hall symbol: -P 2ybc	Mo $K\alpha$ radiation, λ = 0.71073 Å
a = 12.7792 (4) Å	Cell parameters from 9244 reflections
b = 12.4962 (4) Å	θ = 1.7–25.4°
c = 16.5676 (5) Å	μ = 7.07 mm^{-1}
β = 108.1372 (14)°	*T* = 100 K
V = 2514.25 (14) Å^3	Plate, violet
Z = 4	0.46 × 0.30 × 0.10 mm
F(000) = 1436	

Data collection

Bruker APEX-II CCD diffractometer	4622 independent reflections
Radiation source: fine-focus sealed tube	4332 reflections with $I > 2\sigma(I)$
graphite	R_{int} = 0.032
Detector resolution: 16 pixels mm^{-1}	θ_{max} = 25.4°, θ_{min} = 1.7°
phi– and ω–rotation scans	*h* = −15 15
Absorption correction: multi-scan *SADABS*, Bruker, 2008b	*k* = −15 15
T_{min} = 0.427, T_{max} = 0.745	*l* = −20 19
83080 measured reflections	

Refinement

Refinement on F^2	Secondary atom site location: difference Fourier map
Least-squares matrix: full	Hydrogen site location: inferred from neighbouring sites
$R[F^2 > 2\sigma(F^2)]$ = 0.015	H atoms treated by a mixture of independent and constrained refinement
$wR(F^2)$ = 0.038	Weighting scheme based on measured s.u.'s $w = 1/[\sigma^2(F_o^2) + (0.0156P)^2 + 2.281P]$ where $P = (F_o^2 + 2F_c^2)/3$
S = 1.09	$(\Delta/\sigma)_{max}$ = 0.001
4622 reflections	$\Delta\rho_{max}$ = 0.31 e Å^{-3}
289 parameters	$\Delta\rho_{min}$ = −0.42 e Å^{-3}
0 restraints	Extinction correction: none
0 constraints	
Primary atom site location: structure-invariant direct methods	

2. ^{1}H NMR SPECTRA OF COMPLEX 3·MEOH, COMPLEX 3·ACETONE, COMPLEX 4·MEOH AND COMPLEX 2·H_2O

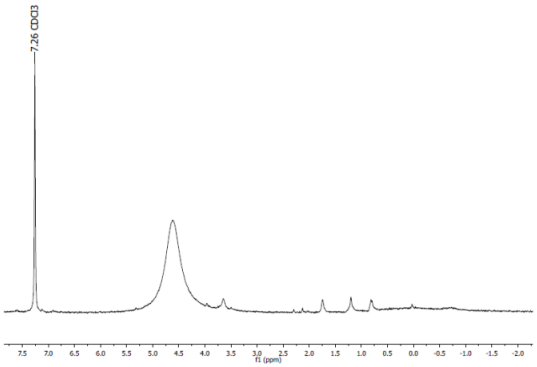

Figure S1. ^{1}H NMR spectrum of catalyst 3·MeOH in $CDCl_3$.

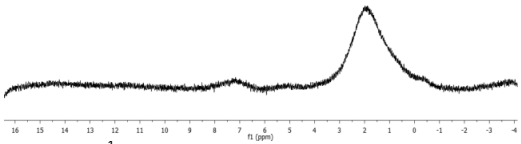

Figure S2. ^{1}H NMR spectrum of catalyst 3·Acetone in $CDCl_3$.

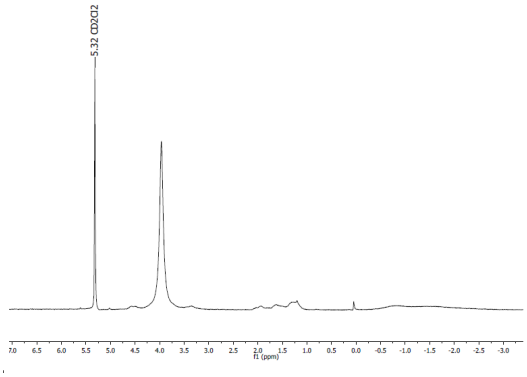

Figure S3. ^{1}H NMR spectrum of catalyst 4·MeOH in CD_2Cl_2.

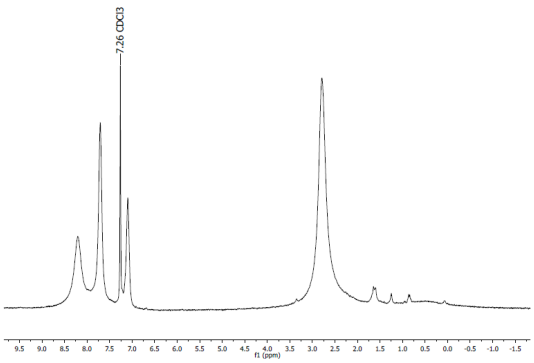

Figure S4. ^{1}H NMR spectrum of catalyst 2·H_2O in $CDCl_3$.

3. SYNTHESIS OF COMPLEX 3·ACETONE

Complex 3·Acetone. Orange pulver was obtained from a saturated acetone solution of compound 3·MeOH at room temperature.

Anal. Calcd for $C_{21}H_{24}CoCl_4N_2O_3$; C, 45,60; H, 4,37; N, 5.06. Found: C, 45,22; H, 4,14; N, 5,31. ESI-MS: 495.3 g/mol $[M- C_3H_6O+H]^+$. μ_{eff} ($CDCl_3$, 298 K) = 4.4μ_B. IR (neat): ũ [cm^{-1}] = 742(s), 857(s), 934(w), 955(w), 1022(m), 1106(w), 1171(m), 1218(m), 2177(m), 1315(m), 1390(s), 1429(s), 1453(s), 1582(w), 1710(m) (v(C=O)), 2847(w), 2891(s).

4. ESI-MS MEASUREMENTS

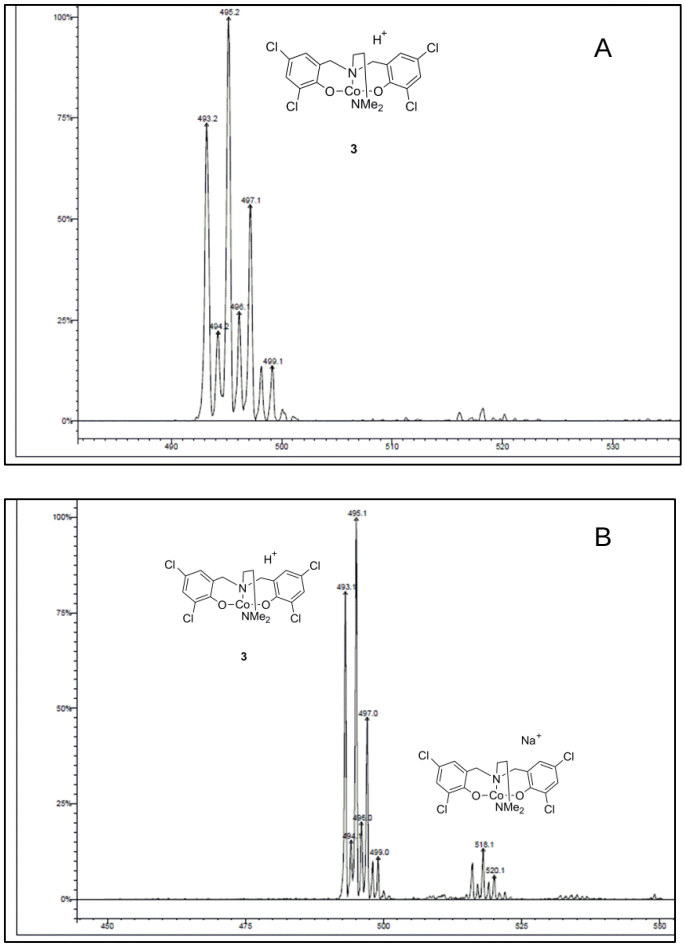

Figure S5. ESI-MS in MeCN of the complex A) before copolymerization B) after copolymerization (catalyst loading of 1:1:100 (cat 3·MeOH:DMAP:CHO) at 80°C and 50 bar CO_2).

5. ENDGROUP ANALYSIS

5.1 POLYMERS PRODUCED BY CATALYST 3·MEOH

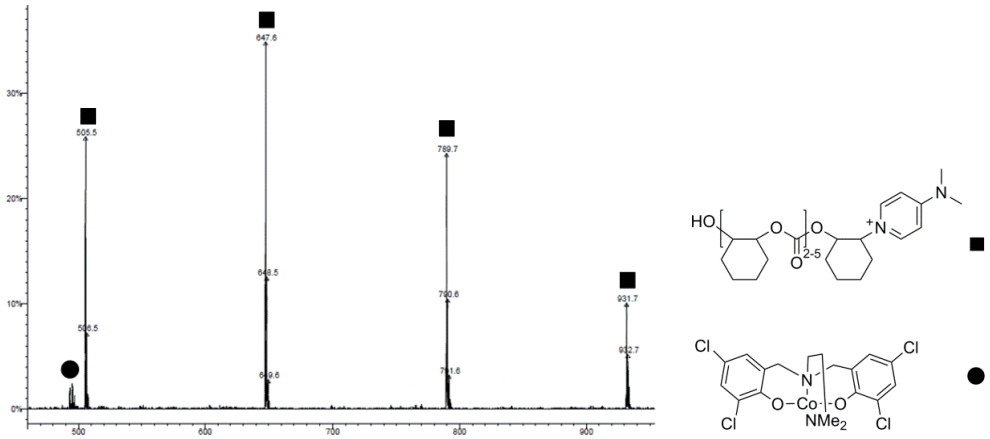

Figure S6. ESI-MS of the oligomer produced with catalyst 3·MeOH at a catalyst loading of 1:1:100 (3·MeOH:DMAP:CHO) at 80°C and 50 bar CO_2.

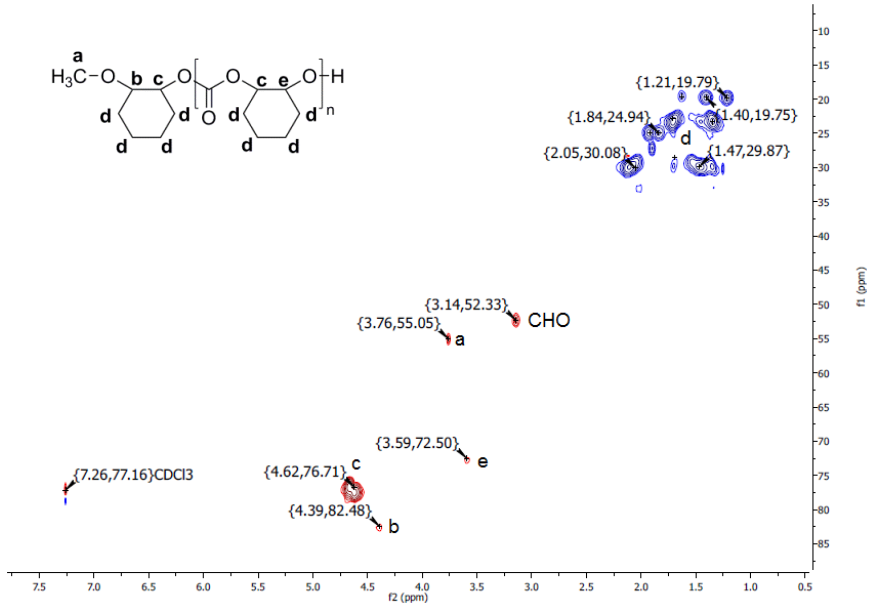

Figure S7. HSQC NMR of PCHC produced by complex 3·MeOH (Table 3, Entry 1, 1:1:500 (3·MeOH:DMAP:CHO)) at 80°C and 50 bar CO_2.

5.2 POLYMERS PRODUCED BY CATALYST 3·ACETONE

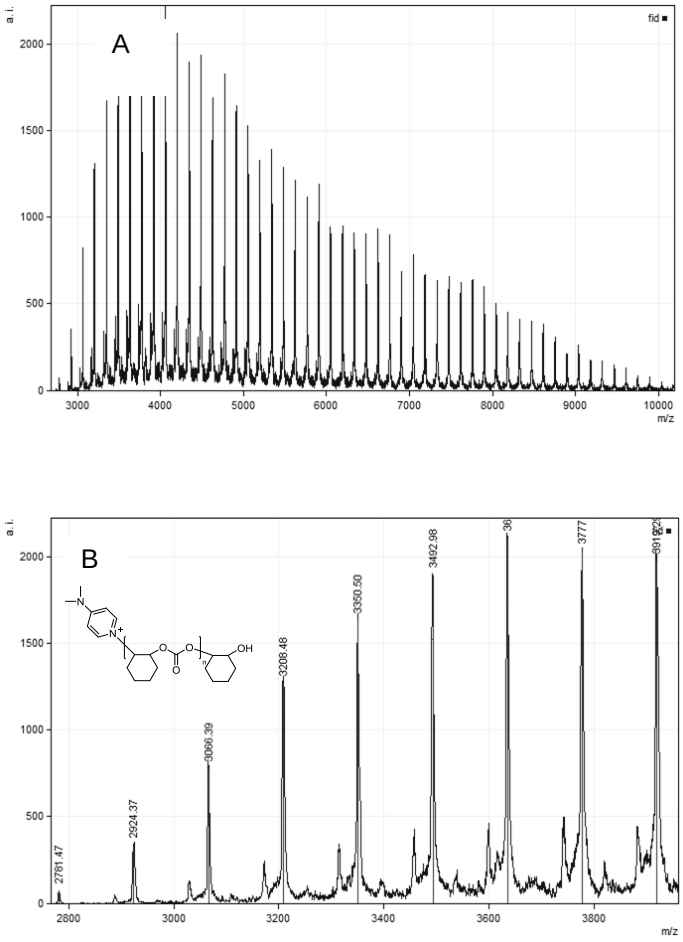

Figure S8. (A) MALDI-TOF MS of PCHC produced according to Table 3, Entry 5 (1:1:500, 3·Acetone: DMAP:CHO, 80 °C, 50 bar CO_2). (B) Labeled section of MALDI spectrum A (2780-3950 g/mol) with modeled polymer chain containing a DMAP initiating group.

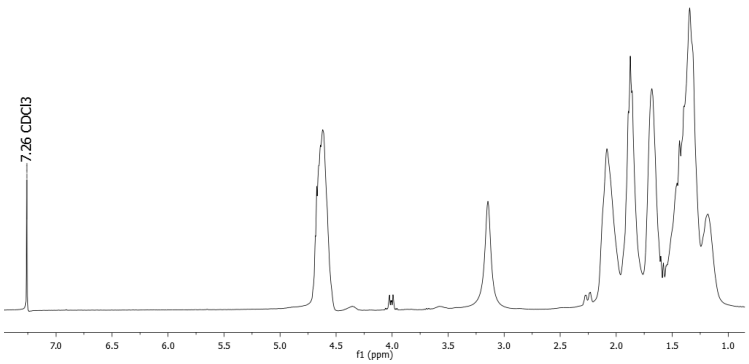

Figure S9. ^{1}H NMR of the polycarbonate catalyzed by 3·Acetone (1:1:500, 3·Acetone: DMAP:CHO; 80°C, 50 bar CO_2), (298 K, $CDCl_3$, 500 MHz).

6. General kinetic considerations in the production of cyclic carbonate

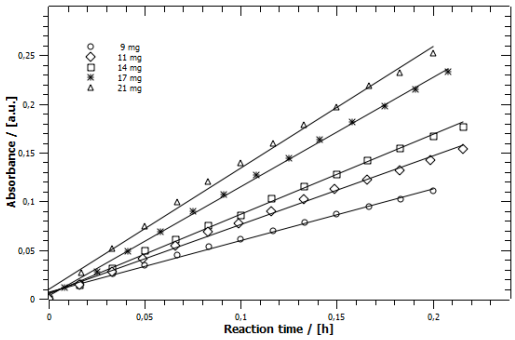

Figure S10. Determination of catalyst/cocatalyst reaction order for the formation of cPC at 60 °C, 30 bar

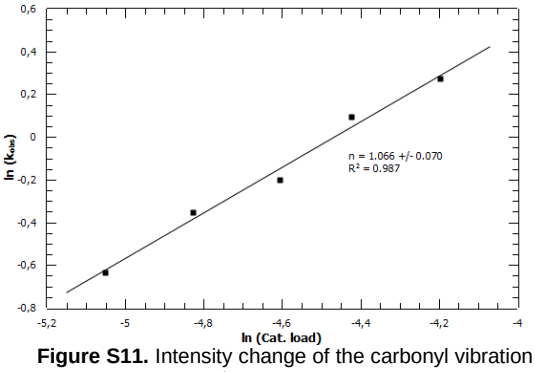

Figure S11. Intensity change of the carbonyl vibration band at 1797 cm^{-1} of cyclic propylene carbonate against time at different loadings of catalyst 3.

To understand the underlying mechanism of the formation of cyclic propylene carbonate for an amine-*bis*-(phenolato)cobalt(II) system, kinetic studies were performed in the in situ ATR-IR. As shown in Figure S8, the logarithmic dependency of the reaction rate on the catalyst/co-catalyst loading resulted in a reaction order of 1.07, however, our preliminary kinetic investigations did not allow further discrimination between the respective contribution of either part, the catalyst and the co-catalyst.

Kinetic Studies. Copolymerization experiments with in situ monitoring were performed using a React-IR/MultiMax four-autoclave system (Mettler-Toledo). 50 mL steel autoclaves equipped with a diamond window, a mechanic stirring and a heating device were heated under vacuum to 130 °C over night prior to use. The required amount of catalyst and co-catalyst were dissolved in 5 mL PO in a vial equipped with an injection septum and afterwards rapidly transferred into the reactor using a syringe. The reactor was pressurized to 30 bar and heated to 60 °C, while the pressure was rising to 39 bar. After 14 hours the autoclave was cooled down and the amount of cyclic propylene carbonate was determined by weight.

7. GPC MEASUREMENTS

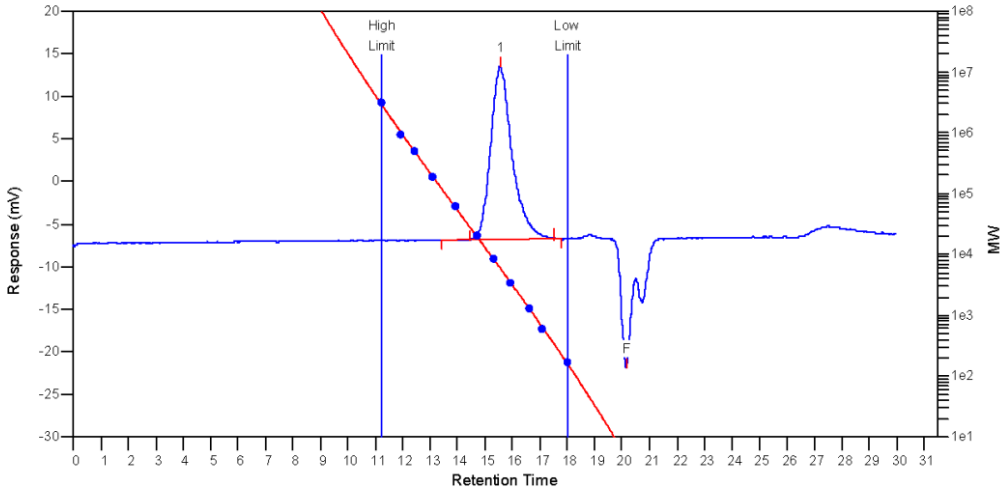

MW Averages

Peak No	Mp	Mn	Mw	Mz	Mz+1	Mv	PD
1	5936	3974	5880	7648	9436	5623	1.47962
2	0	0	0	0	0	0	0

Figure S12. GPC result for PCHC synthesized with catalyst 3·MeOH (3·MeOH/CHO = 1:500, cat/DMAP = 1, 18 h, 80 °C, 50 bar CO_2) (Table 3, Entry 1).

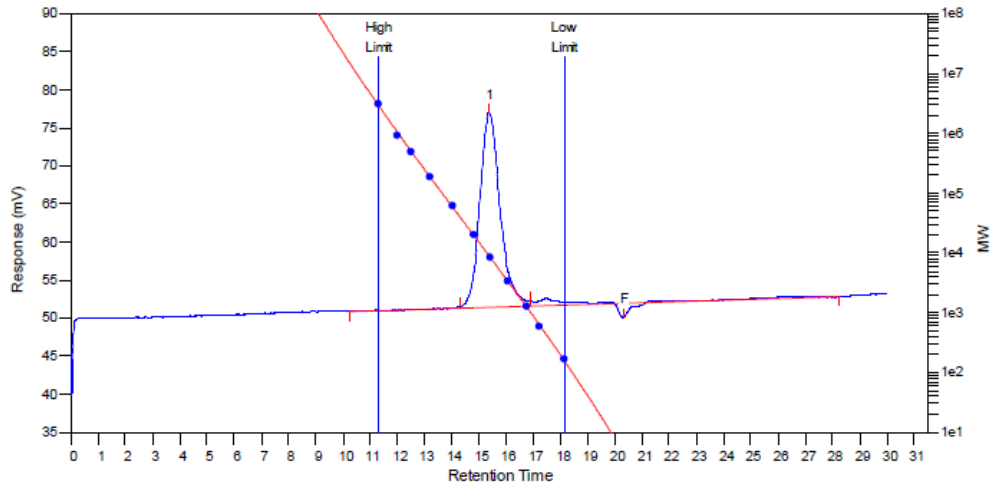

MW Averages

Peak No	Mp	Mn	Mw	Mz	Mz+1	Mv	PD
1	9041	6743	9104	11502	14090	8762	1.35014
2	0	0	0	0	0	0	0

Figure S13. GPC result for PCHC synthesized with catalyst 3·Acetone (3·Acetone/CHO= 1:500, cat/DMAP = 1, 18 h, 80 °C, 50 bar CO_2) (Table 3, Entry 5).

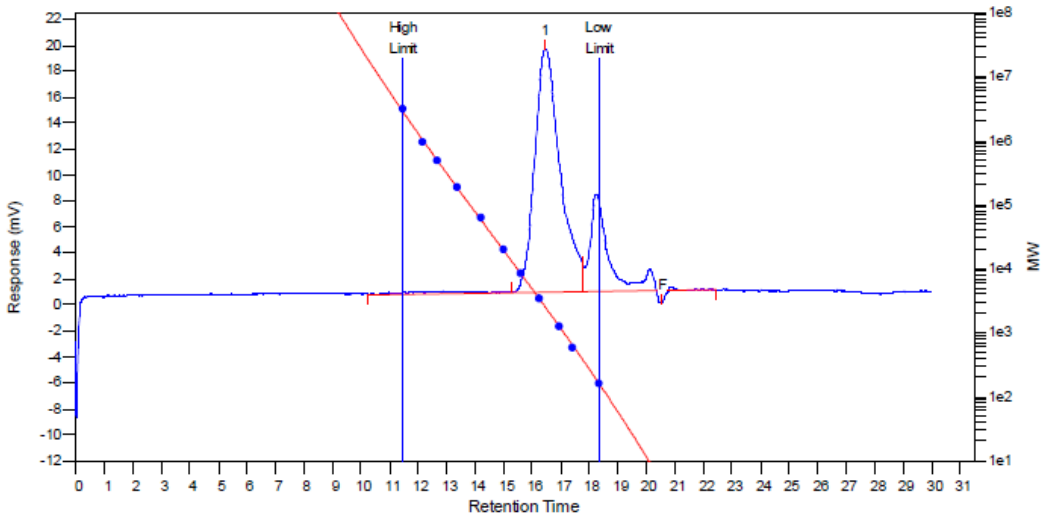

MW Averages

Peak No	Mp	Mn	Mw	Mz	Mz+1	Mv	PD
1	2484	1641	2450	3338	4248	2324	1.49299
2	0	0	0	0	0	0	0

Figure S14. GPC result for PCHC synthesized with catalyst 3·MeOH (3·MeOH/CHO = 1:500, cat/DMAP = 1/3, 18 h, 80 °C, 50 bar) (Table 3, Entry 2).

8. SUSCEPTIBILITY MEASUREMENTS (EVANS' NMR METHOD)

Table S1: Solution magnetic moment of catalyst 3·MeOH in $CDCl_3$ with and without one equivalent DMAP.

Entry	Solvent	DMAP	CHO	Temperature	Conditions	CO_2 [bar]	μ_{eff} [μ_B]
1	$CDCl_3$	No	No	RT	Air	0	4.3
2	$CDCl_3$	DMAP	No	RT	Air	0	4.3

Table S2: Solution magnetic moment of catalyst 3·MeOH in $C_2D_2Cl_4$ with DMAP and CHO (1:1:10) under argon conditions over 15 hours at 80°C.

Entry	Solvent	DMAP	CHO	Temperature [°C]	Conditions	Time [h]	CO_2 [bar]	μ_{eff} [μ_B]
1	$C_2D_2Cl_4$	DMAP	CHO	RT	Argon	0	0	4.3
2	$C_2D_2Cl_4$	DMAP	CHO	80	Argon	1	0	4.3
3	$C_2D_2Cl_4$	DMAP	CHO	80	Argon	15	0	4.3

Table S3: Solution magnetic moment of catalyst 3·MeOH in $C_2D_2Cl_4$ with DMAP and CHO (1:1:10), pressurized with 1 bar CO_2 over 21 hours at 80°C.

Entry	Solvent	DMAP	CHO	Temperature [°C]	Conditions	Time [h]	CO_2 [bar]	μ_{eff} / [μ_B]
1	$C_2D_2Cl_4$	DMAP	CHO	RT	Argon	0	0	4.3
2	$C_2D_2Cl_4$	DMAP	CHO	RT	Argon	0	1	4.3
3	$C_2D_2Cl_4$	DMAP	CHO	80	Argon	0	1	4.3
4	$C_2D_2Cl_4$	DMAP	CHO	80	Argon	1	1	4.3
5	$C_2D_2Cl_4$	DMAP	CHO	80	Argon	2	1	4.3
6	$C_2D_2Cl_4$	DMAP	CHO	80	Argon	3	1	4.3
7	$C_2D_2Cl_4$	DMAP	CHO	80	Argon	4	1	4.3
8	$C_2D_2Cl_4$	DMAP	CHO	80	Argon	5	1	4.3
9	$C_2D_2Cl_4$	DMAP	CHO	80	Argon	6	1	4.3
10	$C_2D_2Cl_4$	DMAP	CHO	80	Argon	7	1	4.3
11	$C_2D_2Cl_4$	DMAP	CHO	80	Argon	21	1	4.3

Table S4: Solution magnetic moment of catalyst 3·MeOH in $C_2D_2Cl_4$ with DMAP and CHO (1:1:10) under air, pressurized with 1 bar CO_2 over 21 hours at 80°C.

Entry	Solvent	DMAP	CHO	Temperature [°C]	Conditions	Time [h]	CO_2 [bar]	μ_{eff} / [μ_B]
1	$C_2D_2Cl_4$	DMAP	CHO	RT	Air	0	0	4.3
2	$C_2D_2Cl_4$	DMAP	CHO	80	Air	21	1	4.2

Table S5: Solution magnetic moment of catalyst 3·MeOH in $C_2D_2Cl_4$ with DMAP and CHO (1:1:10), pressurized with 50 bar CO_2 over 15 hours at 80°C.

Entry	Solvent	DMAP	CHO	Temperature [°C]	Conditions	Time [h]	CO_2 [bar]	μ_{eff} / [μ_B]
1	$C_2D_2Cl_4$	DMAP	CHO	RT	Argon	0	0	4.3
2	$C_2D_2Cl_4$	DMAP	CHO	80	Argon	15	50	4.3

Table S6: Solution magnetic moment of catalyst 3·MeOH in $CDCl_3$ with 3 equivalents $AgNO_3$ over 24 hours at 40 °C.

Entry	Solvent	DMAP	CHO	Temperature [°C]	Conditions	Time [h]	CO_2 [bar]	μ_{eff} / [μ_B]
1	$CDCl_3$	no	no	40	Air	0	0	4.3
2	$CDCl_3$	no	no	40	Air+$AgNO_3$	5	0	4.2
3	$CDCl_3$	no	no	40	Air+$AgNO_3$	24	0	3.5

Table S7: Solution magnetic moment of catalyst 1 in $CDCl_3$ with 3 equivalents $AgNO_3$ over 24 hours at 40 °C.

Entry	Solvent	DMAP	CHO	Temperature [°C]	Conditions	Time [h]	CO_2 [bar]	μ_{eff} / [μ_B]
1	$CDCl_3$	no	no	40	Air	0	0	3.7
2	$CDCl_3$	no	no	40	Air+$AgNO_3$	5	0	3.4
3	$CDCl_3$	no	no	40	Air+$AgNO_3$	24	0	-

Magnetic measurements in solution were performed using Evan´s method on a Bruker AVIII-300 spectrometer with a coaxial insert (Wilmad).[7,8] $CDCl_3$ and $C_2D_2Cl_4$ were used as solvent and TMS as reference.

Figure S15. Copolymerization experiment with catalyst 3·MeOH in an autoclave immediately after CO_2 release and opening of the autoclave (3·MeOH/CHO = 1:500, cat/DMAP = 1, 18 h, 80 °C, 50 bar).

[7] E. M. Schubert, *J. Chem. Educ.* **1992**, *69*, 62.

[8] D. F. Evans, *J. Chem. Soc.* **1959**, 2003-2005.

7.2 Supporting Information: Mechanistic Investigations of the Stereoselective Rare Earth Metal-Mediated Ring-Opening Polymerization of β-Butyrolactone

Status	Published online: 11th August 2015
Journal	Chemistry – A European Journal
Publisher	Wiley-VCH Verlag GmbH & Co. KGaA
Article type	Full paper
DOI	DOI: 10.1002/chem.201501156
Authors	Peter T. Altenbuchner; Alexander Kronast; Stefan Kissling; Sergei I. Vagin; Eberhardt Herdtweck; Alexander Pöthig; Peter Deglmann; Robert Loos; Bernhard Rieger

Supporting Information

1. General Information

Molecular weight determination (GPC)

GPC for Polyhydroxybutyrate samples was carried on a Polymer Laboratories GPC50 Plus chromatograph. As eluent, chloroform with 1.5 g L^{-1} tetrabutylammonium tetrafluoroborate was used. Polystyrene standards were used for calibration.

Activity Measurements and Kinetic Analysis in the *in situ* ATR-IR

For activity measurements, the stated amount of catalyst is dissolved in 5 mL of dry dichloromethane in the glovebox, the reaction mixture is transferred into the *in situ* IR autoclave and the temperature adjusted. Then, the stated amount of monomer is added*via* a syringe. During the course of the experiment the temperature is kept at isotherm (±2 K). After the stated reaction time, the reaction is quenched by addition of hydrous chloroform (0.5 mL) and an aliquot is taken to determine the conversion. The polymer is precipitated in excess methanol, filtered off and dried under vacuum.

TGA-measurements

TGA is carried out on a Texas Instruments TGA-Q5000 with a heating rate of 10 K/min.

DSC measurements

DSC analysisof polymer samplesis carried out on a TA Instruments DSC-Q2000 with heating rates of 5 and 10 K/min.

2. Kinetic Measurements and Eyring-Plots

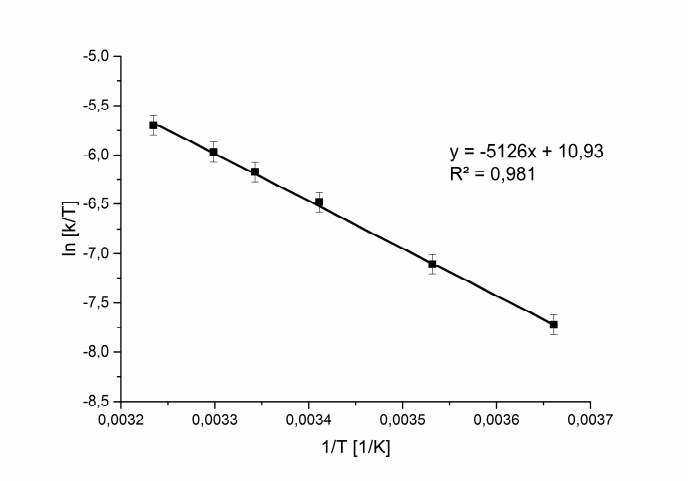

Figure S 1 Eyring-Plot for (ONOO)$^{t\text{Bu}}$Y(N(SiH(CH$_3$)$_2$)$_2$)(thf) (20.3 µmol), BL (14.9 mmol), CH$_2$Cl$_2$ (5 mL), temperature (0 – 36 °C).

Table S 1 Temperature dependent kinetics for (ONOO)$^{t\text{Bu}}$Y(N(SiH(CH$_3$)$_2$)$_2$)(thf) (20.3 µmol), BL (14.9 mmol), CH$_2$Cl$_2$ (5 mL), temperature (0 – 36 °C)

T [°C]	ln(k/T)	c(cat) in [mol/L]	n(cat) in [mmol]	1/T [1/K]
0	-7.723430	0.003134	0.02029	0.00366
10	-7.107724	0.003134	0.02029	0.003531
20	-6.48082	0.003134	0.02029	0.003411
26	-6.17364	0.003134	0.02029	0.003234
30	-5.971246	0.003134	0.02029	0.003298
36	-5.69717	0.003134	0.02029	0.003595

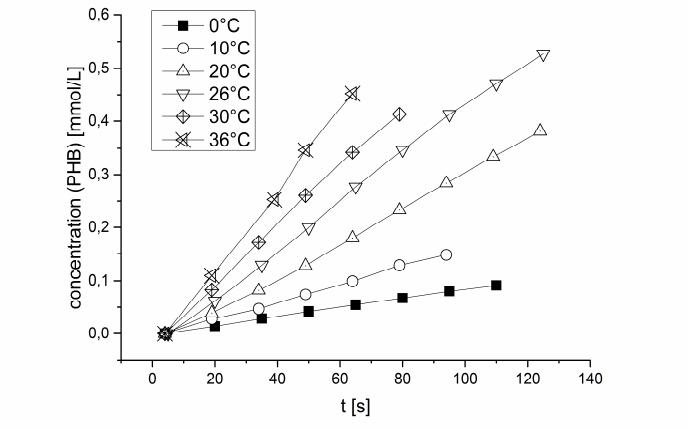

Figure S 2Initial slope of PHB concentration over time: Catalyst 3 (20.3 µmol), BL (14.9 mmol), CH$_2$Cl$_2$ (5 mL), temperature (0 – 36 °C).

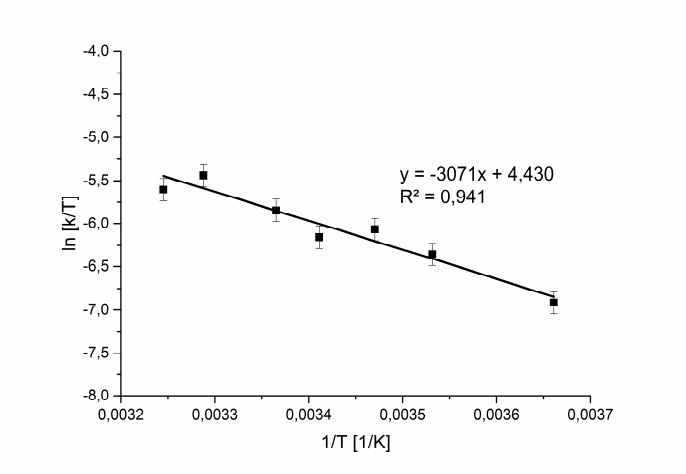

Figure S 3 Eyring-Plot for (ONOO)^{tBu}Lu(N(SiH(CH$_3$)$_2$)$_2$)(thf) (20.3 µmol), BL (14.9 mmol), CH_2Cl_2 (5 mL), temperature (0 – 35 °C).

Table S 2 Temperature dependent kinetics for (ONOO)^{tBu}Lu(N(SiH(CH$_3$)$_2$)$_2$)(thf) (20.3 µmol), BL (14.9 mmol), CH_2Cl_2 (5 mL), temperature (0 – 35 °C)

T [°C]	c(cat) in [mol/L]	n(cat) in [mmol]	1/T [1/K]	ln(k/T)
0	0.003125	0.02024	0.0036610	-6.914729
10	0.003125	0.02024	0.0035317	-6.356631
15	0.003125	0.02024	0.0034704	-6.067925
20	0.003125	0.02024	0.0034112	-6.157890
24	0.003125	0.02024	0.0033653	-5.846309
31	0.003125	0.02024	0.0032879	-5.438691
35	0.003125	0.02024	0.0032452	-5.604176

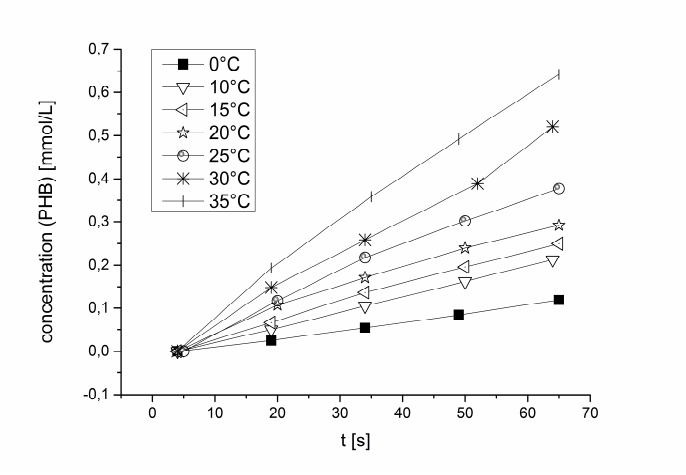

Figure S 4Initial slope of PHB concentration over time: Catalyst 4 (20.3 µmol), BL (14.9 mmol), CH_2Cl_2 (5 mL), temperature (0 – 35 °C).

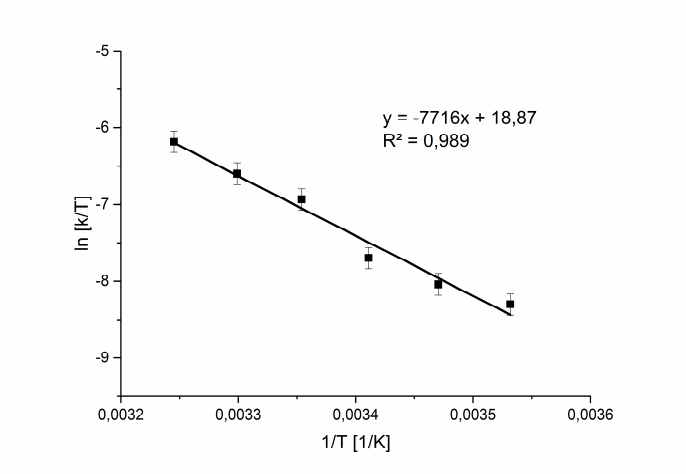

Figure S 5 Eyring-Plot for (ONOO)$^{t\text{Bu}}$Tb(N(SiH(CH$_3$)$_2$)$_2$)(thf) (20.3 µmol), BL (14.9 mmol), CH_2Cl_2 (5 mL), temperature (10 – 35 °C).

Table S 3 Temperature dependent kinetics for (ONOO)$^{t\text{Bu}}$Tb(N(SiH(CH$_3$)$_2$)$_2$)(thf) (20.3 µmol), BL (14.9 mmol), CH_2Cl_2 (5 mL), temperature (10 – 35 °C)

T [°C]	c(cat) [mol/L]	n(cat) [mmol]	1/T [1/K]	ln(k/T)
10	0.003130	0.02027	0.0035317	-8.3027
15	0.003130	0.02027	0.00347041	-8.04026
20	0.003130	0.02027	0.00341122	-7.7016
25	0.003130	0.02027	0.00335	-6.93381
30	0.003130	0.02027	0.0032987	-6.59807
35	0.003130	0.02027	0.00324517	-6.18621

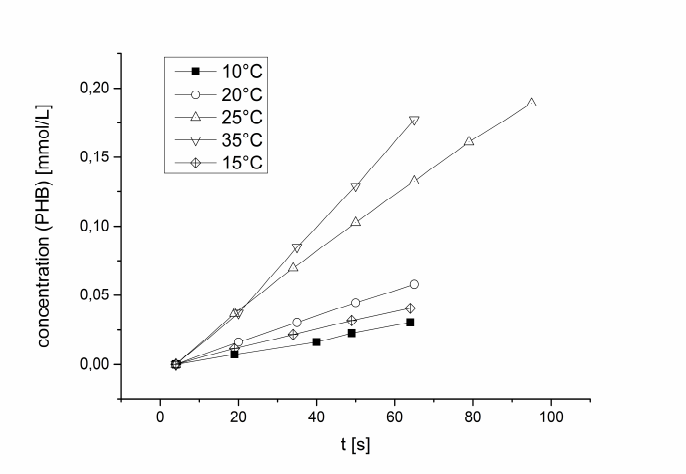

Figure S 6Initial slope of PHB concentration over time: Catalyst 2 (20.3 µmol), BL (14.9 mmol), CH_2Cl_2 (5 mL), temperature (10 – 35 °C).

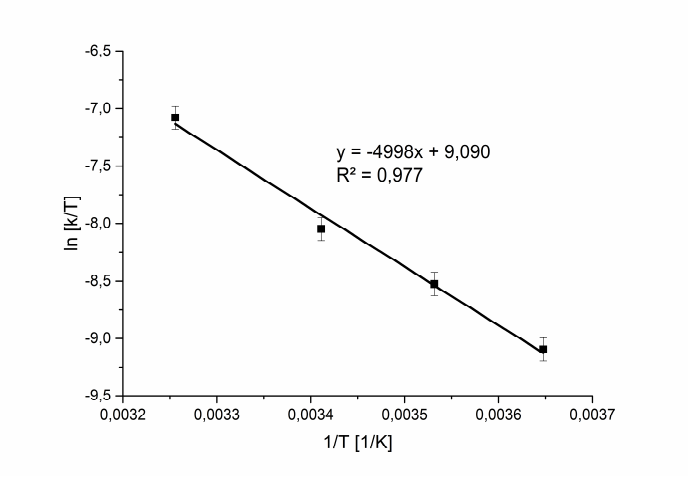

Figure S 7 Eyring-Plot for (ONOO)^{tBu}Sm(N(SiH(CH$_3$)$_2$)$_2$)(thf) (60.7 µmol), BL (14.9 mmol), CH_2Cl_2 (5 mL), temperature (1 – 34 °C).

Table S 4 Eyring-Plot for (ONOO)^{tBu}Sm(N(SiH(CH$_3$)$_2$)$_2$)(thf) (60.7 µmol), BL (14.9 mmol), CH_2Cl_2 (5 mL), temperature (1 – 34 °C)

T [°C]	c(cat) in [mol/L]	n(cat) in [mmol]	1/T [1/K]	ln(k/T)
1	0.009376	0.060723	0.003647	-9.094102239
10	0.009376	0.060723	0.003531	-8.524200301
20	0.009376	0.060723	0.003411	-8.047094986
34	0.009376	0.060723	0.003255	-7.081166039

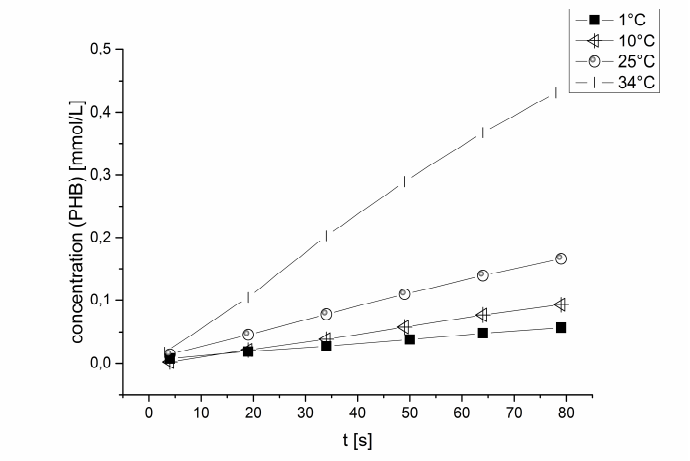

Figure S 8Initial slope of PHB concentration over time: Catalyst 1 (60.7 µmol), BL (14.9 mmol), CH_2Cl_2 (5 mL), temperature (1 – 34 °C).

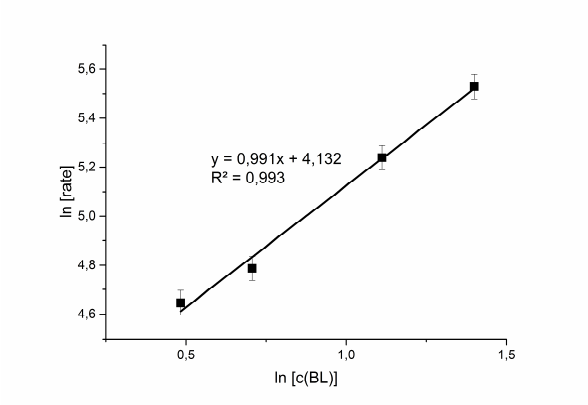

Figure S 9 Determination of monomer order (ONOO)$^{t\text{Bu}}$Y(N(SiH(CH$_3$)$_2$)$_2$)(thf) (10 – 24 mmol of BL, 20 µmol of catalyst, 5 mL CH_2Cl_2, 20 °C).

Table S 5 Determination of monomer order (ONOO)$^{t\text{Bu}}$Y(N(SiH(CH$_3$)$_2$)$_2$)(thf) (10 – 24 mmol of BL, 20 µmol of catalyst, 5 mL CH_2Cl_2, 20 °C)

ln(rate)	c(PHB) in [mmol/Ls]	c(cat) in [mmol/L]	ln(c(BL))
4.7866	0.00346546	0.003136	0.70639241
5.2396	0.00507636	0.003136	1.11185752
5.5294	0.00658424	0.003136	1.39953959
4.6463	0.00282244	0.003136	0.48345443

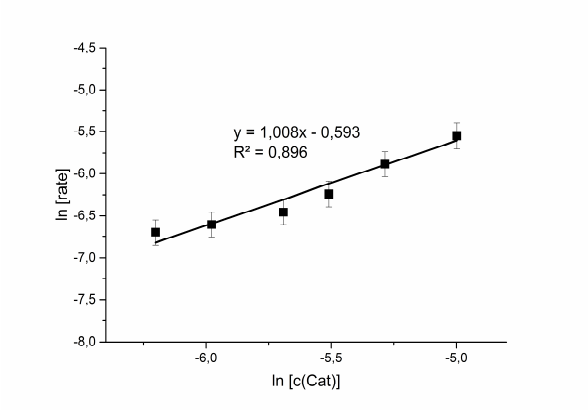

Figure S 10 Determination of catalyst order (ONOO)^{tBu}Y(N(SiH(CH$_3$)$_2$)$_2$)(thf) (12 – 41 µmol of catalyst, 14.9 mmol BL, 5 mL CH_2Cl_2 20 °C).

Table S 6. Determination of catalyst order (ONOO)^{tBu}Y(N(SiH(CH$_3$)$_2$)$_2$)(thf) (12 – 41 µmol of catalyst, 14.9 mmol BL, 5 mL CH_2Cl_2 20 °C)

ln(rate)	c(BL) in [mmol/L]	n(cat) in [mmol/L]	ln[c(BL)]
-6.6077	0.00253	0.0152	-5.9775
-6.7012	0.00202	0.0121	-6.2013
-5.7856	0.00506	0.0304	-5.2850
-5.5493	0.00675	0.0405	-4.9982
-6.3422	0.00405	0.0243	-5.5090
-6.5071	0.00337	0.0202	-5.6908

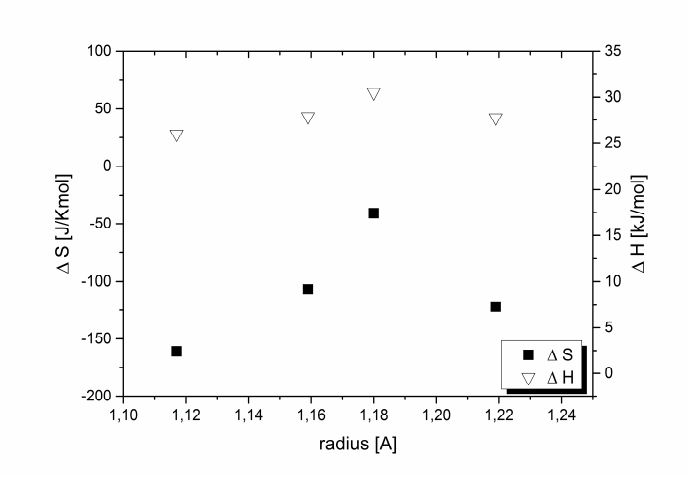

Figure S 11Measured enthalpies $\Delta H^{\ddagger}$ and entropies$\Delta S^{\ddagger}$ for catalysts 1 - 4 (Sm, Tb, Y, Lu).

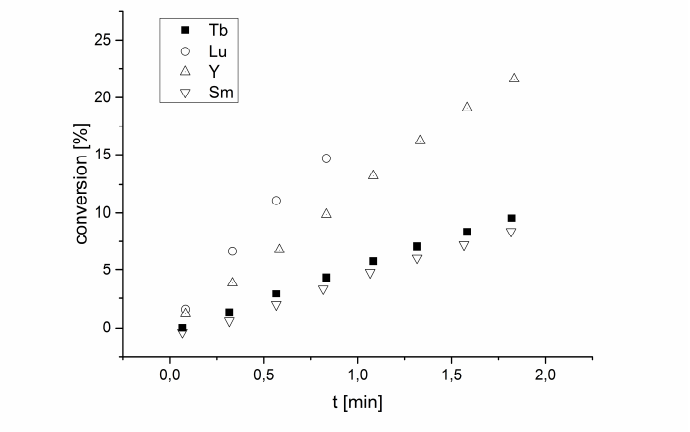

Figure S 12Determination of catalytic activity of $(ONOO)^{tBu}Ln(N(SiH(CH_3)_2)_2)(thf)$ catalysts for the ROP of BL at 298 K, [M] = 14.9 mmol, 5 mL CH_2Cl_2 (Table 1); Catalyst 1 (Sm): [Cat] = 60.7 µmol; Catalysts 2 – 4 (Tb, Y, Lu): [Cat] = 20.3 µmol.

3. Additional Analytics

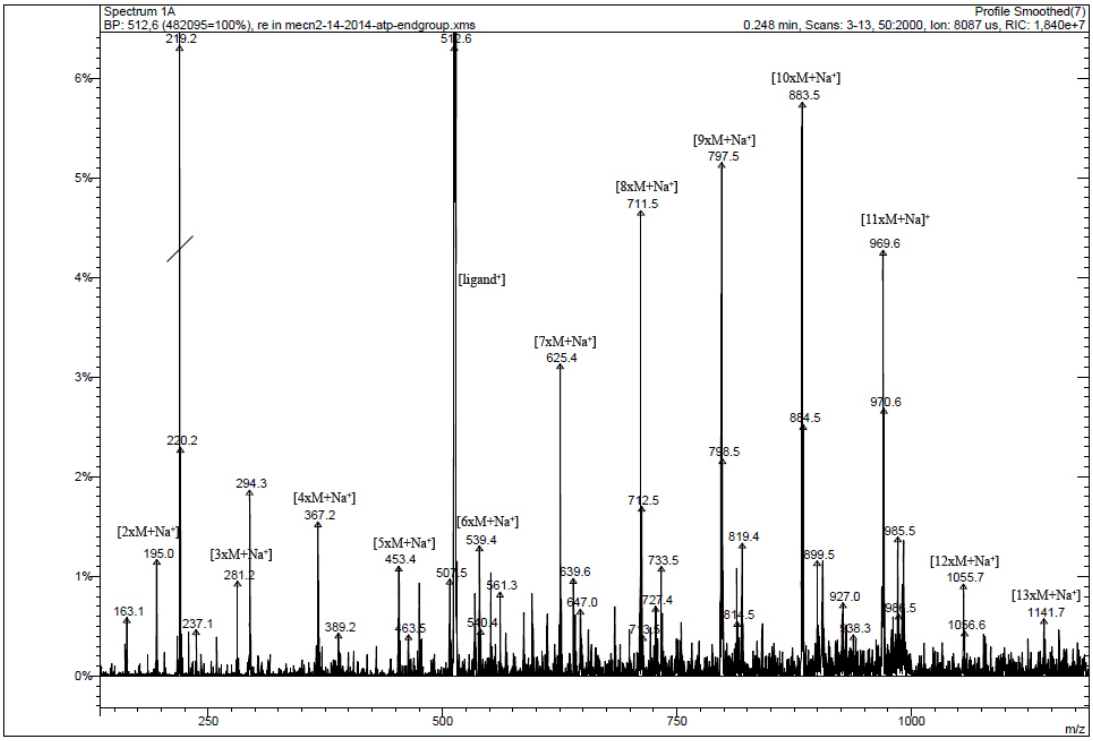

Figure S 13Endgroup analysis (ESI-MS): (ONOO)$^{t\text{Bu}}$Y(N(SiH(CH$_3$)$_2$)$_2$)(thf) (24.9 µmol of catalyst, 0.24 mmol BL, 0.5 mL C$_6$D$_6$, 20 °C).

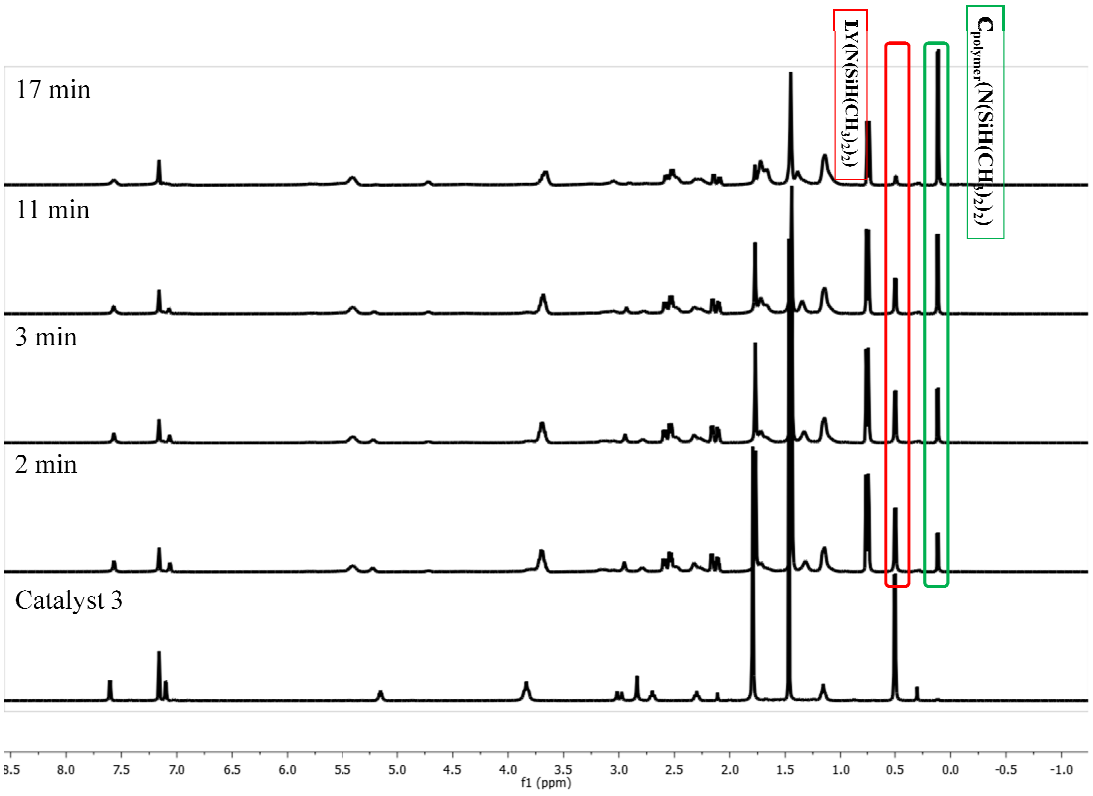

Figure S 14 Endgroup analysis (^{1}H-NMR spectra): (ONOO)^{tBu}Y(N(SiH(CH$_3$)$_2$)$_2$)(thf) (catalyst 3) (24.9 µmol of catalyst, 0.24 mmol BL, 0.5 mL C_6D_6, 20 °C).

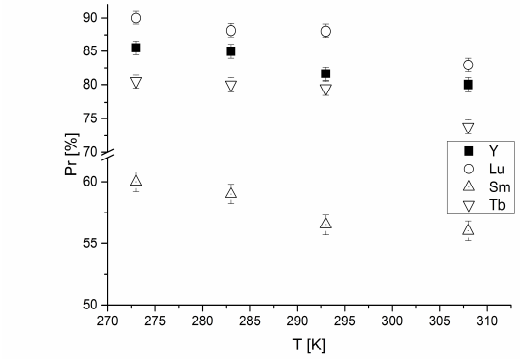

Figure S 15Probability for racemic linkages for (ONOO)^{tBu}Ln(N(SiH(CH$_3$)$_2$)$_2$)(thf) (Ln = Lu, Y, Tb, Sm) at various temperatures (K) (determined by ^{13}C NMR in $CDCl_3$).

Table S 7Probability for racemic linkages for (ONOO)^{tBu}Ln(N(SiH(CH$_3$)$_2$)$_2$)(thf) (Ln = Lu, Y, Tb, Sm) at various temperatures (K)

T [°C] (ONOO)^{tBu}Ln(N(SiH(CH$_3$)$_2$)$_2$)(thf)	P_r [%] Y	P_r [%] Lu	P_r [%] Sm	P_r [%] Tb
0	85.5	89.0	60.0	80.5
10	85.0	88.1	59.0	80.0
20	81.6	88.0	56.0	79.5
35	80.0	80.2	56.0	73.8

Table S 8Thermal analysis of PHB samples prepared with catalysts 1-4 at 25 °C[a]

Entry	[cat]	M_n x10^3 [g/mol]	T_g [°C]	T_m [°C]	T_d[a] [°C]	P_r
1	Sm	13.3	0.65	-	198.00	0.56
2	Tb	69.7	8.34	131.82	217.46	0.77
3	Y	79.6	8.71	144.51	223.40	0.82
4	Lu	91.0	9.88	146.10	239.70	0.88

[a] 5% weight loss from onset temperature as determined by TGA

4. Crystal Structure Data

Compound 1 (CCDC 1040217)

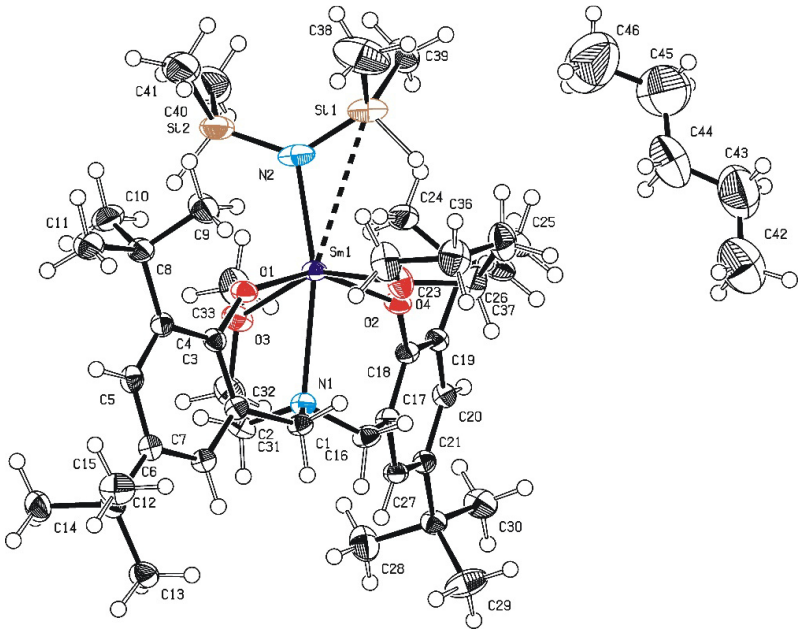

Crystal data

$C_{41}H_{73}N_2O_4Si_2Sm\cdot C_5H_{12}$	$F(000)$ = 994
M_r = 936.70	
Triclinic, *P*	D_x = 1.197 Mg m^{-3}
Hall symbol: -P 1	
a = 11.1919 (4) Å	Mo *K*α radiation, λ = 0.71073 Å
b = 15.3793 (5) Å	Cellparametersfrom9942reflections
c = 15.8676 (5) Å	θ = 1.7–25.4°
α = 99.0051 (13)°	μ = 1.21 mm^{-1}
β = 98.4579 (12)°	*T* = 100 K
γ = 101.5011 (14)°	Plate, colorless
V = 2598.12 (15) Å^3	0.43 × 0.38 × 0.20 mm
Z = 2	

Data collection

Bruker APEX-II CCD diffractometer	9490independentreflections
Radiation source: fine-focus sealed tube	8977 reflections with i> 2σ(i)
graphite	R_{int} = 0.022
Detectorresolution: 16pixels mm^{-1}	θ_{max} = 25.4°, θ_{min} = 1.7°
phi– and ω–rotation scans	h = −13 13
Absorption correction: multi-scan *SADABS*, Bruker, 2008b	k = −18 18
T_{min} = 0.640, T_{max} = 0.745	l = −19 19
43152measuredreflections	

Refinement

Refinement on F^2	Secondary atom site location: difference Fourier map
Least-squaresmatrix: full	Hydrogen site location: inferred from neighbouring sites
$R[F^2 > 2\sigma(F^2)]$ = 0.024	H atoms treated by a mixture of independent and constrained refinement
$wR(F^2)$ = 0.063	Weighting scheme based on measured s.u.'sW = $1/[\Sigma^2(FO^2) + (0.0309P)^2 + 2.3016P]$ WHERE $P = (FO^2 + 2FC^2)/3$
S = 1.08	$(\Delta/\sigma)_{max}$ = 0.001
9490reflections	$\Delta\rho_{max}$ = 1.13 e Å^{-3}
523parameters	$\Delta\rho_{min}$ = –0.51 e Å^{-3}
0restraints	Extinctioncorrection: none
Primary atom site location: structure-invariant direct methods	

Compound 2 (CCDC 1040218)

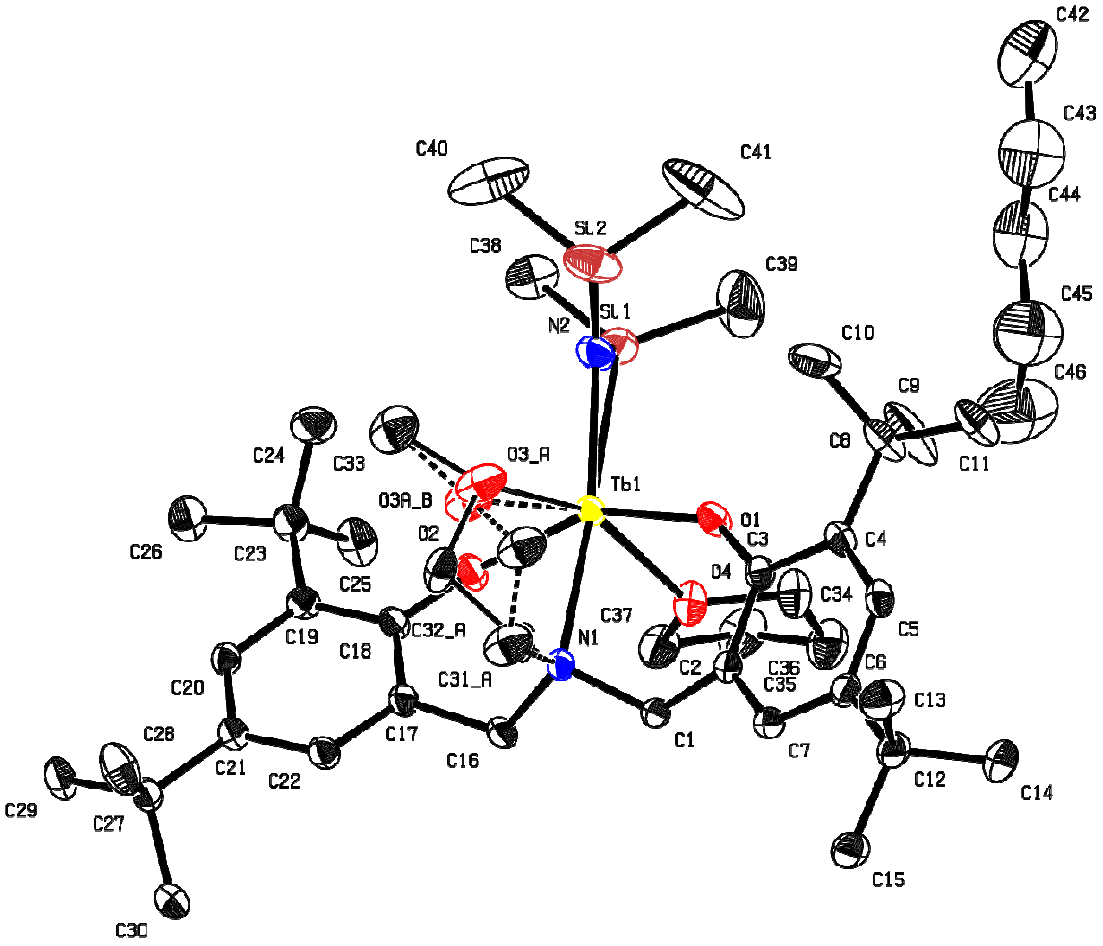

Crystal data

$C_{41}H_{73}N_2O_4Si_2Tb\cdot C_5H_{12}$	$F(000)$ = 1000
M_r = 945.27	
Triclinic, *P*	D_x = 1.222 Mg m^{-3}
Hall symbol: -P 1	
a = 11.1328 (3) Å	Mo *Kα* radiation, λ = 0.71073 Å
b = 15.3175 (5) Å	Cellparametersfrom9663reflections
c = 15.8641 (5) Å	θ = 2.5–25.5°
α = 99.191 (1)°	μ = 1.46 mm^{-1}
β = 98.673 (1)°	*T* = 100 K
γ = 101.521 (1)°	Fragment, colourless

V = 2569.61 (14) Å^3	0.50 × 0.40 × 0.20 mm
Z = 2	

Data collection

Bruker APEX-II CCD diffractometer	9521independentreflections
Radiation source: fine-focus sealed tube	9326 reflections with $I > 2\sigma(I)$
graphite	R_{int} = 0.018
Detectorresolution: 16pixels mm^{-1}	θ_{max} = 25.5°, θ_{min} = 1.7°
phi– and ω–rotation scans	h = −13 13
Absorption correction: multi-scan *SADABS*, Bruker, 2008b	k = −18 18
T_{min} = 0.566, T_{max} = 0.745	l = −19 19
63499measuredreflections	

Refinement

Refinement on F^2	
Least-squaresmatrix: full	Hydrogen sitelocation: mixed
$R[F^2 > 2\sigma(F^2)]$ = 0.022	H atoms treated by a mixture of independent and constrained refinement
$wR(F^2)$ = 0.054	$W = 1/[\Sigma^2(FO^2) + (0.0198P)^2 + 3.1202P]$ WHERE $P = (FO^2 + 2FC^2)/3$
S = 1.13	$(\Delta/\sigma)_{max}$ = 0.001
9521reflections	$\Delta\rho_{max}$ = 0.80 e Å^{-3}
551parameters	$\Delta\rho_{min}$ = −0.61 e Å^{-3}
56restraints	Extinctioncorrection: none

5. ***Entropic corrections***

Model for molecular weight build-up (to be added to the overall reaction)

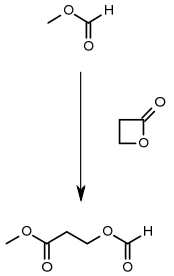

- vibrational correction: $\Delta S = +51.9$ J/mol/K

- conformational correction: $\Delta S = +15.5$ J/mol/K

  for bonds:

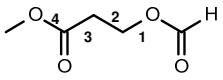

  (used also separately as +15.0 kJ/mol for opening of κ^2-chelates)

→ total correction: $\Delta S = +67.4$ J/mol

used for the sake of simplicity: $\Delta S = +65$ J/mol

Model for catalytic intermediates

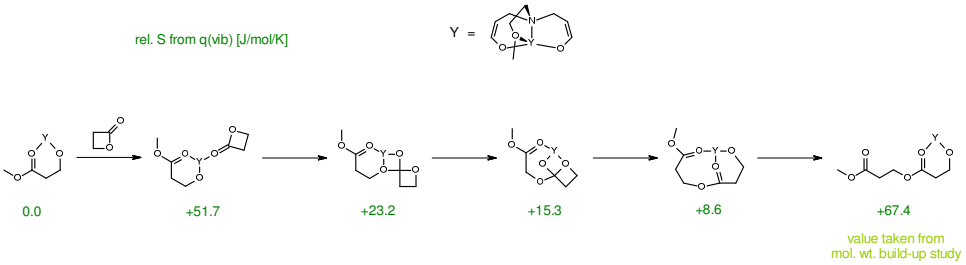

→ used for the sake of simplicity: $\Delta S = +25$ J/mol for species IIa, IIIa, IVa and Va

7.3 Supporting Information: Versatile 2-Methoxyethylaminobis-(phenolate)-yttrium Catalysts: Catalytic Precision Polymerization of Polar Monomers via Rare Earth Metal-Mediated Group Transfer Polymerization

Status	Published online: 10th November 2014
Journal	Macromolecules
Publisher	American Chemical Society
Article type	Full paper
DOI	10.1021/ma501754u
Authors	Peter T. Altenbuchner; Benedikt S. Soller; Stefan Kissling; Thomas Bachmann; Alexander Kronast; Sergei I. Vagin; Bernhard Rieger

Versatile 2-Methoxyethylaminobis(phenolate)yttrium Catalysts: Catalytic Precision Polymerization of Polar Monomers via Rare Earth Metal-Mediated Group Transfer Polymerization

Peter T. Altenbuchner[†], Benedikt S. Soller[†], Stefan Kissling[†], Thomas Bachmann[†], Alexander Kronast[†], Sergei I. Vagin[†], Bernhard Rieger[†*]

[†]WACKER-Lehrstuhl für Makromolekulare Chemie, Technische Universität München, Lichtenbergstraße 4, 85748 Garching bei München, Germany

Table of Contents

1. General Information

Acitivity Measurements and Kinetic Analysis in the *in situ* ATR-IR:
For activity measurements, the stated amount of catalyst (42 – 135 µmol) is dissolved in 5 mL of dichloromethane, and the reaction mixture is transferred into the *in situ* IR autoklave and thermostatted to the desired temperature. Then, the stated amount of monomer (4.3-27 mmol) is added. During the course of the experiment the temperature is kept at the desired temperature (±1 K). In case of block copolymerization experiments, an aliquot sample is taken after complete conversion of the first monomer A for GPC-MALS analysis. Monomer B (4.3 mmol) is added subsequently and the reaction mixture is stirred until full conversion. After the stated reaction time, the reaction is quenched by addition of wet chloroform (0.5 mL) and an aliquot is taken to determine the conversion. The polymer is precipitated in excess hexane, filtered off and freeze dried from destilled H_2O.

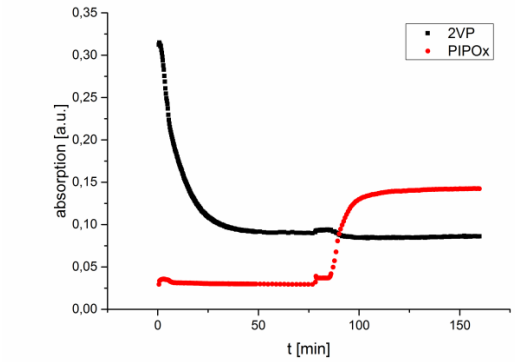

Figure S 1 ATR-IR block copolymerization experiment with block A P2VP (802 cm^{-1}) and block B PIPOx (1607 cm^{-1}).

The block copolymerization of 2VP and PIPOx was monitored in the ATR-IR (Figure S 1) through which the decrease of 2VP to complete conversion and the increase of PIPOx could be observed. The polymerization of IPOx was initiated immediately after the addition and preceded to full conversion within 30 minutes.

Sequential copolymerization

After dissolving the calculated amount of catalyst in dichlormethane at room temperature, the first monomer was added. The reaction mixture was stirred for 2 hours. One aliquot was taken and quenched by the addition of 0.5 mL MeOH while the calculated amount of a second monomer was added to the reaction solution and stirred for another 2 hours at room temperature (in case of DMAA: at – 78 °C) and quenched by addition of 0.5 mL MeOH. The polymers were precipitated by addition of the reaction mixtures to hexane (150 mL) and decanted from solution. Residual solvents were removed by drying the polymers under vacuum at 60 °C overnight.

Molecular weight determination

GPC was carried out on a Varian LC-920 equipped with two PL Polargel columns. As eluent a mixture of 50% THF, 50% water, and 9 g L-1 tetrabutylammonium bromide (TBAB) was used in the case of PDEVP, PIPOx, P2VP, P(2VP-b-PDEVP), P(2VP-b-PIPOx), P(2VP-b-PDMAA) and P(2VP-b-DEVP); for PDIVP analysis, the eluent was THF with 6 g L-1 TBAB. Absolute molecular weights have been determined online by multiangle light scattering (MALS) analysis using a Wyatt Dawn Heleos II in combination with a Wyatt Optilab rEX as concentration source.

GPC for Polyhydroxybutyrate samples was carried on a Polymer Laboratories GPC50 Plus chromatograph. As eluent, chloroform with 1.5 g L-1 tetrabutylammonium tetrafluoroborate was used. Polystyrene standards were used for calibration.

Kinetics by aliquots method

In the Glovebox the calculated amount of catalyst was dissolved in 20mL toluene at room temperature and the calculated amount of monomer was added in one injection. Aliquots were taken from the reaction solution at regular time intervals and quenched by addition to MeOH. For each aliquot, the conversion is determined by gravimetry or ^{1}H NMR spectroscopy and the molecular weight of the formed polymer by GPC-MALS analysis.

2. Analytical Data

2.1 Nuclear Magnetic Resonance Spectroscopy (NMR)

a.)

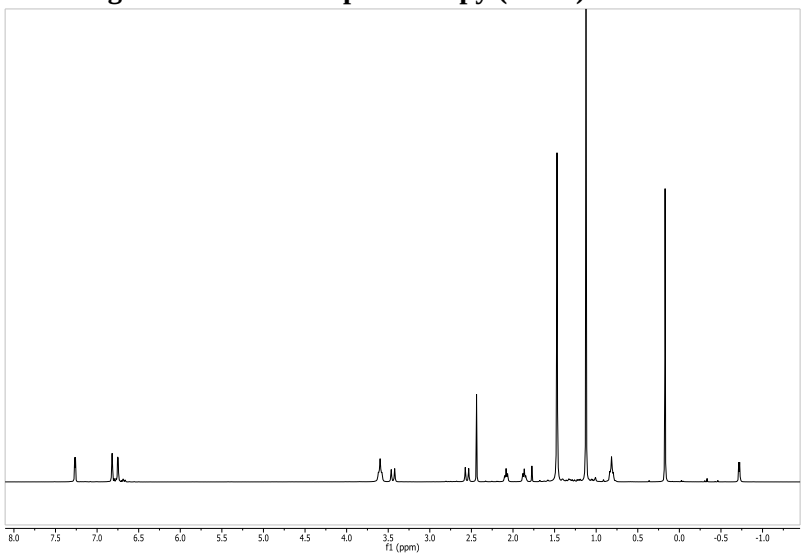

b.)

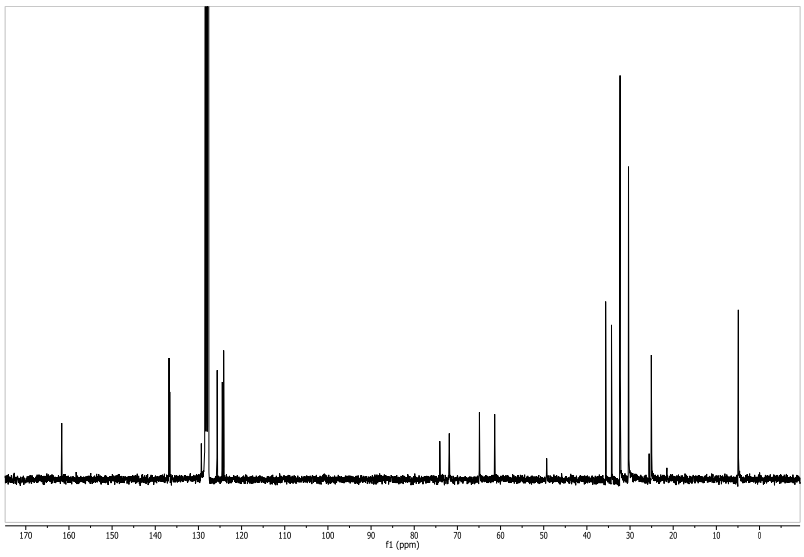

Figure S 2 a.) ^{1}H NMR spectrum b.) ^{13}C NMR spectrum of catalyst (ONOO)^{tBu}Y(CH$_2$Si(CH$_3$)$_3$)(thf) in C_6D_6.

a.)

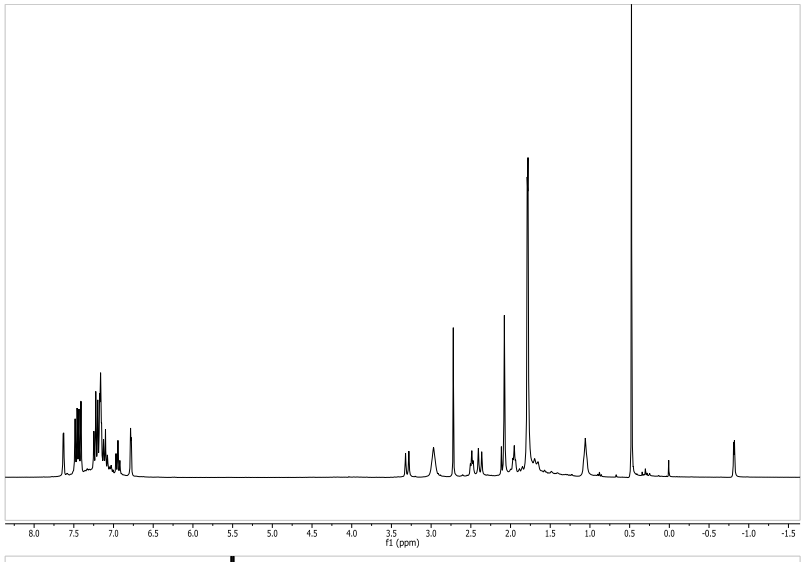

b.)

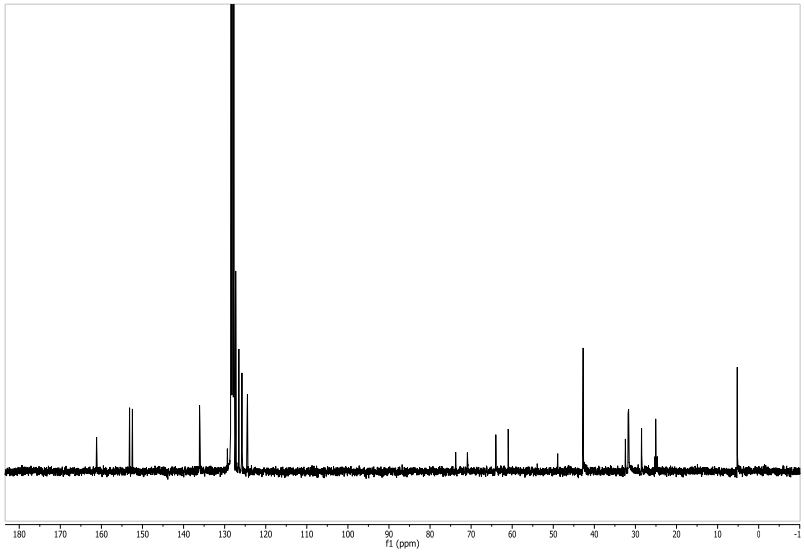

Figure S 3 a.) ^{1}H NMR spectrum b.) ^{13}C NMR spectrum of catalyst (ONOO)^{CMe2Ph}Y($CH_2Si(CH_3)_3$)(thf) in C_6D_6.

5

a.)

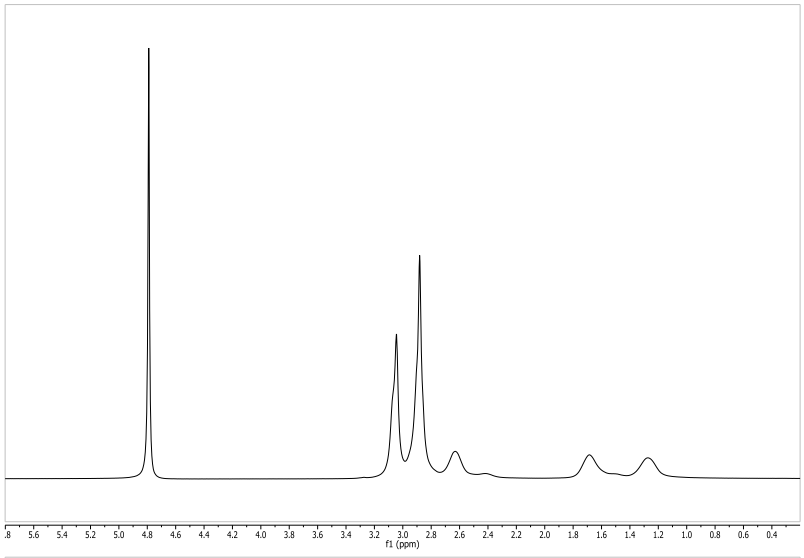

b.)

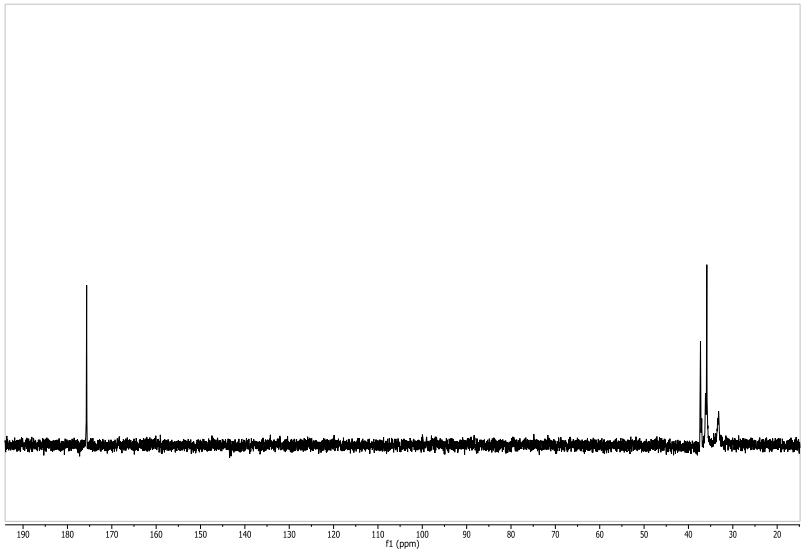

Figure S 4 ^{1}H a.) and ^{13}C b.) NMR spectra of PDMAA in D_2O.

a.)

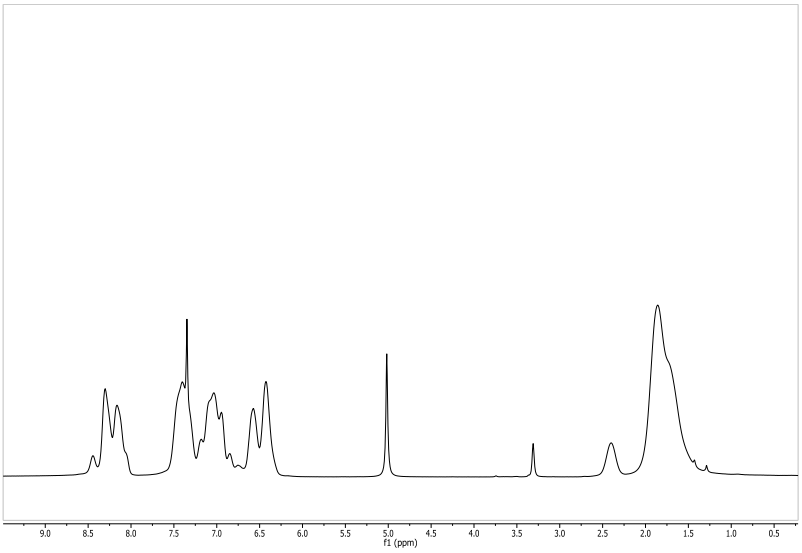

b.)

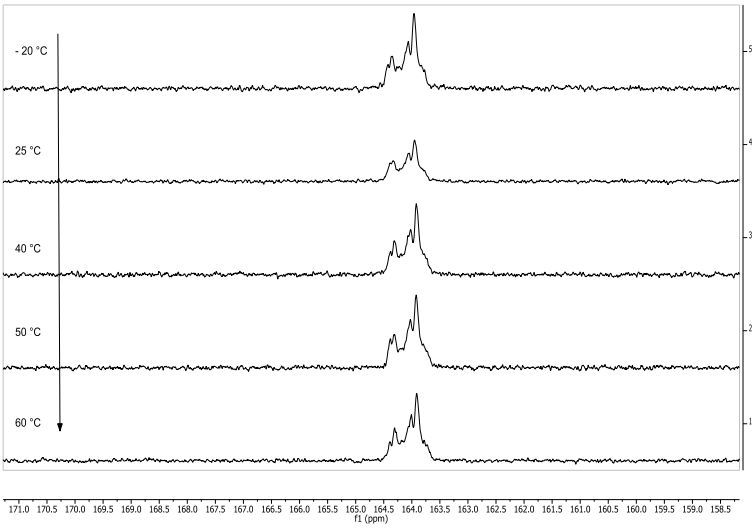

Figure S 5 a.) ^{1}H NMR P2VP b.) Polymer samples synthesized at different temperatures. Aromatic quaternary ^{13}C NMR resonances of P2VP in $CDCl_3$ measured at 25 °C.[1]

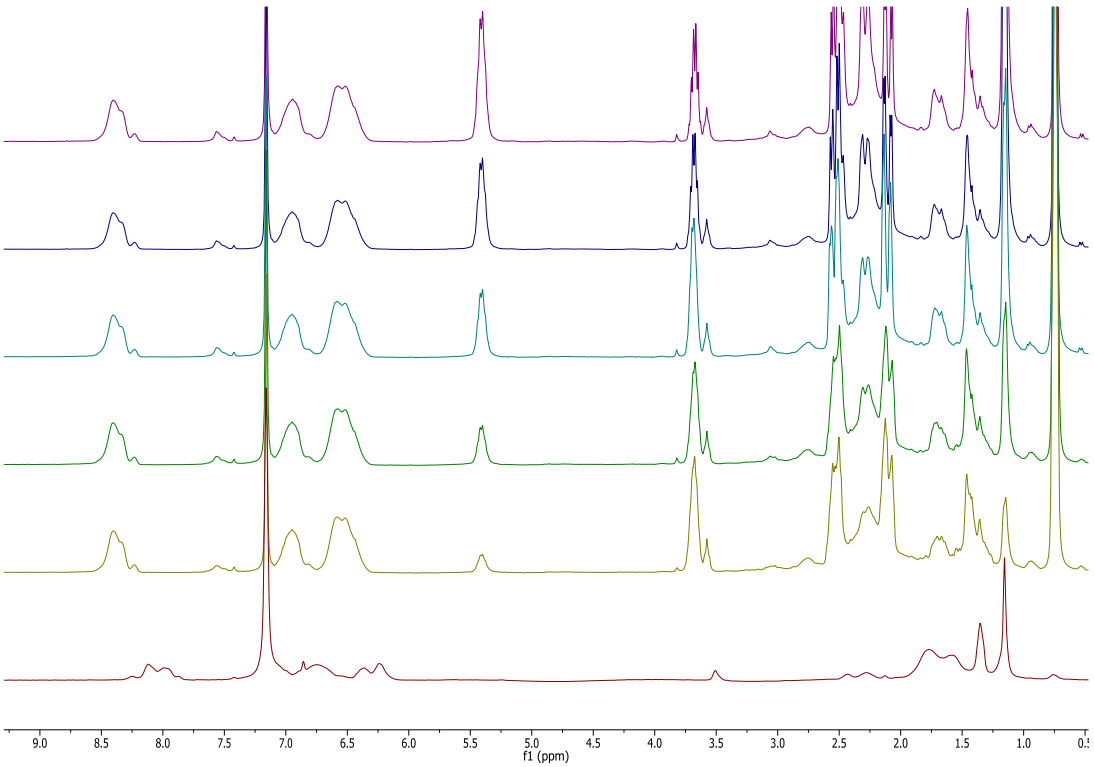

Figure S 6 ^{1}H NMR experiment with (ONOO)^{tBu}Y(CH$_2$Si(CH$_3$)$_3$)(thf) (catalyst 13 µmol, 2VP 0.14 mmol, BL 0.14 mmol, C_6D_6 0.5 mL, T = 25 °C): Polymerization of monomer A (P2VP) and subsequent polymerization of monomer B (BL).

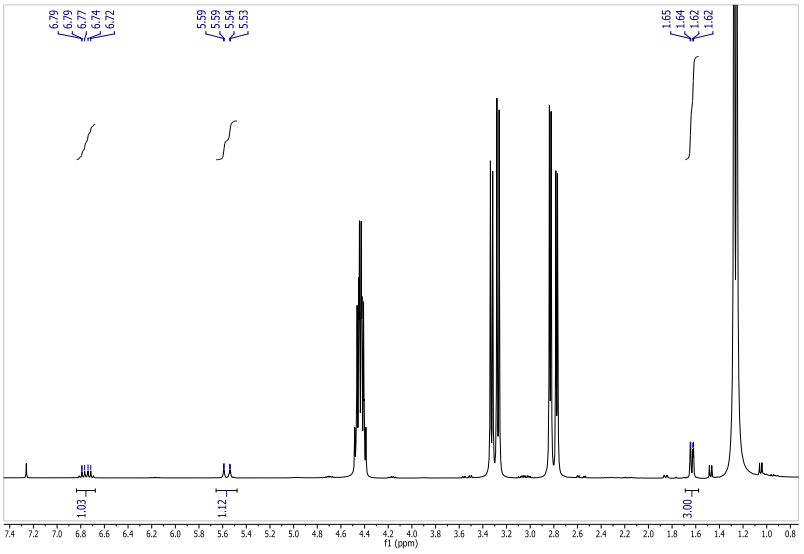

Figure S 7 ^{1}H NMR of BL with traces of crotonic acid in $CDCl_3$.

2.2 Kinetic Data

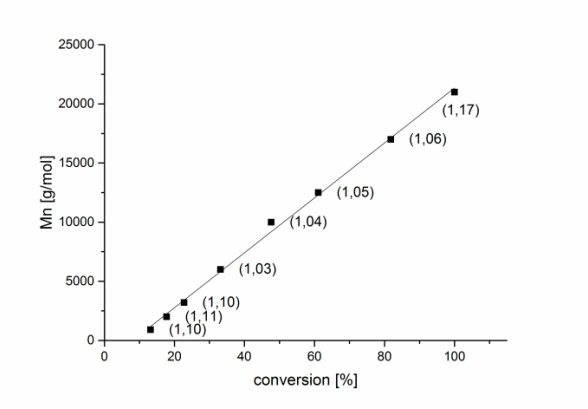

Figure S 8 Growth of the absolute molecular weight (M_n) determined by GPC-MALS as a function of monomer conversion (determined gravimetically), respective PDI values shown in brackets: catalyst 1, 135 µmol, IPOx 27 mmol, toluene 20 mL, 25 °C.

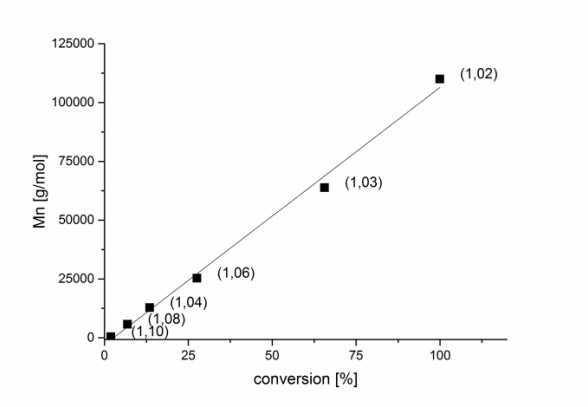

Figure S 9 Growth of the absolute molecular weight (M_n) determined by GPC-MALS as a function of monomer conversion (determined gravimetically), respective PDI values shown in brackets: catalyst 1, 43 µmol, 2VP 27 mmol, toluene 20 mL, 25 °C.

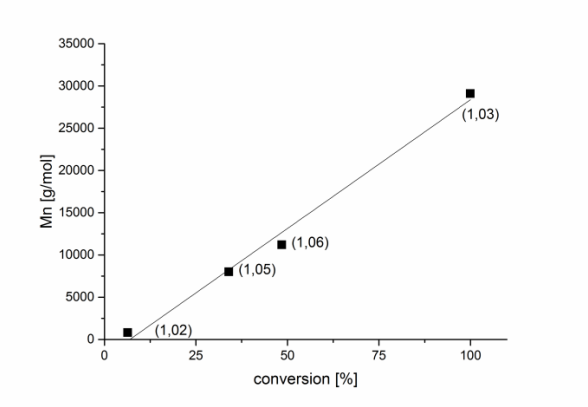

Figure S 10 Growth of the absolute molecular weight (M_n) determined by GPC-MALS as a function of monomer conversion (determined gravimetically), respective PDI values shown in brackets: catalyst 2, 43 µmol, 2VP 135 mmol, toluene 20 mL, 25 °C.

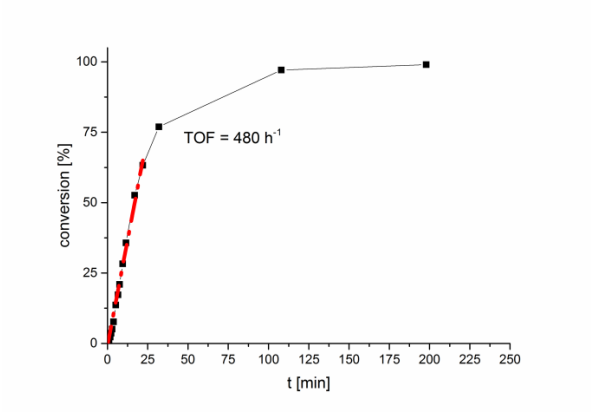

Figure S 11 Determination of catalytic activity of (ONOO)^{tBu}Y($CH_2Si(CH_3)_3$)(thf) (catalyst 135 µmol, DEVP 27 mmol, toluene 20 mL, T = 25 °C).

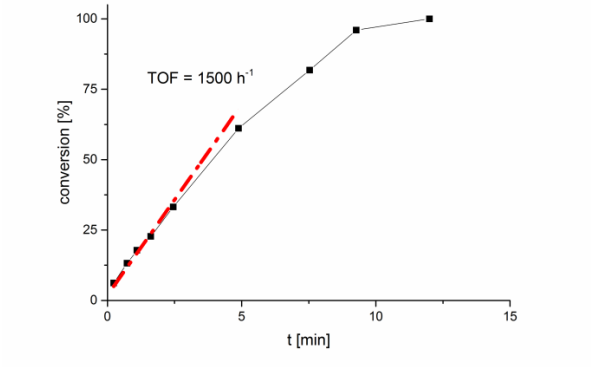

Figure S 12 Determination of catalytic activity of (ONOO)^{tBu}Y($CH_2Si(CH_3)_3$)(thf) (catalyst 135 µmol, IPOx 27 mmol, toluene 20 mL, T = 25 °C).

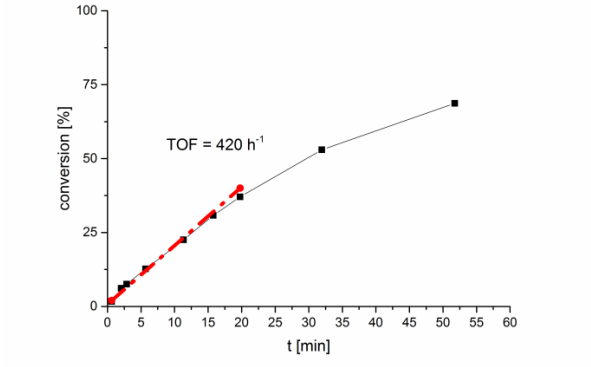

Figure S 13 Determination of catalytic activity of (ONOO)^{tBu}Y($CH_2Si(CH_3)_3$)(thf) (catalyst 43 µmol, 2VP 27 mmol, toluene 20 mL, T = 25 °C).

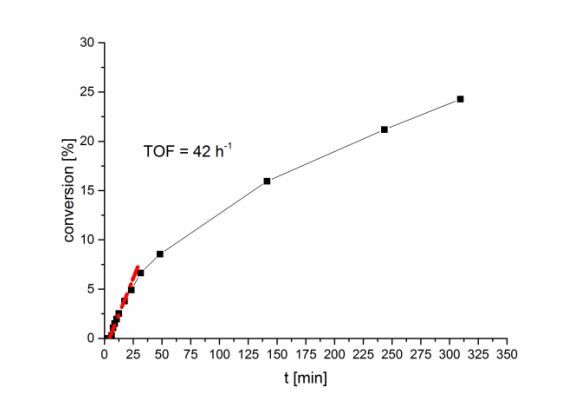

Figure S 14 Determination of catalytic activity of (ONOO)^{tBu}Y($CH_2Si(CH_3)_3$)(thf) (catalyst 135 µmol, DIVP 27 mmol, toluene 20 mL, T = 25 °C).

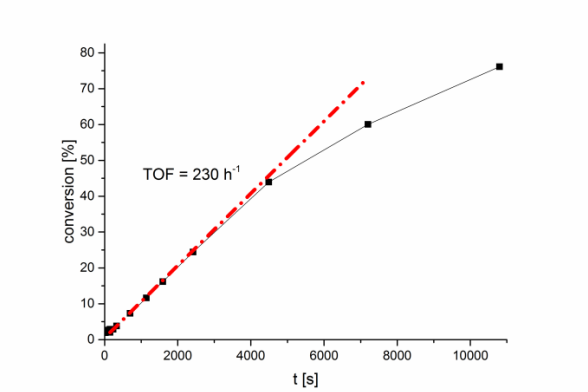

Figure S 15 Determination of catalytic activity of (ONOO)^{CMe2Ph}Y($CH_2Si(CH_3)_3$)(thf) (catalyst 43 µmol, 2VP 27 mmol, toluene 20 mL, T = 25 °C).

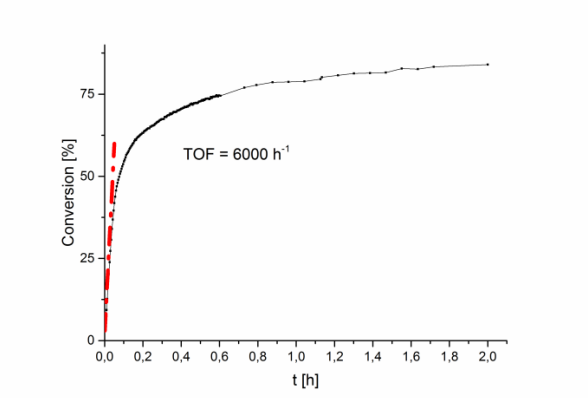

Figure S 16 Determination of catalytic activity of (ONOO)^{tBu}Y($CH_2Si(CH_3)_3$)(thf) (catalyst 14.3 µmol, BL 9 mmol, dichloromethane 5 mL, T = 25 °C).

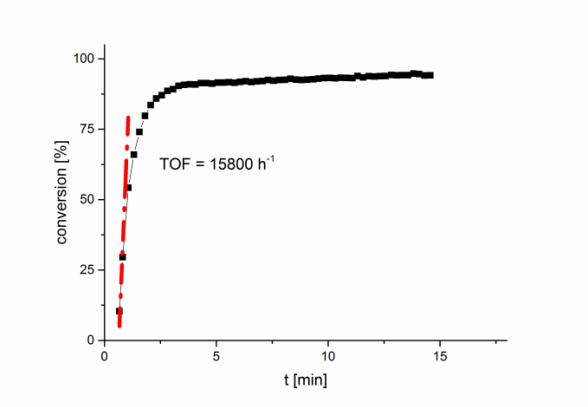

Figure S 17 Determination of catalytic activity of (ONOO)^{CMe2Ph}Y($CH_2Si(CH_3)_3$)(thf) (catalyst 14.3 µmol, BL 9 mmol, dichloromethane 5 mL, T = 25 °C).

2.3 Endgroup Analysis

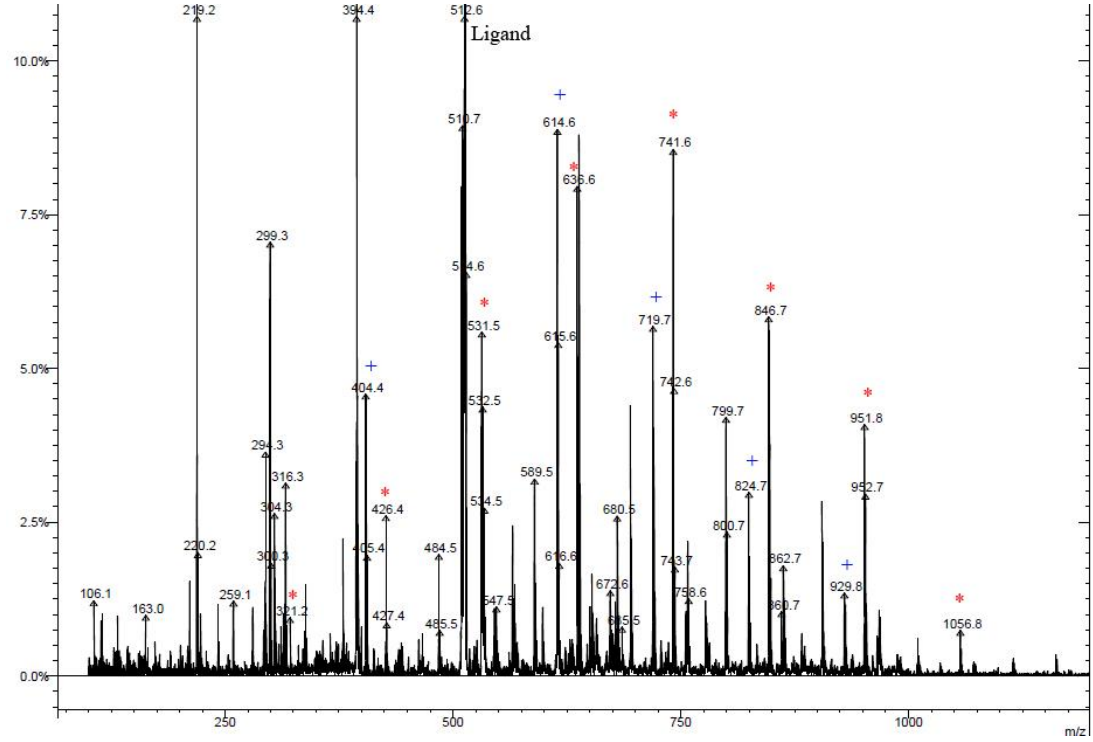

Figure S 18 Endgroup analysis ESI-MS measured in *i*PrOH; Catalyst 1 (40 µmol of catalyst, 0.4 mmol 2VP, 0.5 mL C_6D_6, 20 °C): (*) [(n x M) + (CH_2TMS) + (Na)]$^+$ (+) [(n x M) + (CH_2TMS) + H]$^+$.

2.4 LCST (Lower critical solution temperature)

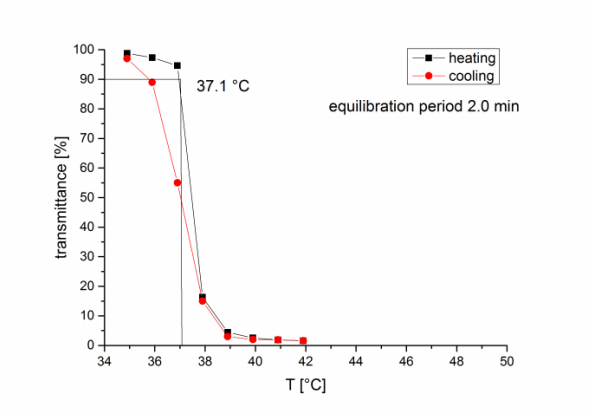

Figure S 19 Determination of the cloud point (lower critical solution temperature, LCST) of P2VP homopolymer. The cloud point was determined at 10% decrease of transmittance for a 5.0 wt % dest. H_2O:THF =1:1, $M_n = 2.2x10^4$ g/mol, PDI = 1.01.

2.5 Eyring-Plot Data

Table S 1 Eyring plot for (ONOO)^{tBu}Y($CH_2Si(CH_3)_3$)(thf) initiated 2VP (catalyst 42 µmol, 2VP 8.6 mmol, toluene 5.5 mL, temperature 298 – 331 K).

T [K]	$v_{initial}$ [mol/L]	c(Mon) [mol/L]	n(Mon) [mol]	k (L/mols)	ln(k/T)	1/T
313	0,00215641	1,177845	0,008560015	0,31321527	-6,907067763	0,00319489
298	0,00043782	1,177845	0,008560015	0,06359269	-8,452350272	0,0033557
298	0,00046452	1,177845	0,008560015	0,06747082	-8,393153525	0,0033557
323	0,00557182	1,177845	0,008560015	0,80929836	-5,989239946	0,00309598
308	0,0014717	1,177845	0,008560015	0,21376218	-7,272990962	0,00324675
331	0,00997805	1,177845	0,008560015	1,44929656	-5,431040069	0,00302115

Table S 2 Eyring plot for (ONOO)^{CMe2Ph}Y($CH_2Si(CH_3)_3$)(thf) initiated 2VP (catalyst 42 µmol, 2VP 8.6 mmol, toluene 5.5 mL, temperature 303 – 333 K.

T [K]	$v_{initial}$ [mmol/mL]	c(Mon) [mol/L]	n(Mon) [mol]	k (L/mols)	ln(k/T)	1/T
333	0,00774761	1,177845	0,008560015	1,11611147	-5,698291743	0,003003
313	0,00108568	1,177845	0,008560015	0,15640177	-7,601530334	0,00319489
323	0,00198724	1,177845	0,008560015	0,28627943	-7,028439244	0,00309598
303	0,00026055	1,177845	0,008560015	0,03753452	-8,996226965	0,00330033
341	0,01309903	1,177845	0,008560015	1,88703067	-5,196877958	0,00293255

2.6 Thermogravimetric analysis (TGA) and Differential scanning calorimetry (DSC)

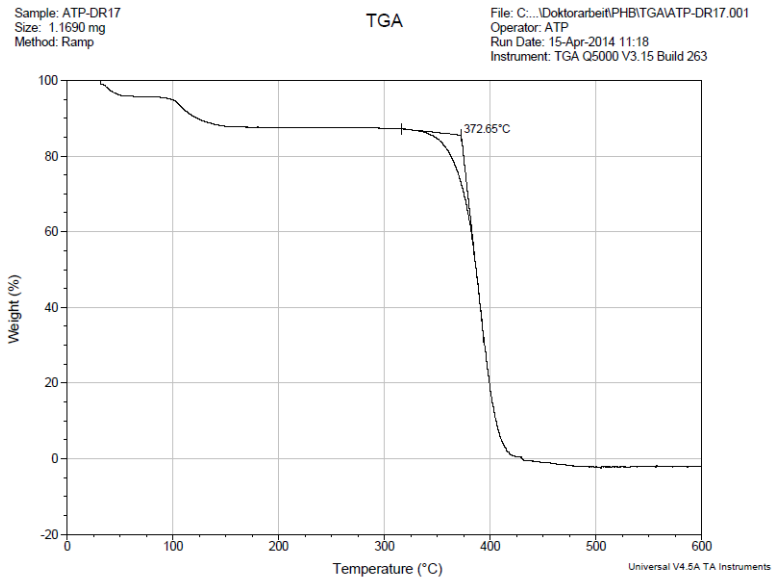

Figure S 20 TGA thermogram for P2VP reported in table 2, entry 2

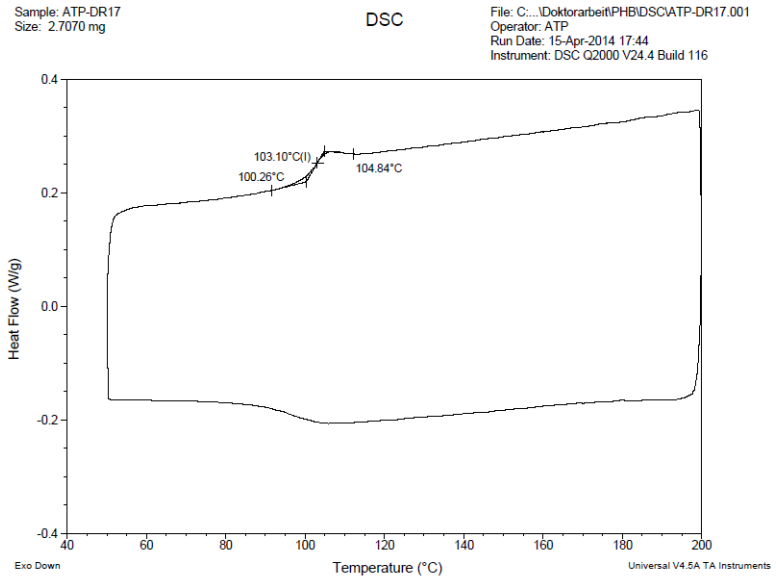

Figure S 21 DSC thermogram for P2VP reported in table 2, entry 2.

2.7 Gel-permeation chromatography (GPC) Data

2.7.1 Homopolymerization

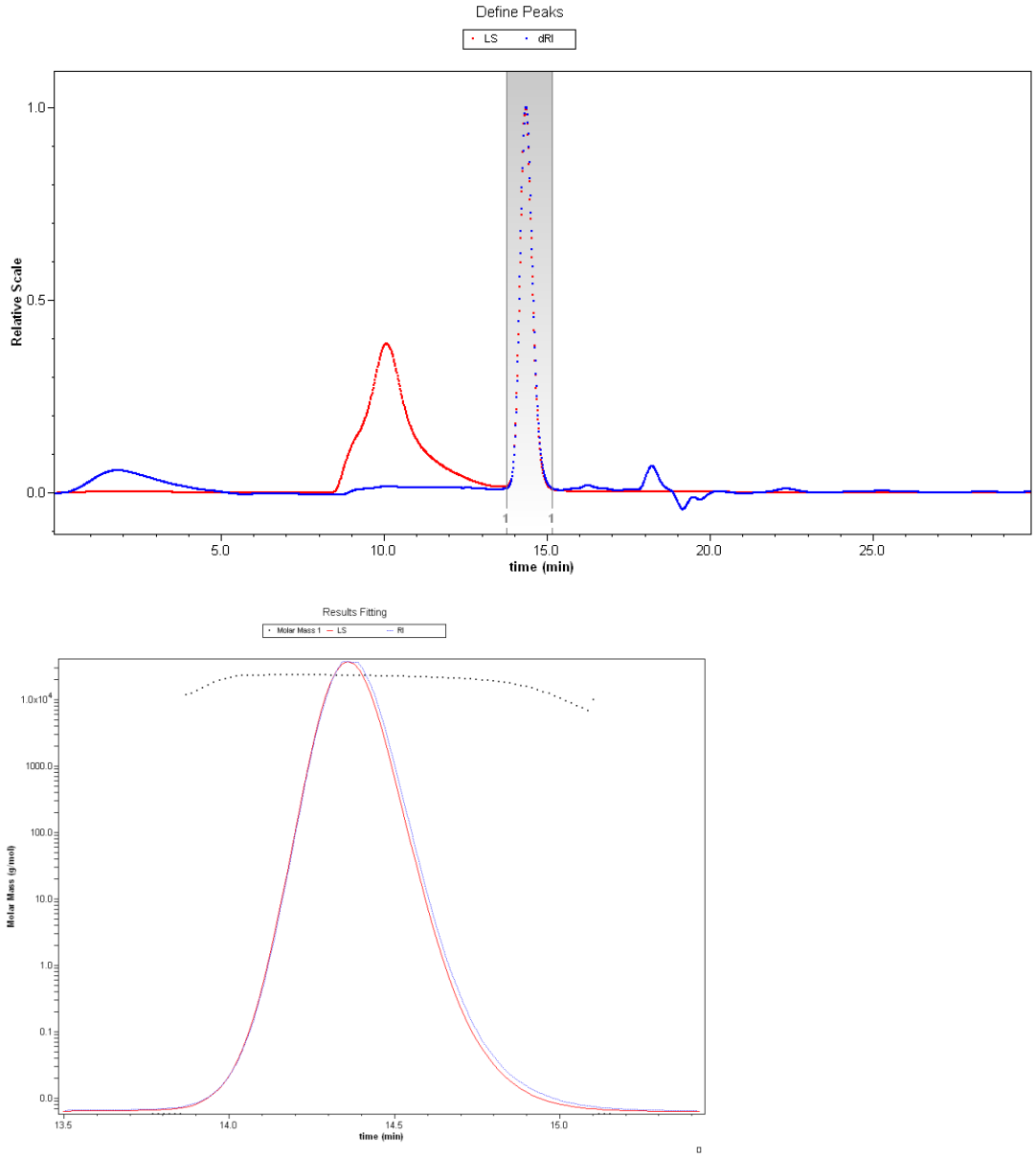

Figure S 22 REM-GTP (2VP), table 1, entry 1, conversion 99%.

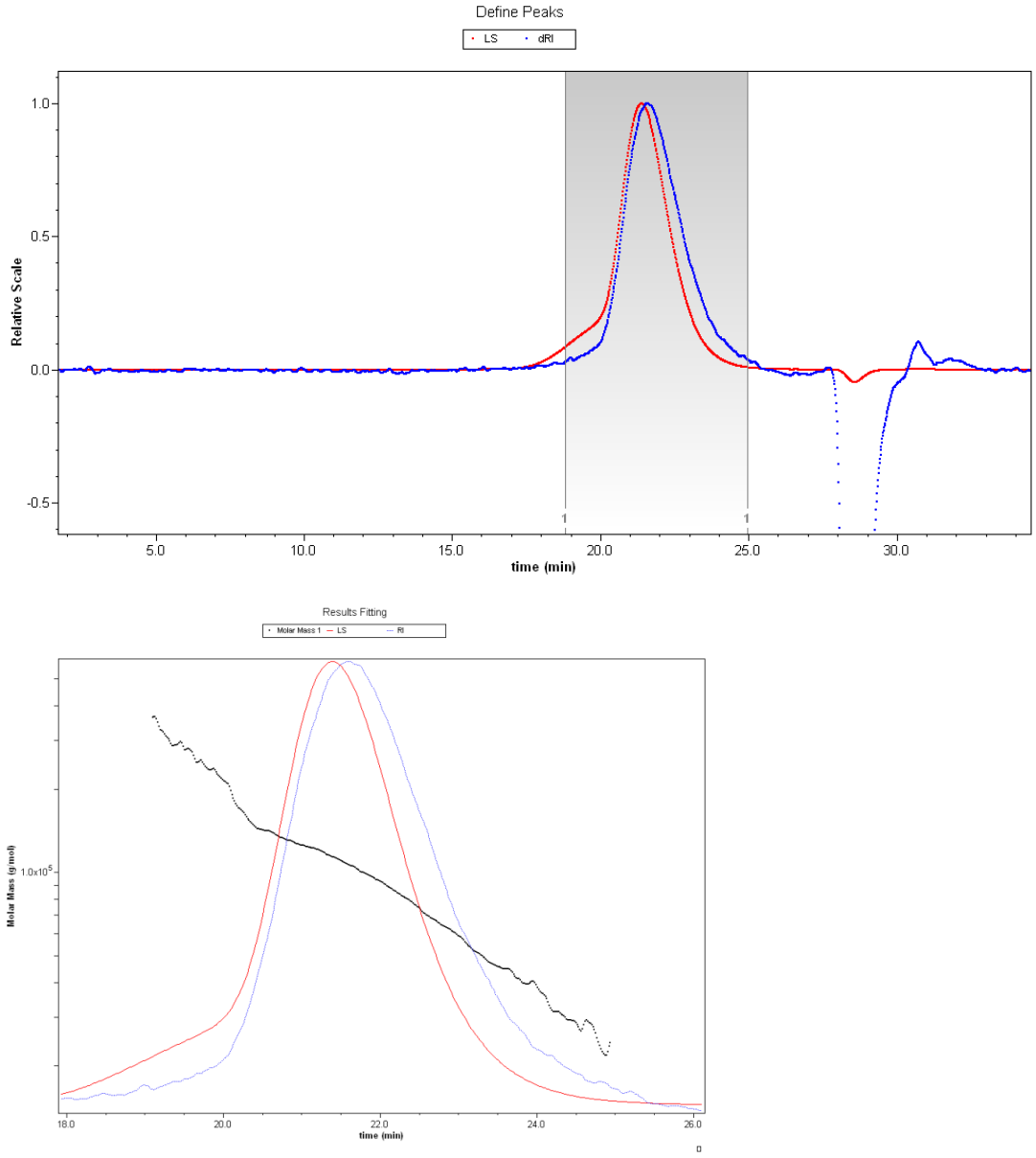

Figure S 23 REM-GTP (DEVP), table 1, entry 2, conversion 99%.

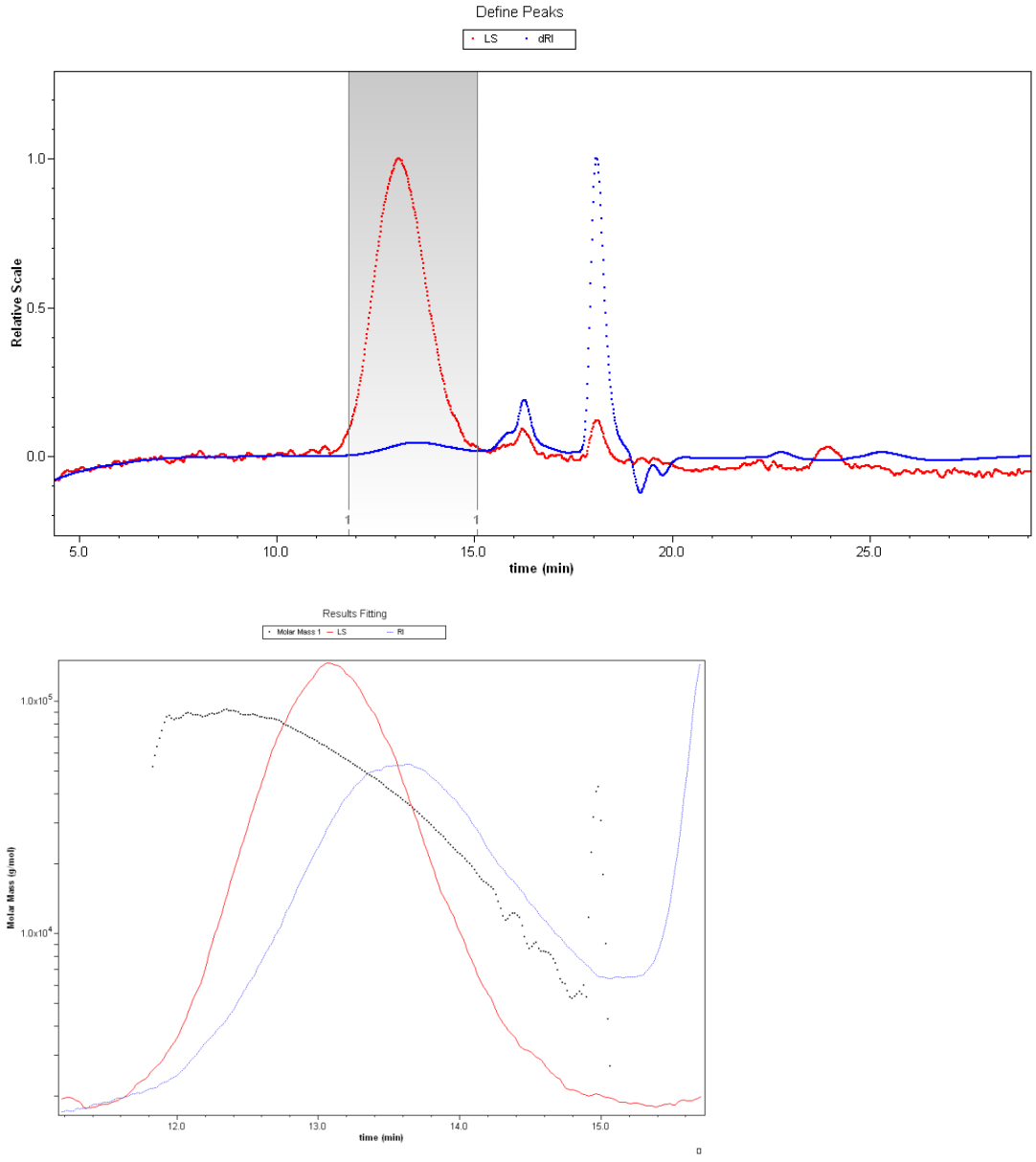

Figure S 24 REM-GTP (DIVP), table 1, entry 3, conversion 25%.

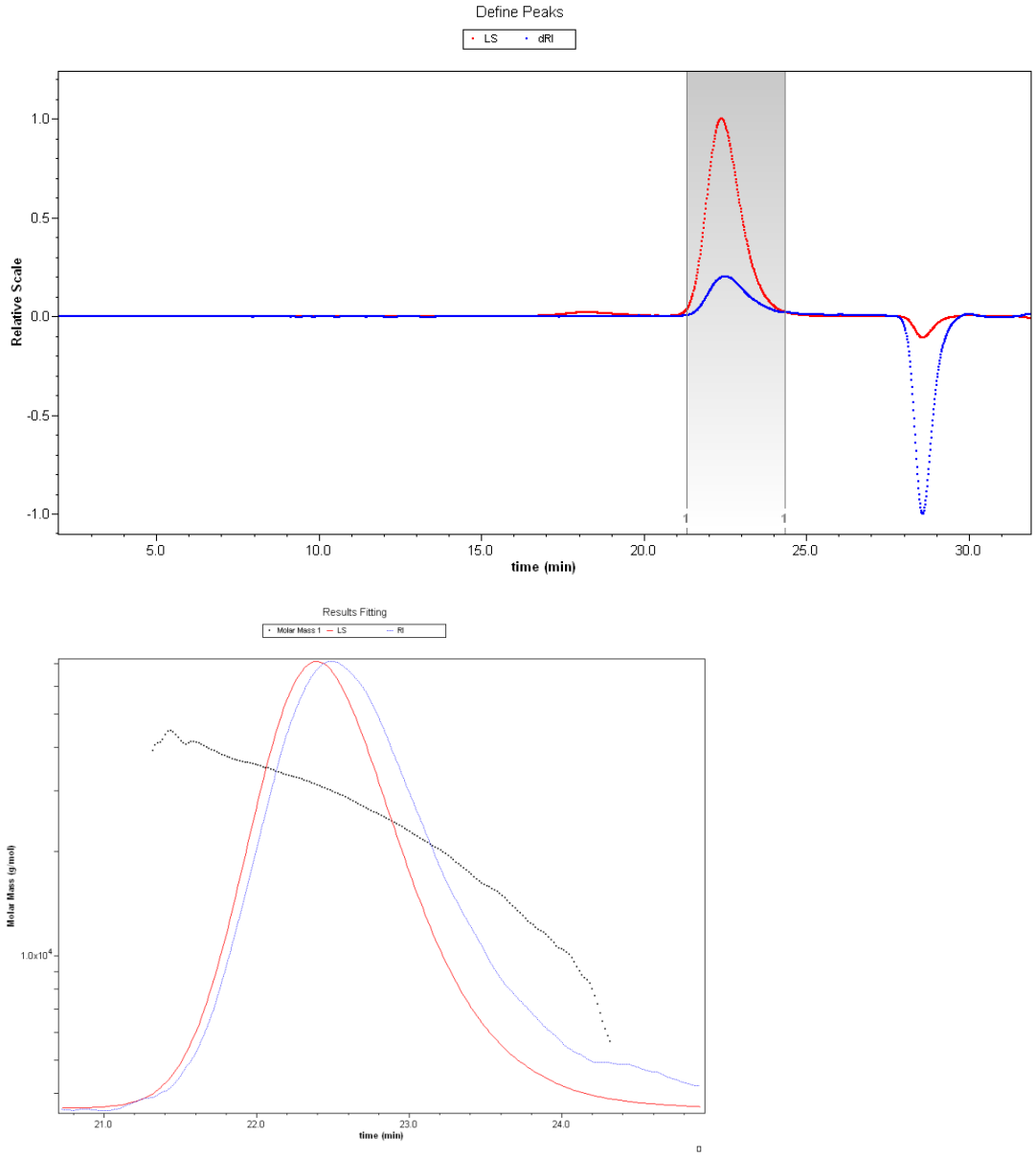

Figure S 25 REM-GTP (IPOx), table 1, entry 4, conversion 99%.

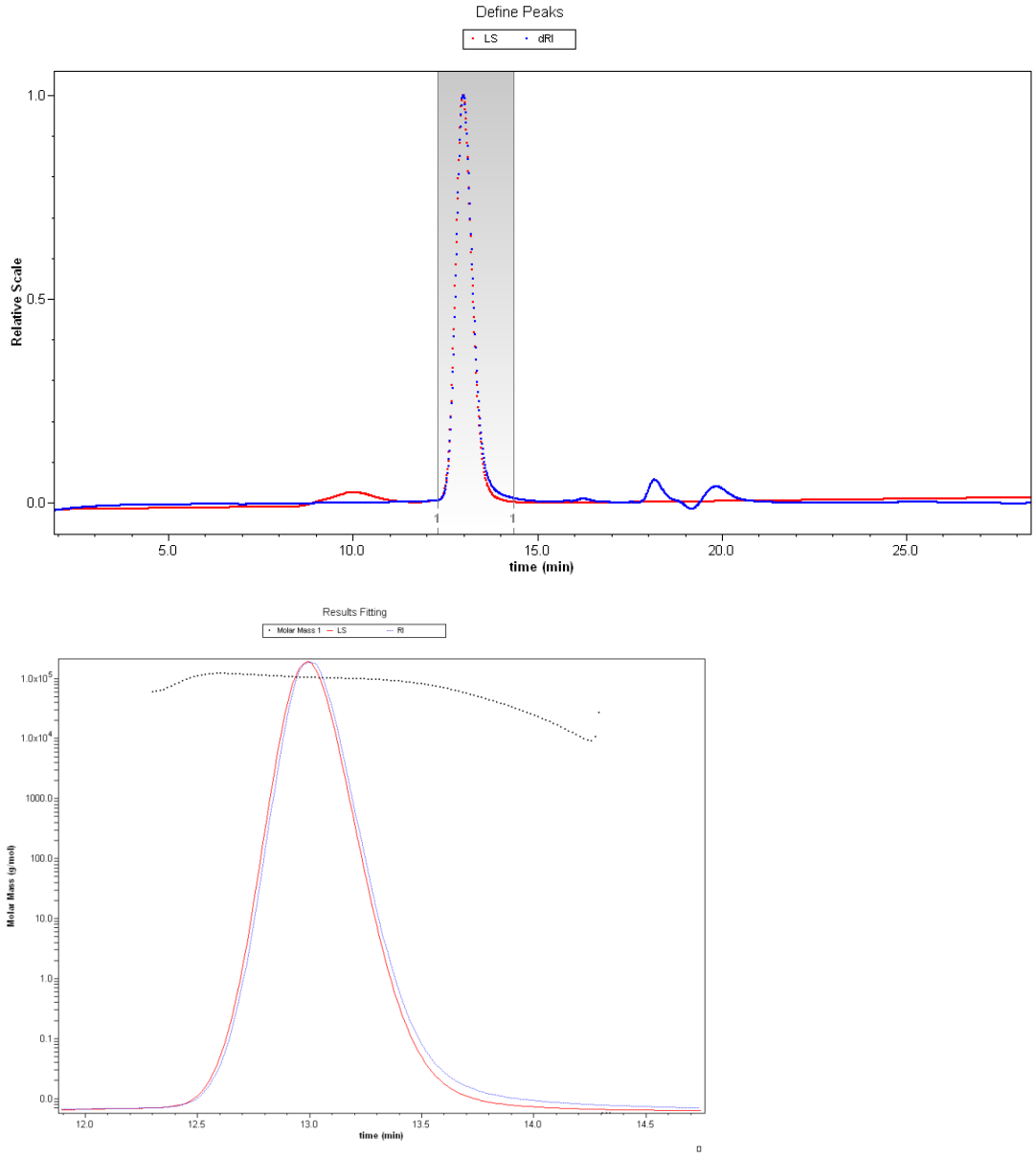

Figure S 26 REM-GTP (2VP), table 1, entry 5, conversion 99%.

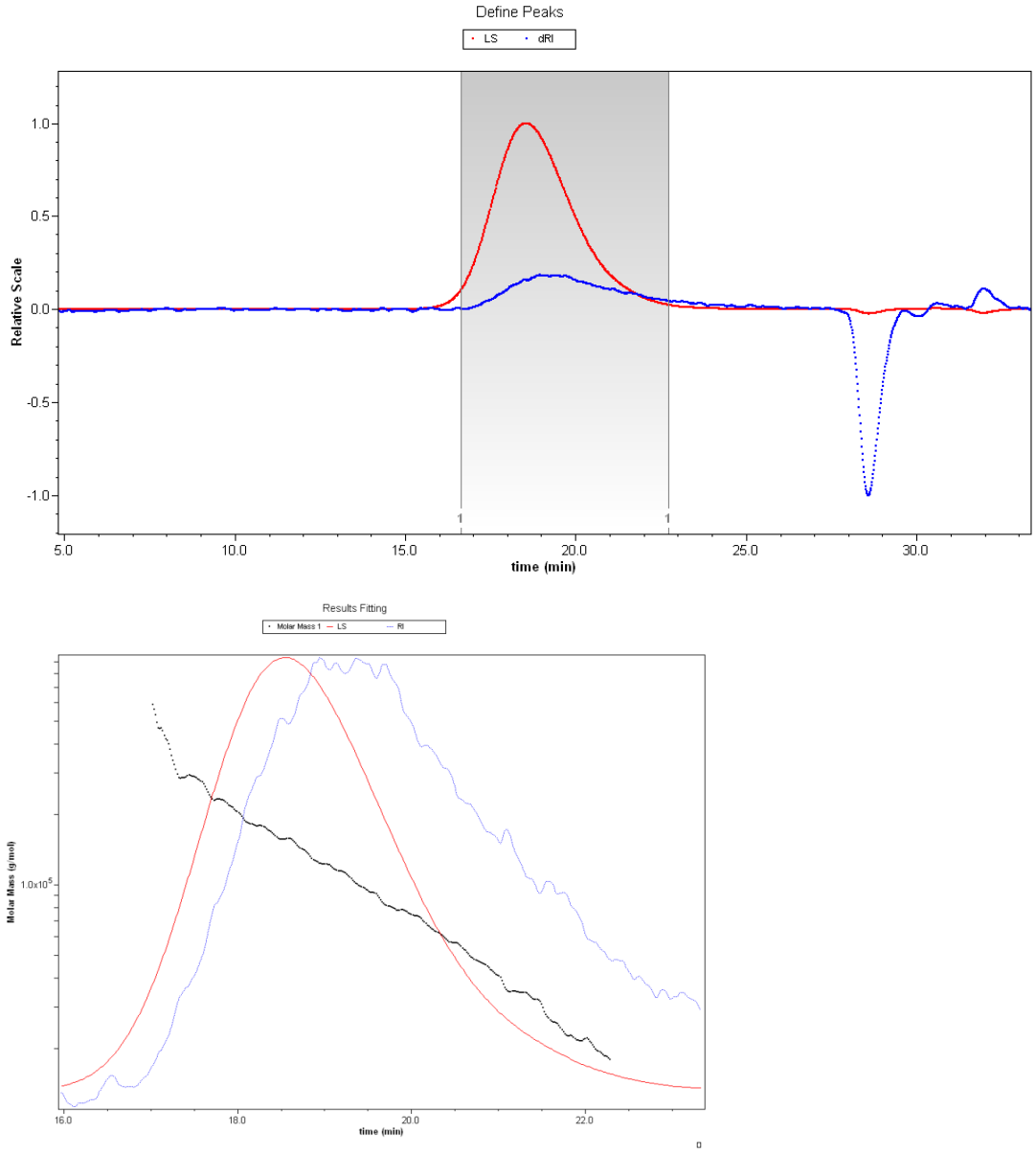

Figure S 27 REM-GTP (DMAA), table 1, entry 6, conversion 99%.

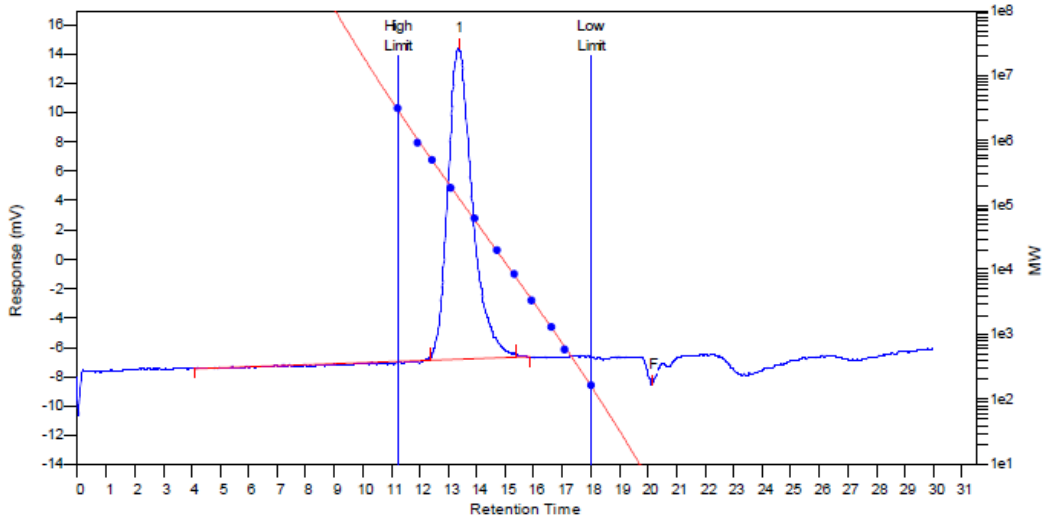

MW Averages

Peak No	Mp	Mn	Mw	Mz	Mz+1	Mv	PD
1	129276	85510	130306	173311	216079	124085	1.52387
2	0	0	0	0	0	0	0

Figure S 28 ROP (BL), table 1, entry 7, conversion 89%.

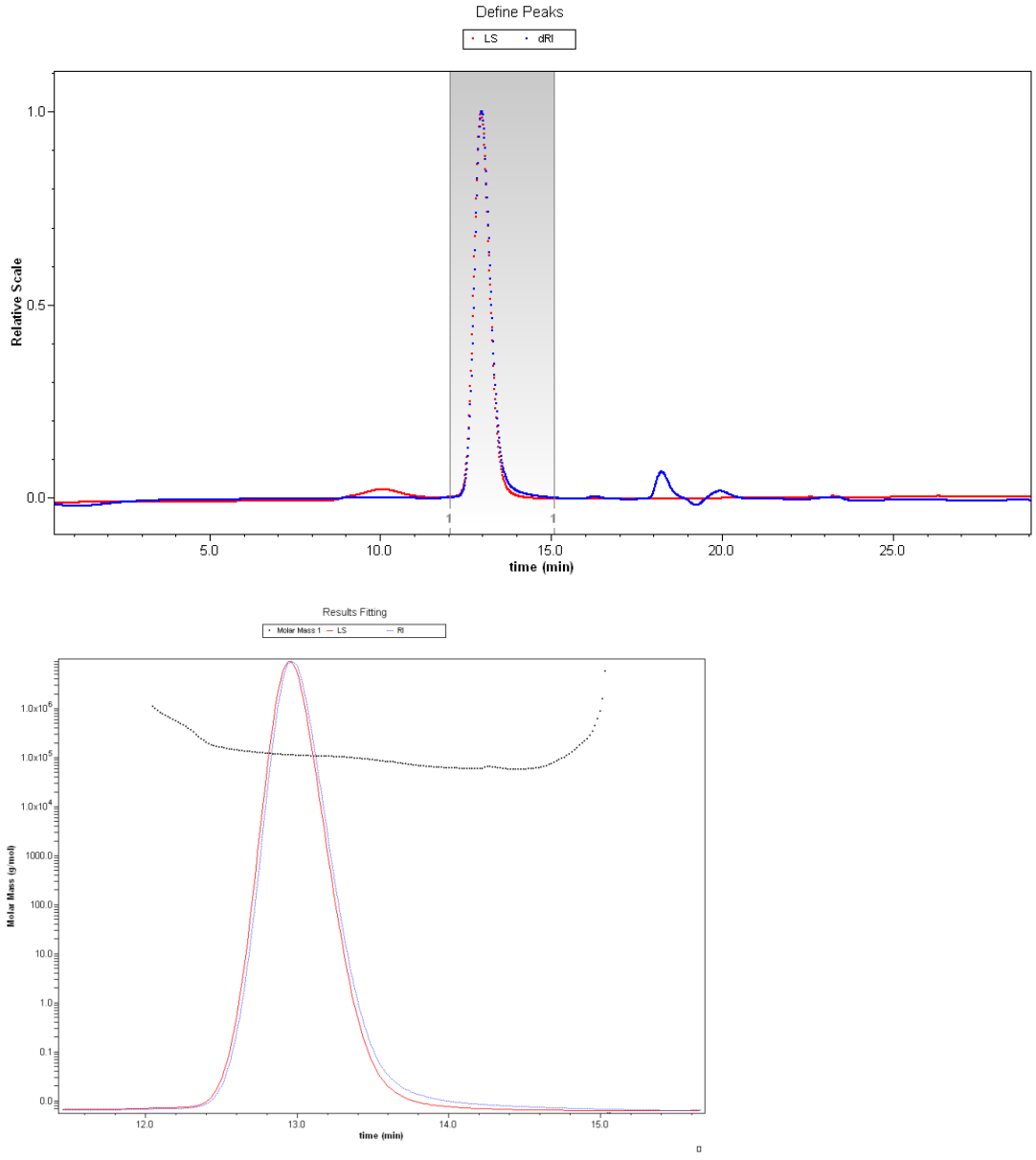

Figure S 29 REM-GTP (2VP), table 2, entry 1, conversion 99%.

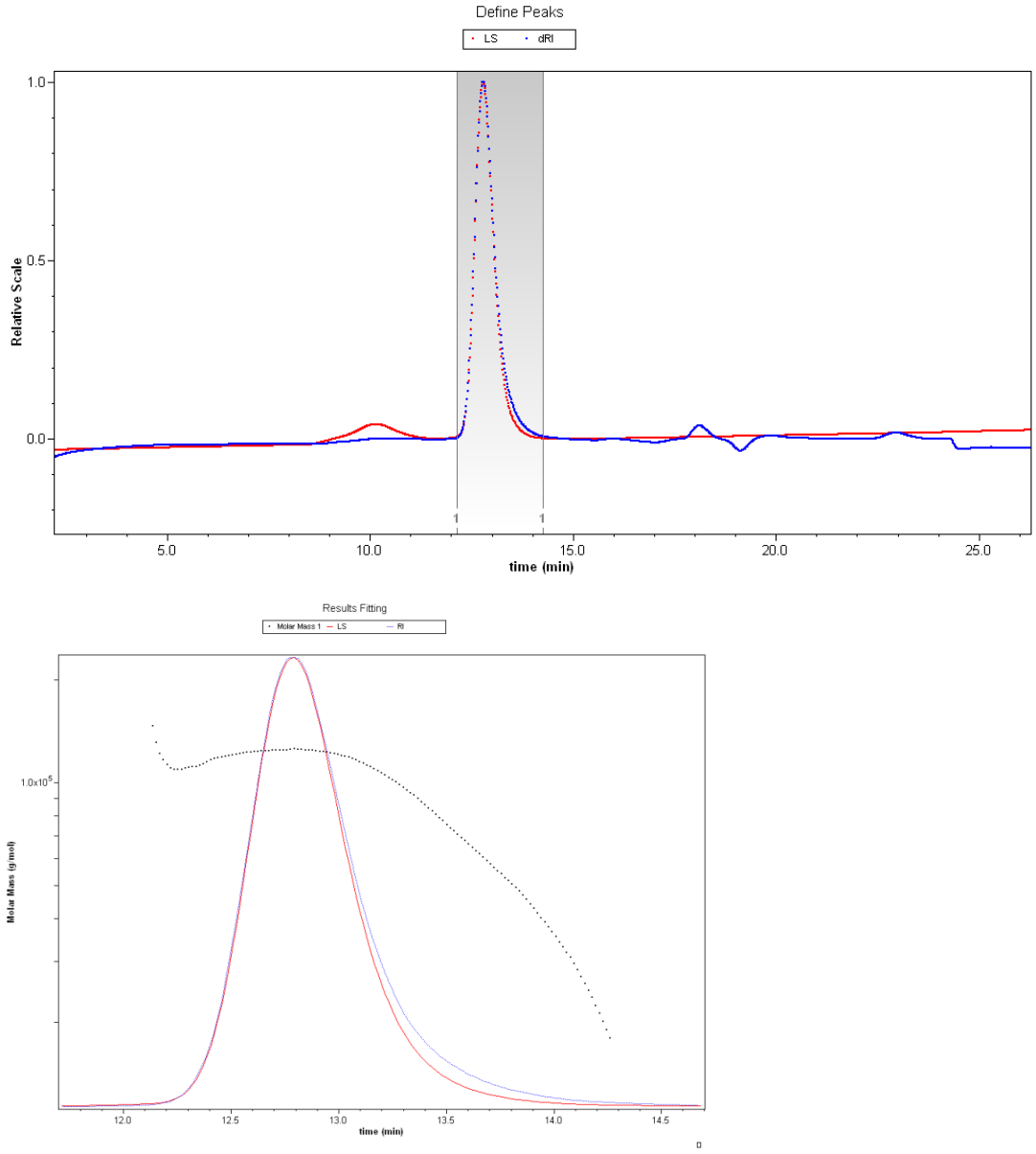

Figure S 30 REM-GTP (2VP), table 2, entry 2, conversion 82%.

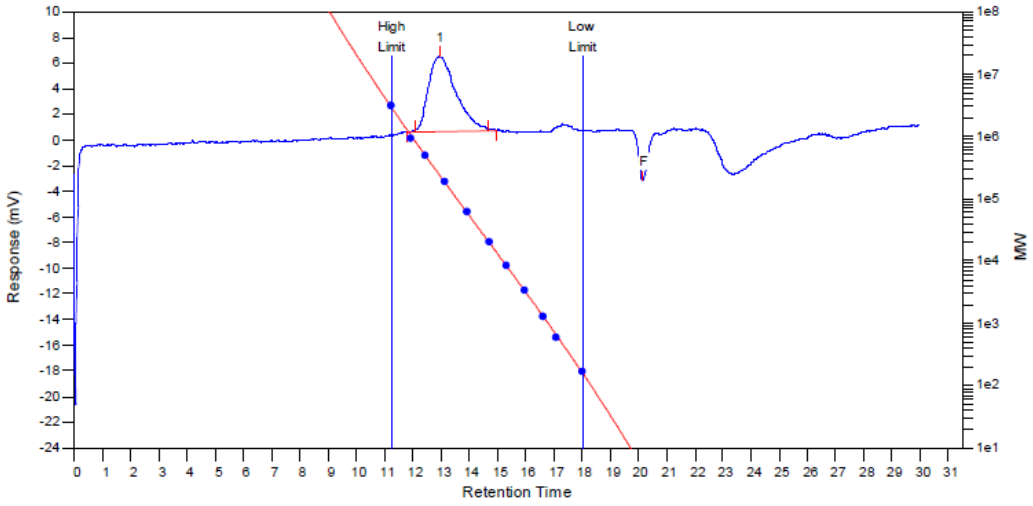

MW Averages

Peak No	Mp	Mn	Mw	Mz	Mz+1	Mv	PD
1	232020	141585	222664	303406	374741	210730	1.57265
2	0	0	0	0	0	0	0

Figure S 31 ROP (BL), table 2, entry 3, conversion 99%.

2.7.2 Block copolymerization

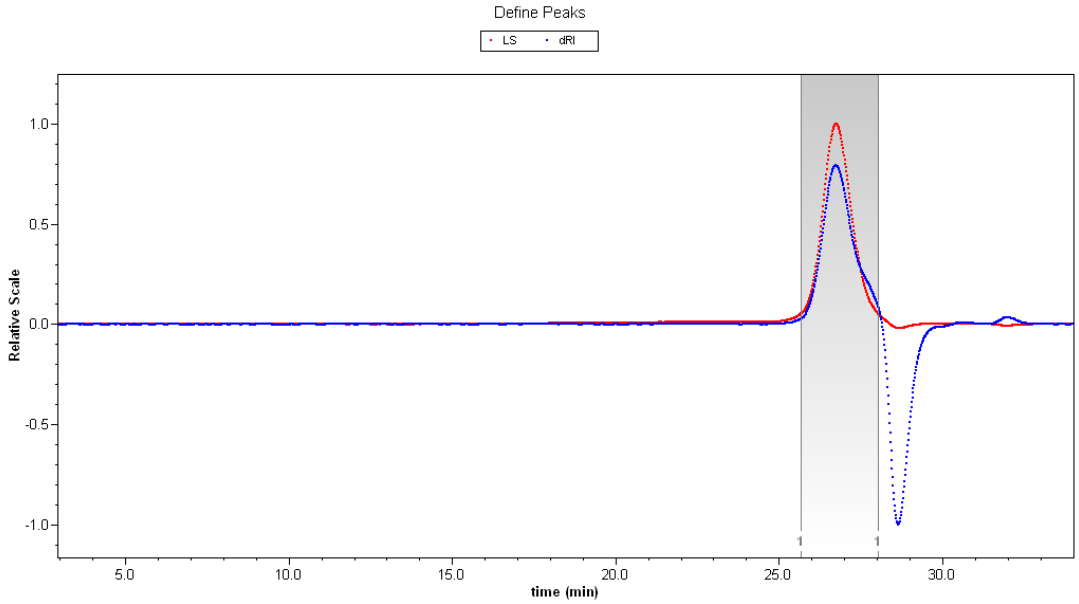

Figure S 32 REM-GTP (P2VP-b-PDEVP), table 4, entry 1.

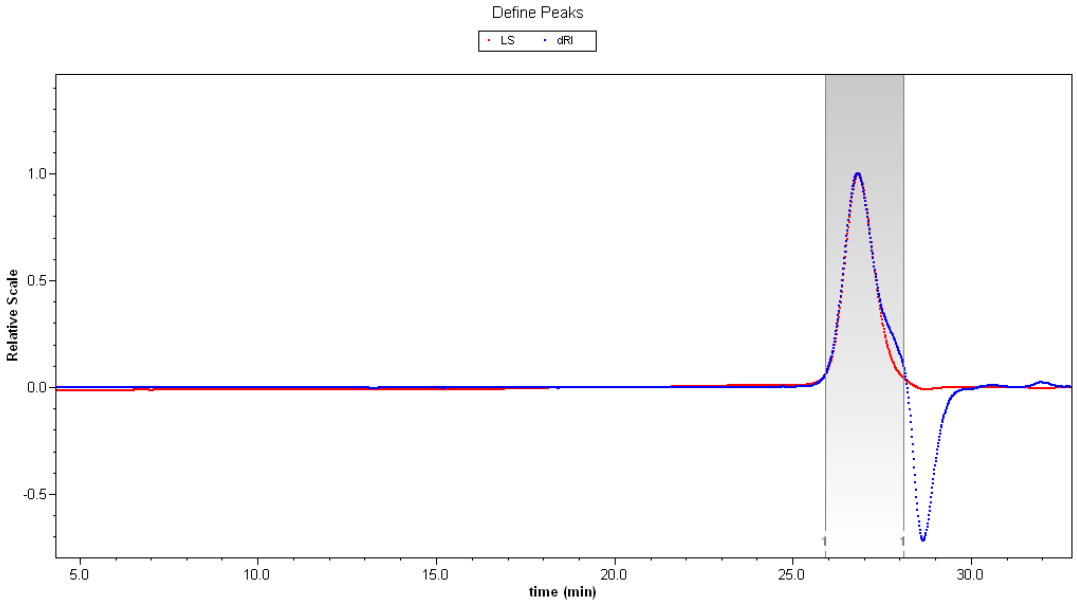

Figure S 33 REM-GTP (P2VP), table 4, entry 2 (aliquot sample).

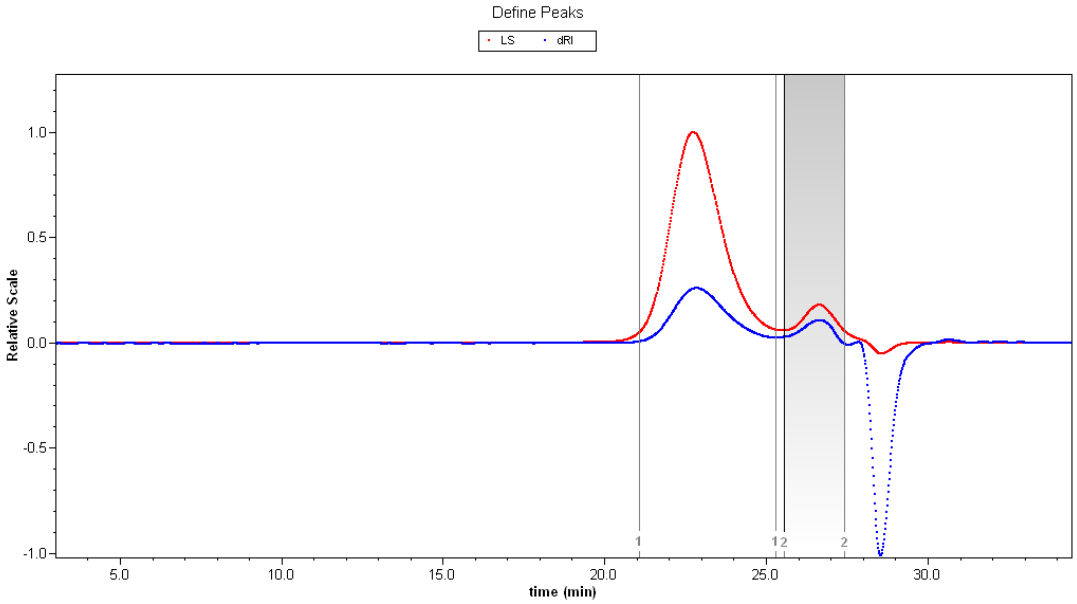

Figure S 34 REM-GTP (P2VP-b-PIPOx), table 4, entry 2.

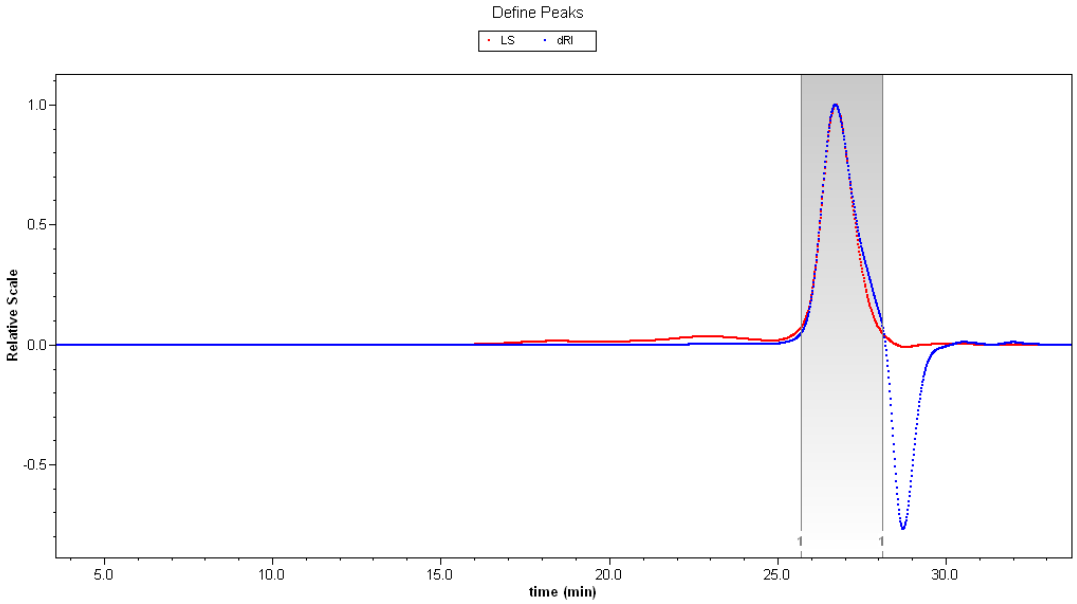

Figure S 35 REM-GTP (P2VP), table 4, entry 3 (aliquot sample).

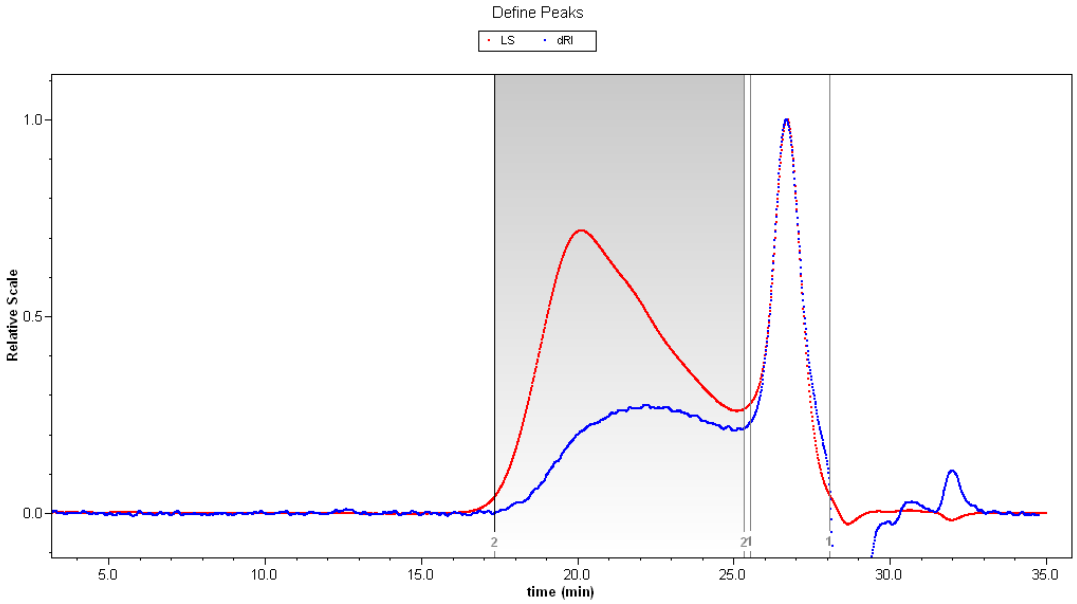

Figure S 36 REM-GTP (P2VP-b-PDMAA), table 4, entry 3.

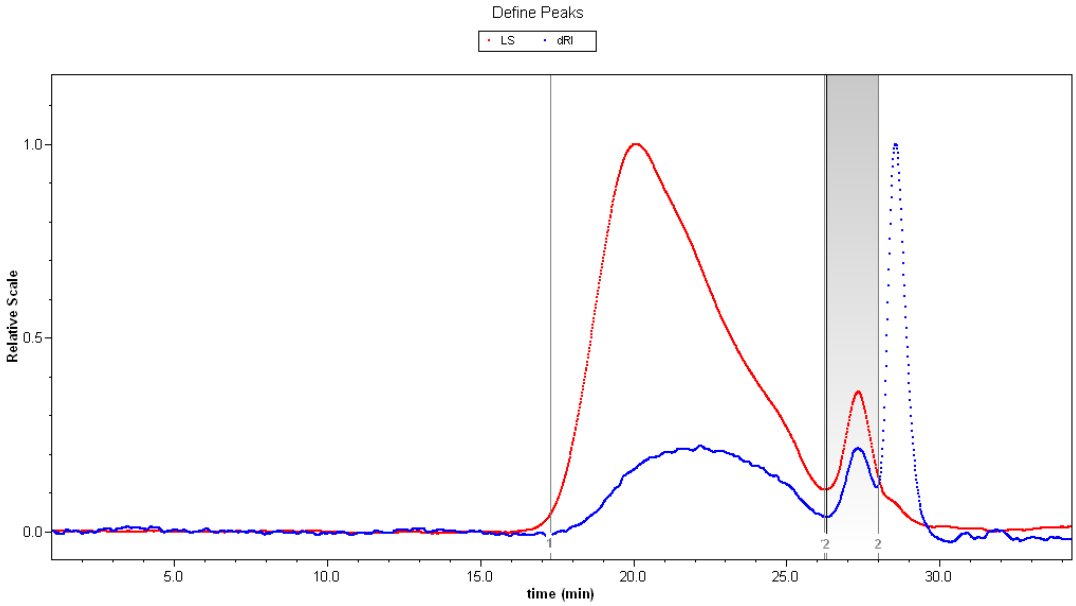

Figure S 37 REM-GTP (P2VP-b-PDMAA), table 4, entry 3: 2 hours washing with toluene.

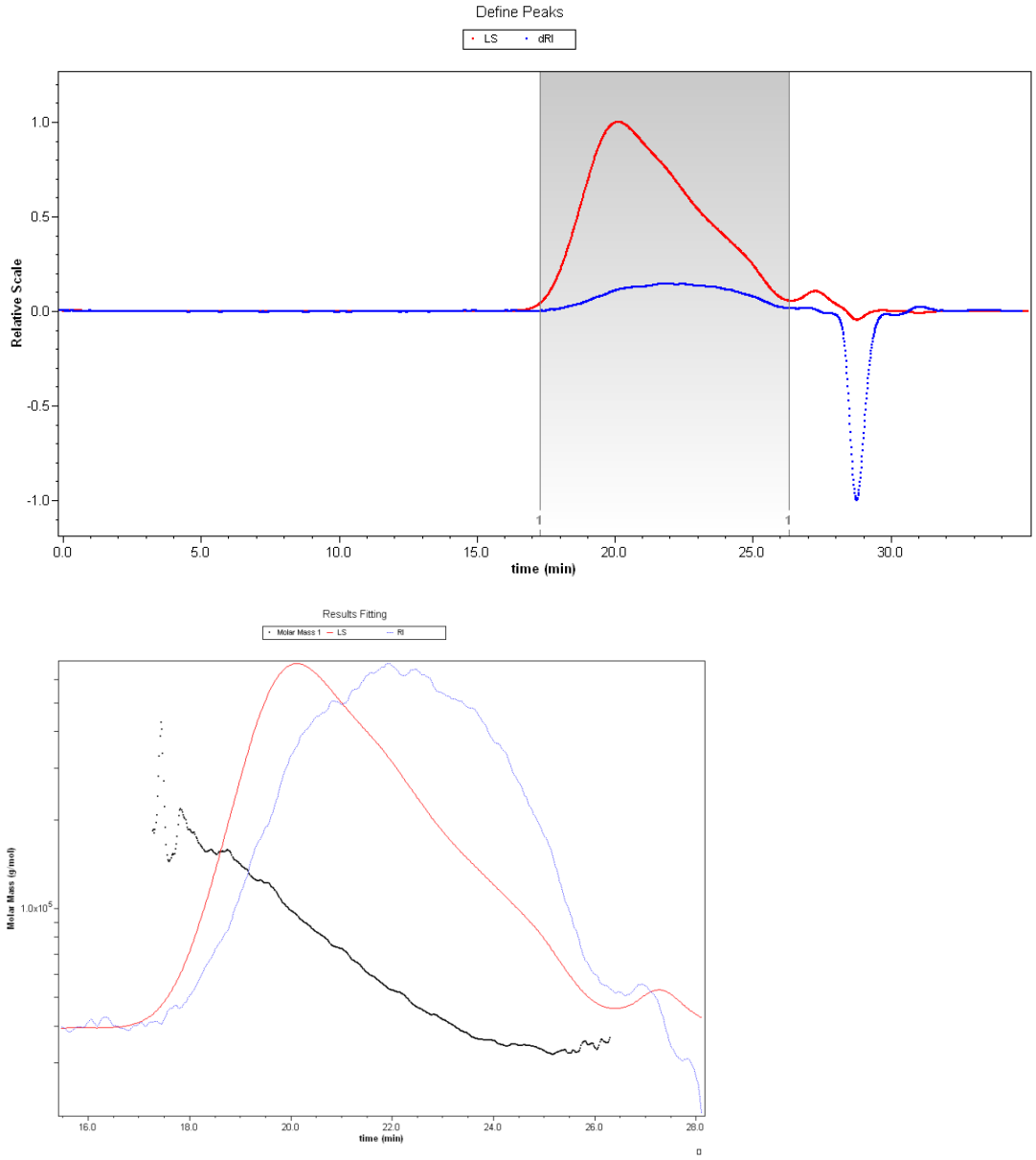

Figure S 38 REM-GTP (P2VP-b-PDMAA), table 4, entry 3: 48 hours washing with toluene.

1. Dimov, D. K.; Hogen-Esch, T. E. *Macromolecules* **1995,** 28, (22), 7394-400.

7.4 Supporting Information: Stereospecific Catalytic Precision Polymerization of 2-Vinylpyridine via Rare Earth Metal-Mediated Group Transfer Polymerization with 2-Methoxyethylamino-bis(phenolate)-Yttrium Complexes

Status	Published online: 13th August 2015
Journal	Polymer Chemistry
Publisher	RSC Publishing
Article type	Communication
DOI	DOI: 10.1039/c5py01146a
Authors	Peter T. Altenbuchner; Friederike Adams; Alexander Kronast; Eberhardt Herdtweck; Alexander Pöthig; Bernhard Rieger

Supporting Information for the Manuscript Entitled

Stereospecific Catalytic Precision Polymerization of 2-Vinylpyridine via Rare Earth Metal-Mediated Group Transfer Polymerization with 2-Methoxyethylamino-bis(phenolate)-Yttrium Complexes

P. T. Altenbuchner,[a] F. Adams,[a] A. Kronast,[a] E. Herdtweck[b], A. Pöthig[b] and B. Rieger[a*]

Table of Contents

1 Experimental procedures

Materials and Methods.

All reactions were carried out under argon atmosphere using standard Schlenk or glovebox techniques. All glassware was heat dried under vacuum prior to use. Unless otherwise stated, all chemicals were purchased from Sigma-Aldrich, Acros Organics, or ABCR and used as received. Toluene, thf and pentane were dried using a MBraun SPS-800 solvent purification system. Hexane was dried over 3 Å molecular sieves. The precursor complexes $Ln(CH_2Si(CH_3)_3)_3(thf)_2$ (Ln = Y,Lu) and $Y(N(SiH(CH_3)_2)_2)_3(thf)_2$, $LiCH_2TMS$ and catalysts 4 and 5 are prepared according to literature procedures.[1-4] Triethylamine and 2-vinylpyridine were dried over calcium hydride and distilled prior to use.

Initiator efficiency ($I^* = M_{n,calc}/M_{n,exp}$) is determined by taking aliquots and at the end of the polymerization. I^*_t is determined for polymerization kinetics as the average initiator efficiency of I^* at the maximum rate of the reaction (maximum slope of the conversion-reaction time plot).

NMR spectra were recorded on a Bruker AVIII-300, AVIII-500 Cryo and AVIII 900 Cryo spectrometer. Unless otherwise stated, ^{1}H- and ^{13}C-NMR spectroscopic chemical shifts δ are reported in ppm relative to δ (^{1}H) is calibrated to the residual proton signal, δ (^{13}C) to the carbon signal of the solvent. Unless otherwise stated, coupling constants J are averaged values and refer to couplings between two protons. Deuterated solvents were obtained from Sigma-Aldrich and dried over 3 Å molecular sieves.

Elemental analyses were measured at the Laboratory for Microanalysis at the Institute of Inorganic Chemistry at the Technische Universität München.

ESI-MS analytical measurements were performed with methanol, isopropanol, ethyl acetate and toluene solutions on a Varian 500-MS spectrometer.

Single Crystal X-ray Crystallography was performed in the SCXRD laboratory of the Catalysis Research Center at the Technische Universität München. Additional crystallographic information is given below.

Polymerization Procedures. To a solution of 13.5 µmol catalyst (1.0 eq.) in 2 mL solvent at room temperature, 2.7 mmol monomer (200 eq.; 27 mmol [2VP]/ 20 mL solvent) was added in one portion. The polymerization is quenched by addition of methanol. Conversion is determined by ^{1}H-NMR-spectroscopy. The polymers were precipitated by addition of the reaction mixtures to pentane (100 mL) and the solution was decanted of. Residual solvent was removed by freeze-drying from benzene (100 mL) over night.

Kinetic measurements by aliquots method. To a solution of 135 µmol catalyst in 20 mL toluene at room temperature, the corresponding amount of monomer (27 mmol, 200 eq.) was added in one portion. Aliquots were taken from the reaction solution at regular time intervals and quenched by addition of MeOH. Solvent and not polymerized monomer were removed by drying the polymers under vacuum at

60 °C overnight. For each aliquot, the conversion is determined gravimetrically and the molecular weight of the polymer is determined by GPC-MALS analysis.

Characterization of P2VP Samples. The tacticity determination of P2VP was performed by ^{13}C-NMR-spectroscopy at room temperature. Spectra for the analysis of P2VP *mm*, *mr*/*rm* and *rr* triads were recorded with a sample concentration of 15% (w/w; 75 mg/0.6 mL CD_3OD) on a AVIII 500 Cryo spectrometer and analyzed according to literature.[5] Spectra for the analysis of P2VP pentades were recorded with a sample concentration of 6% (w/w; 30 mg/0.6 mL CD_3OD) on a AVIII 900 Cryo spectrometer and analyzed according to literature.[6] Unless otherwise stated, ^{13}C-NMR-spectra are measured with 2000 scans, a relaxation delay of 4 seconds and calibrated to the *mmmm*-pentade of the aromatic quaternary carbon-atom of P2VP due to better possibility of comparison.

Gel permeation chromatography (GPC) was carried out with samples of 5 mg/mL concentration on a Varian LC-920 equipped with two PL Polargel columns. As eluent a mixture of THF/water (1:1; v:v), 9 g/L tetrabutylammonium bromide (TBAB) and 680 mg/L_{THF} 3,5-di-tert-butyl-4-hydroxytoluene (BHT), was used. Absolute molecular weights have been determined online by multiangle light scattering (MALS) analysis using a Wyatt Dawn Heleos II in combination with a Wyatt Optilab rEX as concentration source.

Proligand Synthesis

Synthesis of 4-(tert-butyl)-2-tritylphenol after a modified literature procedure:[7]

4-tert-butylphenol (10.0 eq.) is heated up to 111 °C and sodium metal (1.39 eq.) is added to the molten phenol. The reaction mixture is stirred till melting of the sodium and triphenylchloromethane (1.0 eq) was added. The resulting mixture is heated for 3 h at 140 °C with vigorous stirring. After cooling down to 90 °C the reaction mixture is treated with 7% $NaOH_{aq.}$ and diethylether. The organic layer is separated, washed with 7% $NaOH_{aq.}$, water and brine and dried over anhydrous $MgSO_4$. After evaporation of the solvent, the crude product is recrystallized from hot ethanol. Yield: 65% (light yellow powder)

Synthesis route of formation of 2-methoxyethylamino-bis(phenolate)ligands (L_1-L_3):

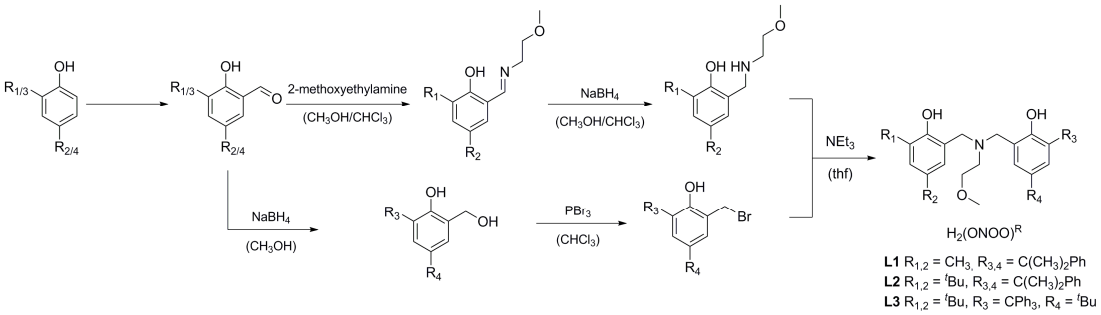

General procedure for the formylation of phenols after a modified literature procedure:[7]

The respective phenol (1.0 eq.), hexamethylenetetramine (1.0 eq.) and CF_3COOH are mixed and heated to 110 °C for 22 h and then cooled to 80 °C. 2 M HCl is added and the reaction mixture is cooled to room temperature. Chloroform is added and the organic layer is separated. The aqueous layer is extracted with chloroform two more times. The combined organic layers are washed with 2 M HCl, water and brine, separated and dried over $MgSO_4$. The solvents are evaporated and the residue is purified by recrystallization from methanol or column chromatography (SiO_2, hexane/EtOAc = 12:1).

General procedure for the synthesis of the secondary amines:

2-methoxyethylenamine (1.0 eq.) is added to a solution of the respective 2-hydroxybenzaldehyde (1.0 eq.) in methanol/chloroform (1:1, v:v). The reaction mixture is heated to reflux for 24 hours, cooled to 0 °C and $NaBH_4$ (2.1 eq.) is added in small portions. The reaction is kept at 50 °C for 48 h. After cooling to room temperature, the solution is acidified by adding concentrated HCl. All volatiles are removed under vacuum and the residue is dissolved in saturated aqueous Na_2CO_3. The aqueous layer is extracted with chloroform and the combined organic layers are dried over anhydrous $MgSO_4$ and concentrated *in vacuo*. Recrystallization from ethanol leads to the desired product.

4-(tert-Butyl)-2-(((2-methoxyethyl)imino)methyl)-6-tritylphenol

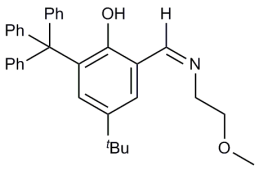

$C_{33}H_{35}NO_2$
M: 477.65

Yield: 61% (yellow powder)

^{1}H-NMR (300 MHz, $CDCl_3$, 300 K): δ (ppm) = 13.37 (s, 1H, C*H*O), 8.33 (s, 1H), 7.33 (d, ^4J = 2.4 Hz, 1H, H_{arom}), 7.25 – 7.09 (m, 16H, H_{arom}), 3.63 (t, ^3J = 5.5 Hz, 2H, CH_2), 3.54 (t, ^3J = 5.5 Hz, 2H, CH_2), 3.29 (s, 3H, CH_3), 1.17 (s, 9H, ^{t}Bu).

^{13}C-NMR (75 MHz, $CDCl_3$, 300 K): δ (ppm) = 166.7, 145.5, 133.9, 131.0, 128.3, 127.0, 126.9, 125.5, 118.0, 77.2, 71.6, 63.3, 58.9, 34.0, 31.3.

ESI-MS (toluene): 478.2 $[M]^+$.

4-(tert-butyl)-2-(((2-methoxyethyl)amino)methyl)-6-tritylphenol

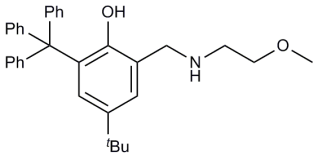

$C_{33}H_{37}NO_2$
M: 479.66

Yield: 67% (yellow powder)

^{1}H-NMR (300 MHz, $CDCl_3$, 300 K): δ (ppm) = 7.14 – 7.09 (m, 15H, H_{arom}), 7.00 (d, ^4J = 2.4 Hz, 1H, H_{arom}), 6.83 (d, ^4J = 2.4 Hz, 1H, H_{arom}), 3.81 (s, 2H, ArCH_2), 3.21 – 3.04 (m, 5H, CH_2, CH_3), 2.46 (t, ^3J = 5.0 Hz, 2H, CH_2), 1.05 (s, 9H, *t*Bu).

^{13}C-NMR (75 MHz, $CDCl_3$, 300 K): δ (ppm) = 154.2, 146.2, 140.1, 133.6, 131.1, 128.4, 127.7, 127.5, 127.0, 125.4, 124.3, 122.0, 71.0, 63.5, 58.9, 52.6, 47.2, 34.1, 31.6.

EA: calculated: C 82.63 H 7.73 N 2.92
found: C 83.48 H 7.92 N 2.73

2-(((2-methoxyethyl)amino)methyl)-4,6-bis(2-phenylpropan-2-yl)phenol

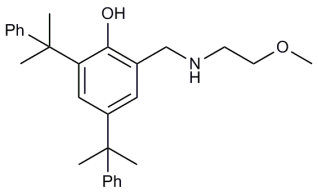

$C_{28}H_{35}NO_2$
M: 417.59

Yield: 74% (yellow powder)

^{1}H-NMR (300 MHz, $CDCl_3$, 298 K): δ (ppm) = 7.37 – 7.12 (m, 11H, H_{arom}), 6.81 (d, ^4J = 2.2 Hz, 1H, H_{arom}), 3.87 (s, 2H. ArCH_2), 3.43 (t, ^3J = 5.0 Hz, 2H), 3.26 (s, 3H, O*Me*), 2.74 (t, ^3J = 5.0 Hz, 2H), 1.69 (s, 6H, CMe_2Ph), 1.64 (s, 6H, CMe_2Ph).

^{13}C-NMR (75 MHz, $CDCl_3$, 298 K): δ (ppm) = 154.2, 151.5, 151.4, 139.9, 135.2, 128.0, 127.8, 126.9, 125.6, 125.5, 125.0, 124.9, 122.2, 70.9, 58.9, 52.8, 47.8, 42.5, 42.2, 31.2, 29.7.

ESI-MS (EtOAc): 418.3 $[M]^+$

2-(((2-methoxyethyl)amino)methyl)-4,6-dimethylphenol

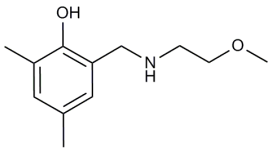

$C_{12}H_{19}NO_2$
M: 209.29

Yield: 63% (yellow powder)

^{1}H-NMR (300 MHz, $CDCl_3$, 300 K): δ (ppm) = 6.89 – 6.82 (m, 1H, H_{arom}), 6.66 – 6.61 (m, 1H, H_{arom}), 3.94 (s, 2H), 3.51 (m, 2H), 3.36 (s, 3H), 2.81 (m, 2H), 2.21 (s, 3H), 2.20 (s, 3H).

^{13}C-NMR (75 MHz, $CDCl_3$, 300 K): δ (ppm) = 153.9, 130.5, 127.5, 126.5, 124.9, 121.5, 71.1, 58.9, 52.4, 47.9, 20.5, 15.7.

ESI-MS (EtOAc): 210.4 $[M]^+$

2,4-di-tert-butyl-6-(((2-methoxyethyl)amino)methyl)phenol

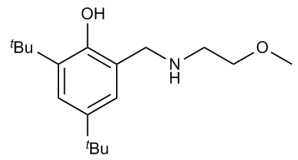

$C_{18}H_{31}NO_2$
M: 293.45

Yield: 78% (yellow powder)

^{1}H-NMR (300 MHz, $CDCl_3$, 300 K): δ (ppm) = 7.21 (virt. s, 1H, H_{arom}), 6.86 (d, ^4J = 2.5 Hz, 1H, H_{aron}), 3.96 (s, 2H), 3.53 (s, 2H), 3.36 (s, 3H), 2.84 (s, 2H), 1.42 (s, 9H, ^{t}Bu), 1.28 (s, 9H, ^{t}Bu).

^{13}C-NMR (75 MHz, $CDCl_3$, 300 K): δ (ppm) = 151.7, 144.4, 141.3, 127.0, 125.9, 121.1, 67.5, 59.1, 48.5, 45.6, 35.2, 34.5, 31.6, 30.2.

ESI-MS (EtOAc): 294.6 $[M]^+$

General procedure for the synthesis of bromomethyl-compounds:[8-10]

$NaBH_4$ (2.0 eq.) is slowly added to a stirred solution of the respective 2-hydroxybenzaldehyde (1.0 eq.) in methanol. The solution is stirred at room temperature for 1 h. All volatiles are removed in vacuum and the resulting residue is dissolved in water. The resulting aqueous mixture is neutralized with glacial acetic acid and extracted with CH_2Cl_2. The combined organic layers are dried with anhydrous $MgSO_4$ and concentrated to give a white solid which is immediately converted in the next step.

PBr_3 (0.5 eq.) is added to a stirred solution of 2-hydroxybenzyl alcohol (1.0 eq.) in chloroform. The mixture is stirred for 1 h at room temperature. Within 5 minutes cold water is added with vigorous stirring. The organic layer is separated and the aqueous residue is extracted with chloroform. The combined organic layers are dried with anhydrous $MgSO_4$ and concentrated *in vacuo* to yield the desired product.

General procedure for the synthesis of $H_2(ONOO)^R$:

One equivalent of the methylbromide is dissolved in tetrahydrofurane and added dropwise to a solution of one equivalent of the respective secondary amine in tetrahydrofurane. The solution is stirred for 30 minutes at room temperature before 1.5 equivalents of triethylamine are added slowly. The solution is heated up to 75 °C for 14 hours. The solid is filtered off and the solvent is removed *in vacuo*. A respective purification leads to the desired product.

$H_2(ONOO)^{Me,C(CH_3)_2Ph}$ (L1):

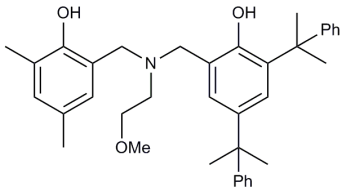

$C_{37}H_{45}NO_3$
M: 551.77

L1

A gradient column chromatographic purification (SiO_2, hexane / EtOAc = 12: 1 → 9: 1) yields the desired product. Yield: 64% (white powder)

DC: R_f = 0.25 (hexane/EtOAc = 20:1) [UV]

^{1}H-NMR (300 MHz, $CDCl_3$, 300 K): δ (ppm) = 7.33 – 7.12 (m, 11H, H_{arom}), 6.84 (s, 2H, H_{arom}), 6.57 (d, ^4J = 2.2 Hz, 1H, H_{arom}), 3.63 (d, ^2J = 3.0 Hz, 4H, ArCH_2), 3.33 (t, ^3J = 5.3 Hz, 2H, $H_{sidearm}$), 3.22 (s, 3H, O*Me*), 2.56 (t, ^3J = 5.3 Hz, 2H, $H_{sidearm}$), 2.18 (s, 6H), 1.69 (s, 6H), 1.63 (s, 6H).

^{13}C-NMR (75 MHz, $CDCl_3$, 300 K): δ (ppm) = 151.3, 150.2, 135.2, 128.3, 128.2, 127.9, 126.7, 125.8, 125.4, 120.9, 71.1, 58.7, 56.3, 56.0, 50.9, 42.5, 42.0, 31.0, 29.5, 20.4, 16.0.

EA: calculated: C 80.54 H 8.22 N 2.54
found: C 80.50 H 8.32 N 2.56

ESI-MS (iso-propanol): 552.5 $[M]^+$

H_2(ONOO)$^{tBu,C(CH_3)_2Ph}$(L2):

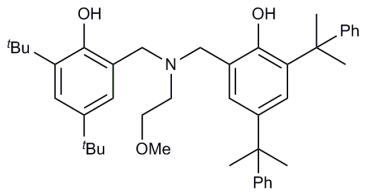

$C_{43}H_{57}NO_3$
M: 635.93

L2

A column chromatographic purification (SiO_2, hexane / EtOAc = 12: 1) yields the desired product. Yield: 49% (white powder)

DC: R_f = 0.46 (hexane/EtOAc = 12:1) [UV]

^{1}H-NMR (300 MHz, $CDCl_3$, 300 K): δ (ppm) = 7.37 – 7.11 (m, 12H, H_{arom}), 6.91 (d, ^4J = 2.4 Hz, 1H, H_{arom}), 6.83 (d, ^4J = 2.4 Hz, 1H, H_{arom}), 3.68 (s, 2H), 3.61 (s, 2H), 3.27 (t, ^3J = 5.4 Hz, 2H, H_{Henkel}), 3.17 (s, 3H, O*Me*), 2.59 (t, ^3J = 5.4 Hz, 2H, H_{Henkel}), 1.71 (s, 6H, C*Me*$_2$Ph), 1.64 (s, 6H, C*Me*$_2$Ph),1.42 (s, 9H, *t*Bu), 1.29 (s, 9H, *t*Bu).

^{13}C-NMR (75 MHz, $CDCl_3$, 300 K): δ (ppm) = 153.3, 151.7, 151.2, 150.2, 140.7, 140.4, 135.7, 135.4, 128.0, 127.8, 127.4, 126.7, 125.9, 125.4, 125.4, 124.8, 124.4, 123.1, 122.8, 121.6, 71.0, 58.5, 58.3, 56.0, 51.4, 42.5, 41.9, 34.9, 34.0, 31.7, 31.0, 29.6, 29.3.

EA: calculated: C 81.22 H 9.03 N 2.20
found: C 81.39 H 9.24 N 2.01

ESI-MS (iso-propanol): 636.6 $[M]^+$

$H_2(ONOO)^{tBu,tBu,CPh3}$ (L3):

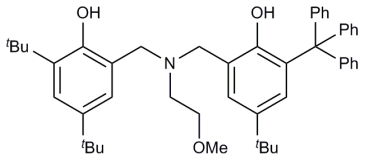

$C_{48}H_{59}NO_3$
M: 698.00

L3

A gradient column chromatographic purification (SiO_2, hexane / EtOAc = 20: 1 → 11: 1) yields the desired product. Yield: 43% (white powder)

DC: R_f = 0.25 (hexane/EtOAc = 20:1) [UV]

^{1}H-NMR (300 MHz, $CDCl_3$, 300 K): δ (ppm) = 7.17 – 7.13 (m, 6H, H_{arom}), 7.10 (m, 10H, H_{arom}), 7.06 (d, ^4J = 2.4 Hz, 1H, H_{arom}), 6.96 (d, ^4J = 2.4 Hz, 1H, H_{arom}), 6.75 (d, ^4J = 2.4 Hz, 1H, H_{arom}), 3.68 (s, 2H, ArCH_2), 3.55 (s, 2H, ArCH_2), 3.21 (t, ^3J = 5.6 Hz, 2H, $H_{sidearm}$), 3.07 (s, 3H, O*Me*), 2.48 (t, ^3J = 5.6 Hz, 2H, $H_{sidearm}$), 1.18 (s, 9H, ^{t}Bu), 1.04 (s, 9H, ^{t}Bu).

^{13}C-NMR (126 MHz, $CDCl_3$, 300 K): δ (ppm) = 153.9, 151.6, 145.2, 141.6, 140.5, 135.8, 133.2, 131.2, 128.5, 127.9, 127.6, 127.2, 126.2, 124.3, 123.8, 123.1, 121.7, 70.9, 63.4, 58.8, 58.7, 54.7, 51.3, 35.1, 34.3, 34.2, 31.8, 31.6, 29.9.

EA: calculated: C 82.60 H 8.52 N 2.01
found: C 82.58 H 8.63 N 2.00

Catalyst Synthesis

General procedure for the synthesis of $(ONOO)^{R}Y(CH_2Si(CH_3)_3)(thf)$:[4]

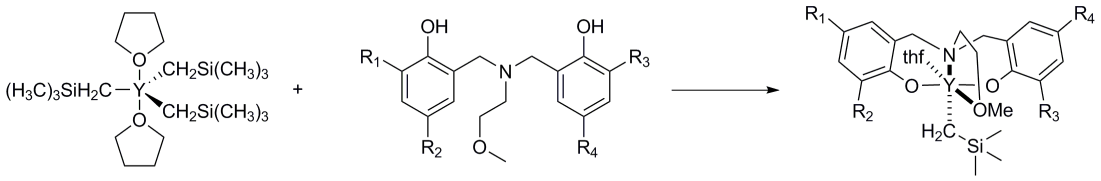

$[Y(CH_2Si(CH_3)_3)_3(thf)_2]$ $H_2(ONOO)^{R}$ $(ONOO)^{R}Y(CH_2Si(CH_3)_3)(thf)$

1 $R_{1,2} = CH_3$, $R_{3,4} = C(CH_3)_2Ph$
2 $R_{1,2} = {}^{t}Bu$, $R_{3,4} = C(CH_3)_2Ph$
3 $R_{1,2,4} = {}^{t}Bu$, $R_3 = CPh_3$
4 $R_{1,2,3,4} = {}^{t}Bu$
5 $R_{1,2,3,4} = C(CH_3)_2Ph$

One equivalent of proligand $H_2(ONOO)^{R}$ in toluene is added to a stirred solution of $Y(CH_2Si(CH_3)_3)_3(thf)_2$ in pentane at 0 °C. The resulting solution is stirred overnight at room temperature. The solvent is removed *in vacuo* and the resulting solid is washed with pentane.

$[(ONOO)^{Me,C(CH_3)_2Ph}Y(X)]_2$ (1):

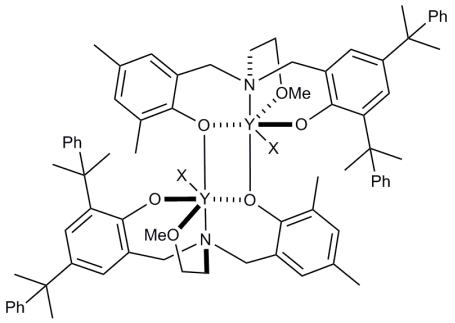

1 X = $CH_2Si(CH_3)_3$
1a X = $N(SiH(CH_3)_2)_2$

Catalyst 1:

Synthesis led to a dimeric structure. Yield: 56% (white powder)

^{1}H-NMR (500 MHz, C_6D_6, 300 K): δ (ppm) = 7.44 (d, ^{4}J = 2.5 Hz, 2H, H_{arom}), 7.37 – 7.30 (m, 8H, H_{arom}), 7.20 (t, ^{3}J = 7.6 Hz, 4H, H_{arom}), 7.12 – 7.06 (m, 6H, H_{arom}), 6.97 (d, ^{4}J = 2.5 Hz, 2H, H_{arom}), 6.95 (t, ^{3}J = 7.6 Hz, 2H, H_{arom}), 6.74 (d, ^{4}J = 2.3 Hz, 2H, H_{arom}), 6.61 (d, ^{4}J = 2.3 Hz, 2H, H_{arom}), 4.96 (d, ^{2}J = 12.7 Hz, 2H, CH_2Ar), 4.71 (d, ^{2}J = 12.7 Hz, 2H, CH_2Ar), 3.18 (d, ^{2}J = 12.7 Hz, 2H, CH_2Ar), 2.74 (d, ^{2}J = 12.7 Hz, 2H, CH_2Ar), 2.45 (s, 6H, O*Me*), 2.39 – 2.21 (m, 4H, H_{Henkel}), 2.20 (s, 6H), 2.14 (s, 6H), 2.12 – 2.08 (m, 4H, H_{Henkel}), 1.84 (s, 6H), 1.77

(s, 6H), 1.69 (s, 6H), 1.69 (s, 6H), 0.27 (s, 18H, H_{TMS}), -0.91 (dd, ^2J = 11.2 Hz, $^2J_{H,Y}$ = 3.1 Hz, 2H, CH_2TMS), -1.00 (dd, ^2J = 11.2 Hz, $^2J_{H,Y}$ = 3.1 Hz, 2H, CH_2TMS).

^{13}C-NMR (126 MHz, C_6D_6, 300 K): δ (ppm) = 160.8 (d, $^2J_{C,Y}$ = 3.4 Hz), 153.8, 152.1, 151.6, 137.3, 136.5, 133.4, 129.5, 129.3, 129.2, 128.8, 127.5, 127.2, 126.5, 125.7, 125.6, 125.0, 124.2, 73.0, 64.6, 63.3, 60.8, 49.7, 43.0, 42.7, 31.5 (d, $^1J_{C,Y}$ = 11.3 Hz), 31.2, 28.9, 26.9, 26.5, 20.6, 17.6, 5.3.

EA: calculated: C 67.84 H 7.50 N 1.93
found: C 67.87 H 7.35 N 2.02

Catalyst 1a:

Monomeric structure (333 K):

^{1}H-NMR (300 MHz, THF-d_8, 333 K): δ (ppm) = 7.28 – 6.93 (m, 11H, H_{arom}), 6.79 (d, ^4J = 2.5 Hz, 1H, H_{arom}), 6.77 – 6.76 (m, 1H, H_{arom}), 6.59 (m, 1H, H_{arom}), 4.80 (m, 2H, Si-*H*), 3.84 (d, ^2J = 12.6 Hz, 1H, CH_2Ar), 3.67 (d, ^2J = 12.6 Hz, 1H, CH_2Ar), 3.36 (m, 2H), 3.29 (s, 3H, OCH_3), 3.07 (d, ^2J = 12.9 Hz, 1H, CH_2Ar), 2.66 – 2.45 (m, 2H), 2.30 (br s, 1H), 2.12 (s, 3H), 2.11 (s, 3H), 1.82 (s, 3H), 1.65 - 1.63 (m, 9H), 0.19 (d, ^3J = 3.1 Hz, 6H, Si-CH_3), 0.15 (d, ^3J = 3.1 Hz, 6H, Si-CH_3).

^{13}C-NMR (101 MHz, THF-d_8, 333 K): δ (ppm) = 161.9 (d, $^2J_{C,Y}$ = 2.5 Hz), 161.4 (d, $^2J_{C,Y}$ = 2.5 Hz), 153.5, 153.0, 136.3, 136.2, 132.0, 129.6, 129.2, 128.9, 128.5, 128.4, 128.0, 127.5, 127.3, 127.2, 126.0, 125.9, 125.8, 125.2, 125.0, 123.5, 123.3, 73.6, 63.7, 63.3, 61.6, 51.2, 43.4, 43.0, 31.7, 31.6 (d, J = 1.6 Hz), 29.8 , 20.6 , 17.4 , 4.1, 4.0.

For dimeric structure ($C_{82}H_{114}N_4O_6Si_4Y_2$):

EA: calculated: C 63.87 H 7.45 N 3.63
found: C 63.95 H 7.45 N 3.58

(ONOO)$^{t\text{Bu,C(CH}_3)_2\text{Ph}}$Y(CH$_2$Si(CH$_3$)$_3$)(thf) (2):

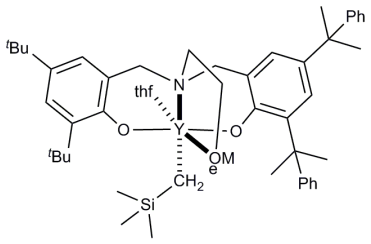

$C_{51}H_{74}NO_4SiY$
M: 882.15

2

Yield: 47% (white powder)

^{1}H-NMR (300 MHz, C_6D_6, 300 K): δ (ppm) = 7.68 (d, ^4J = 2.6 Hz, 1H, H_{arom}) 7.58 (d, ^2J = 2.6 Hz, 1H, H_{arom}), 7.50 (d, ^3J = 7.5 Hz, 2H, H_{arom}), 7.46 – 7.40 (m, 2H, H_{arom}), 7.25 – 7.18 (m, 4H, H_{arom}), 7.11 (t, ^3J = 7.5 Hz, 1H, H_{arom}), 7.00 (d, ^4J = 2.6 Hz, 1H, H_{arom}), 6.97 (t, ^3J = 7.5 Hz, 1H, H_{arom}), 6.88 (d, ^4J = 2.6 Hz, 1H, H_{arom}), 3.63 – 3.28 (m, 6H, ArCH_2+H_{THF}), 2.72 (s, 3H), 2.64 (m, 2H, ArCH_2), 2.49 – 2.37 (m, 2H), 2.16 – 2.10 (m, 1H), 2.07 (s, 3H), 2.02 (m, 1H), 1.80 (m, 18H), 1.45 (s, 9H), 1.14 – 1.05 (m, 4H, H_{THF}), 0.49 (s, 9H, H_{TMS}), -0.55 – -0.65 (m, 2H, CH_2TMS).

^{13}C-NMR (126 MHz, C_6D_6, 300 K): δ (ppm) = 161.6 (d, $^2J_{C,Y}$ = 2.4 Hz), 161.2 (d, $^2J_{C,Y}$ = 2.3 Hz), 136.7, 136.5, 136.2, 136.1, 128.5, 128.4, 128.3, 128.1, 127.9, 127.3, 126.4, 125.9, 125.8, 125.6, 124.5, 124.4, 124.3, 124.0, 73.9, 71.3, 64.6, 64.2, 61.2, 49.0, 42.7, 42.6, 35.6, 34.4, 34.2, 32.4, 32.3, 31.7 (d, $^1J_{C,Y}$ = 14.9 Hz), 30.4, 28.2, 25.2, 25.0, 24.9, 22.7.

EA: calculated: C 69.44 H 8.46 N 1.59
found: C 68.99 H 8.48 N 1.61

(ONOO)$^{t\text{Bu}\ t\text{Bu,CPh}_3}$Y($CH_2Si(CH_3)_3$)(thf) (3):

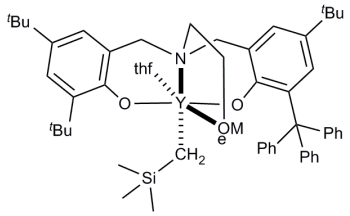

$C_{56}H_{76}NO_4SiY$
M: 944.22

3

Yield: 45% (white powder)

^{1}H-NMR (500 MHz, C_6D_6, 300 K): δ (ppm) = 7.63 (d, ^4J = 2.6 Hz, 1H, H_{arom}), 7.59 (d, ^4J = 2.6 Hz, 1H, H_{arom}), 7.58 – 7.53 (m, 7H, H_{arom}), 7.18 (d, J = 2.6 Hz, 1H, H_{arom}), 7.14 (t, ^3J = 7.6 Hz, 4H, H_{arom}), 7.05 (d, ^2J = 2.6 Hz, 1H, H_{arom}), 6.99 (t, ^3J = 7.6 Hz, 4H, H_{arom}), 3.66 (d, ^2J = 12.4 Hz, 1H, C$H_a$$H_b$Ar), 3.59 (d, ^2J = 12.4 Hz, 1H, CH$_a$$H_b$Ar), 3.52 – 3.37 (m, 4H, H_{THF}), 2.91 – 2.78 (m, 2H), 2.77 (s, 3H, O*Me*), 2.62 – 2.55 (m, 1H), 2.52 – 2.44 (m, 1H), 2.40 – 2.31 (m, 1H), 2.02 – 1.94 (m, 1H), 1.77 (s, 9H, *t*Bu), 1.46 (s, 9H, *t*Bu), 1.37 (s, 9H, *t*Bu), 1.16 (br s, 4H, H_{THF}), 0.30 (s, 9H, H_{TMS}), -1.05 (dd, $^2J_{H,Y}$ = 3.2 Hz, ^2J = 10.9 Hz, 1H, CH_2TMS), -1.29 (dd, $^2J_{H,Y}$ = 3.4 Hz, ^2J = 10.9 Hz, 1H, CH_2TMS).

^{13}C-NMR (126 MHz, C_6D_6, 300 K): δ (ppm) = 161.6 (d, $^2J_{C,Y}$ = 19.4 Hz), 136.6, 136.4, 136.1, 134.8, 131.8, 130.3, 128.1, 127.9, 127.4, 126.9, 125.3, 124.4, 74.0, 71.4, 65.0, 64.6, 64.3, 61.7, 49.6, 35.7, 34.4, 34.2 (d, $^1J_{C,Y}$ = 3.7 Hz), 32.3, 32.1, 30.5, 25.0, 22.7, 14.3, 4.9, 1.4.

EA: calculated: C 71.24 H 8.11 N 1.48
found: C 70.98 H 8.32 N 1.60

2 Crystallographic data of Complex 1a

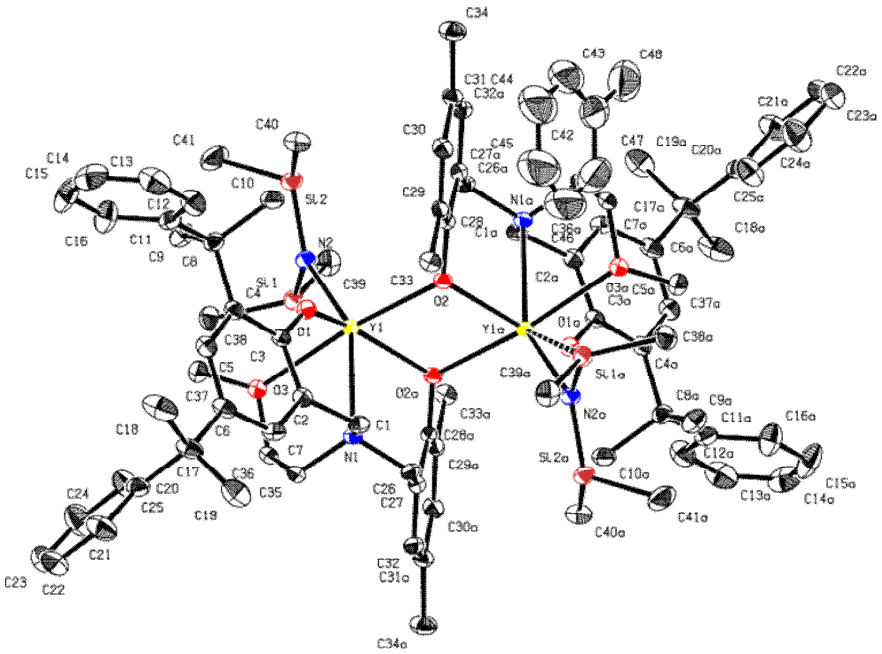

Figure S 1 ORTEP structure of complex 1a with 50% thermal ellipsoid. All H-atoms have been omitted for clarity. Selected bond distances [Å] and angles [deg]: Y(1)-O(1), 2.1181(18); Y(1)-O(2), 2.2883(19); Y(1)-O(3), 2.4661(19); Y(1)-N(1), 2.593(2); Y(1)-N(2), 2.280(2); Y(1)-Si(1), 3.2238(2); Y(1)-O(2a), 2.3170(18); O(1)-Y(1)-O(2), 94.92(7); O(1)-Y(1)-O(3), 85.17(7); O(2)-Y(1)-O(3), 172.89(7); O(1)-Y(1)-N(1), 78.20(7); O(1)-Y(1)-N(2), 105.11(8); O(1)-Y(1)-O(2a), 146.58(7); O(2)-Y(1)-N(1), 105.58(7); O(2)-Y(1)-N(2), 105.07(7); O(2)-Y(1)-O(2a), 70.24(6); N(1)-Y(1)-N(2), 148.74(8); O(3)-Y(1)-N(1), 67.45(7); O(3)-Y(1)-N(2), 81.72(7); O(2a)-Y(1)-O(3), 105.98(6); O(2a)-Y(1)-N(1), 77.45(7); O(2a)-Y(1)-N(2), 107.61(7); Y(1)-O(2)-Y(1a), 109.76(7).

Compound 1a adopts a dimeric structure in the solid state with a distorted octahedral-environment at both yttrium-centers as also found in a similar structure analyzed by Carpentier and co-workers.[11] Both complexes are THF-free complexes and each metal center is coordinated by an amido-ligand and a tetradentade 2-methoxyethylamino-bis(phenolate)-ligand. The dimeric structure originates from the insufficient bulkiness of the methyl-group as an ortho-substituent. The oxygen(phenolate)-atoms O(2) and O(2a) are able to form two µ-bridges between the two metal centers (Y(1)-Y(1a) = 3.767 Å) which leads to a planar Y(1)O(2)Y(1a)O(2a) metallacycle.

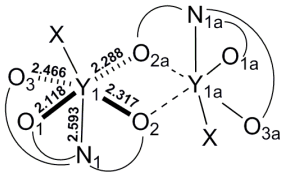

Figure S 2 Metallacycle Y(1)O(2)Y(1a)O(2a) originated from µ-bridges of the oxygen-atoms between the two metal centers. Selected bond distances are marked.

In this metallacycle the opposite bonds have the same lengths (Y(1)-O(2) = Y(1a)-O(2a), 2.2883(19); Y(1)-O(2a) = Y(1a)-O(2), 2.3170(18)) which leads to a high symmetrical rhombic-structure with bond angles of O(2)-Y(1)-O(2a) = O(2)-Y(1a)-O(2a) = 70.24° and Y(1)-O(2)-Y(1a) = Y(1)-O(2)-Y(1a) = 109.76°. This metallacycle is also found in the dimeric structure of Carpentier et al., with slightly different Y-(µ-O)-bond lengths ((Y(1)-O(1), 2,380(3); O(4)-Y(2), 2.381(3); Y(1)-O(4), 2.247(3); Y(2)-O(1), 2.344(3) which lead to a trapezoid-structure. The present close Y-Si contact of 3.224 Å already resemble Y-Si σ-bond distances suggesting an interaction in the solid state. Due to the close Y(1)-Si(1) distance of 3.224 Å (an interaction between these two centers is suggested. In addition, the relatively short Y-H distances of 2.875 Å show an interaction which leads to a formation of a four-membered Y(1)-N(2)-Si(1)-H(1)-ring with small torsional angles of -8°.The Si(1)-N(2)-Si(2) bond angle of 117.65(13) is not – as expected for Y-H-Si-agostic interaction- widened, because of an unsymmetrically interaction only on one site of the initiator.[4, 11-14]

Crystal data

$C_{82}H_{114}N_4O_6Si_4Y_2 \cdot 2(C_7H_8)$	$F(000) = 916$
$M_r = 1726.22$	
Triclinic, P	$D_x = 1.265$ Mg m^{-3}
Hall symbol: -P 1	
$a = 10.7741$ (3) Å	Mo $K\alpha$ radiation, $\lambda = 0.71073$ Å
$b = 13.3826$ (4) Å	Cell parameters from 9916 reflections
$c = 16.2750$ (5) Å	$\theta = 2.5–25.4°$
$\alpha = 82.3193$ (16)°	$\mu = 1.38$ mm^{-1}
$\beta = 83.5313$ (13)°	$T = 120$ K
$\gamma = 77.9230$ (13)°	Fragment, colourless
$V = 2265.39$ (12) Å^3	0.51 × 0.18 × 0.10 mm
$Z = 1$	

Data collection

Bruker APEX-II CCD diffractometer	8250 independent reflections
Radiation source: fine-focus sealed tube	7301 reflections with $I > 2\sigma(I)$
graphite	$R_{int} = 0.038$
Detector resolution: 16 pixels mm^{-1}	$\theta_{max} = 25.4°$, $\theta_{min} = 1.9°$
phi– and ω–rotation scans	$h = -12 \quad 12$
Absorption correction: multi-scan *SADABS*, Bruker, 2008b	$k = -16 \quad 16$
$T_{min} = 0.539$, $T_{max} = 0.874$	$l = -19 \quad 19$
39534 measured reflections	

Refinement

Refinement on F^2	Secondary atom site location: difference Fourier

	map
Least-squares matrix: full	Hydrogen site location: inferred from neighbouring sites
$R[F^2 > 2\sigma(F^2)] = 0.040$	H atoms treated by a mixture of independent and constrained refinement
$wR(F^2) = 0.114$	$w = 1/[\sigma^2(F_o^2) + (0.0662P)^2 + 2.1916P]$ where $P = (F_o^2 + 2F_c^2)/3$
$S = 1.06$	$(\Delta/\sigma)_{max} < 0.001$
8250 reflections	$\Delta\rho_{max} = 1.20$ e Å^{-3}
525 parameters	$\Delta\rho_{min} = -0.62$ e Å^{-3}
0 restraints	Extinction correction: none
Primary atom site location: structure-invariant direct methods	

3 High-temperature ^{1}H-NMR-spectroscopy of complex 1a

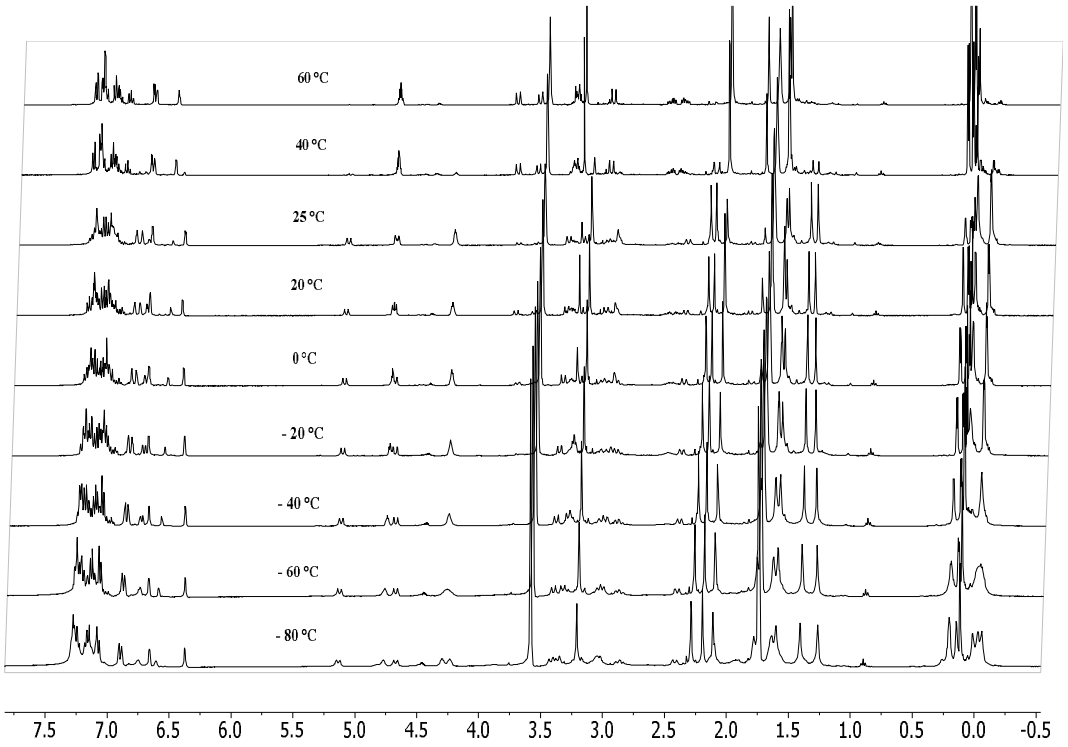

Figure S 3 ^{1}H NMR spectra of catalyst 1a at different temperatures (-80 °C-60 °C) in THF-d_8. Dissociation process at ~40 °C.

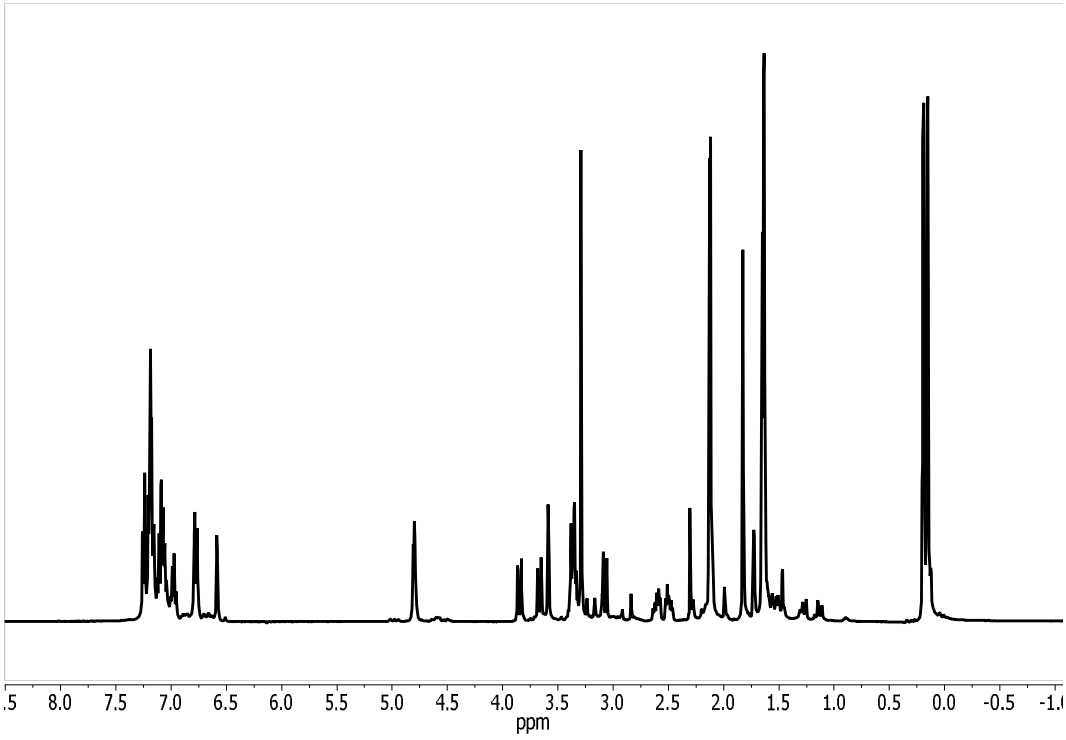

Figure S 4 ^{1}H NMR spectra of catalyst 1a at 60 °C in THF-d_8.

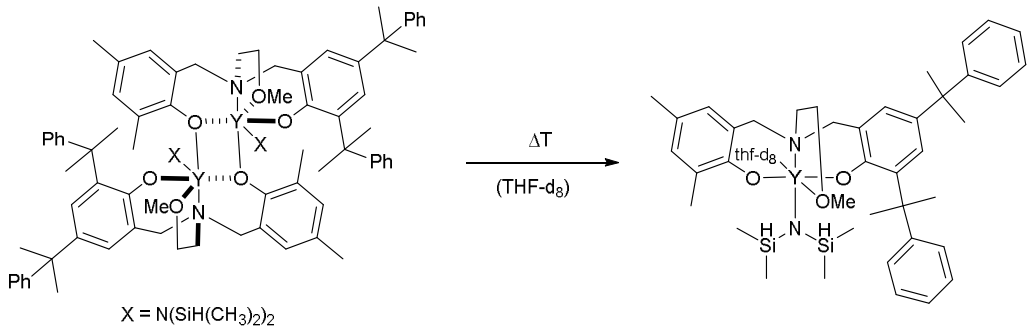

Figure S 5 Dissociation of complex 1a in THF-d_8 at elevated temperatures..

4 Kinetic investigations

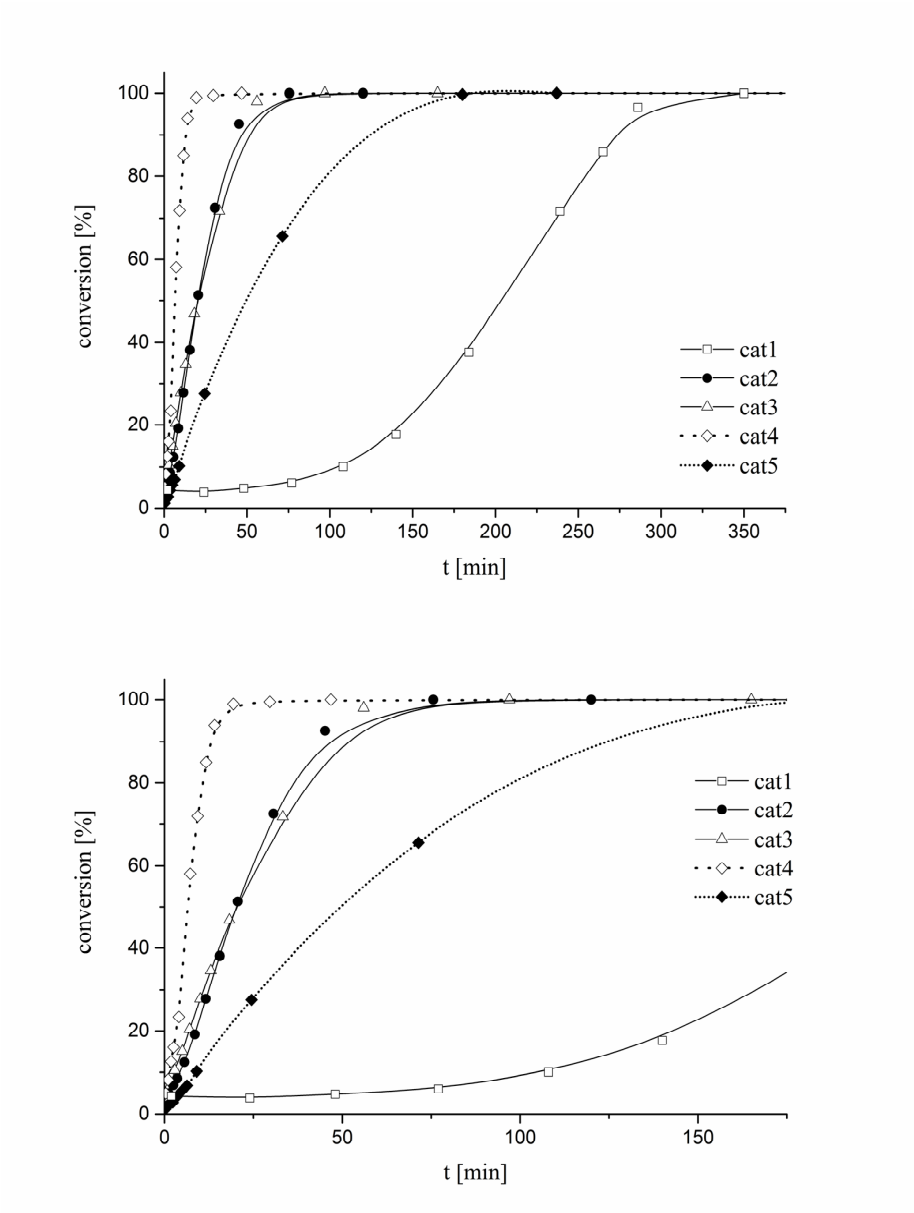

Figure S 6 Catalytic activity of catalyst 1 (square), 2 (circle), 3 (triangle), 4 (diamond, dotted), and 5 (diamond, short dotted) (catalyst 135 μmol, 2VP 27 mmol, toluene 20 mL, T = 25 °C) (table 1).

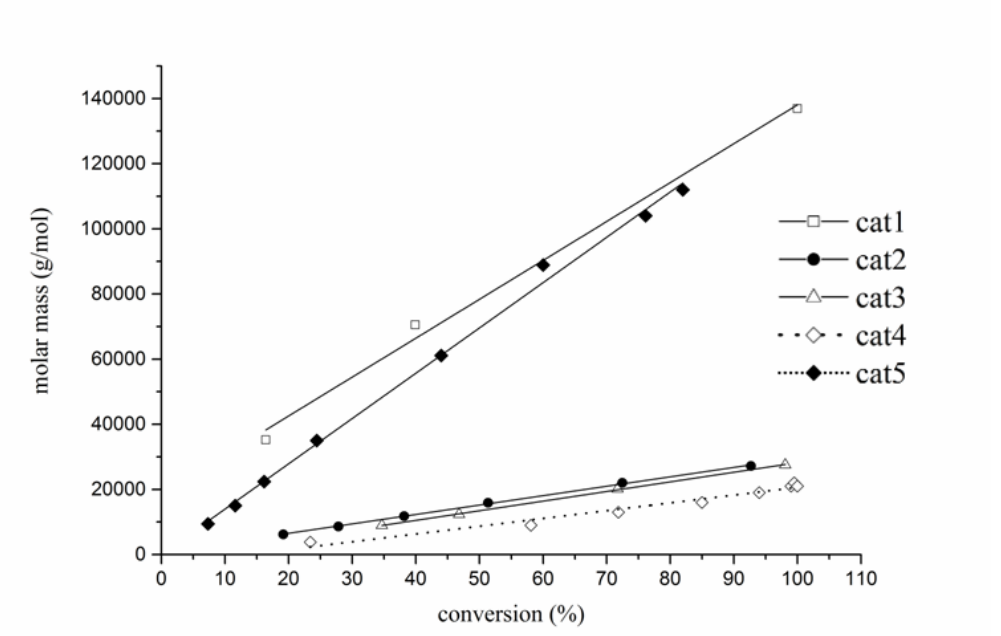

Figure S 7 Linear growth of the absolute molecular weight (M_n) for catalyst 1-5 (determined by GPC-MALS) as a function of monomer conversion (determined gravimetrically) (table 1).

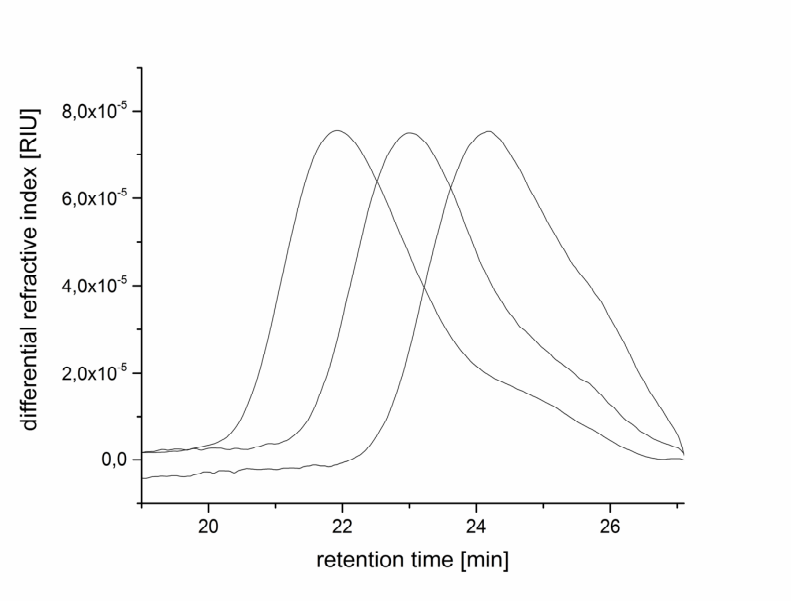

Figure S 8 GPC traces of P2VP produced with catalyst 1 (table 1, entry 1).

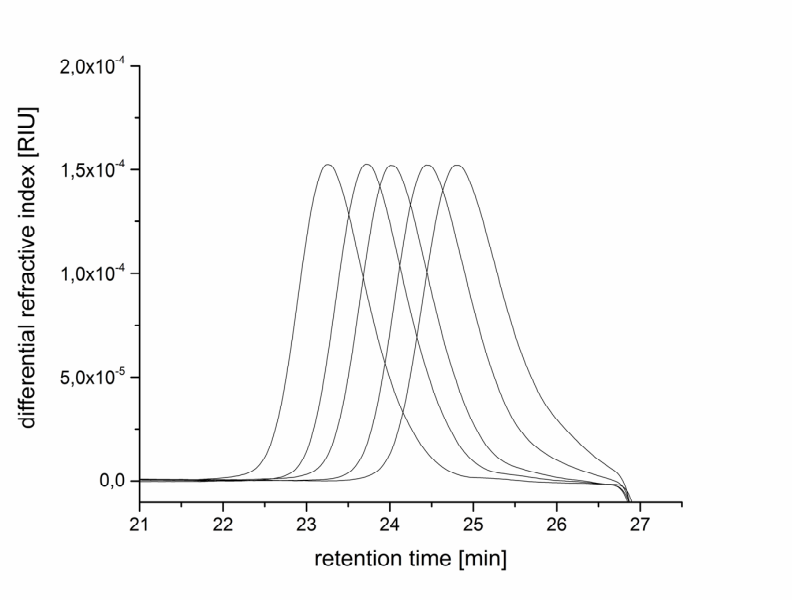

Figure S 9 GPC traces of P2VP produced with catalyst 2 (table 1, entry 2).

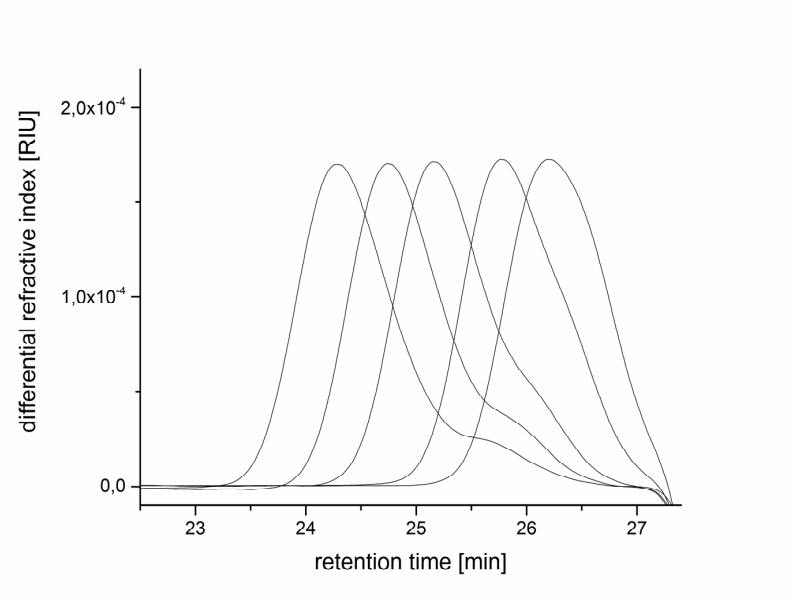

Figure S 10 GPC traces of P2VP produced with catalyst 3 (table 1, entry 3).

5 NMR-Analysis of P2VP

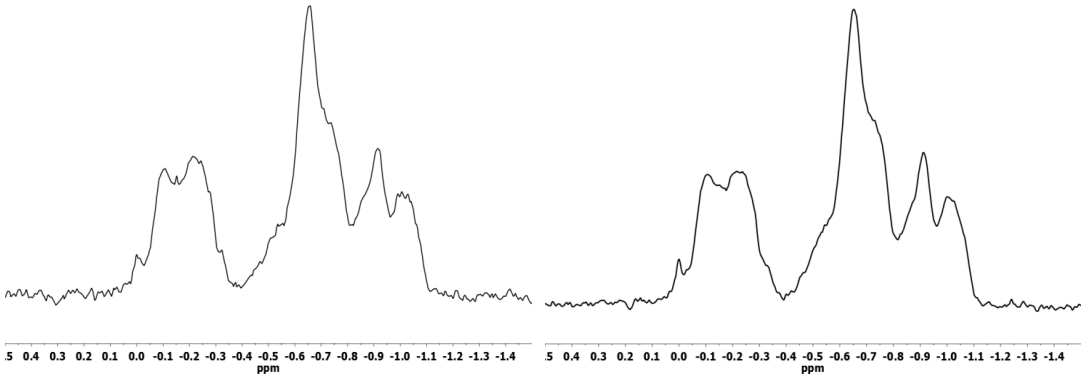

Figure S 11 Aromatic quarternary ^{13}C NMR resonances of P2VP produced with catalyst 4 (left) and 5 (right). Calibration on *mmmm*-pentade (126 MHz, Cryo, 2000 scans, CD_3OD, table 1, entry 4 and 5).

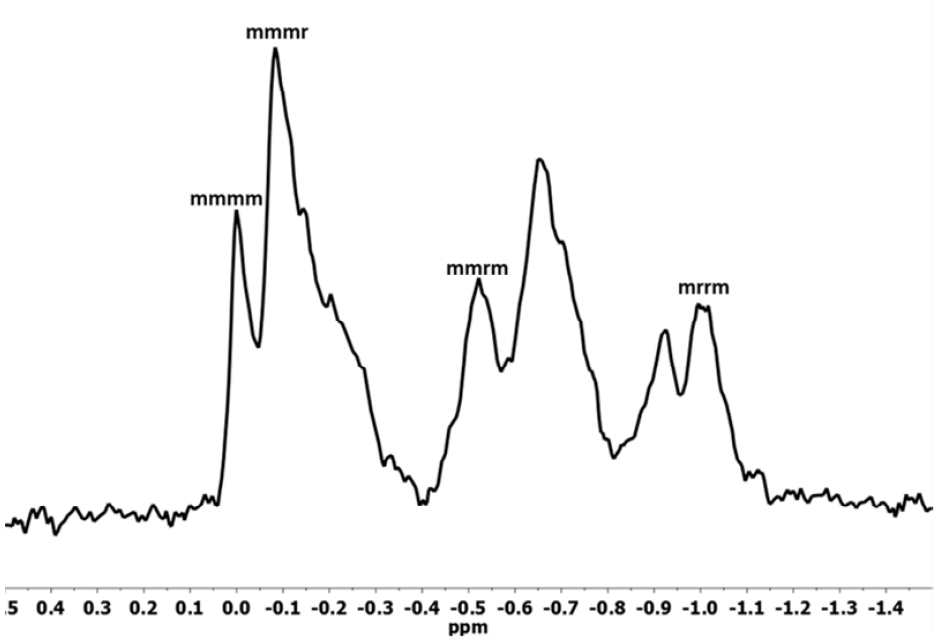

Figure S 12 Aromatic quarternary ^{13}C NMR resonance of P2VP produced with catalyst 1. Calibration on *mmmm*-pentade (126 MHz, Cryo, 2000 scans, MeOD, table 1, entry 1).

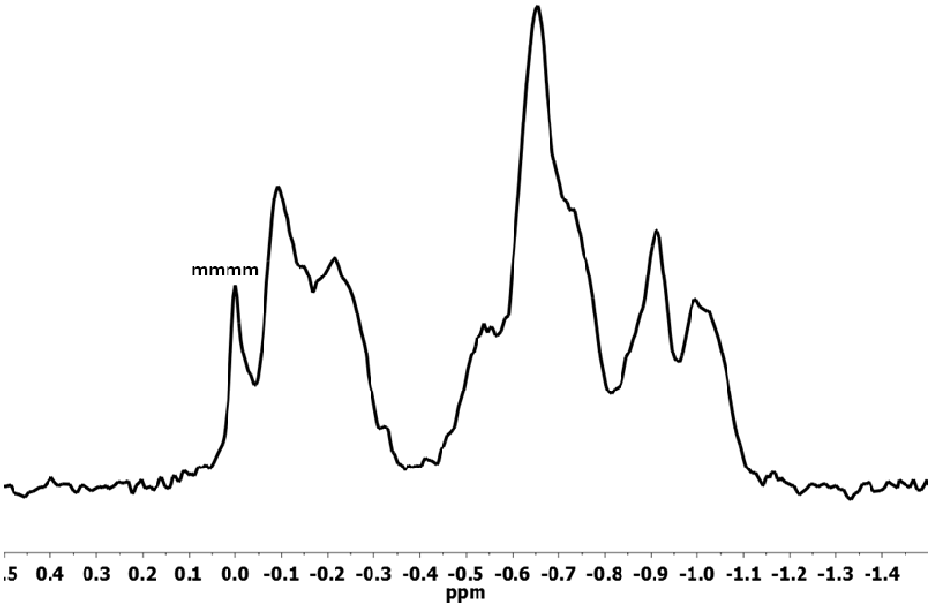

Figure S 13 Aromatic quarternary ^{13}C NMR resonance of P2VP produced with catalyst 2. Calibration on *mmmm*-pentade (126 MHz, Cryo, 2 000 scans, CD_3OD, table 1, entry 2).

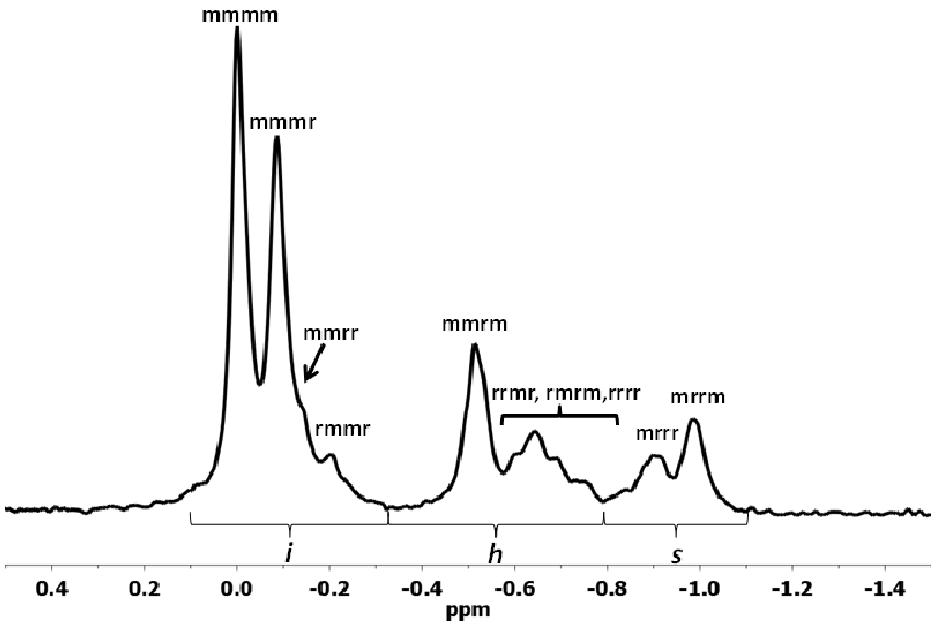

Figure S 14 Aromatic quarternary ^{13}C NMR resonance (i,h,s :proportions of isotactic, heterotactic and syndiotactic triad) of P2VP produced with catalyst 3 (226 MHz, Cryo, 1 000 scans, relaxations delay: 2 seconds, 30 mg/0.6 mL CD_3OD, table 1, entry 3).

Table S 1 Triad- and pentade-assignment of the aromatic quarternary ^{13}C NMR resonance of P2VP produced with catalyst 3.[a] chemical shifts are stated as positive values and calibrated on the *mmmm*-pentade (table 1, entry 3).

		chemical shift [ppm][a]	proportions
triad-splitting	i (mm)	0.00-0.38	0.61
	h (mr)	0.38-0.80	0.26
	s (rr)	0.80-1.11	0.13
pentade-splitting	mmmm	0.00	
	mmmr	0.09	
	mmrr	0.14	
	rmmr	0.20	
	mmrm	0.51	
	rrmr		
	rrrr	0.64-0.81	
	rmrm		
	mrrr	0.90	
	mrrm	0.98	

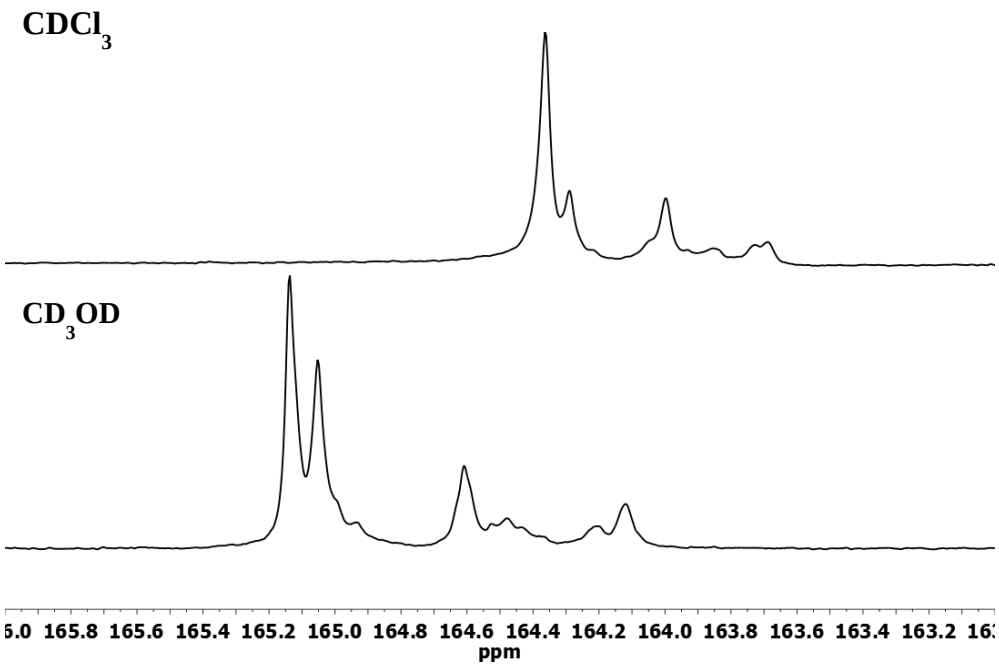

Figure S 15 ^{13}C-NMR-spectra of the quaternary carbon atom of P2VP produced by catalyst 3 measured in $CDCl_3$ (top) and CD_3OD (bottom) (126 MHz, Cryo, 2 000 scans). Spectra in $CDCl_3$ show different chemical shifts, intensities and coupling constants.

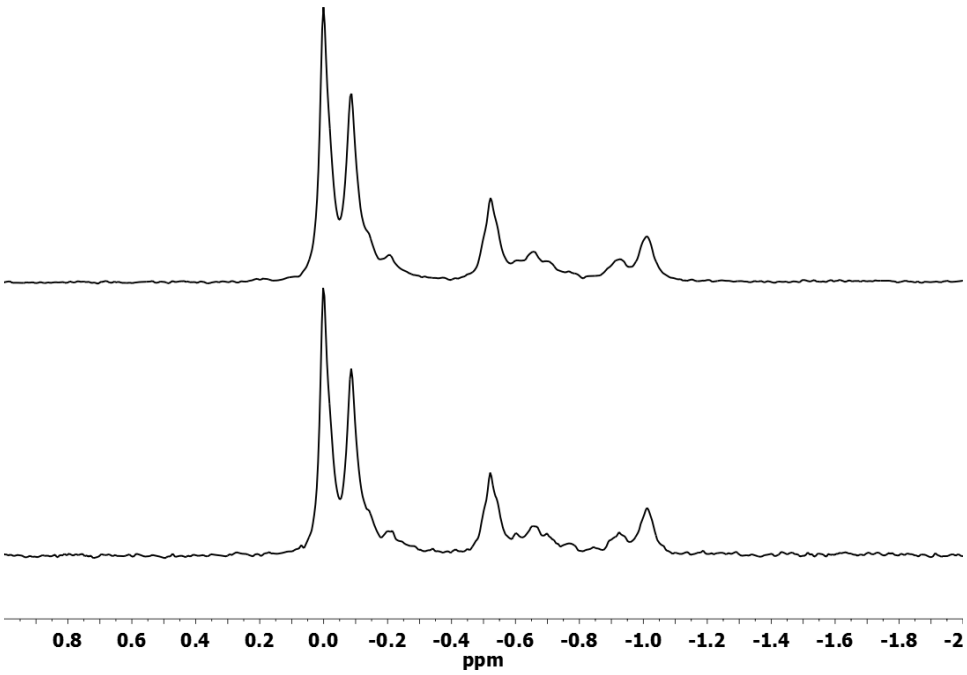

Figure S 16 ^{13}C-NMR-spectra of the quaternary carbon atom of P2VP produced by catalyst 3 measured in CD_3OD with a concentration of 30 mg/0.6 mL (top) and 15 mg/mL (bottom) (126 MHz, Cryo, 4 000 scans). Lower concentrations led to an increased signal-to-noise ratio, but without a better pentade resolution.

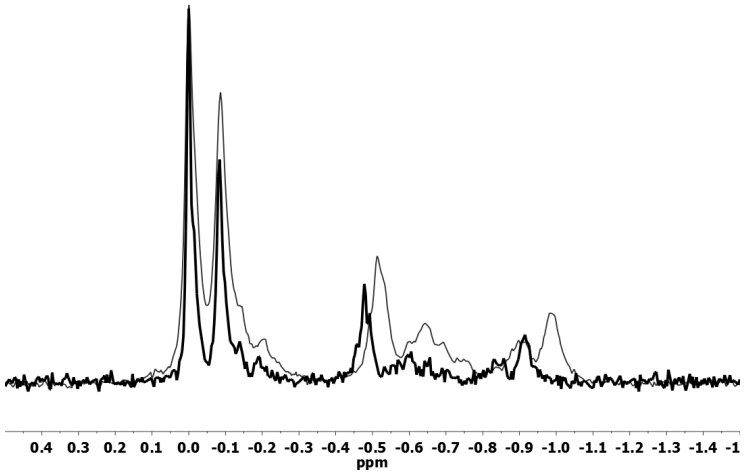

Figure S 17 ^{13}C-NMR-spectra of the quaternary carbon atom of P2VP produced by catalyst 3 measured in CD_3OD at 40 °C (black, 75 mg/0.6 mL; 72 MHz, 12 000 scans, relaxation delay: 3.5 sec, CD_3OD) and at room temperature (gray, 30 mg/0.6 mL; 226 MHz, Cryo, 2 000 scans, relaxation delay: 2 sec, CD_3OD). High temperature measurements led to incomparable chemical shifts, but with a better splitting of *mmmm*- and *mmmr*-pentade. A higher signal-to-noise ratio is observed due to a weaker magnetic field.

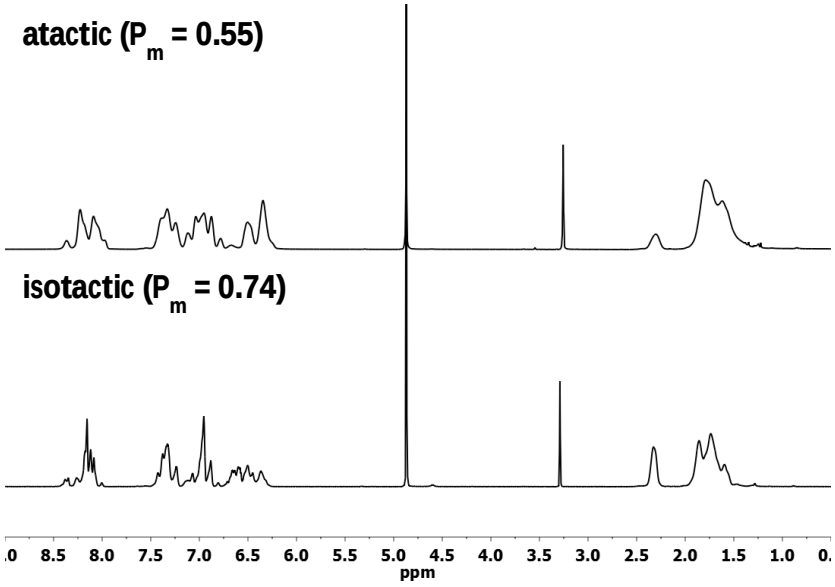

Figure S 18 ^{1}H-NMR-spectra of atactic and isotactic P2VP produced by catalysts 3 (bottom) and 4 (top) (500/900 MHz, Cryo, CD_3OD)

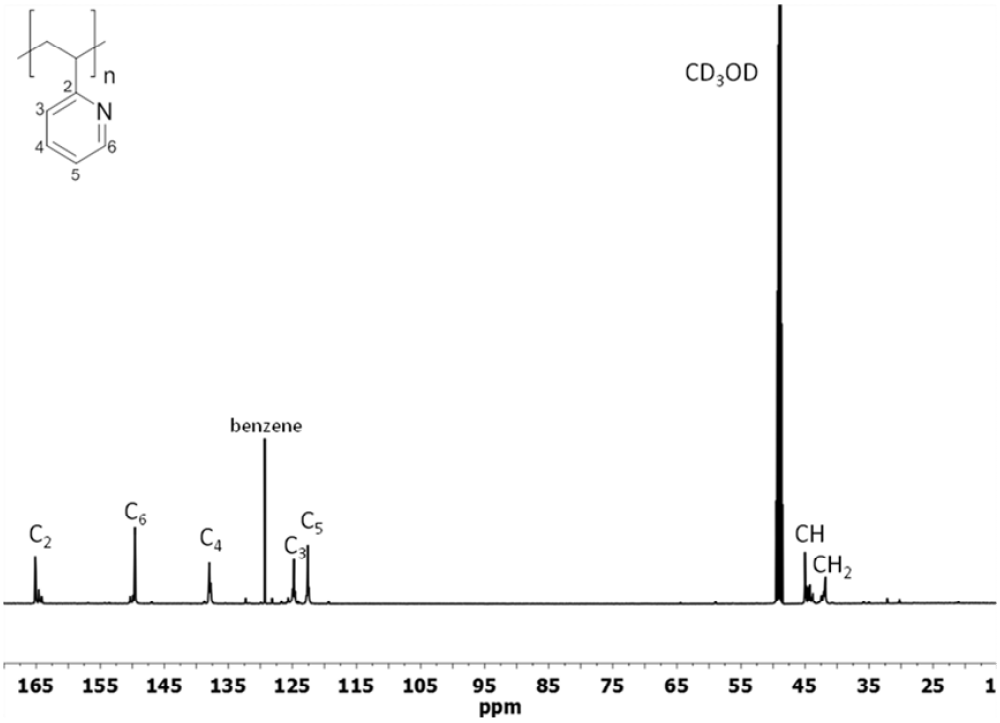

Figure S 19 ^{13}C-NMR-spectra of isotactic P2VP produced by catalysts 3 (500 MHz, Cryo, CD_3OD). Assignment according to Matsumoto and coworkers [15]

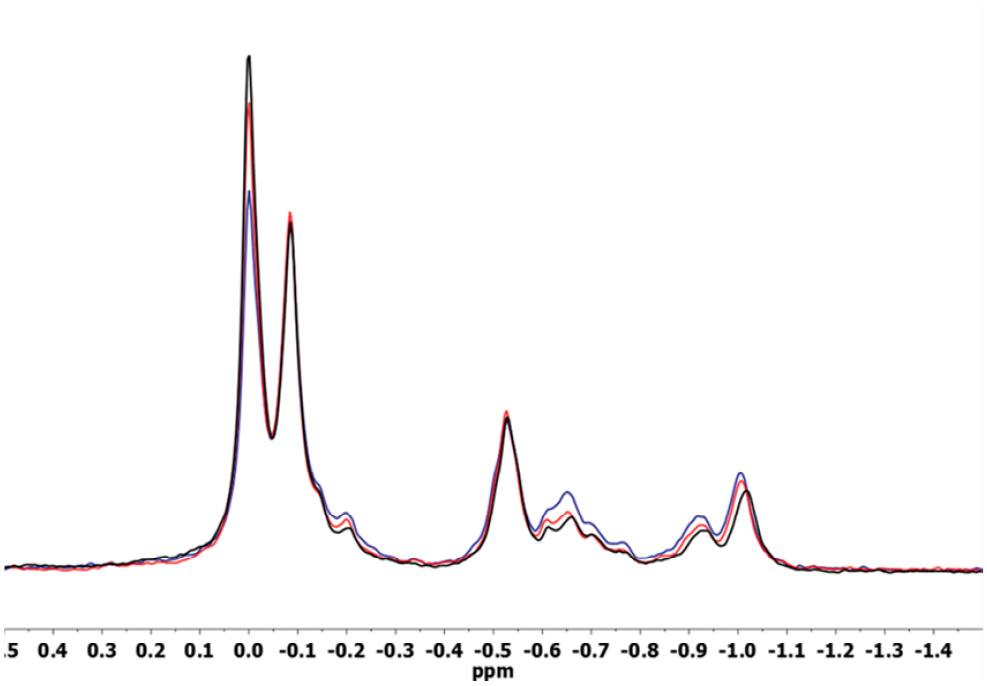

Figure S 20 ^{13}C-NMR-spectra of the quaternary carbon atom of P2VP produced by catalyst 3 in toluene (black), thf (blue) and dichloromethane (red) measured in CD_3OD at room temperature (75 mg/0.6 mL; 226 MHz, Cryo, 2 000 scans, relaxation delay: 2 sec, CD_3OD).

6 Mechanistic investigations and polymerization data

Table S 2 Experimental and calculated triad distributions in the aromatic quaternary ^{13}C resonance for mechanistic investigations.[a]

Catalyst	triad distributions							B[d]	E[e]	σ[f]
	experimental values				theoretical values[c]					
	i (mm)	h (mr)	s (rr)	P_m[b]	i	h	s			
1	0.44	0.37	0.19	0.63	0.45	0.37	0.18	2.44	1.03	0.755
2	0.35	0.43	0.22	0.57	0.36	0.43	0.21	1.67	1.02	0.687
3	0.61	0.26	0.13	0.74	0.61	0.26	0.13	4.69	1.00	0.846
4	0.34	0.43	0.23	0.55	0.32	0.45	0.23	1.69	1.07	0.658
5	0.31	0.45	0.24	0.54	0.34	0.44	0.22	1.47	1.07	0.673

Table S 3 Experimental and calculated triad distributions in the aromatic quaternary ^{13}C resonance for mechanistic investigations of P2VP produced with catalyst 3 in different solvents and at different temperatures.[g]

Entry	Solvent	Temp.	triad distributions							B[d]	E[e]	σ[f]
			experimental values				theoretical values[c]					
			i (mm)	h (mr)	s (rr)	P_m[b]	i	H	s			
1	thf	rt	0.59	0.27	0.14	0.73	0.59	0.27	0.14	4.53	1.04	0.839
2	CH_2Cl_2	rt	0.63	0.24	0.13	0.75	0.63	0.25	0.12	5.68	1.08	0.854
3	toluene	-30 °C	0.57	0.29	0.14	0.72	0.58	0.28	0.14	3.80	0.97	0.831
4	toluene	50 °C	0.58	0.27	0.15	0.72	0.58	0.28	0.14	4.72	1.11	0.831
5	pyridine	rt	-	-	-	-	-	-	-	-	-	-

[a] 75 mg P2VP in 0.6 mL CD_3OD; NMR AV500C; ^{13}C NMR resonances of poly(2-vinylpyridine) produced with catalyst 1-5, at 25 °C, ([Cat]:[2VP] =1:200, [2VP] = 27 mmol, 20 mL toluene).

[b] Pm is the probability of *meso* linkages between monomer units and is determined by ^{13}C NMR spectroscopy:

$$P_m = mm + 0.5mr$$

[c] Theoretical triad distributions calculated for enantiomorphic site control model:

$$mm = m^2 = 1 - 3\sigma(1-\sigma)$$

$$mr = m(1-m) = 2\sigma(1-\sigma)$$

$$rr = (1-m)^2 = \sigma(1-\sigma)$$

[d] Bernoulli model triad test B:

$$B = \frac{4(mm)(rr)}{(mr)^2}$$

With B = 1 for chain end control.

[e] Enantiomorphic site control triad test E:

$$E = \frac{2(rr)}{(mr)}$$

With E = 1 for enantiomorphic site control.

[f] Probability of prochiral monomer addition *via re* or *si* side of the catalyst:

$$P_m = m = \sigma^2 + (1-\sigma)^2$$

[g]75 mg P2VP in 0.6 mL CD_3OD; NMR AV500C; ^{13}C NMR resonances of poly(2-vinylpyridine) produced with catalyst 3, at given temperature, ([Cat]:[2VP] =1:200, [2VP] = 2.7 mmol, 2.0 mL solvent).

Table S 4 REM-GTP of 2VP with catalyst 3 at various reaction conditions.[a]

Entry	Solvent	Temp [°C]	Time [h]	Conversion [%]	$M_{n,calc}$ ($x10^4$) [g/mol][b]	$M_{n,exp}$ ($x10^4$) [g/mol]	M_w/M_n	I^* [c]	P_m[d]
1	THF	25	2.0	10	0.22	3.3	1.14	0.06	0.73
2	THF	25	24w	>99	2.1	9.2	1.15	0.22	0.73
3	CH_2Cl_2	25	2.0	>99	1.9	4.6	1.07	0.41	0.75
4	toluene	-30	26	6	0.11	0.43	1.30	0.26	0.72
5	toluene	50	0.75	>99	2.2	3.9	1.07	0.57	0.72
6	toluene	25	1.6	>99	2.0	3.3	1.06	0.60	0.74

[a] Reactions performed with [2VP] = 2.7 mmol, [2VP]/[Cat] = 200/1, in 2.0 mL solvent, conversions determined by gravimetry and $M_{n,exp}$ determined by GPC-MALS. [b] $M_{n,calc}$ = M x (([M]/[Cat]) x conversion). [c] I^* at the end of the reaction. [d] P_m is the probability of *meso* linkages between monomer units and is determined by ^{13}C NMR spectroscopy.

7 References

1. P. T. Altenbuchner, B. S. Soller, S. Kissling, T. Bachmann, A. Kronast, S. I. Vagin and B. Rieger, *Macromolecules*, 2014, 47, 7742-7749.
2. K. C. Hultzsch, P. Voth, K. Beckerle, T. P. Spaniol and J. Okuda, *Organometallics*, 2000, 19, 228-243.
3. G. D. Vaughn, K. A. Krein and J. A. Gladysz, *Organometallics*, 1986, 5, 936-942.
4. C.-X. Cai, L. Toupet, C. W. Lehmann and J.-F. Carpentier, *J. Organomet. Chem.*, 2003, 683, 131-136.
5. M. Brigodiot, H. Cheradame, M. Fontanille and J. P. Vairon, *Polymer*, 1976, 17, 254-256.
6. D. K. Dimov and T. E. Hogen-Esch, *Macromolecules*, 1995, 28, 7394-7400.
7. A. I. Kochnev, I. I. Oleynik, I. V. Oleynik, S. S. Ivanchev and G. A. Tolstikov, *Russ. Chem. Bull.*, 2007, 56, 1125-1129.
8. Y.-L. Wong, L. H. Tong, J. R. Dilworth, D. K. P. Ng and H. K. Lee, *Dalton Transactions*, 2010, 39, 4602-4611.
9. S. Barroso, S. R. M. M. de Aguiar, R. F. Munhá and A. M. Martins, *Journal of Organometallic Chemistry*, 2014, 760, 60-66.
10. M. Konkol, M. Nabika, T. Kohno, T. Hino and T. Miyatake, *Journal of Organometallic Chemistry*, 2011, 696, 1792-1802.
11. M. Bouyahyi, N. Ajellal, E. Kirillov, C. M. Thomas and J.-F. Carpentier, *Chemistry*, 2011, 17, 1872-1883.
12. J. Eppinger, M. Spiegler, W. Hieringer, W. A. Herrmann and R. Anwander, *Journal of the American Chemical Society*, 2000, 122, 3080-3096.
13. W. A. Herrmann, J. Eppinger, M. Spiegler, O. Runte and R. Anwander, *Organometallics*, 1997, 16, 1813-1815.
14. A. Amgoune, C. M. Thomas, T. Roisnel and J.-F. Carpentier, *Chemistry*, 2005, 12, 169-179.
15. K. Matsuzaki, T. Kanai, T. Matsubara and S. Matsumoto, *Journal of Polymer Science: Polymer Chemistry Edition*, 1976, 14, 1475-1484.

8. Bibliography

(1) (a) Richard Forrest, O. S., Thomas Rings, Dr. Joachim von Hoyningen-Huene *Chemical Industry Vision 2030: A European Perspective*, A.T. Kearney, 2012; (b) Jan Friese, S. G., Andreas Gocke, Frank Plaschke, Hubert Schönberger, Yves-Pierre Willers *The 2012 Chemical Industry Value Creators Report - Rebounding from the Storm*, The Boston Consulting Group, 2013.
(2) Andres Gocke, Y.-P. W., Jan Friese, Sarah Gehrlein, Hubert Schönberger, Hady Farag *The 2013 Chemical Industry Value Creators Report - How 20 Years have Transformed the Chemical Industry*, The Boston Consulting Group, 2013.
(3) Stirling, C. *The Future of the European Chemical Industry*, KPMG International Cooperative, 2010.
(4) Gellrich, T. *Shale Gas - Reshaping the US Chemicals Industry*, PWC, 2012.
(5) Udo Jung, A. K., Peter Nowotnik, Alexander Roos, Sebastian Stange *Maintaining M&A Momentum in Chemicals - A Perspective for 2012 and Beyond*, The Boston Consulting Group, 2012.
(6) Dickson, D. *The Decade Ahead - Preparing for an Unpredictable Future in the Global Chemical Industry*, Deloitte Touche Tohmatsu Chemical Group, 2010.
(7) Sven Wydra, K.-H. H., Andre Jungmittag, Thomas Reiss, Axel Thielmann *Economic Forsight Study on Industrial Trends and the Research Needed to Support the Competitivness of European Industry Around 2025*; Europäische Kommission, Generaldirektion Forschung und Innovation 2012.
(8) (a) Rosenberg, N.; Nelson, R. R. *Research Policy* **1994**, *23*, 323; (b) Beise, M.; Stahl, H. *Research Policy* **1999**, *28*, 397; (c) Cohen, W. M.; Nelson, R. R.; Walsh, J. P. *Management Science* **2002**, *48*, 1; (d) Perkmann, M.; Walsh, K. *International Journal of Management Reviews* **2007**, *9*, 259; (e) Henrik Meincke, J. U. *Evolution of competitiveness in the German chemical industry: historical trends and future*, VCI - Oxford Economics, 2014.
(9) Trans, P.; U.S. Department of Commerce, National Oceanic & Atmospheric Administration: NOAA/ESRL, 2015.
(10) (a) MacDowell, N.; Florin, N.; Buchard, A.; Hallett, J.; Galindo, A.; Jackson, G.; Adjiman, C. S.; Williams, C. K.; Shah, N.; Fennell, P. *Energy & Environmental Science* **2010**, *3*, 1645; (b) Markewitz, P.; Kuckshinrichs, W.; Leitner, W.; Linssen, J.; Zapp, P.; Bongartz, R.; Schreiber, A.; Muller, T. E. *Energy & Environmental Science* **2012**, *5*, 7281; (c) Aresta, M.; Dibenedetto, A.; Angelini, A. *Chem. Rev.* **2013**.
(11) (a) Peters, M.; Köhler, B.; Kuckshinrichs, W.; Leitner, W.; Markewitz, P.; Müller, T. E. *ChemSusChem* **2011**, *4*, 1216; (b) Lee, S. H.; Cyriac, A.; Jeon, J. Y.; Lee, B. Y. *Polymer Chemistry* **2012**, *3*, 1215; (c) Langanke, J.; Wolf, A.; Hofmann, J.; Bohm, K.; Subhani, M. A.; Muller, T. E.; Leitner, W.; Gurtler, C. *Green Chemistry* **2014**, *16*, 1865.
(12) Sakakura, T.; Choi, J. C.; Yasuda, H. *Chem. Rev.* **2007**, *107*, 2365.
(13) (a) Kawaguchi, T.; Nakano, M.; Juni, K.; Inoue, S.; Yoshida, Y. *Chem. Pharm. Bull.* **1983**, *31*, 1400; (b) Du, L. C.; Meng, Y. Z.; Wang, S. J.; Tjong, S. C. *J. Appl. Polym. Sci.* **2004**, *92*, 1840; (c) Jung, J. H.; Ree, M.; Kim, H. *Catal. Today* **2006**, *115*, 283; (d) Luinstra, G. A. *Polym. Rev.* **2008**, *48*, 192; (e) Kim, G.; Ree, M.; Kim, H.; Kim, I.; Kim, J.; Lee, J. *Macromol. Res.* **2008**, *16*, 473; (f) Qin, Y.; Wang, X. *Biotechnol. J.* **2010**, *5*, 1164.
(14) (a) Klaus, S.; Lehenmeier, M. W.; Herdtweck, E.; Deglmann, P.; Ott, A. K.; Rieger, B. *J. Am. Chem. Soc.* **2011**, *133*, 13151; (b) Klaus, S.; Lehenmeier, M. W.; Anderson, C. E.; Rieger, B. *Coord. Chem. Rev.* **2011**, *255*, 1460.

(15) (a) Inoue, S.; Koinuma, H.; Tsuruta, T. *Makromol. Chem.* **1969**, *130*, 210; (b) Inoue, S.; Koinuma, H.; Tsuruta, T. *J. Polym. Sci., Part B: Polym. Lett.* **1969**, *7*, 287.
(16) (a) Sugimoto, H.; Inoue, S. *J. Polym. Sci., Part A: Polym. Chem.* **2004**, *42*, 5561; (b) Coates, G. W.; Moore, D. R. *Angew. Chem., Int. Ed.* **2004**, *43*, 6618; (c) Darensbourg, D. J. *Chem. Rev.* **2007**, *107*, 2388; (d) Darensbourg, D. J. *Inorg. Chem.* **2010**, *49*, 10765; (e) Cokoja, M.; Bruckmeier, C.; Rieger, B.; Herrmann, W. A.; Kuehn, F. E. *Angew. Chem., Int. Ed.* **2011**, *50*, 8510; (f) Kember, M. R.; Buchard, A.; Williams, C. K. *Chem. Commun.* **2011**, *47*, 141; (g) Darensbourg, D. J.; Wilson, S. J. *Green Chemistry* **2012**, *14*, 2665; (h) Darensbourg, D. J.; Yeung, A. D. *Polymer Chemistry* **2014**, *5*, 3949.
(17) Lu, X.-B.; Ren, W.-M.; Wu, G.-P. *Acc. Chem. Res.* **2012**, *45*, 1721.
(18) (a) Moore, D. R.; Cheng, M.; Lobkovsky, E. B.; Coates, G. W. *J. Am. Chem. Soc.* **2003**, *125*, 11911; (b) Darensbourg, D. J.; Mackiewicz, R. M.; Rodgers, J. L.; Phelps, A. L. *Inorg. Chem.* **2004**, *43*, 1831; (c) Vagin, S. I.; Reichardt, R.; Klaus, S.; Rieger, B. *J. Am. Chem. Soc.* **2010**, *132*, 14367; (d) Nakano, K.; Hashimoto, S.; Nozaki, K. *Chem. Sci.* **2010**, *1*, 369; (e) Kember, M. R.; Jutz, F.; Buchard, A.; White, A. J. P.; Williams, C. K. *Chemical Science* **2012**, *3*, 1245; (f) Lehenmeier, M. W.; Kissling, S.; Altenbuchner, P. T.; Bruckmeier, C.; Deglmann, P.; Brym, A.-K.; Rieger, B. *Angew. Chem., Int. Ed.* **2013**, *52*, 9821; (g) Darensbourg, D. J.; Yeung, A. D. *Polymer Chemistry* **2014**.
(19) Lu, X.-B.; Darensbourg, D. J. *Chem. Soc. Rev.* **2012**, *41*, 1462.
(20) Darensbourg, D. J.; Yarbrough, J. C.; Ortiz, C.; Fang, C. C. *J. Am. Chem. Soc.* **2003**, *125*, 7586.
(21) (a) Soga, K.; Hyakkoku, K.; Ikeda, S. *Die Makromolekulare Chemie* **1978**, *179*, 2837; (b) Lu, X.-B.; Feng, X.-J.; He, R. *Appl. Catal., A* **2002**, *234*, 25.
(22) (a) Shen, Y.-M.; Duan, W.-L.; Shi, M. *J. Org. Chem.* **2003**, *68*, 1559; (b) Lu, X.-B.; Xiu, J.-H.; He, R.; Jin, K.; Luo, L.-M.; Feng, X.-J. *Appl. Catal., A* **2004**, *275*, 73.
(23) (a) Tokunaga, M.; Larrow, J. F.; Kakiuchi, F.; Jacobsen, E. N. *Science* **1997**, *277*, 936; (b) Qin, Z.; Thomas, C. M.; Lee, S.; Coates, G. W. *Angew. Chem., Int. Ed.* **2003**, *42*, 5484.
(24) (a) Nakano, K.; Kamada, T.; Nozaki, K. *Angew. Chem., Int. Ed.* **2006**, *45*, 7274; (b) Noh, E. K.; Na, S. J.; S, S.; Kim, S.-W.; Lee, B. Y. *J. Am. Chem. Soc.* **2007**, *129*, 8082; (c) Ren, W.-M.; Liu, Z.-W.; Wen, Y.-Q.; Zhang, R.; Lu, X.-B. *J. Am. Chem. Soc.* **2009**, *131*, 11509.
(25) (a) Min, S. S. J. K.; Seong, J. E.; Na, S. J.; Lee, B. Y. *Angew. Chem., Int. Ed.* **2008**, *47*, 7306; (b) Na Sung, J.; Sujith, S.; Cyriac, A.; Kim Bo, E.; Yoo, J.; Kang Youn, K.; Han Su, J.; Lee, C.; Lee Bun, Y. *Inorg. Chem.* **2009**, *48*, 10455; (c) Yoo, J.; Na, S. J.; Park, H. C.; Cyriac, A.; Lee, B. Y. *Dalton Trans.* **2010**, *39*, 2622.
(26) (a) Sugimoto, H.; Ohshima, H.; Inoue, S. *J. Polym. Sci., Part A: Polym. Chem.* **2003**, *41*, 3549; (b) Xiao, Y.; Wang, Z.; Ding, K. *Chemistry – A European Journal* **2005**, *11*, 3668; (c) Vitanova, D. V.; Hampel, F.; Hultzsch, K. C. *J. Organomet. Chem.* **2005**, *690*, 5182; (d) Xiao, Y.; Wang, Z.; Ding, K. *Macromolecules* **2006**, *39*, 128; (e) Sugimoto, H.; Kuroda, K. *Macromolecules* **2008**, *41*, 312; (f) Kember, M. R.; Knight, P. D.; Reung, P. T. R.; Williams, C. K. *Angew. Chem., Int. Ed.* **2009**, *48*, 931; (g) Nakano, K.; Nakamura, M.; Nozaki, K. *Macromolecules* **2009**, *42*, 6972; (h) Kember, M. R.; White, A. J. P.; Williams, C. K. *Macromolecules* **2010**, *43*, 2291; (i) Ren, W.-M.; Zhang, X.; Liu, Y.; Li, J.-F.; Wang, H.; Lu, X.-B. *Macromolecules* **2010**, *43*, 1396.
(27) Cohen, C. T.; Chu, T.; Coates, G. W. *J. Am. Chem. Soc.* **2005**, *127*, 10869.
(28) Ren, W.-M.; Wang, Y.-M.; Zhang, R.; Jiang, J.-Y.; Lu, X.-B. *The Journal of Organic Chemistry* **2013**, *78*, 4801.

(29) (a) Chatterjee, C.; Chisholm, M. H.; El-Khaldy, A.; McIntosh, R. D.; Miller, J. T.; Wu, T. *Inorg. Chem.* **2013**, *52*, 4547; (b) Anderson, C. E.; Vagin, S. I.; Hammann, M.; Zimmermann, L.; Rieger, B. *ChemCatChem* **2013**, *5*, 3269.
(30) Xia, W.; Salmeia, K. A.; Vagin, S. I.; Rieger, B. *Chemistry – A European Journal* **2015**, *21*, 4384.
(31) (a) Dean, R. K.; Granville, S. L.; Dawe, L. N.; Decken, A.; Hattenhauer, K. M.; Kozak, C. M. *Dalton Trans.* **2010**, *39*, 548; (b) Dean, R. K.; Dawe, L. N.; Kozak, C. M. *Inorg. Chem.* **2012**, *51*, 9095; (c) Saunders, L. N.; Ikpo, N.; Petten, C. F.; Das, U. K.; Dawe, L. N.; Kozak, C. M.; Kerton, F. M. *Catal. Commun.* **2012**, *18*, 165; (d) Dean, R. K.; Devaine-Pressing, K.; Dawe, L. N.; Kozak, C. M. *Dalton Trans.* **2013**, *42*, 9233; (e) Saunders, L. N.; Pratt, M. E.; Hann, S. E.; Dawe, L. N.; Decken, A.; Kerton, F. M.; Kozak, C. M. *Polyhedron* **2012**, *46*, 53.
(32) (a) Abe, H.; Matsubara, I.; Doi, Y.; Hori, Y.; Yamaguchi, A. *Macromolecules* **1994**, *27*, 6018; (b) Abe, H.; Doi, Y. *Macromolecules* **1996**, *29*, 8683; (c) Wu, B.; Lenz, R. W.; Scherer, T. *Macromol. Chem. Phys.* **1998**, *199*, 2079; (d) Bachmann, B. M.; Seebach, D. *Macromolecules* **1999**, *32*, 1777; (e) Van der Walle, G. A. M.; De Koning, G. J. M.; Weusthuis, R. A.; Eggink, G. *Adv. Biochem. Eng./Biotechnol.* **2001**, *71*, 263; (f) Chen, G.-Q.; Patel, M. K. *Chem. Rev.* **2012**, *112*, 2082.
(33) Chen, G.-Q. *Chem. Soc. Rev.* **2009**, *38*, 2434.
(34) (a) Choi, J.-i.; Lee, S. Y. *Bioprocess. Eng.* **1997**, *17*, 335; (b) Reichardt, R.; Rieger, B. *Adv. Polym. Sci.* **2012**, *245*, 49.
(35) (a) Carpentier, J.-F.; Kirillov, E.; Sarazin, Y. In *PATAI'S Chemistry of Functional Groups*; John Wiley & Sons, Ltd: 2009; (b) Thomas, C. M. *Chem. Soc. Rev.* **2010**, *39*, 165; (c) Carpentier, J.-F. *Macromol. Rapid Commun.* **2010**, *31*, 1696; (d) Miyake, G. M.; Chen, E. Y. X. *Polym. Chem.* **2011**, *2*, 2462.
(36) (a) Getzler, Y. D. Y. L.; Mahadevan, V.; Lobkovsky, E. B.; Coates, G. W. *J. Am. Chem. Soc.* **2002**, *124*, 1174; (b) Lee, J. T.; Thomas, P. J.; Alper, H. *The Journal of Organic Chemistry* **2001**, *66*, 5424; (c) Dunn, E. W.; Coates, G. W. *J. Am. Chem. Soc.* **2010**, *132*, 11412; (d) Mulzer, M.; Coates, G. W. *The Journal of Organic Chemistry* **2014**, *79*, 11851; (e) Mulzer, M.; Lamb, J. R.; Nelson, Z.; Coates, G. W. *Chem. Commun.* **2014**, *50*, 9842.
(37) Guillaume, S. M.; Carpentier, J.-F. *Catal. Sci. Technol.* **2012**, *2*, 898.
(38) (a) Bloembergen, S.; Holden, D. A.; Bluhm, T. L.; Hamer, G. K.; Marchessault, R. H. *Macromolecules* **1989**, *22*, 1656; (b) Kemnitzer, J. E.; McCarthy, S. P.; Gross, R. A. *Macromolecules* **1993**, *26*, 1221; (c) Hocking, P. J.; Marchessault, R. H. *Macromolecules* **1995**, *28*, 6401; (d) Ajellal, N.; Bouyahyi, M.; Amgoune, A.; Thomas, C. M.; Bondon, A.; Pillin, I.; Grohens, Y.; Carpentier, J.-F. *Macromolecules* **2009**, *42*, 987.
(39) Rieth, L. R.; Moore, D. R.; Lobkovsky, E. B.; Coates, G. W. *J. Am. Chem. Soc.* **2002**, *124*, 15239.
(40) (a) Cheng, M.; Attygalle, A. B.; Lobkovsky, E. B.; Coates, G. W. *J. Am. Chem. Soc.* **1999**, *121*, 11583; (b) Chamberlain, B. M.; Cheng, M.; Moore, D. R.; Ovitt, T. M.; Lobkovsky, E. B.; Coates, G. W. *J. Am. Chem. Soc.* **2001**, *123*, 3229.
(41) (a) Zintl, M.; Molnar, F.; Urban, T.; Bernhart, V.; Preishuber-Pfluegl, P.; Rieger, B. *Angew. Chem., Int. Ed.* **2008**, *47*, 3458; (b) Reichardt, R.; Vagin, S.; Reithmeier, R.; Ott, A. K.; Rieger, B. *Macromolecules* **2010**, *43*, 9311.
(42) (a) Amgoune, A.; Thomas, C. M.; Ilinca, S.; Roisnel, T.; Carpentier, J.-F. *Angew. Chem., Int. Ed.* **2006**, *45*, 2782; (b) Bouyahyi, M.; Ajellal, N.; Kirillov, E.; Thomas, C. M.; Carpentier, J.-F. *Chem. - Eur. J.* **2011**, *17*, 1872; (c) Nie, K.; Fang, L.; Yao, Y.; Zhang, Y.; Shen, Q.; Wang, Y. *Inorg. Chem.* **2012**, *51*, 11133; (d) Chapurina, Y.; Klitzke, J.; Casagrande Jr, O. d. L.; Awada, M.; Dorcet, V.; Kirillov, E.; Carpentier, J.-F. *Dalton Transactions* **2014**, *43*, 14322.

(43) (a) Amgoune, A.; Thomas, C. M.; Carpentier, J.-F. *Macromol. Rapid Commun.* **2007**, *28*, 693; (b) Ajellal, N.; Carpentier, J.-F.; Guillaume, C.; Guillaume, S. M.; Helou, M.; Poirier, V.; Sarazin, Y.; Trifonov, A. *Dalton Trans.* **2010**, *39*, 8363.
(44) (a) Cai, C.-X.; Amgoune, A.; Lehmann, C. W.; Carpentier, J.-F. *Chem. Commun.* **2004**, 330; (b) Amgoune, A.; Thomas, C. M.; Roisnel, T.; Carpentier, J.-F. *Chemistry – A European Journal* **2006**, *12*, 169; (c) Amgoune, A.; Thomas, C. M.; Carpentier, J.-F. *Pure Appl. Chem.* **2007**, *79*, 2013.
(45) Jaffredo, C. G.; Chapurina, Y.; Guillaume, S. M.; Carpentier, J.-F. *Angew. Chem. Int. Ed.* **2014**, *53*, 2687.
(46) (a) Yasuda, H.; Yamamoto, H.; Yokota, K.; Miyake, S.; Nakamura, A. *J. Am. Chem. Soc.* **1992**, *114*, 4908; (b) Collins, S.; Ward, D. G. *J. Am. Chem. Soc.* **1992**, *114*, 5460.
(47) (a) Webster, O. W. *Adv. Polym. Sci.* **2004**, *167*, 1; (b) Chen, E. Y. X. *Chem. Rev.* **2009**, *109*, 5157; (c) Salzinger, S.; Rieger, B. *Macromol. Rapid Commun.* **2012**, *33*, 1327.
(48) (a) Pike, R. M.; Cohen, R. A. *J. Polym. Sci.* **1960**, *44*, 531; (b) Banks, M.; Ebdon, J. R.; Johnson, M. *Polymer* **1994**, *35*, 3470; (c) Jin, S.; Gonsalves, K. E. *Macromolecules* **1998**, *31*, 1010; (d) Wu, Q.; Weiss, R. A. *J. Polym. Sci., Part B: Polym. Phys.* **2004**, *42*, 3628; (e) Wu, Q.; Weiss, R. A. *Polymer* **2007**, *48*, 7558; (f) Parvole, J.; Jannasch, P. *Macromolecules* **2008**, *41*, 3893; (g) Perrin, R.; Elomaa, M.; Jannasch, P. *Macromolecules* **2009**, *42*, 5146; (h) Wagner, T.; Manhart, A.; Deniz, N.; Kaltbeitzel, A.; Wagner, M.; Brunklaus, G.; Meyer, W. H. *Macromol. Chem. Phys.* **2009**, *210*, 1903.
(49) Seemann, U. B.; Dengler, J. E.; Rieger, B. *Angew. Chem., Int. Ed.* **2010**, *49*, 3489.
(50) (a) Yasuda, H.; Yamamoto, H.; Yamashita, M.; Yokota, K.; Nakamura, A.; Miyake, S.; Kai, Y.; Kanehisa, N. *Macromolecules* **1993**, *26*, 7134; (b) Salzinger, S.; Seemann, U. B.; Plikhta, A.; Rieger, B. *Macromolecules* **2011**, *44*, 5920.
(51) Fang, J.; Tschan, M. J. L.; Brule, E.; Robert, C.; Thomas, C. M.; Maron, L. *Dalton Transactions* **2013**, *42*, 9226.
(52) Salzinger, S.; Soller, B. S.; Plikhta, A.; Seemann, U. B.; Herdtweck, E.; Rieger, B. *J. Am. Chem. Soc.* **2013**, *135*, 13030.
(53) (a) Watson, P. L. *J. Am. Chem. Soc.* **1983**, *105*, 6491; (b) Watson, P. L. *J. Chem. Soc., Chem. Commun.* **1983**, 276.
(54) Quiroga Norambuena, V. F.; Heeres, A.; Heeres, H. J.; Meetsma, A.; Teuben, J. H.; Hessen, B. *Organometallics* **2008**, *27*, 5672.
(55) (a) Deelman, B.-J.; Booij, M.; Meetsma, A.; Teuben, J. H.; Kooijman, H.; Spek, A. L. *Organometallics* **1995**, *14*, 2306; (b) Duchateau, R.; van Wee, C. T.; Teuben, J. H. *Organometallics* **1996**, *15*, 2291; (c) Duchateau, R.; Brussee, E. A. C.; Meetsma, A.; Teuben, J. H. *Organometallics* **1997**, *16*, 5506; (d) Ringelberg, S. N.; Meetsma, A.; Hessen, B.; Teuben, J. H. *J. Am. Chem. Soc.* **1999**, *121*, 6082; (e) Ringelberg, S. N.; Meetsma, A.; Troyanov, S. I.; Hessen, B.; Teuben, J. H. *Organometallics* **2002**, *21*, 1759.
(56) (a) Sadow, A. D.; Tilley, T. D. *J. Am. Chem. Soc.* **2003**, *125*, 7971; (b) Fontaine, F.-G.; Tilley, T. D. *Organometallics* **2005**, *24*, 4340; (c) Barros, N.; Eisenstein, O.; Maron, L.; Tilley, T. D. *Organometallics* **2008**, *27*, 2252.
(57) (a) Labinger, J. A.; Bercaw, J. E. *Nature* **2002**, *417*, 507; (b) Waterman, R. *Organometallics* **2013**, *32*, 7249.
(58) Kaneko, H.; Nagae, H.; Tsurugi, H.; Mashima, K. *J. Am. Chem. Soc.* **2011**, *133*, 19626.
(59) Soller, B. S.; Salzinger, S.; Jandl, C.; Pöthig, A.; Rieger, B. *Organometallics* **2015**.
(60) Zhang, N.; Salzinger, S.; Rieger, B. *Macromolecules* **2012**, *45*, 9751.

(61) (a) Zhang, N.; Salzinger, S.; Deubel, F.; Jordan, R.; Rieger, B. *J. Am. Chem. Soc.* **2012**, *134*, 7333; (b) Yang, J.; Liang, Y.; Salzinger, S.; Zhang, N.; Dong, D.; Rieger, B. *J. Polym. Sci., Part A: Polym. Chem.* **2014**, n/a; (c) Kehrle, J.; Höhlein, I. M. D.; Yang, Z.; Jochem, A.-R.; Helbich, T.; Kraus, T.; Veinot, J. G. C.; Rieger, B. *Angew. Chem. Int. Ed.* **2014**, *53*, 12494.
(62) Zhang, N.; Salzinger, S.; Soller, B. S.; Rieger, B. *J. Am. Chem. Soc.* **2013**, *135*, 8810.
(63) Cai, C.-X.; Toupet, L.; Lehmann, C. W.; Carpentier, J.-F. *J. Organomet. Chem.* **2003**, *683*, 131.
(64) (a) Kang, N.-G.; Kang, B.-G.; Koh, H.-D.; Changez, M.; Lee, J.-S. *React. Funct. Polym.* **2009**, *69*, 470; (b) Changez, M.; Kang, N.-G.; Kim, D. W.; Lee, J.-S. *Nanoscale* **2013**, *5*, 11554; (c) Popescu, M.-T.; Korogiannaki, M.; Marikou, K.; Tsitsilianis, C. *Polymer* **2014**, *55*, 2943; (d) Dyakonova, M. A.; Stavrouli, N.; Popescu, M. T.; Kyriakos, K.; Grillo, I.; Philipp, M.; Jaksch, S.; Tsitsilianis, C.; Papadakis, C. M. *Macromolecules* **2014**, *47*, 7561; (e) Gao, Y.; Qiu, H.; Zhou, H.; Li, X.; Harniman, R.; Winnik, M. A.; Manners, I. *J. Am. Chem. Soc.* **2015**.
(65) Klinger, D.; Wang, C. X.; Connal, L. A.; Audus, D. J.; Jang, S. G.; Kraemer, S.; Killops, K. L.; Fredrickson, G. H.; Kramer, E. J.; Hawker, C. J. *Angew. Chem. Int. Ed. Engl.* **2014**, *53*, 7018.
(66) Kang, N.-G.; Cho, B.; Kang, B.-G.; Song, S.; Lee, T.; Lee, J.-S. *Adv. Mater.* **2012**, *24*, 385.
(67) (a) Natta, G.; Mazzanti, G.; Longi, P.; Dall'Asta, G.; Bernardini, F. *Journal of Polymer Science* **1961**, *51*, 487; (b) Matsushita, Y.; Shimizu, K.; Nakao, Y.; Choshi, H.; Noda, I.; Nagasawa, M. *Polym. J.* **1986**, *18*, 361; (c) Soum, A.; Fontanille, M. *Die Makromolekulare Chemie* **1982**, *183*, 1145; (d) Kumar, S.; Changez, M.; Murthy, C. N.; Yamago, S.; Lee, J.-S. *Macromol. Rapid Commun.* **2011**, *32*, 1576.